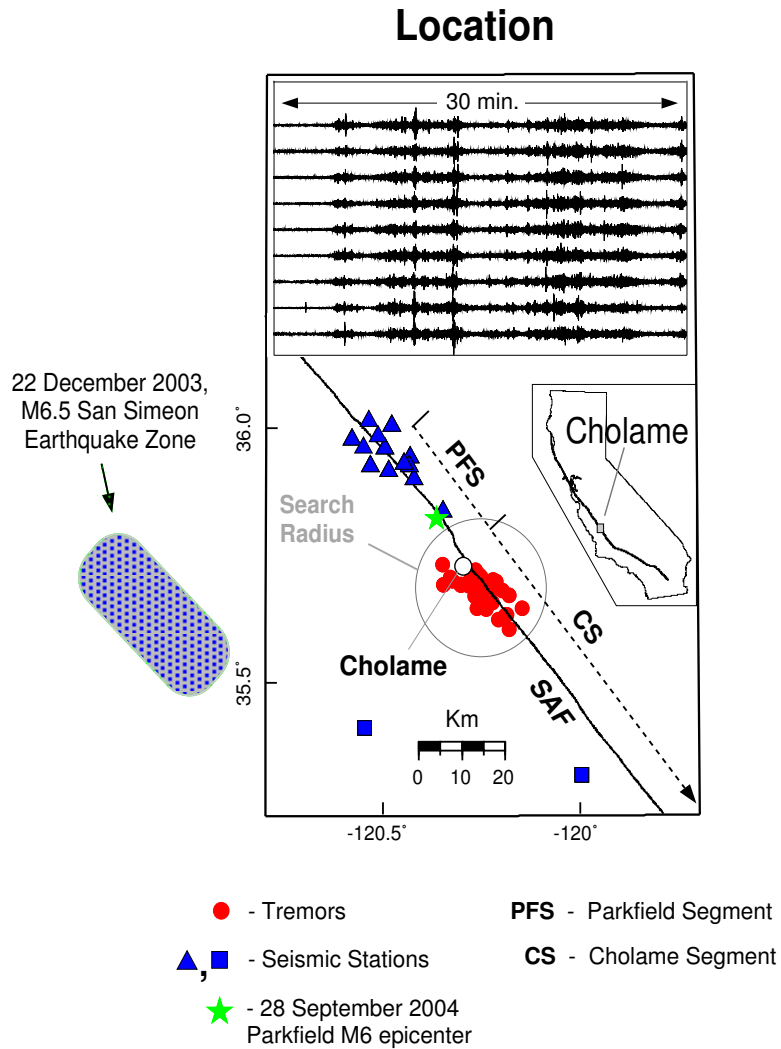


Berkeley Seismological Laboratory



Annual Report July 2004 - June 2005

Contents

1	Director's Report	4
1.	Background and Facilities	5
2.	Highlights of 2004-2005	6
3.	A tribute to Christina Jordan	8
4.	BSL staff news	9
5.	Acknowledgements	9
2	Glossary of Common Acronyms	10
3	Berkeley Digital Seismic Network	12
1.	Introduction	12
2.	BDSN Overview	12
3.	2004-2005 Activities	15
4.	Acknowledgements	24
5.	References	24
4	California Integrated Seismic Network	25
1.	Introduction	25
2.	CISN Background	25
3.	2004-2005 Activities	26
4.	Acknowledgements	34
5.	References	34
5	Northern Hayward Fault Network	35
1.	Introduction	35
2.	NHFN Overview	35
3.	2004-2005 Activities	37
4.	Acknowledgements	43
5.	References	43
6	Parkfield Borehole Network (HRSN)	44
1.	Introduction	44
2.	HRSN Overview	44
3.	2004-2005 Activities	48
4.	Acknowledgements	53
5.	References	53
7	Bay Area Regional Deformation Network	54
1.	Introduction	54
2.	2004-2005 Activities	56
3.	Data Analysis and Results	59
4.	Real-Time Processing	59
5.	Acknowledgements	61
6.	References	61

8	Plate Boundary Deformation Project	63
1.	Introduction	63
2.	Mini-PBO Station Configuration	63
3.	Broadband Deformation Data	65
4.	Acknowledgements	67
9	Data Acquisition and Quality Control	68
1.	Introduction	68
2.	McCone Hall Facilities	68
3.	Data Acquisition	69
4.	Seismic Noise Analysis	71
5.	Sensor Testing Facility	71
6.	Acknowledgements	72
7.	References	72
10	Northern California Earthquake Monitoring	73
1.	Introduction	73
2.	Northern California Management Center	73
3.	2004-2005 Activities	74
4.	Routine Earthquake Analysis	76
5.	Acknowledgements	79
6.	References	80
11	Northern California Earthquake Data Center	82
1.	Introduction	82
2.	2004-2005 Activities	82
3.	Data Collections	82
4.	Hardware and Software Systems	89
5.	Data Quality Control	90
6.	User Interface	90
7.	Database Development	91
8.	Data Distribution	92
9.	Acknowledgements	93
12	Outreach and Educational Activities	94
1.	Introduction	94
2.	Outreach Overview	94
3.	2004-2005 Activities	94
4.	Acknowledgements	95
13	Research Studies	96
1.	Nonvolcanic Tremors on the Central San Andreas Fault	97
2.	Kinematic Modeling of the 2004 Parkfield Earthquake	100
3.	The Parkfield Earthquakes: Then and Now	103
4.	A View of the 2004 Parkfield Earthquake from InSAR	105
5.	Frictional Afterslip Following the 2004 Parkfield, California Earthquake	107
6.	The Orinda Earthquake Sequence: Scaling of Small Earthquakes	110
7.	Inversion for the Velocity Structure of the Santa Clara Valley, California	112
8.	Analysis of Bridge Structures Crossing Fault Rupture Zones: Seismic Ground Motion Simulation	114
9.	Investigation of Deep Earthquake Mechanics	116
10.	ElarmS: A Methodology for Earthquake Early Warning	118
11.	Northern California Seismicity Project	121
12.	Seismogram Scanning Project	123
13.	Insight into the Origin of Earth's hum and Microseisms	125

14.	Observations of Infragravity Waves at the Monterey Ocean Bottom Broadband Station (MOBB) . . .	127
15.	Seismic Imaging OF the Newberry Hotspot Track	130
16.	Fluid-Influenced Faulting in the Long Valley Volcanic Region	132
17.	Measuring and Modeling Fluid Movements in Volcanoes: Insights from Continuous Broadband Seismic Monitoring at Galeras Volcano, Colombia	134
18.	Independent Okhotsk and Amurian Microplate Tectonics of Northeast Asia	136
19.	Crustal Deformation Along the Northern San Andreas Fault System	138
20.	Strong Ground Motions Derived from Geodetic Slip Models	140
21.	Joint Inversion for 3D Velocity Structure of the Middle East and North Africa to Improve Nuclear Explosion Monitoring	142
22.	Constraints on Shear Wave Attenuation in the Earth's Inner Core from an observation of PKJKP . .	144
23.	High Resolution Anisotropic Structure of the North American Upper Mantle from Inversion of Body and Surface Waveform Data	146
24.	Development of a Regional Velocity Model Using 3D Broadband Waveform Sensitivity	149
25.	Toward the Constraints on Lateral S Wave Velocity Gradients and the Shape of the Pacific Superplume	151
26.	Towards Inverting Seismic Waveform Data for Temperature and Composition of the Earth's Upper Mantle	153
27.	Europa Scenarios: Preliminary Physically Consistent Models of Europa	155

Chapter 1

Director's Report

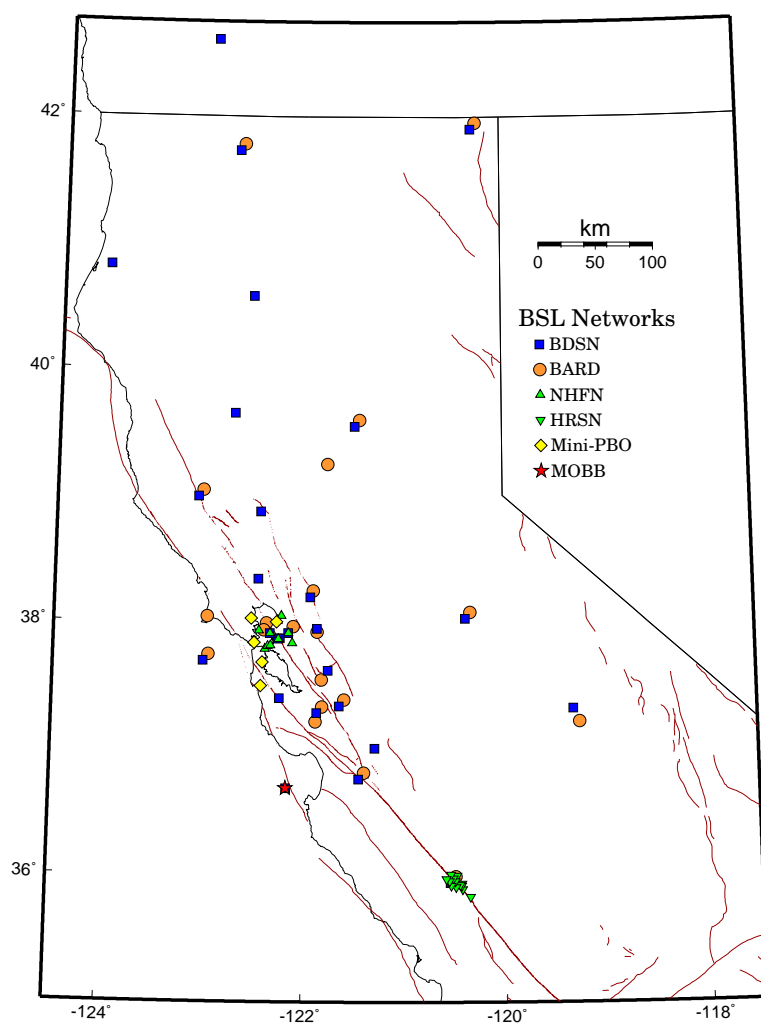


Figure 1.1: Map illustrating the distribution of stations in the BDSN, NHFN, HRSN, BARD, and Mini-PBO networks in northern and central California. A star indicates the location of the MOBB deployment.

1. Background and Facilities

The Berkeley Seismological Laboratory (BSL), formerly the Berkeley Seismographic Station (BSS), is the oldest Organized Research Unit (ORU) on the U. C. Berkeley campus. Its mission is unique in that, in addition to research and education in seismology and earthquake-related science, it is responsible for providing timely information on earthquakes (particularly those that occur in northern and central California) to the UC Berkeley constituency, the general public, and various local and state government and private organizations. The BSL is therefore both a research center and a facility/data resource, which sets it apart from most other ORUs. A major component of our activities is focused on developing and maintaining several regional observational networks, and participating, along with other agencies, in various aspects of the collection, analysis, archival, and distribution of data pertaining to earthquakes, while maintaining a vigorous research program on earthquake processes and Earth structure. In addition, the BSL staff spends considerable time with public relations activities, including tours, talks to public groups, responding to public inquiries about earthquakes, and, more recently, World-Wide-Web presence (<http://www.seismo.berkeley.edu/seismo/>).

U.C. Berkeley installed the first seismograph in the Western Hemisphere at Mount Hamilton (MHC) in 1887. Since then, it has played a leading role in the operation of state-of-the-art seismic instruments and in the development of advanced methods for seismic data analysis and interpretation. Notably, the installation, starting in 1927, of Wood-Anderson seismographs at 4 locations in northern California (BKS, ARC, MIN and MHC) allowed the accurate determination of local earthquake magnitude (M_L) from which a unique historical catalog of regional earthquakes has been maintained to this day, providing crucial input to earthquake probabilities studies.

Over the years, the BSS continued to keep apace of technological improvements. The first centrally telemetered network using phone lines in an active seismic region was installed by BSS in 1960. The BSS was the first institution in California to operate a 3-component “broadband” system (1963). Notably, the BSS played a major role in the early characterization of earthquake sources using “moment tensors” and source-time functions, and made important contributions to the early definitions of detection/discrimination of underground nuclear tests and to earthquake hazards work, jointly with UCB Engineering. Starting in 1986, the BSS acquired 4 state-of-the-art broadband instruments (STS-1), while simultaneously developing PC-based digital telemetry, albeit with limited resources. As the telecommunication and computer technology made rapid progress, in parallel with broadband instrument development, paper record reading could be completely abandoned in favor of largely

automated digital data analysis.

The current modern facilities of BSL have been progressively built over the last 14 years, initiated by significant “upgrade” funding from U.C. Berkeley in 1991-1995. The BSL currently operates and acquires data, continuously and in real-time, from over 60 regional observatories, housing a combination of broadband and strong motion seismic instrumentation installed in vaults, borehole seismic instrumentation, permanent GPS stations of the BARD network, and electromagnetic sensors. The seismic data are fed into the BSL real-time processing and analysis system and are used in conjunction with data from the USGS NCSN network in the joint earthquake notification program for northern California, started in 1996. This program capitalizes on the complementary capabilities of the networks operated by each institution to provide rapid and reliable information on the location, size and other relevant source parameters of regional earthquakes. In recent years, a major emphasis in BSL instrumentation has been in densifying the state-of-the-art seismic and geodetic networks, while a major on-going emphasis in research has been the development of robust methods for quasi-real time automatic determination of earthquake source parameters and predicted strong ground motion, using a sparse network combining broadband and strong motion seismic sensors, as well as permanent geodetic GPS receivers.

The backbone of the BSL operations is a regional network of 27+ digital broadband and strong motion seismic stations, the Berkeley Digital Seismic Network (BDSN), with continuous telemetry to UC Berkeley. This network provides the basic regional data for the real-time estimation of location, size and rupture parameters for earthquakes of M 3 and larger in central and northern California, within our Rapid Earthquake Data Integration (REDI) program and is the Berkeley contribution to the California Integrated Seismic Network (CISN). It also provides a fundamental database for the investigation of three-dimensional crustal structure and its effects on regional seismic wave propagation, which is ultimately crucial for estimating ground shaking for future earthquakes. Most stations also record auxiliary temperature/pressure channels, valuable in particular for background noise quality control. Complementing this network is a ~ 25 station “high-resolution” network of borehole seismic sensors located along the Hayward Fault (HFN) and under the Bay Area bridges, operated jointly with the USGS/Menlo Park and linked to the Bridge Safety Project of the California Department of Transportation (Caltrans). The latter has facilitated the installation of sensor packages at 15 bedrock boreholes along 5 east-bay bridges in collaboration with Lawrence Livermore National Laboratory (LLNL). A major science goal of this network is to collect high signal-to-noise data for micro-earthquakes along the Hayward Fault to gain

insight into the physics that govern fault rupture and its nucleation. The BSL is also involved in the operation and maintenance of the 13 element Parkfield borehole seismic array (HRSN), which is yielding enlightening results on quasi-periodic behavior of micro-earthquake clusters and important new constraints on earthquake scaling laws and is currently playing an important role in the characterization of the site for the future San Andreas Fault Observatory at Depth (SAFOD). Since April 2002, the BSL is also involved in the operation of a permanent broadband ocean bottom station, MOBB, in collaboration with MBARI (Monterey Bay Aquarium Research Institute).

In addition to the seismic networks, the BSL is involved in data archival and distribution for the permanent geodetic BARD (Bay Area Regional Deformation) Network as well as the operation, maintenance, and data processing of 22 out of its 70+ sites. Whenever possible, BARD sites are collocated with BDSN sites in order to minimize telemetry costs. In particular, the development of analysis methods combining the seismic and geodetic data for the rapid estimation of source parameters of significant earthquakes has been one focus of BSL research.

Finally, two of the BDSN stations (PKD, SAO) also share data acquisition and telemetry with 5-component electromagnetic sensors installed with the goal of investigating the possibility of detection of tectonic signals. In 2002-2003, an automated quality control software was implemented to monitor the electromagnetic data.

Archival and distribution of data from these and other regional networks is performed at the Northern California Earthquake Data Center (NCEDC), operated at the BSL in collaboration with USGS/Menlo Park. The data reside on a mass-storage device (current holdings ~ 6 TerraBytes), and are accessible “on-line” over the Internet (<http://www.quake.geo.berkeley.edu>). Among others, data from the USGS Northern California Seismic Network (NCSN), are archived and distributed through the NCEDC. The NCEDC also maintains, archives and distributes the ANSS/CNSS earthquake catalog.

Core University funding to our ORU has suffered from permanent budget cuts to research programs from the State of California, and currently provides salary support for 2 field engineers, one computer expert, 2 data analysts, 1 staff scientist and 2 administrative staff. This supports a diminishing portion of the operations of the BDSN and provides seed funding for our other activities. All other programs are supported through extramural grants primarily from the USGS and NSF, and in the past four years, the Governor’s Office of Emergency Services (OES). We acknowledge valuable recent contributions from other sources such as Caltrans, the CLC program, PEER, as well as our Earthquake Research Affiliates.

2. Highlights of 2004-2005

2.1 Infrastructure and Earthquake Notification

In 2004-2005, BSL’s activities have centered around two major projects: the continuation of CISN and our participation, at various levels, in three components of the national Earthscope program: the deployment in California of the *BigFoot* component of USArray, the preparation for archival of borehole strainmeter data and for acting as “analysis center” for continuous GPS data, in the framework of the Plate Boundary Observatory (PBO), and the preparation for archival of the data from the San Andreas Fault Observatory at Depth (SAFOD).

The main goal of the CISN (see Chapter 4) is to ensure a more uniform system for earthquake monitoring and reporting in California. The highest priority, from the point of view of emergency responders in California, is to improve the robustness of statewide real-time notification and to achieve a uniform interface across the State to the California OES and other emergency responders. This represents a major challenge, as the CISN started as a heterogeneous collection of networks with disparate instrumentation, software systems and culture. The M 6.0 September 28th Parkfield earthquake provided a significant opportunity to test the CISN capabilities. CISN funds were used to establish new broadband stations at Alder Springs, CA (GASB), which has been completed, and at the Marconi Conference Center near Point Reyes (MCCM), which is under construction. We also upgraded remote diagnostic capabilities at 23 of our sites equipped with Quanterra Q4120 data loggers. As in previous years, the emphasis has been on improvement of Statewide Communications. In the past year, BSL has worked with SBC to distribute the acquisition of seismic data between the two frame-relay T1 circuits connecting BSL and USGS/Menlo Park, and to establish a second Permanent Virtual Circuit (PVC) at each frame-relay site, to improve the robustness of data acquisition. Efforts to develop the next generation of the northern California joint notification system are underway and described in chapter 9.

The CISN partners completed the final stage of a system to exchange peak ground motion data this year, which improves the robustness of ShakeMaps and their quality on the boundary between northern and southern California. Efforts have also gone towards improving the standardization of ShakeMaps across the State and statewide software calibration.

BSL staff continue to spend considerable efforts in organizational activities for CISN, notably by participating in the CISN Project Management Group (Gee and now Neuhauser), which includes weekly 2 hour phone conferences, and the Standards Committee (Neuhauser-chair, Gee, Lombard), which strives to define and coordinate

software development tasks. Romanowicz and Gee have continued to serve on the CISN Steering Committee. The CISN also represents California as a designated region of ANSS (Advanced National Seismic System) and the BSL is actively involved in planning activities for the ANSS.

The BSL concluded an agreement in June 2004 with IRIS to contribute 19 stations of the BDSN to USArray, while the experiment is deployed in California. This includes 17 existing stations and the two new sites mentioned above: GASB and MCCM. The 19 BDSN sites provide USArray with a running start in Northern California. In the past year, BSL staff have worked with USArray to establish several new USArray sites in northern and central California, from which data are being sent both to BSL and the Array Network Facility. BSL staff have been working to identify 8 potential sites that may become permanent BDSN sites, many at UC reserves and field stations. As part of the USArray collaboration, the BSL has converted most of the BDSN broadband data streams from 20 samples per second to 40 samples per second.

The BSL has been actively working to relocate the critical operations of data acquisition, processing, archiving and data distribution to 2195 Hearst (“SRB-1”), a recently completed building on Oxford Tract, which was constructed to current seismic codes, with special attention to post-earthquakes operability of the campus computer facility. The computer center contains state-of-the-art seismic bracing, UPS power and air conditioning with generator back-up and extensive security and equipment monitoring. BSL has moved almost all of its data acquisition, real-time earthquake processing computers and data archive and distribution computers to the new facility, including telemetry equipment. The latter is in the course of being completed.

This past year has been exceptionally busy for the borehole Parkfield project (HRSN, see chapter 6), with the 28 September 2004 repeat of the long awaited M6 Parkfield earthquake, the discovery of nonvolcanic tremor activity (see research part of the report) and the on-going SAFOD project. Several steps have been taken towards enhancing the performance, and in particular upgrading aging components of the systems. HRSN data have played a key role in characterizing the SAFOD drilling site. Monitoring the evolution of nonvolcanic tremors and microseismicity, particularly in the SAFOD drilling and target zone, are primary objectives of the HRSN project. The numerous and on-going aftershocks from the December 2003 M6.5 San Simeon and Sept 2004 M6.0 Parkfield earthquakes have called for a significant revision of the “traditional” processing scheme used since 1987.

The Northern Hayward Fault Network (NHFN, see chapter 5) has seen equipment upgrades in anticipation of installing Q4120 data loggers and real time telemetry.

Mini-PBO stations SVIN and SBRN, which became fully operational this past year (see chapter 8) have added coverage to the north side of the north bay and east side of the south bay, respectively.

Continued acquisition of data from the BARD GPS network (see chapter 7) has been occurring at a sampling rate of 30 seconds. We have now converted the acquisition rate to 1 sec at 7 stations in the San Francisco Bay Area, which allows us to measure dynamic displacements due to large earthquakes. Additional conversions await resolving telemetry bandwidth limitations. The GPS team has also been busy preparing for the transfer of several UC Berkeley operated and maintained BARD stations to PBO. Berkeley will retain control over those stations that have real time telemetry and are collocated with broadband instrumentation. We are, in particular, continuing to develop joint real-time analysis methods of GPS and seismic broadband data.

The NCEDC (see Chapter 11), continues archiving and distribution of on-line of data from expanding BDSN, NHFN, HRSN, BARD, Mini-PBO, and other networks and data collections in northern California and Nevada. In 2005, the NCEDC started acquiring telemetered continuous data from USArray stations in northern California and vicinity. We are continuing to receive data from the SAFOD pilot hole and main hole, and data from 15 SCSN (southern California) broadband sites as part of the CISN robust “backbone”. Efforts are continuing to develop software and acquire hardware to archive continuous NCSN seismograms directly onto the NCEDC archive for the future, as well as transfer from tapes to complete the collection retroactively.

Finally, through Dr Lind Gee’s (and now Peggy Hellweg’s) efforts, BSL has continued to be actively involved in the preparation of UC Berkeley’s participation in the commemoration activities of the centennial anniversary of the 1906 earthquake (see Chapter 12). These activities include a joint SSA/EERI/DRC conference to be held in San Francisco in April 2006 as well as many exhibits, classes, and public lectures on the UC Berkeley Campus, the first of which was held on October 20th, 2005.

2.2 Research Accomplishments

Chapter 13 documents the main research contributions of the past year. Research at the BSL spans a broad range of topics, from the study of microseismicity at the local scale to global deep earth structure, and includes the use of seismological, geodetic, and remote sensing (InSAR) techniques.

I wish to highlight several prominent research results of the past year. First, the invested effort in the HRSN network is continuing to pay off. Nadeau and collaborators (see research report 1.) have discovered the presence of non-volcanic tremor activity on the San Andreas Fault at Parkfield. Previously, such tremors had been only ob-

served in subduction zones, and an important role had been attributed to fluids in their generation. The new discovery, reported in *Science*, presents a challenge to this simple interpretation.

Second, at the other end of the spectrum of BSL research, the report by Cao et al. (see research report 22.) describes a convincing observation of the PKJKP wave, a seismic wave that travels through the inner core as a shear wave. Only three detections of this wave, whose existence is predicted from the solidity of the inner core, had previously been claimed, with controversial observations. In contrast, Aimin's observation, published in *Science* and based on data from the Gräffenberg array in Germany, is much clearer.

The 09/28/04 Parkfield earthquake resulted in several studies: a kinematic model of the earthquake, combining seismic and geodetic data (see research study 2.), comparison of the 2004 earthquake with previous repeating Parkfield earthquakes of 1922, 1934 and 1966 (see research report 3.), as well as studies of the earthquake rupture and afterslip using InSAR and GPS data (see research reports 4. and 5.). An intriguing swarm of small earthquakes near Orinda, CA, has provided a unique dataset for the study of earthquake scaling behavior (see research report 6.).

Studies devoted to the source and effects of earthquakes also include investigation of the generation mechanism of deep earthquakes (research report 9.), ground motion simulation of structures (research report 8.), and the development and testing of an early warning system (research report 10.). Dr Uhrhammer continues to lead the analysis and preservation of historical data (research report 11. and 12.).

BSL researchers have used microseismic noise data to study detailed structure of the Santa Clara Valley (research report 7.), have investigated further the oceanic origin of the low frequency "hum", and its relation to ocean storms (research reports 13., 14.). In collaboration with Peter Bromirski of UC San Diego, selected analog seismograms of the Berkeley historical collection have been scanned to study the relation of microseisms and wave climate, with important applications for climate studies (research report 12.).

We note an increasing interest in the study of structure and processes in volcanic areas: imaging the Newberry hotspot track (research report 15.), investigating fluid-influenced faulting in Long Valley (research report 16.), and fluid motion in Galeras Volcano, Colombia (research report 17.).

Geodetic studies also include the estimation of strong ground motions in real time from geodetic data (research report 20.), and the study of crustal deformation along the northern San Andreas Fault system (research report 13.38), and the tectonics of northeast Asia (research report 18.).

BSL researchers image earth structure at a variety of scales, investigating various theoretical improvements to the forward and inverse problems: 1) regional, in the Middle East (research report 21.) and in north America (research report 23.), in southeast Asia (research report 24.), in the deep mantle under the Pacific and African "superplumes" (research report 25.), and 2) global: this year, an on-going study attempts direct inversion of seismic waveforms for lateral variations in temperature and composition (research report 26.).

And finally, an investigation of physically consistent models of Europa is the first explicit study of planetary structures at BSL (research report 27.).

3. A tribute to Christina Jordan

Christina Jordan passed away on April 23, 2005, at age 50, after suffering a massive brain hemorrhage, leaving the BSL staff and faculty in deep shock and sorrow. Christina came to BSL as an administrative assistant in 1999 and soon became an invaluable resource for all of us. Always smiling and available to help in emergencies, Christina had an exceptional ability to anticipate everyone's needs, follow up on tasks, and, perhaps more importantly, catch all the loose ends that I, in particular, would leave behind when jumping around my overbooked schedule. In addition to her incredible attention to detail, which saved many a letter, report, and proposal I wrote, she helped me and others meet deadlines. Christina had artistic talents and skills which we only had a glimpse of when she prepared our BSL Annual Reports.

Christina earned a B.A. in Biological Sciences from UC Berkeley in 1977 (a Regents Scholar all four years), and a B.A. in Studio Arts from Cal State Hayward, after which she studied medical and biological illustration at UC San Francisco (M.A., 1984). Christina's first job at UC Berkeley was as Illustrator with the Department of Entomological Sciences, College of Natural Resources (CNR), from 1985 to 1996, where, in particular, she produced many astounding drawings of birds. After working for two years with the CNR Dean's Office on the alumni magazine, Breakthroughs, Christina was a free-lance scientific illustrator and graphic designer for 2 years. She joined the BSL in January 1999 as an Administrative Assistant II. She had just been promoted to Administrative Specialist, a position that she deserved for a long time because of her role as executive assistant to the Director and Contracts and Grants Analyst. In recognition of her special place in the hearts of her many friends and colleagues on Campus, we have planted two trees in front of McCone Hall, an Eastern Redbud and a California Buckeye. These trees will be dedicated to Christina in a special ceremony held on October 14, 2005. A webpage dedicated to Christina's life and work is available at <http://seismo.berkeley.edu/memorial>

4. BSL staff news

There have been many other changes in BSL staff this past year. Lind Gee was offered and accepted the position of Chief Scientist at the Albuquerque Seismological Laboratory of the USGS. We are proud of Lind, and at the same time, very sorry that she has left, at the beginning of September 2005. Lind has served the BSL remarkably for the past 14 years. Peggy Hellweg has assumed part of Lind's responsibilities, those pertaining to the operation of the Berkeley Digital Seismic Network, the alarm response and the outreach. In particular, Peggy has been heavily involved in the last two months in the organization of the 1906 centennial activities. With Lind, we also lose Mark Murray, who is leaving at the end of October 2005 and will assume a research position at New Mexico Tech. Mark Murray's responsibilities for operation of the BARD network and real time GPS data acquisition will be transferred to Nicolas Houlié, who recently arrived from Institut de Physique du Globe in Paris, as a post-doc. Unfortunately, Nicolas will not benefit from the assistance of Cédric de la Beaujardière, who is also leaving at the end of October.

As if the changes were not sufficient, Eleanor Blair, our Manager, decided to retire at the end of October. A retirement party was held in her honor at the Women's Faculty Club on October 19th, 2005. Eleanor served the University for 36 years, and the BSL for 12 years. For her outstanding service, she earned the Chancellor's Distinguished Service Award, which will be presented to her on November 1st.

On the bright side, our field engineering team is back in shape: Rick Lellinger joined the BSL engineering team in October 2004, and Jarrett Gardner in August 2005, both as assistant development engineers. Kate Conner and Jenny Pehl joined the BSL administrative office in September 2005 to replace Christina and assist with an overflow of projects. In addition to Nicolas Houlié, two new post-docs joined the BSL in this past year: Fabio Cammarano, who earned his PhD from the ETH in Zurich, Switzerland, and Gareth Funning, from Cambridge University.

5. Acknowledgements

I wish to thank our technical and administrative staff, scientists and students for their efforts throughout the year and their contributions to this annual report. Individual contributions to activities and report preparation are mentioned in the corresponding sections, except for the Appendix section, prepared by Kate Conner and Eleanor Blair.

I also wish to specially thank the individuals who

have regularly contributed to the smooth operation of the BSL facilities: Sierra Boyd, Rich Clymer, Cédric de la Beaujardière, Doug Dreger, John Friday, Lind Gee, Wade Johnson, Bill Karavas, Rick Lellinger, Pete Lombard, Rick McKenzie, Mark Murray, Bob Nadeau, Doug Neuhauser, Charley Paffenbarger, Bob Uhrhammer, and Stephane Zuzlewski. I particularly want to thank Doug Dreger for serving as Associate Director of the BSL, and Doug Neuhauser for stepping in to help and serve on the CISN Program Management Group after Lind Gee's departure.

I also wish to thank our undergraduate assistants, Amanda Austin, Chi Chan, Jonathan Hsu, Kevin Lee, Rose Li, Tomasz Matlak, Gretchen Sites, Miles Traer, Sean Tsa and Noli Valera, for their contributions to our research and operational activities.

I am particularly thankful to Jenny Pehl, Kate Conner as well as Lind Gee, for their help in putting together this Annual Report (the latter remotely).

The Annual Report of the Berkeley Seismological Laboratory is available on the WWW at http://www.seismo.berkeley.edu/seismo/annual_report/.

Barbara Romanowicz
October 24, 2005

Chapter 2

Glossary of Common Acronyms

Table 2.1: Standard abbreviations used in this report.

Acronym	Definition
AGU	American Geophysical Union
ANSS	Advanced National Seismic System
BARD	Bay Area Regional Deformation
BDSN	Berkeley Digital Seismic Network
BSL	Berkeley Seismological Laboratory
BSS	Berkeley Seismographic Station
CISN	California Integrated Seismic Network
CGS	California Geological Survey
CLC	Campus Laboratory Collaboration
CNSS	Council of the National Seismic System
CSRC	California Spatial Reference Center
DRC	Disaster Resistent California
EM	Electromagnetic
EPRI	Electric Power Research Institute
EERI	Earthquake Engineering Research Institute
FBA	Force Balance Accelerometer
FIR	Finite Impulse Response
FRAD	Frame Relay Access Device
GPS	Global Positioning System
HFN	Hayward Fault Network
HRSN	High Resolution Seismic Network
IGS	International Geodetic Service
IMS	International Monitoring System
InSAR	Interferometric Synthetic Aperture Radar
IRIS	Incorporated Research Institutions for Seismology
ISC	International Seismological Center
ISTAT	Integrating Science, Teaching, and Technology
JPL	Jet Propulsion Laboratory
LBNL	Lawrence Berkeley National Laboratory
LLNL	Lawrence Livermore National Laboratory
MBARI	Monterey Bay Aquarium Research Institute
MHH	Murdock, Hutt, and Halbert
MOA	Memorandum of Agreement
MOBB	Monterey Ocean Bottom Broadband observatory
MOISE	Monterey Bay Ocean Bottom International Seismic Experiment
MPBO	Mini-Plate Boundary Observatory

continued on next page

Table 2.1: *continued*

Acronym	Definition
MRI	Major Research Initiative
MRE	Major Research Equipment
MT	Magnetotelluric
NCEDC	Northern California Earthquake Data Center
NCSN	Northern California Seismic Network
NEHRP	National Earthquake Hazards Reduction Program
NEIC	National Earthquake Information Center
NHFN	Northern Hayward Fault Network
NGS	National Geodetic Survey
NSF	National Science Foundation
NSN	National Seismic Network
OES	Office of Emergency Services
ORU	Organized Research Unit
PBO	Plate Boundary Observatory
PEER	Pacific Earthquake Engineering Center
PH	Pilot Hole
PPE	Parkfield Prediction Experiment
PREM	Preliminary Reference Earth Model
PSD	Power Spectral Density
QDDS	Quake Data Distribution System
REDI	Rapid Earthquake Data Integration
SAF	San Andreas Fault
SAFOD	San Andreas Fault Observatory at Depth
SAR	Synthetic Aperture Radar
SCEC	Southern California Earthquake Center
SCEDC	Southern California Earthquake Data Center
SCIGN	Southern California Integrated GPS Network
SEED	Standard for the Exchange of Earthquake Data
SEM	Spectral Element Method
SHFN	Southern Hayward Fault Network
SIO	Scripps Institutions of Oceanography
SNCL	Station Network Channel Location
SSA	Seismological Society of America
STP	Seismogram Transfer Program
UCB	University of California at Berkeley
UNAVCO	University NAVSTAR Consortium
UrEDAS	Urgent Earthquake Detection and Alarm System
USGS	United States Geological Survey

Chapter 3

Berkeley Digital Seismic Network

1. Introduction

The Berkeley Digital Seismic Network (BDSN) is a regional network of very broadband and strong motion seismic stations spanning northern California and linked to UC Berkeley through continuous telemetry (Figure 3.1 and Table 3.1). This network is designed to monitor regional seismic activity at the magnitude 3+ level as well as to provide high quality data for research projects in regional and global broadband seismology.

The network upgrade and expansion initiated in 1991 has continued, and it has grown from the original 3 broadband stations installed in 1986-87 (BKS, SAO, MHC) to 28 stations in 2004, including the ocean-bottom seismometer in Monterey Bay. One new station was added in the past year (MCCM), while one station was closed (POTR).

We take particular pride in high quality installations, which often involve lengthy searches for appropriate sites away from sources of low-frequency noise, as well as continuous improvements in installation procedures and careful monitoring of noise conditions at existing stations.

Future expansion of our network is contingent on the availability of funding and coordination with other institutions for the development of a denser state-of-the-art strong motion/broadband seismic network and joint earthquake notification system in this seismically hazardous region.

2. BDSN Overview

Twenty-five of the BDSN sites are equipped with 3 component broadband seismometers and strong-motion accelerometers, and a 24-bit digital data acquisition system or datalogger. Two additional sites (RFSB and SCCB) consist of a strong-motion accelerometer and a 24-bit digital datalogger. Data from all BDSN stations are transmitted to UC Berkeley using continuous telemetry. In order to insure against data loss during utility disruptions, each site has a 3-day supply of battery power and is accessible via a dialup phone line. The combina-

tion of high-dynamic range sensors and digital dataloggers ensures that the BDSN has the capability to record the full range of earthquake motion for source and structure studies. Table 3.2 lists the instrumentation at each site.

Most BDSN stations have Streckeisen STS-1 or STS-2 three-component broadband sensors (*Wielandt and Streckeisen, 1982; Wielandt and Steim, 1986*). Guralp CMG-3T downhole broadband sensors contributed by LLNL are deployed in post-hole installations at BRIB and FARB. The strong-motion instruments are Kinemetrics FBA-23 or FBA-ES-T with ± 2 g dynamic range. The recording systems at all sites are either Q330, Q680, Q730, or Q4120 Quanterra dataloggers, with 3, 6, 8, or 9 channel systems. The Quanterra dataloggers employ FIR filters to extract data streams at a variety of sampling rates. In general, the BDSN stations record continuous data at .01, 0.1, 1.0, 20.0 or 40.0, and 80 or 100 samples per second, although some sites send triggered data at the highest sampling rate using the Murdock, Hutt, and Halbert event detection algorithm (*Murdock and Hutt, 1983*) (Table 3.3). In addition to the 6-channels of seismic data, signals from thermometers and barometers are recorded at nearly every site (Figure 3.2).

In parallel with the upgrade of the broadband network, a grant from the CalREN Foundation (California Research and Education Network) in 1994 enabled the BSL to convert data telemetry from analog leased lines to digital frame-relay connections. The frame-relay network uses digital phone circuits that can support 56 Kbit/s to 1.5 Mbit/s throughput. Since frame-relay is a packet-switched network, a site may use a single physical circuit to communicate with multiple remote sites through the use of “permanent virtual circuits”. Frame Relay Access Devices (FRADs), which replace modems in a frame-relay network, can simultaneously support multiple interfaces such as RS-232 async ports, synchronous V.35 ports, and ethernet connections. In practical terms, the upgrade to frame relay communication provides faster data telemetry between the remote sites and the BSL, remote console control of the dataloggers, additional services such as FTP and telnet to the dataloggers, data

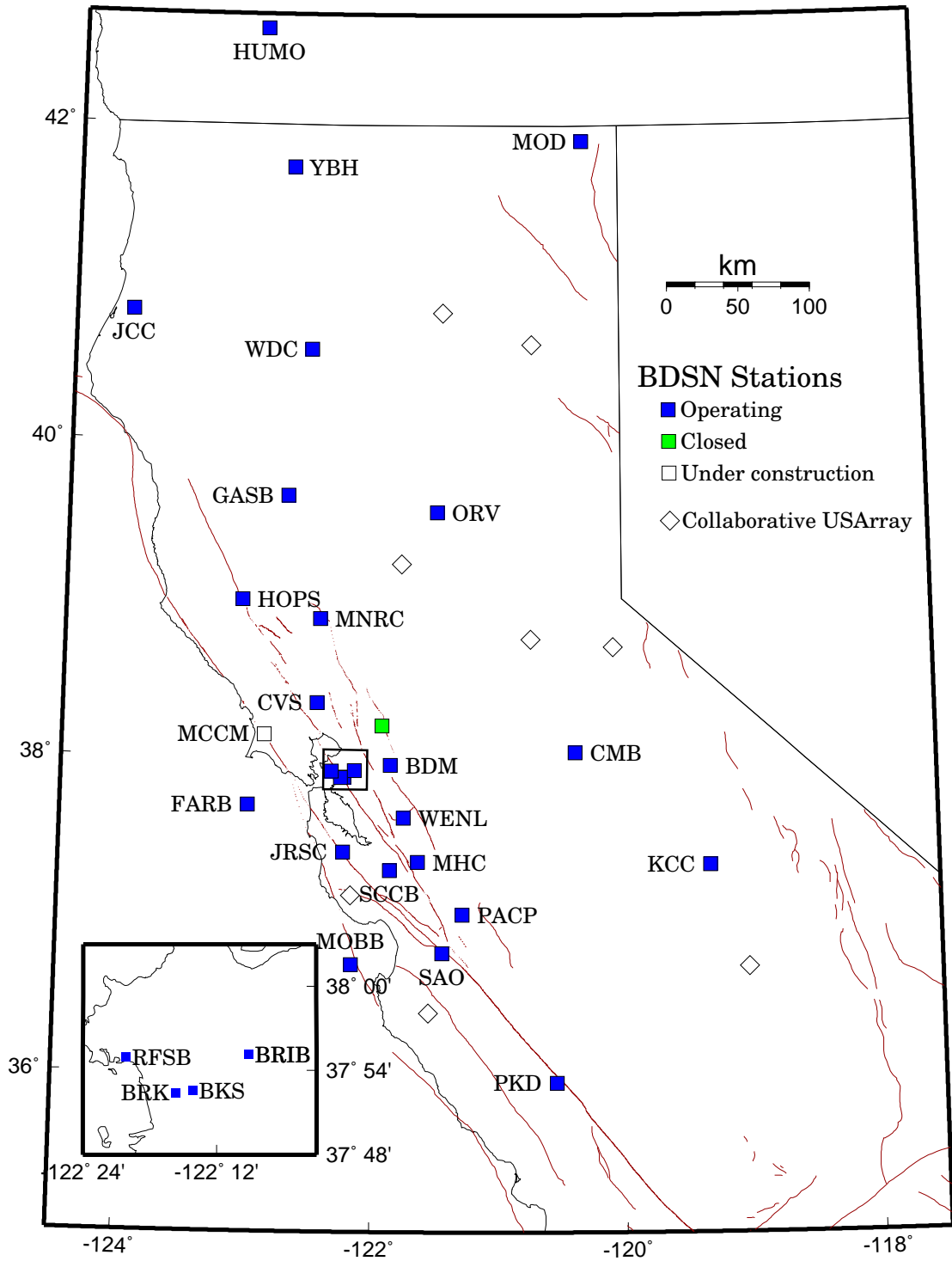


Figure 3.1: Map illustrating the distribution of operational (filled squares), planned (open squares), and closed (grey squares) BDSN stations in northern and central California. The open diamonds indicate new sites developed in collaboration with USArray

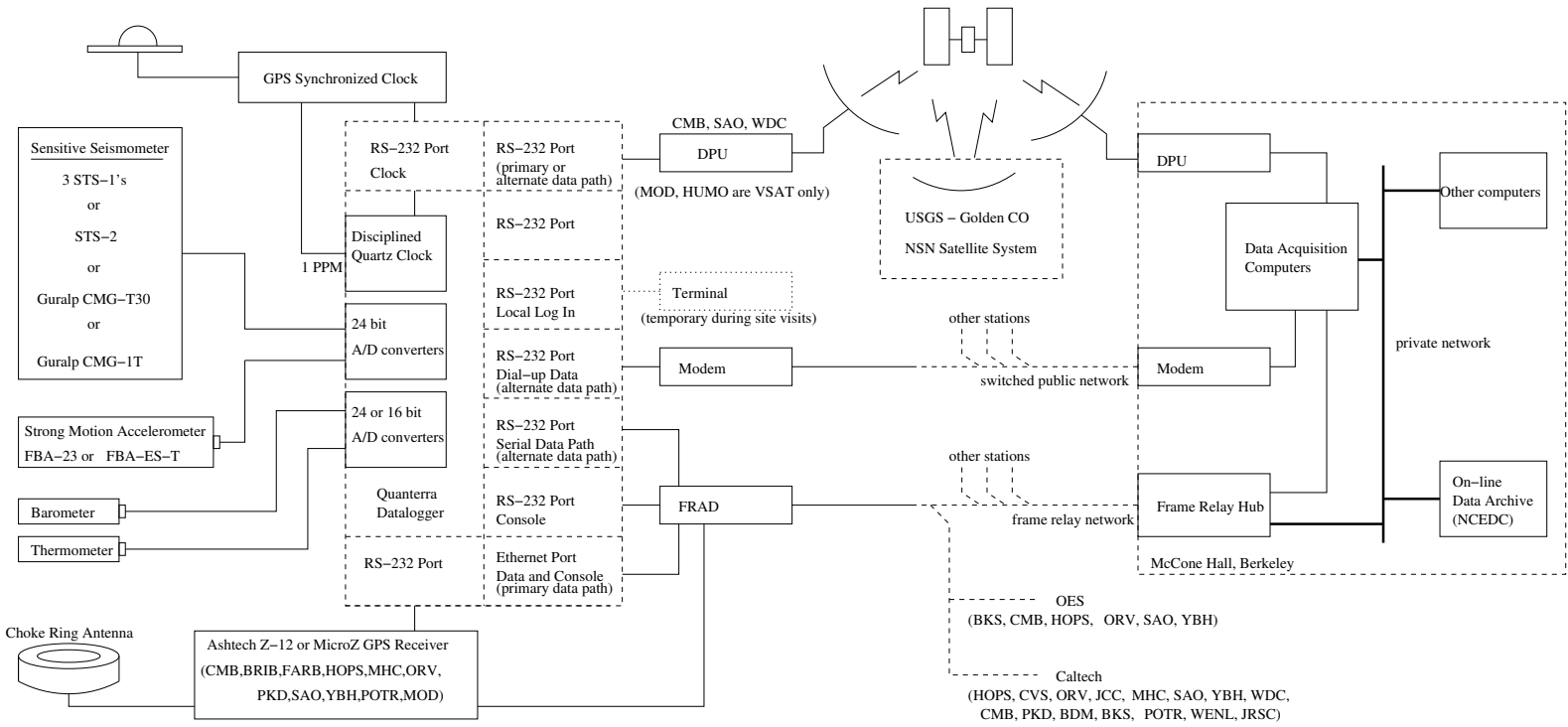


Figure 3.2: Schematic diagram showing the flow of data from the sensors through the dataloggers to the central acquisition facilities of the BSL.

transmission to multiple sites, and the ability to communicate and transmit data from multiple instruments such as GPS receivers and/or multiple dataloggers at a single site. Today, 23 of the BDSN sites use frame-relay telemetry for all or part of their communications system.

As described in Chapter 9, data from the BDSN are acquired centrally at the BSL. These data are used for rapid earthquake reporting as well as for routine earthquake analysis (Chapters 4 and 10). As part of routine quality control (Chapter 9), power spectral density (PSD) analyses are performed weekly and Figure 3.3 shows a summary of the results for 2004-2005.

The occurrence of a significant teleseism also provides the opportunity to review station health and calibration. Figure 3.4 displays BDSN waveforms for a M_w 7.1 deep focus earthquake in the Fiji region on July 15, 2004.

BDSN data are archived at the Northern California Earthquake Data Center. This is described in detail in Chapter 11.

Sensor	Channel	Rate (sps)	Mode	FIR
Broadband	UH?	0.01	C	Ac
Broadband	VH?	0.1	C	Ac
Broadband	LH?	1	C	Ac
Broadband	BH?	20/40	C	Ac
Broadband	HH?	80/100	C	Ac/Ca
SM	LL?	1	C	Ac
SM	BL?	20/40	C	Ac
SM	HL?	80/100	C	Ac/Ca
Thermometer	LKS	1	C	Ac
Barometer	LDS	1	C	Ac

Table 3.3: Typical data streams acquired at BDSN stations, with channel name, sampling rate, sampling mode, and the FIR filter type. SM indicates strong-motion; C continuous; T triggered; Ac acausal; Ca causal. The LL and BL strong-motion channels are not transmitted over the continuous telemetry but are available on the Quanterra disk system if needed. The HH channels are recorded at two different rates, depending on the datalogger type. Q4120s provide 100 sps and causal filtering; Q680/980s provide 80 sps and acausal filtering. The BH channels were changed from 20 to 40 sps this year as described below.

2.1 Electromagnetic Observatories

In 1995, the BSL installed two well-characterized electric and magnetic field measuring systems at two sites along the San Andreas Fault which are part of the Berkeley Digital Seismic Network in collaboration with Dr. Frank Morrison. Since then, magnetotelluric (MT) data have been continuously recorded at 40 Hz and 1 Hz and archived at the NCEDC (Table 3.4). At least one set of

Sensor	Channel	Rate (sps)	Mode	FIR
Magnetic	VT?	0.1	C	Ac
Magnetic	LT?	1	C	Ac
Magnetic	BT?	40	C	Ac
Electric	VQ?	0.1	C	Ac
Electric	LQ?	1	C	Ac
Electric	BQ?	40	C	Ac

Table 3.4: Typical MT data streams acquired at SAO and PKD, with channel name, sampling rate, sampling mode, and FIR filter type. C indicates continuous; T triggered; Ac acausal.

orthogonal electric dipoles measures the vector horizontal electric field, E, and three orthogonal magnetic sensors measure the vector magnetic field, B. These reference sites, now referred to as electromagnetic (EM) observatories, are co-located with seismographic sites so that the field data share the same time base, data acquisition, telemetry and archiving system as the seismometer outputs.

The MT observatories are located at Parkfield (PKD1, PKD) 300 km south of the San Francisco Bay Area and Hollister (SAO), halfway between San Francisco and Parkfield (Figure 3.1). In 1995, initial sites were established at PKD1 and SAO, separated by a distance of 150 km, and equipped with three induction coils and two 100 m electric dipoles. PKD1 was established as a temporary seismic site, and when a permanent site (PKD) was found, a third MT observatory was installed in 1999 with three induction coils, two 100 m electric dipoles, and two 200 m electric dipoles. PKD and PKD1 ran in parallel for one month in 1999, and then the MT observatory at PKD1 was closed.

Data at the MT sites are fed to Quanterra dataloggers, shared with the collocated BDSN stations, synchronized in time by GPS and sent to the BSL via dedicated communication links.

3. 2004-2005 Activities

3.1 USArray

The BSL concluded an agreement with IRIS during 2003-2004 to contribute 19 stations of the BDSN to USArray while the experiment is deployed in California. This includes 17 existing stations: CMB, CVS, FARB, HOPS, HUMO, JCC, JRSC, KCC, MNRC, MOD, ORV, PACP, PKD, POTR, WDC, WENL, and YBH as well as two new sites: GASB and MCCM.

The 19 BDSN sites provide USArray with a running start in northern California. In June of 2004, the BSL set up the software necessary to exchange data with USArray and made modifications to the dataloggers to change the

BDSN PSD Low Noise Synopsis (2004–2005)

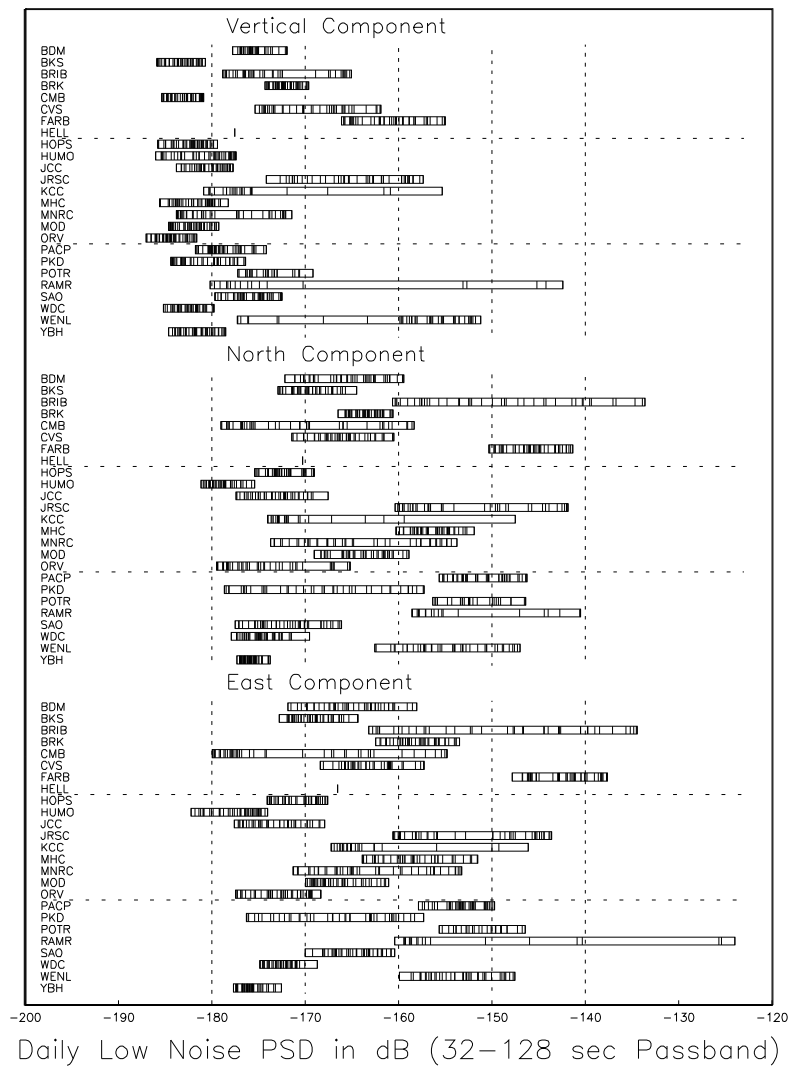


Figure 3.3: PSD noise analysis for BDSN stations, by channel, in the period range from 32-128 sec from 7/1/2004-6/30/2005. BRIB (situation in a shallow vault that is prone to tilting) and FARB (located on the Farallon Islands) stand out as sites with high noise levels. HUMO (located in an abandoned mine) stands out as an exceptionally quiet site.

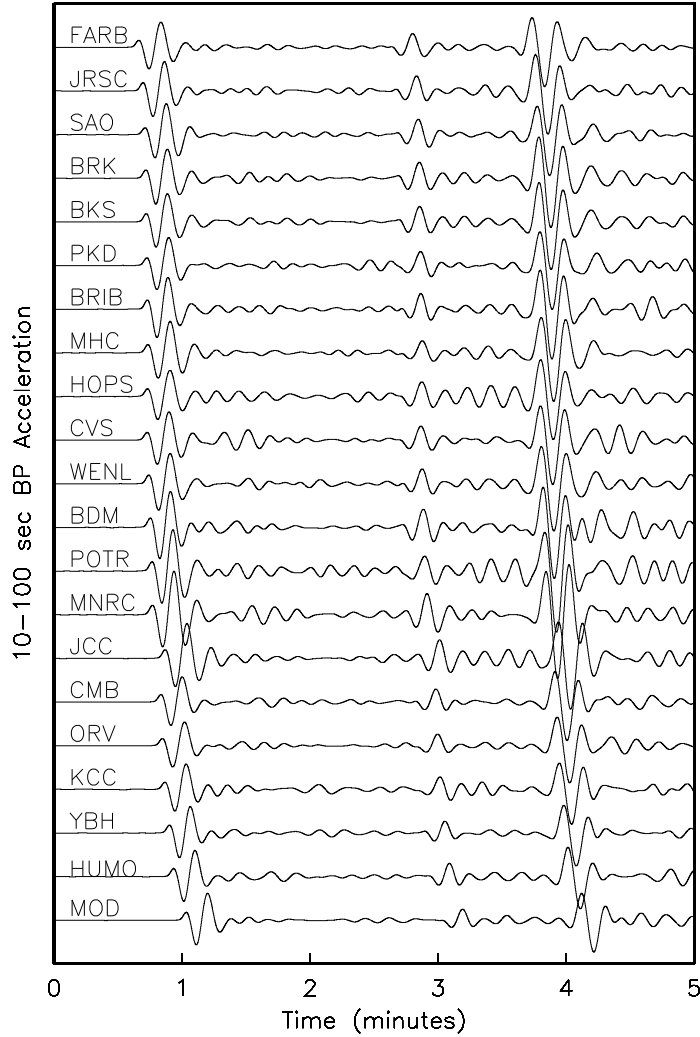


Figure 3.4: BDSN broadband vertical-component waveforms for a M_w 7.1 deep focus earthquake (565 km) which occurred in the Fiji Region on July 15, 2004. The waveforms were deconvolved to absolute ground acceleration, 10-100 second band pass filtered, and plotted in order of increasing distance from FARB at 76.0 degrees to MOD at 80.1 degrees. Shown are the P, pP, and sP body wave phases. Note that the body waves are highly similar across the BK network and that most noticeable differences are in the coda detail and the absolute amplitudes. This provides confirmation that the station transfer function and polarities are correct. The stations MNRC and POTR especially stand out in that their amplitudes are significantly larger than is observed at the other BDSN stations, owing primarily to their siting in the proximity of thick alluvial deposits which amplify the ground motions.

Code	Net	Latitude	Longitude	Elev (m)	Over (m)	Date	Location
BDM	BK	37.9540	-121.8655	219.8	34.7	1998/11 -	Black Diamond Mines, Antioch
BKS	BK	37.8762	-122.2356	243.9	25.6	1988/01 -	Byerly Vault, Berkeley
BRIB	BK	37.9189	-122.1518	219.7	2.5	1995/06 -	Briones Reservation, Orinda
BRK	BK	37.8735	-122.2610	49.4	2.7	1994/03 -	Haviland Hall, Berkeley
CMB	BK	38.0346	-120.3865	697.0	2	1986/10 -	Columbia College, Columbia
CVS	BK	38.3453	-122.4584	295.1	23.2	1997/10 -	Carmenet Vineyard, Sonoma
FARB	BK	37.6978	-123.0011	-18.5	0	1997/03 -	Farallon Island
GASB	BK	39.6547	-122.716	1354.8	2	2004/06 -	Alder Springs
HOPS	BK	38.9935	-123.0723	299.1	3	1994/10 -	Hopland Field Stat., Hopland
HUMO	BK	42.6071	-122.9567	554.9	50	2002/06 -	Hull Mountain, Oregon
JCC	BK	40.8175	-124.0296	27.2	0	2001/04 -	Jacoby Creek
JRSC	BK	37.4037	-122.2387	70.5	0	1994/07 -	Jasper Ridge, Stanford
KCC	BK	37.3236	-119.3187	888.1	87.3	1995/11 -	Kaiser Creek
MCCM	BK	38.1448	237.120	-7.7	2	2005/09 -	Marconi Conference Center, Marshall
MHC	BK	37.3416	-121.6426	1250.4	0	1987/10 -	Lick Obs., Mt. Hamilton
MNRC	BK	38.8787	-122.4428	704.8	3	2003/06 -	McLaughlin Mine, Lower Lake
MOBB	BK	36.6907	-122.1660	-1036.5	1	2002/04 -	Monterey Bay
MOD	BK	41.9025	-120.3029	1554.5	5	1999/10 -	Modoc Plateau
ORV	BK	39.5545	-121.5004	334.7	0	1992/07 -	Oroville
PACP	BK	37.0080	-121.2870	844	0	2003/06 -	Pacheco Peak
PKD	BK	35.9452	-120.5416	583.0	3	1996/08 -	Bear Valley Ranch, Parkfield
POTR	BK	38.2026	-121.9353	20.0	6.5	1998/02 -	Potrero Hill, Fairfield (closed 02/2005)
RFSB	BK	37.9161	-122.3361	-26.7	0	2001/02 -	RFS, Richmond
SAO	BK	36.7640	-121.4472	317.2	3	1988/01 -	San Andreas Obs., Hollister
SCCB	BK	37.2874	-121.8642	98	0	2000/04 -	SCC Comm., Santa Clara
WDC	BK	40.5799	-122.5411	268.3	75	1992/07 -	Whiskeytown
WENL	BK	37.6221	-121.7570	138.9	30.3	1997/06 -	Wente Vineyards, Livermore
YBH	BK	41.7320	-122.7104	1059.7	60.4	1993/07 -	Yreka Blue Horn Mine, Yreka

Table 3.1: Currently operating stations of the Berkeley Digital Seismic Network. Each BDSN station is listed with its station code, network id, location, operational dates, and site description. The latitude and longitude (in degrees) are given in the WGS84 reference frame and the elevation (in meters) is relative to the WGS84 reference ellipsoid. The elevation is either the elevation of the pier (for stations sited on the surface or in mining drifts) or the elevation of the well head (for stations sited in boreholes). The overburden is given in meters. The date indicates either the upgrade or installation time.

BH sampling rate from 20 Hz to 40 Hz. In this second year of USArray, the BDSN has continued to use the 40 Hz sampling rate for the BH channels.

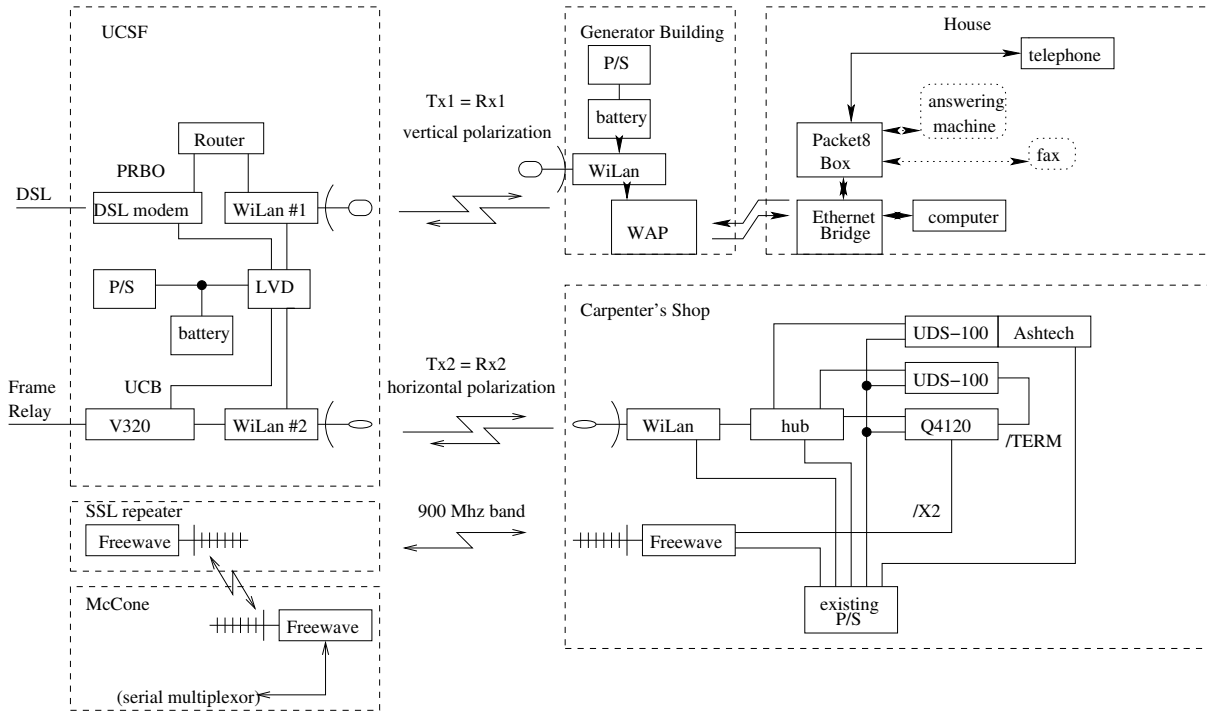
In addition, the BSL is collaborating with USArray to identify other sites that may be suitable to become BDSN stations. During the past year, BSL staff have been working to identify 8 potential sites for USArray/BDSN instrumentation, many at UC reserves and field stations (shown in Figure 3.1).

In the past year, BSL staff have worked with USArray to establish several new sites in northern and central California, including sites at Sutter Buttes, Hat Creek Radio Observatory, Eagle Lake Biological Field Station, Kirkwood Ski Area, Ben Lomond Conservation Camp, and at the summer home of a BSL staff member (P. Hellweg) in the Sierra Nevada foothills. All these sites have been installed by USArray and data from several of them are

being sent directly to the BSL as well as to the Array Network Facility. The BSL is currently evaluating the performance of these stations to determine which sites should be continued after USArray moves on across the country. In particular, noise comparisons are being conducted in different frequency bands for all BDSN and USArray stations in northern California (see Chapter 9 for further details).

3.2 Station Maintenance

Given the remoteness of the off-campus stations, BDSN data acquisition equipment and systems have been designed, configured, and installed for both cost effectiveness and reliability. As a result, the need for regular station visits has been reduced. Most station visits are necessitated by some catastrophic failure. The 2004-2005 fiscal year was no exception.



UNIVERSITY OF CALIFORNIA – BERKELEY
SEISMOGRAPH STATION
 PHONE (510) 642-3976
 FARB BDSN Telemetry, and USFWS VoIP Telephone System

2004/12/20	"farb_telemetry.fig"
------------	----------------------

Figure 3.5: Schematic of the communication collaboration between the BSL, UCSF, Point Reyes Bird Observatory, and US Fish and Wildlife Service.

Code	Broadband	Strong-motion	datalogger	T/B	GPS	Other	Telemetry	Dial-up
BDM	STS-2	FBA-23	Q4120	X			FR	
BKS	STS-1	FBA-23	Q980	X		Baseplates	FR	X
BRIB	CMG-3T	FBA-23	Q980		X	Vol. Strain	FR	X
BRK	STS-2	FBA-23	Q680				POTS	
CMB	STS-1	FBA-23	Q980	X	X	Baseplates	FR	X
CVS	STS-2	FBA-23	Q4120	X			FR	
FARB	CMG-3T	FBA-23	Q4120	X	X		R-FR/R	
GASB	STS-2	FBA-ES-T	Q4120	X			R-FR	
HOPS	STS-1	FBA-23	Q980	X	X	Baseplates	FR	X
HUMO	STS-2	FBA-ES-T	Q4120	X			VSAT	X
JCC	STS-2	FBA-23	Q980	X			FR	X
JRSC	STS-2	FBA-23	Q680				FR	X
KCC	STS-1	FBA-23	Q980	X		Baseplates	R-Mi-FR	X
MCCM	STS-2	FBA-ES-T	Q4120				VSAT	
MHC	STS-1	FBA-23	Q980	X	X		FR	X
MNRC	STS-2	FBA-ES-T	Q4120	X			None	X
MOBB	CMG-1T		GEOSense			Current meter, DPG	None	
MOD	STS-1	FBA-ES-T	Q980	X	X	Baseplates	VSAT	X
ORV	STS-1	FBA-23	Q980	X	X	Baseplates	FR	X
PACP	STS-2	FBA-ES-T	Q4120	X			Mi/FR	
PKD	STS-2	FBA-23	Q980	X	X	EM	R-FR	X
POTR	STS-2	FBA-ES-T	Q4120	X	X		FR	X
RFSB		FBA-ES-T	Q730				FR	
SAO	STS-1	FBA-23	Q980	X	X	Baseplates, EM	FR	X
SCCB		FBA-ES-T	Q730		X		FR	
WDC	STS-2	FBA-23	Q980	X			FR	X
WENL	STS-2	FBA-23	Q4120	X			FR	
YBH	STS-1 & STS-2	FBA-23	Q980	X	X	Baseplates	FR	X

Table 3.2: Instrumentation of the BDSN as of 06/30/2005. Every BDSN station consists of collocated broadband and strong-motion sensors, with the exception of PKD1, RFSB and SCCB which are strong-motion only, with a 24-bit Quanterra datalogger and GPS timing. Additional columns indicate the installation of a thermometer/barometer package (T/B), collocated GPS receiver as part of the BARD network (GPS), and additional equipment (Other) such as warless baseplates or electromagnetic sensors (EM). The obs station MOBB also has a current meter and differential pressure gauge (DPG). The main and alternate telemetry paths are summarized for each station. FR - frame relay circuit, R - radio, Mi - microwave, POTS - plain old telephone line, VSAT - USGS ANSS satellite link, None - no telemetry at this time. An entry like R-Mi-FR indicates multiple telemetry links, in this case, radio to microwave to frame relay.

NSN VSAT modifications

The BSL cooperates with the USGS ANSS on the following sites in northern California: SAO, CMB, WDC, MOD, and HUMO. At each of these sites, the ANSS (previously NSN) has provided a VSAT to support a communications link. The MOD and HUMO sites are sufficiently remote that the VSAT is the only communications link available.

In 2003, the US NSN began to replace the older VSAT systems and, in February 2004, the USGS turned off the original satellite system. Prior to the end of February, BSL staff traveled to HUMO and MOD to work with USGS contractors on the installation of the new VSAT

system. Fortunately, these two installations were completed just before the older system was turned off, avoiding the loss of communications.

Unfortunately, we have not completed the VSAT modifications at the three remaining sites. Hopefully this task will be completed during FY05/06, as the VSATs provide an important secondary communication link at these stations. At this time, data from the non-upgraded stations is provided to NEIC via the BSL data acquisition.

Problems with accelerometers

The 2003 San Simeon earthquake highlighted problems with the FBA-23s and Episensors at several BDSN sites.

JRSC (FBA-23), MHC (FBA-23), WENL (FBA-23), and RFSB (Episensor) showed problems with the San Simeon recording (primarily poor response to ground motions). Over the past year, we have continued our program to replace the older FBA-23s with Episensors as well as address other noise-related issues. Seven stations (FARB, JCC, MHC, WENL, YBH, HUMO) have been upgraded and a new one (GASB) installed.

MNRC telemetry

The McLaughlin Mine property in Lake and Yolo counties is on property owned and formerly operated by Homestake Mining Company as a surface gold mine. The site is now managed as a UC Davis reserve.

Due to the remoteness of the site, digital telephone data circuits are not available. During 2003-2004, BSL engineers permitted, designed, prefabricated and installed a two-hop wireless radio bridge to a State of California radio and microwave facility at Mt Saint Helena, twenty five kilometers away. From the Mt Saint Helena site, data are relayed to the California Department of Forestry and Fire Protection (CDF) command center in the Napa Valley. At that point, a frame-relay circuit provides communications to UC Berkeley.

During early 2005, the State of California began installation of upgrades to the radio facilities atop Mt Saint Helena site. These upgrades are to include a new antenna tower. The State of California requested that BSL relocate and remount our directional antennas at Mt Saint Helena site. Concurrent with remounting the antennas, BSL engineers installed battery back-up for the radio system.

PKD telemetry

At the time the station PKD was installed in 1996, continuous telemetry from the site was achieved by interconnection of a digital spread spectrum radio (900 MHz) with the frame-relay circuit at Carr Hill. Radios in this spectrum have the advantage of not requiring federal licensing or permits and the BSL installation in 1996 was the first use of such equipment in Parkfield. Since the initial installation, at least two other investigating groups in Parkfield have installed similar radios, ultimately causing interference and a reduction in data bandwidth.

In December of 2003, BSL and USGS engineers went to Parkfield to coordinate frequencies, align antennas, and replace and move radio equipment in order to minimize future interference. Over two days, the telemetry path from the PKD vault to the Carr hill site was redirected to a repeater site operated by UCSD. RF signal levels were tested and confirmed. By January 2004, however, the signal levels on the new path had faded as much as 20 db, apparently due to the increased water absorption by vegetation. During a January trip by BSL engineers, antennas were once again redirecting the data path directly

to Carr Hill. Unfortunately, that solution was short lived as the signal level fell again and faded more than 10 db in the following two weeks. During a third trip, BSL engineers installed a solar-powered radio repeater, which operated satisfactorily through the dry summer months of 2004.

For a more robust solution, the BSL sought and obtained permission from a private landowner to install a solar-powered repeater at a different site. In December of 2004, engineers from BSL successfully installed the new repeater. This installation worked reliably through both winter and summer months.

FARB refurbishment

The Farallon Islands are located approximately 30 kilometers west of the Golden Gate, on the Pacific plate. The BSL has operated instrumentation on Southeast Farallon Island (FARB) since January of 1994. Broadband seismic instruments were initially deployed in March of 1997. The unique location of FARB makes it a valued BDSN station, although it is both difficult to access and subject to a highly corrosive environment.

As part of the BSL collaboration with USArray, the BSL decided to rebuild the FARB station, including datalogger, seismometers, radios, cables and power supplies. In early summer of 2004, the BSL gained permission from the US Department of Fish and Wildlife (USFW) for a site visit. The USFW arranged transportation to and from the Island for BSL engineers via US Coast Guard rescue boat and helicopter. In August of 2004, BSL engineers went to the island and successfully removed the old instrumentation and replaced it with new equipment. Testing was also performed for upgrade of the radio telemetry described below. Of particular note, the Guralp CMG-3T was replaced with an STS-2.

FARB/PTRB telemetry

During the past year, the BSL received notice that the government-owned radio facility atop Mt Tamalpais in Marin County would be privatized. At the Mt Tamalpais facility, the BSL operated digital radio telemetry to the station FARB located on the Farallon Islands west of the Golden Gate, and PTRB (the BARD GPS) site at Point Reyes.

Access to the Mt Tamalpais radio facility began in the early 1990's. Initially, digital data from the station ARC and later HOPS was telemetered via the USGS-operated microwave system there. In March of 1997, the BSL worked with the USGS to establish radio connections to FARB and later PTRB from Mt Tamalpais, with a frame-relay circuit back to UC Berkeley.

Concurrently, in November of 2004, the managing biologist from USFW contacted the BSL's engineers for assistance with the radio telephone at the Farallon's. The

license to operate their 30-year-old equipment was expiring and, worse, their mainland repeater site at a firehouse on the Marin county coast was scheduled to be removed. Without the radio phone, there would be no voice communications to the islands.

BSL engineers began a search for a site on the mainland which could accommodate radio telemetry from both the seismic instrumentation and the new voice circuit. The new location would need line-of-sight to the Farallon's and have existing phone services. With only a few months to identify and permit the new location, an obvious choice was the University of California at San Francisco (UCSF). After contacting UCSF physical plant, a rooftop location was found and an internal University agreement put in place.

The BSL engineers designed, built, and tested communications systems for both the BSL and USFW. Two separate radio links were installed. The BSL radio link is connected to a frame-relay circuit; the USFW radio link is connected to a digital subscriber line (DSL). The BSL engineers used wireless Ethernet bridge radios to effectively extend the DSL service to the Farallons, providing high-quality voice and Internet connectivity. Biologists on the island can now transfer files and images, send email and faxes, access the Internet, and make simple telephone calls.

The collaborative efforts and solution between BSL, UCSF, Point Reyes Bird Observatory, and the US Fish and Wildlife Service are shown schematically in Figure 3.5

KCC Clock Failure

The station at Kaiser Creek (KCC) was installed in January of 1996. The station is located in a hydropower facility operated by Edison International within the Sierra Nevada range. Due to the remoteness of the site, access to the area is limited after the first snowfall.

In January of 2005, the internal clock of the datalogger began to exhibit large daily drifts indicative of hardware failure. The clock voltage controlled oscillator (VCO) was reset over the remote telemetry link several times in an attempt to control the clock drift. In late January the system became completely unstable. Coincidentally, snowfall in the area was at or near the highest levels recorded over the past 100 years making a site visit impossible.

In early June 2005, BSL engineers were finally able to drive to the site and replace the entire datalogger. The newly installed instrument was complete with hardware and software necessary to upgrade the telemetry. With Edison's assistance, upgrade of data telemetry from the site is planned for late 2005.

Upgrade and Addition of Equipment at YBH

The BSL Station YBH was initially installed in July of 1993. Since that time, instruments and telemetry have been reconfigured several times. In 1996 a geodetic GPS receiver was added to the site. In 2002 an second seismometer (STS-2) was installed and added to the existing datalogger on behalf of CTBTO.

During November of 2004, CTBTO requested a site visit to install UPS power on their auxiliary instrumentation and telemetry (VSAT) at the site. BSL engineers took this opportunity to replace the strong motion FBA-23 with a newer model Episensor, as well as replacement of the telemetry FRAD.

Stations Closures

POTR

The BSL station at Portero Hills (POTR) was installed in December of 1998. The site is located in the Sacramento River Delta in one of the few areas of competent rock (sandstone). The instruments were placed in a 1960's-vintage missile silo that was being used by a contractor to the US Air Force.

In late 2004, BSL received word that the contractor would no longer be leasing the silo from the Air Force and could thus no longer grant BSL permission to operate there. Direct discussions between BSL and the US Army Corps of Engineers on behalf of the US Air Force were not fruitful. In February of 2005, power was cut to the site and the instruments went dead. BSL engineers removed all instrumentation.

Discussions between BSL and the Air Force contract have continued toward the goal of finding a replacement site on the adjacent property. In the summer of 2005, a background noise test was performed at one such site. That site was found noisier than the High Noise Model and was not pursued as a replacement for POTR.

3.3 New Installations

Alder Springs

The Alder Springs (GASB) site located approximately 35 kilometers west of the central valley town of Willows. Local geology is mostly serpentine and Franciscan. Previously, a short period observatory has been operated at the Alder Springs site by the California Department of Water Resources. The GASB site is being developed in cooperation with the CREST (Consolidated Reporting of EarthquakeS and Tsunamis) network.

In June 2004, construction began on a steel and concrete seismographic vault similar to those at JCC, PKD, HOPS, and MNRC. On-site excavation was contracted. Inmates from the CDF Valley View Conservation Camp provided labor for the concrete pour and back filling of the excavation. BSL engineers built the forms and framing for the concrete, as well as all electrical wiring at the

site. The permit for this site was provided by the US Forest Service, Mendocino National Forest.

Due to reduced staff and medical problems, physical work at the site was stopped in September 2004. In early January of 2005, a frame-relay circuit was installed at the CDF camp and local loop connectivity to the vault was achieved via wireless Ethernet bridge (radio). Installation of the seismic instruments at GASB was completed in September 2005.

Marconi Conference Center

In 2003-2004, we permitted a site at the Marconi Conference Center, near Marshall, CA. The conference center is operated by the State of California. This site is planned in collaboration with the USGS and will form part of the ANSS backbone network.

In January of 2005, BSL contractors and engineers broke ground on construction and development of a steel and concrete seismographic vault similar to those at JCC, PKD, HOPS, and MNRC. Construction activities at the vault were completed in April. The site is awaiting connection to power, scheduled for the fall of 2005.

Telemetry at the Marconi will primarily be achieved via an USGS ANSS VSAT. The BSL has also initiated planning of radio telemetry. Radio telemetry will require additional site permits from California State Parks. This permitting process is on-going and may take up to six months.

3.4 MOBB: An Ocean Floor Broadband Station

The Monterey Ocean Bottom Broadband observatory (MOBB) is a collaborative project between the Monterey Bay Aquarium Research Institute (MBARI) and the BSL. Supported by funds from the Packard Foundation to MBARI, NSF/OCE funds and UC Berkeley funds to BSL, its goal has been to install and operate a long-term seafloor broadband station as a first step towards extending the on-shore broadband seismic network in northern California, to the seaside of the North-America/Pacific plate boundary, providing better azimuthal coverage for regional earthquake and structure studies. It also serves the important goal of evaluating background noise in near-shore buried ocean floor seismic systems, such as may be installed as part of temporary deployments of “leap-frogging” arrays (e.g. Ocean Mantle Dynamics Workshop, September 2002).

BSL staff put significant effort in the development of procedures to minimize instrumental noise caused by air circulation inside the seismometer package casing (see 2001-2002 and 2002-2003 BSL Annual Reports). These procedures were later applied to the preparation of 3 similar packages destined for installation on the Juan de Fuca plate in the framework of University of Washington’s Keck project.

This project follows the 1997 MOISE experiment, in which a three component broadband system was deployed for a period of 3 months, 40 km off shore in Monterey Bay, with the help of MBARI’s “Point Lobos” ship and ROV “Ventana” (Figure 3.7). MOISE was a cooperative program sponsored by MBARI, UC Berkeley and the INSU, Paris, France (*Stakes et al.*, 1998; *Romanowicz et al.*, 1999; *Stutzmann et al.*, 2001). During the MOISE experiment, valuable experience was gained on the technological aspects of such deployments, which contributed to the success of the present MOBB installation.

The successful MOBB deployment took place April 9-11, 2002 and the station is currently recording data autonomously (e.g. *Romanowicz et al.*, 2003). It comprises a 3 component very broadband CMG-1T seismometer system, a differential pressure gauge (DPG, *Cox et al.*, 1984) and a current meter. Data from the DPG are acquired with a sampling rate of 1 sps, and are crucial for the development and implementation of a posteriori noise deconvolution procedures to help counteract the large contribution of infragravity wave noise in the period range 20-200 sec. Figure 3.6 shows preliminary results of removing the infragravity noise from the seismic channel by using a simple linear regression in the time domain (*Zuern and Widmer*, 1995). We are also developing a procedure in frequency domain that will routinely remove coherent noise derived from pressure measurements, following the approach described in *Crawford and Webb* (2000). Removal of infragravity noise from the MOBB seismic channel will make station MOBB an important addition to the BDSN land stations for use in studies that utilize high quality long-period seismic data as well as provide directions for data processing from the future ocean bottom broadband seismic stations.

Fifteen “dives” involving the MBARI ship “Point Lobos” and ROV “Ventana” have so far taken place to exchange dataloggers and battery packages, the last one on June 16, 2005. In February 2004, the N/S component seismometer failed. It was temporarily replaced, from 05/19/04 to 07/09/04 by one of the Keck seismometer packages which was conveniently available at that time. The original seismometer was sent back to Guralp Inc. for repair and successfully reinstalled on 07/09/04.

The data collection from the broadband seismic system is fairly complete. However, there have been recurring DPG sensor as well as DPG data storage problems in the first two years of the MOBB operation. Well recorded DPG data are available since 03/18/2004.

With input from BSL staff, MBARI engineers are currently working on hardware and software developments needed to connect the MOBB sensors to the MARS (Monterey Accelerated Research System; <http://www.mbari.org/mars/>) cable (Figure 3.7). This will provide access to real-time, continuous seismic data from MOBB to be merged with the rest of the northern California

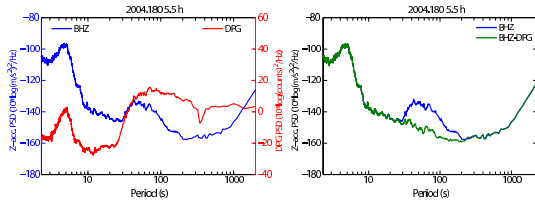


Figure 3.6: Left: Comparison of the power spectral density (PSD) calculated for a 5.5 hour period without earthquakes for the vertical acceleration (blue) and DPG signal (red). The DPG signal has not been corrected for the instrument response. Increased noise level for periods between 30 and 200 seconds that is due to infragravity waves is observed in both datasets. Right: Vertical acceleration PSD before (blue) and after (green) correction to remove the noise due to infragravity waves from the seismic channel.

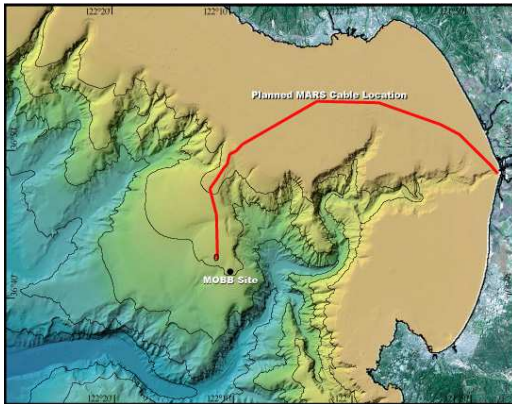


Figure 3.7: Location of the MOBB station in Monterey Bay, California, against seafloor and land topography. The projected path of the MARS cable is indicated by the solid line.

real-time seismic system.

4. Acknowledgements

Under Barbara Romanowicz's general supervision, Lind Gee and Doug Neuhauser oversee the BDSN data acquisition operations and Bill Karavas is head of the engineering team. John Friday, Dave Rapkin, and Bob Uhrhammer contribute to the operation of the BDSN. Sierra Boyd has been responsible for the operation of the EM observatories. Bill Karavas, Bob Uhrhammer, and Lind Gee contributed to the preparation of this chapter.

The California Governor's Office of Emergency Services provided funding toward the development of sites MCCM and GASB as part of the CISN. The Incorporated

Research Institutions in Seismology provided matching funds for the installation of MCCM. The CREST project provided a datalogger for GASB.

MOBB is a collaboration between the BSL and MBARI, involving Barbara Romanowicz, Bob Uhrhammer, Doug Neuhauser and David Dolenc from the BSL and Debra Stakes and Paul McGill from MBARI. The MBARI team also includes Steve Etchemendy (Director of Marine Operations), Jon Erickson, John Ferreira, Tony Ramirez and Craig Dawe. The MOBB effort at the BSL is supported by funds from NSF/OCE and UC Berkeley. The MOBB seismometer package was funded by NSF/OCE grant #9911392.

5. References

- Cox, C., T. Deaton and S. Webb, A deep-sea differential pressure gauge, *J. Atm. Ocean. Tech.*, 1, 237-245, 1984.
- Crawford W. C., and S. C. Webb, Identifying and removing tilt noise from low-frequency (<0.1 Hz) seafloor vertical seismic data, *Bull. Seis. Soc. Am.*, 90, 952-963, 2000.
- Murdock, J., and C. Hutt, A new event detector designed for the Seismic Research Observatories, *USGS Open-File-Report 83-0785*, 39 pp., 1983.
- Romanowicz, B., D. Stakes, J. P. Montagner, P. Tarits, R. Uhrhammer. M. Begnaud, E. Stutzmann, M. Pasyanos, J.F. Karczewski, S. Etchemendy, MOISE: A pilot experiment towards long term sea-floor geophysical observatories, *Earth Planets Space*, 50, 927-937, 1999.
- Romanowicz, B., D. Stakes, R. Uhrhammer, P. McGill, D. Neuhauser, T. Ramirez and D. Dolenc, The MOBB experiment: a prototype permanent off-shore ocean bottom broadband station, *EOS Trans. AGU*, Aug 28 issue, 2003.
- Stakes, D., B. Romanowicz, J.P. Montagner, P. Tarits, J.F. Karczewski, S. Etchemendy, D. Neuhauser, P. McGill, J-C. Koenig, J.Savary, M. Begnaud and M. Pasyanos, MOISE: Monterey Bay Ocean Bottom International Seismic Experiment, *EOS Trans. AGU*, 79, 301-309, 1998.
- Stutzmann, E., J.P. Montagner et al., MOISE: a prototype multiparameter ocean-bottom station, *Bull. Seism. Soc. Am.*, 81, 885-902, 2001.
- Wielandt, E., and J. Steim, A digital very broad band seismograph, *Ann. Geophys.*, 4, 227-232, 1986.
- Wielandt, E., and G. Streckeisen, The leaf spring seismometer: design and performance, *Bull. Seis. Soc. Am.*, 72, 2349-2367, 1982.
- Zürn, W., and R. Widmer, On noise reduction in vertical seismic records below 2 mHz using local barometric pressure, *Geophys. Res. Lett.*, 22, 3537-3540, 1995.

Chapter 4

California Integrated Seismic Network

1. Introduction

Advances in technology have made it possible to integrate separate earthquake monitoring networks into a single seismic system as well as to unify earthquake monitoring instrumentation. In California, this effort was first started under the TriNet Project in southern California, where Caltech, the then California Division of Mines and Geology, and the USGS combined their efforts to create a unified seismic system for southern California. With major funding provided by FEMA, OES, and the USGS, the TriNet project provided the opportunity to upgrade and expand the monitoring infrastructure, combining resources in federal, state, and university partnership. More recently, the integration effort was expanded to the entire State in a cooperation between the California Geological Survey, Caltech, UC Berkeley, USGS Menlo Park, and the USGS Pasadena called the California Integrated Seismic Network (CISN).

In the 2000-2001 Annual Report, we described the initial efforts to create this collaboration through the establishment of a memorandum of agreement and the development of the CISN strategic and implementation plans. The CISN is now in its fifth year of collaboration and its fourth year of funding from the California Governor's Office of Emergency Services.

2. CISN Background

2.1 Organization

The core CISN institutions (California Geological Survey, Caltech, UC Berkeley, USGS Menlo Park, and USGS Pasadena) and OES have signed a MOA (included in the 2000-2001 Annual Report) that describes the CISN organizational goals, products, management, and responsibilities of member organizations. To facilitate coordination of activities among institutions, the CISN has formed three management centers:

- Southern California Management Center: Caltech/USGS Pasadena

- Northern California Management Center: UC Berkeley/USGS Menlo Park
- Engineering Strong Motion Data Center: California Geological Survey/USGS National Strong Motion Program

A goal of the CISN is for the Northern and Southern California Management Centers to operate as twin statewide earthquake processing centers while the Engineering Strong Motion Data Center has the responsibility for producing engineering data products and distributing them to the engineering community.

The Steering Committee oversees CISN projects and is comprised of two representatives from each core institution and a representative from OES. The position of chair rotates among the institutions; Woody Savage is the current chair of the Steering Committee.

An external Advisory Committee, representing the interests of structural engineers, seismologists, emergency managers, industry, government, and utilities, has been formed for review and oversight. The Advisory Committee is chaired by Ron Tognazinni, formerly of the LA Department of Water and Power and Stu Nishenko of Pacific Gas and Electric Company serves as the vice-chair. The Advisory Committee last met in October 2004. The agenda from that meeting and resulting report may be accessed through the CISN Web site (<http://www.cisn.org/advisory>). The next meeting is planned for October 2005.

The Steering Committee has formed other committees, including a Program Management Group to address planning and coordination, a Strong Motion Working Group to focus on issues related to strong-motion data, and a Standards Committee to resolve technical design and implementation issues.

In addition to the core members, several organizations contribute data that enhances the capabilities of the CISN. Contributing members of the CISN include: University of California, Santa Barbara; University of California, San Diego; University of Nevada, Reno; University of Washington; California Department of Water

Resources; Lawrence Livermore National Lab; and Pacific Gas and Electric.

2.2 CISN and ANSS

The USGS Advanced National Seismic System (ANSS) is being developed along a regionalized model. Eight regions have been organized, with the CISN representing California. David Oppenheimer of the USGS serves as the CISN representative to the ANSS National Implementation Committee (NIC).

Over the last 6 years, ANSS funding in California has been directed primarily to the USGS Menlo Park to expand the strong-motion instrumentation in the San Francisco Bay Area. As a result, more than 100 sites have been installed or upgraded, significantly improving the data available for ShakeMaps.

As the ANSS moves forward, committees and working groups are being established to address issues of interest. Lind Gee has served on the Technical Integration Committee (TIC), which oversees technical issues for the ANSS. Other BSL faculty and staff have been involved in several TIC working groups, including Doug Dreger, Pete Lombard, Doug Neuhauser, Bob Uhrhammer, and Stephane Zuzlewski.

2.3 CISN and OES

The California Governor's Office of Emergency Services has had a long-term interest in coordinated earthquake monitoring. The historical separation between northern and southern California and between strong-motion and weak-motion networks resulted in a complicated situation for earthquake response.

OES has been an advocate of increased coordination and collaboration in California earthquake monitoring and encouraged the development of the CISN Strategic and Implementation Plans. In FY01/02, Governor Gray Davis requested support for the CISN, to be administered through OES. Funding for the California Geological Survey, Caltech and UC Berkeley was made available in spring 2002, officially launching the statewide coordination efforts.

Following the first year of funding, OES support led to the establishment of 3-year contracts to the UC Berkeley, Caltech, and the California Geological Survey for CISN activities. 2004-2005 marked the last year of the multi-year award, and the CISN partners submitted proposals to OES for new 3-year contracts to begin on July 1, 2005.

3. 2004-2005 Activities

The CISN funding from OES facilitated a number of activities at the BSL during the past year.

3.1 Parkfield Earthquake

In late 2003, the CISN experienced the first significant test of its capabilities with the M6.5 San Simeon earthquake. A brief 9 months later, an M6.0 earthquake occurred along the San Andreas fault in Parkfield, California.

Overall, the CISN performance for the distribution of information following the San Simeon and Parkfield earthquakes were good. Automatic information about the location was available within 30 seconds and a final location with a reliable magnitude was released about 4.5 minutes after the event. The first ShakeMap was issued 8 minutes after origin time and distributed to OES and multiple Web servers. During the next 24 hours, additional information about aftershock probabilities, the fault rupture, and seismological/engineering aspects of interest were made available by the CISN.

Unlike San Simeon, the Parkfield earthquake occurred during a weekday in a densely instrumented area of the Northern California network (although much of that instrumentation was analog). Like San Simeon, however, the earthquake illustrated some issues with CISN operations. For example, some difficulties were encountered with rarely exercised software, some clients were unhappy with the number of earthquake notifications received, firewalls (both within the CISN and with CISN client) continue to be problematic, and some aspects of the human response showed a lack of familiarity with appropriate procedures.

More information about the Parkfield earthquake is available in Chapter 13 in research contributions.

3.2 San Simeon HGMP funds

Both the San Simeon and Parkfield earthquakes highlighted the sparseness of instrumentation in central California, outside of the Bay Area. In both cases, the initial ShakeMaps were not well constrained, due to the lack of digital instrumentation with real-time communications. One major difference between these two events is that the Parkfield area was very densely instrumented, particularly with accelerometers deployed by the California Geological Survey. However, since these instruments were primarily analog, the data were not available for several days after the event.

As a result of the San Simeon earthquake, FEMA made funds available to OES. The BSL, Caltech, and CGS submitted a joint application for Hazard Mitigation Grant Program funds, which was funded in Spring of 2005. The funds received by BSL will be expended to add one broadband station in the vicinity of the San Simeon event and to relocate the data acquisition and processing systems from McCone Hall to 2195 Hearst (described in Chapter 9).

3.3 Expanded Instrumentation

In 2001-2002, the BSL purchased equipment for 5 BDSN stations, including STS-2 seismometers, Episen-sors, and Q4120 data loggers, and initiated efforts to identify potential sites, considering such factors as the current distribution of stations, private versus public property, location of power and telecommunications, and geologic materials. This equipment allowed the BSL to add two broadband stations in 2002-2003 (PACP and MNRC, Figure 3.1).

In the past year, the BSL continued the installation of a site at Alder Springs (GASB), California. This site has been under discussion for a number of years, initially as part of the National Tsunami Hazards Program.

The BSL also initiated the installation of a site near Pt. Reyes, California, at the Marconi Conference Center (MCCM). This site is partially funded by IRIS (part of the permanent component of USArray), USGS, and OES. The site will be completed in the fall 2005, with the installation of power and an ANSS VSAT system.

With the completion of GASB and MCCM, the BSL has installed 4 of the 5 sets of site equipment purchased in the first year of the CISN. The efforts at GASB and MCCM more fully described in Chapter 3.

3.4 Network Operations

As part of the CISN project, the BSL purchased 23 upgrade kits for their Q4120 data loggers with the goal of improving remote diagnostic capabilities. Three different kits were purchased – power board only, calibration board only, and combined power and calibration boards – in order to ensure that every Q4120 has a power board and that every 8-channel Q4120 also has a calibration board. The power boards provide the capability to monitor battery voltage, allowing staff to discriminate between power and telemetry problems remotely. The calibration boards provide the capability to monitor mass position as well as allow remote calibration of the seismic sensors. Both boards also record data logger temperature.

Successful upgrade of the dataloggers requires a site visit to remove the datalogger and bring it back to the lab, installation of the boards, replacement of lattices on the CPU board, construction of new cables to transmit the mass position signals, and redeployment of the datalogger in the field. At this point, 3 upgrades remain although a few sites still require new cables or replacement of the lattices.

3.5 Collaboration with USArray

In late 2003, the CISN concluded a memorandum of agreement with the Incorporated Research Institutions in Seismology (IRIS) covering the duration of the USArray project in California. As a result 19 stations operated by

the BSL and 41 stations operated by Caltech are part of USArray during its California deployment.

Both Caltech and the BSL needed to modify some aspects of their station operation in order to meet the US-Array specifications. In particular, USArray calls for BH data sampling at 40 Hz, rather than the 20 Hz rate that has been standard in California. In the case of the BSL, all surface broadband stations were converted to 40 Hz over June 15-16th, 2004.

Also as part of this collaboration, the BSL has worked with USArray to survey and permit several sites in Northern California.

The collaboration between the BSL and USArray is discussed more fully in Chapters 3 and 9.

3.6 Statewide Communications

One of the major accomplishments in FY01/02 was the design and initial implementation of a CISN communications infrastructure. Doug Neuhauser of the BSL took the lead in investigating options and the CISN partners decided to establish a “ring” of T1 communication links (Figure 4.1) with dual routers at each node.

As described last year, the CISN ring is up and operational. It is being used to transmit seismic waveform data and parametric data, including strong motion parameters, between the management centers and to distribute ShakeMaps to OES. It is also used to support mirroring of the CISN Web server.

During 2003-2004, the CISN performed a test to verify the failover and redundancy capabilities of the CISN ring. The goals of the test were to 1) verify that if a single segment of the CISN ring fails, the backbone routers will detect the outage in a timely fashion and will reroute traffic to all CISN sites around the remaining CISN ring segments, and 2) verify that if a site is completely disconnected from the CISN ring, the backbone routers will detect the outage in a timely fashion and will reroute traffic to/from that site over the backup Internet tunnels between the disconnected site and all other CISN sites.

The test conducted demonstrated that the CISN routers and ring are performing according to design. However, the CISN OES routers do NOT have public Internet connections yet, so they have no Internet tunnel connections. If the CISN T1 circuits were to go down at OES, OES would be completely isolated from the CISN network and all CISN partners. This continues to be an issue of major concern.

During the last year, the BSL began the process to upgrade the Cisco IOS (Internetworking Operating System) installed on the routers, only to discover that additional memory was required in order to support the latest version. The BSL ordered memory for all the routers, sent the needed modules to Caltech, CGS, and USGS Menlo Park, and installed memory on the BSL and OES routers. As of the end of June, the only CGS routers were waiting

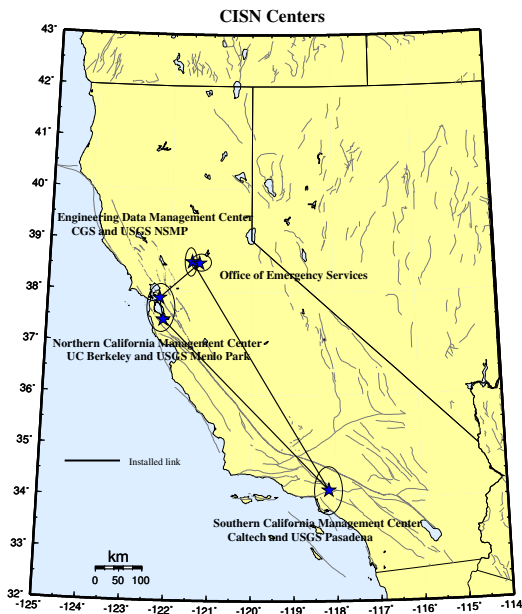


Figure 4.1: Map showing the geographical distribution of the CISN partners and centers. The communications “ring” is shown schematically with installed links (solid lines).

for the upgrade to be completed. When all the memory is installed, then the BSL plans to begin testing the new IOS (which supports ssh and scp), prior to rolling it out on all the routers. Once the new IOS is fully deployed, then CISN will perform another test of the ring.

3.7 Northern California Management Center

As part of their effort within the CISN, the BSL and the USGS Menlo Park have begun to plan for the next generation of the northern California joint notification system. Chapter 10 describes the operations of the existing Management Center and reports on design discussions.

Communications Infrastructure

In order to move ahead with plans for restructuring the northern California earthquake monitoring system, the USGS Menlo Park and BSL have been working to improve their communications infrastructure.

At present, the BSL and the USGS Menlo Park are connected by two dedicated T1 circuits. One circuit is a component of the CISN ring, while the second circuit was installed last year (Figure 4.3) to support the anticipated level of dedicated traffic between Berkeley and Menlo Park above and beyond that associated with the CISN.

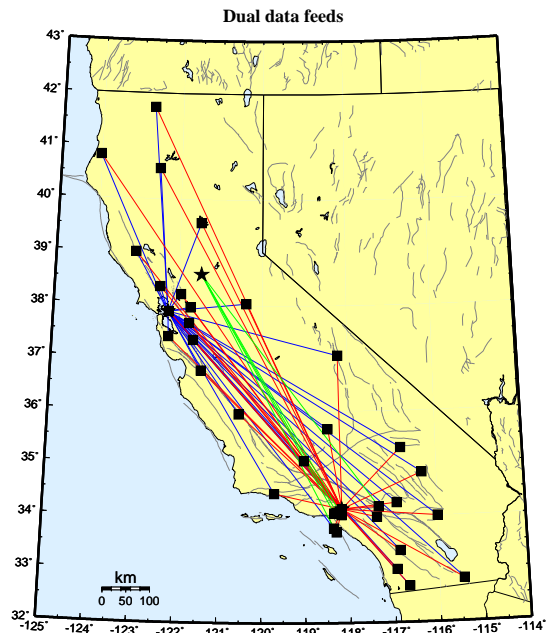


Figure 4.2: Map showing the 30 stations selected to send data directly to the Northern and Southern California processing centers, and the 5 stations that send data directly to the Engineering Data Center and the Southern California processing center.

The installation of the second dedicated T1 between Berkeley and Menlo Park freed up a frame-relay connection deployed by the BSL as part of the CalREN project in mid-1990s. In the past year, the BSL has been reconfiguring the frame-relay circuit to serve as a second data acquisition link. The plan is to distribute the BDSN data acquisition between the two frame-relay T1 circuits, eliminating what had been a single point of failure. A second component of the plan is to establish an additional Permanent Virtual Circuit (PVC) at each BDSN site so that each station has connections to both T1s.

During the past year, the BSL worked with SBC to distribute the acquisition of seismic data between the two T1s and to establish a second PVC at each frame-relay site. This effort has improved the robustness of data acquisition at the BSL by providing redundancy in the incoming circuit.

In the long term, the BSL and USGS Menlo Park hope to have a high-bandwidth microwave or satellite connection in addition to the current land lines. Unfortunately, we have not been able to obtain funding for this additional communication link at this time.

3.8 Statewide Integration

BSL staff are involved in many elements of the statewide integration effort. The Standards Committee continues to define and prioritize projects necessary to

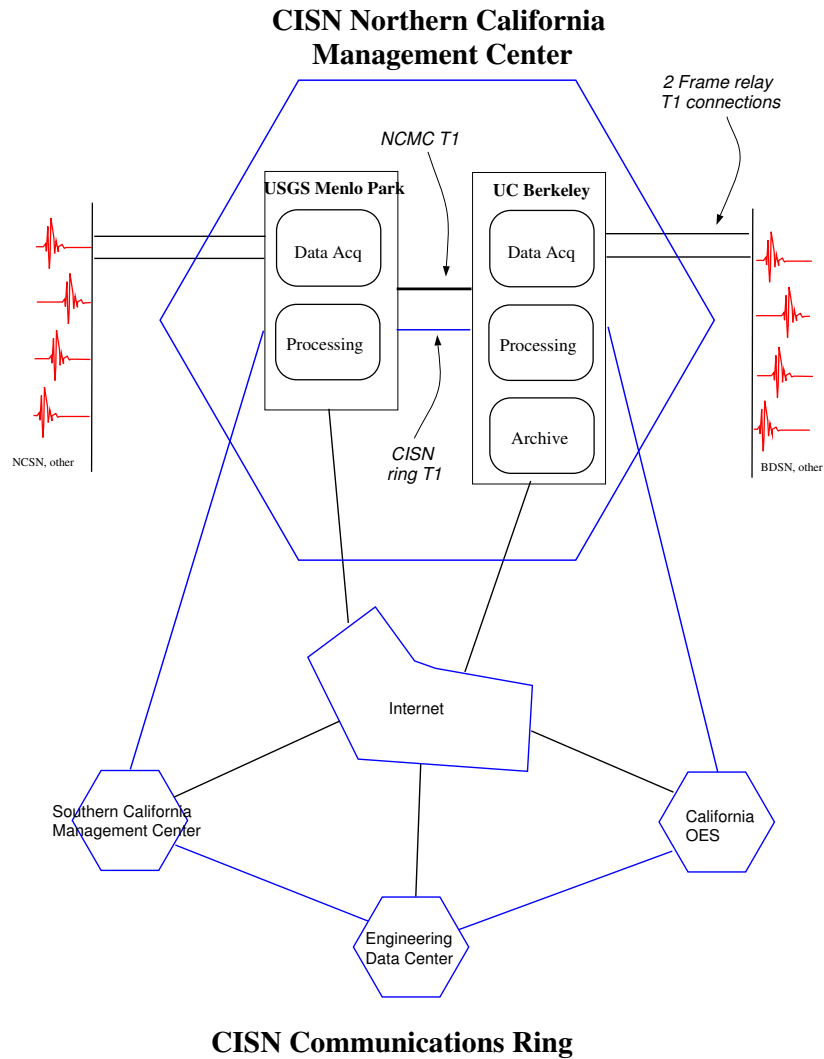


Figure 4.3: Schematic diagram illustrating the connectivity between the real-time processing systems at the USGS Menlo Park and UC Berkeley, forming the northern California Management Center, and with other elements of the CISN.

develop a prototype system and establish working groups to address them (see the minutes from meetings and conference calls at <http://www.cisn.org/standards/meetings.html>).

Dual Station Feeds

One of the major accomplishments in the first few years has been the establishment of “dual station feeds” at 30 stations (15 in northern California and 15 in southern California) (Figure 4.2). To achieve this, the BSL and Caltech both ordered the DLCIs (data link connection

identifier) that allow the 2nd center to establish a PVC to each station using the frame-relay network.

The Northern California Management Center is using data from the Southern California stations to estimate magnitudes on a routine basis. A subset of these stations are being used for the moment tensor inversions, a computation that is more sensitive to the background noise level.

Data Exchange

Pick exchange was initiated between the Northern and Southern California Management Centers in 2001-2002. Although the CISON has developed software to exchange the reduced amplitude timeseries, this aspect of data exchange has been delayed while certain problems in the codes that generate the time series are addressed.

The CISON partners completed the final stage of a system to exchange peak ground motion data this year. Using a common format, the CISON partners are exchanging observations with one another following an event or a trigger. This step increases the robustness of generating products such as ShakeMap, since all CISON partners are now exchanging data directly with one another. It also improves the quality of ShakeMaps on the boundary between northern and southern California, such as the San Simeon earthquake, by allowing all data to be combined in a single map. Finally, it is a necessary step toward the goal of generating statewide ShakeMaps.

Software Calibration & Standardization

The CISON partners are working together on the problem of software calibration, particularly as it pertains to automated earthquake processing. Currently, the software implemented in the Northern and Southern California Management Centers is very different. Initially, the CISON focused on the issue of calibration although the last year has seen an increased focus on standardization.

In 2002-2003, effort was focused on phase pickers (*pick-ew*), the association algorithm (*binder*), the location algorithm (*hypoinverse*), and magnitude estimation (various). Since then, magnitude estimation continues to be a significant area of focus, as well as ShakeMap configuration, metadata exchange, and database standardization.

At this point, the issues of a statewide detection and location system are largely addressed. Configuration files have been standardized and a statewide system has been running in Menlo Park for nearly a year. It performed well during the December 2003 San Simeon sequence and the 2004 Parkfield earthquake.

However, a number of outstanding issues remain to be addressed.

Magnitude: Calibrating magnitude estimates has proven to be more difficult than the CISON originally anticipated. As described last year (in some detail), it appears as if there is a bias between the northern and southern California magnitude estimates, as illustrated by three lines of evidence. First, a comparison of nearly 500 earthquakes over a 20 year period in central California recorded by both networks shows a bias of 0.14 magnitude units, with NC magnitudes higher than SC magnitudes. Second, efforts to invert Wood Anderson amplitudes using a differential approach, a constraint that the BKS and PAS adjustments sum to zero, and fixing the

attenuation relationship to one determined by *Kanamori* (1993), indicates a bias of 0.14. Finally, an independent inversion of a different dataset (absolute approach, a different set of station constraints, and simultaneous inversion for attenuation) suggests a bias of 0.20.

Efforts to understand this issue have been hampered by the lack of a good statewide dataset. In the past year, Bob Uhrhammer has started to clean up the data set by removing outliers and events with a small number of observations and analyze these data. His results examine variations among networks, component, orientation, and processing system as well as station adjustments.

A final component of the magnitude efforts is the designation of a magnitude reporting hierarchy. There is general agreement at the low end and at the high end, but the working group is still reviewing issues related to transition points from one magnitude type to another.

ShakeMap: In addition to the efforts in standardizing earthquake locations and magnitudes, a CISON working group has been addressing issues related to ShakeMaps. At present, ShakeMaps are currently generated on 5 systems within the CISON. 2 systems in Pasadena generate “SoCal” Shakemaps; 2 systems in the Bay area generate “NoCal” Shakemaps; and 1 system in Sacramento generates ShakeMaps for all of California. The Sacramento system uses QDDS to provide the authoritative event information for northern and southern California.

Over last 18 months, the Working Group has addressed a number of issues in the standardization of ShakeMap. Initially focusing on the look and feel of the maps (topography, geology, faults, road, lake outlines, cities, and fonts), the Working Group has just started to review a comprehensive compilation of the differences in configuration among the 3 implementations. The remaining differences between the centers range from the small (URL used in the “addon” message) to the significant (use of regressions, linear versus log amplitude weighting). This effort will move the CISON forward toward having fully standardized ShakeMaps.

The lack of stations in the near source region of the 2003 San Simeon earthquake raised a number of issues related to ShakeMap and how to measure the quality of the product as well as quantify the uncertainty. Over the past 6 months, a subset of the Working Group has been working on this issue, based on the work of *Hok and Wald* (2003). One of the first projects has been to make a map to illustrate current CISON capabilities, based on the existing station distribution. The next step is to look at calculating uncertainty for some example earthquakes and comparing the uncertainty estimates with different realizations of the ShakeMap produced by using various subsets of the data. Once the method to quantify the uncertainty is validated, then we can use this information to determine a grade.

Toward the goal of improving access to ShakeMap, the

working group has put together an outline of how to create a unified set of Web pages. With general agreement about what to do, not much progress was made on actual implementation. The primary difficulty has been time, since creating unified Web pages requires a separation between product generation and Web page generation.

A second goal of this effort was to improve the robustness of ShakeMap generation and delivery by taking advantage of the fact that ShakeMaps are generated in the Bay Area, Pasadena, and Sacramento.

Lind Gee and Bruce Worden recently drafted a updated proposal to address both of these problems. The proposal is still being reviewed by various parties (including the working group) but hopefully will begin to move forward during the next fiscal year.

Location Codes: The CISON adopted a standard for the use of "location" codes (part of the Standard for the Exchange of Earthquake Data (SEED) nomenclature to describe a timeseries based on network-station-channel-location) in the late fall of 2003. Over the past few months, USGS and UC Berkeley developers have been working to modify the Earthworm software to support the use of location codes. This effort is nearly complete and the centers are working on a plan to begin migration to the modified codes.

Metadata Exchange: The CISON is also working on issues related to metadata exchange. This is an important component of CISON activities, as correct metadata are required to insure valid interpretation of data. A Standards Working Group has developed and initiated testing of a model for database replication of metadata, and is currently reviewing how much of the schema to exchange and how to address metadata from partners such as CGS, who do not currently maintain their metadata in a database.

Two years ago, the Metadata Working Group compiled a list of metadata necessary for data processing and developed a model for exchanging metadata. In this model, each CISON member is responsible for the metadata of their stations and other stations that enter into CISON processing through them. For example, Menlo Park is responsible for the NSMP, Tremor, and PG&E stations and Caltech is responsible for the Anza data. The Working Group believes that metadata exchange should proceed on a timely basis, not just when data are generated, and is testing an approach using database replication.

For database exchange, the Working Group proposed that each group or organization have a working or interim database as a staging area (a private sandbox) and a master database. The interim database would contain snapshots of the master tables (that the group/organization is responsible for) and the changes would be pushed manually to the master database by snapshot replication. Changes would be propagated among the master databases by multi-master replication.

To start this off, the Working Group agreed to test replication with a limited number of tables, focusing initially on tables relevant to the real-time system (but not sufficient for archiving). In order to test this solution, the NCMC and SCMC needed to resolve some inconsistencies in the database implementations. This included both differences in the physical schema as well as differences in use of the schema. The Working Group initiated a pilot test in early 2004, using the tables SimpleResponse and StaMapping and a test database at the NCMC and SCMC. The initial results were successful and the effort has expanded to other tables. As of June 2005, 11 tables are being replicated between the test databases. The next step for the Working Group is to validate the use of the metadata in the real-time system. When this is done, the database replication can be migrated to the primary databases.

In parallel, the Working Group has developed a plan for importing metadata from CGS. Their metadata is not currently stored in a database and is maintained in simple files. Their policy is to distribute the metadata as part of a waveform package and the V0 format was developed to allow for that. The Working Group developed the concept of a "dataless" V0 format (analogous to the dataless SEED files) which will be used to distribute the metadata. In the current plan, CGS will initially prepare and distribute dataless V0 files providing the current metadata for ShakeMap quality stations (i.e., with channels meeting CISON Reference Station or better standards) in the CGS network. These current-information metadata files for the stations will be distributed (probably using a mechanism like sendfile/getfile) and will also be placed at the CGS FTP site. As agreed, the comment field in the V0 header will be used to define the valid time period for the metadata. Each dataless V0 file will contain the 3 channels of the reference sensor at the site. The Working Group plan includes the ability to handle corrections, as well as updates as stations are serviced.

In order to make use of the dataless V0 file, tools have been developed to parse the file and write an XML file containing the information (an expansion of capabilities of the v02ms program). The NCMC has taken advantage of previously existing tools to create a system where the XML is converted into a spreadsheet format and then imported into the database. This plan will be further tested as CGS generates more dataless V0 files and the database is populated.

As part of this process, the issue of mapping the sensor orientation into the SEED channel nomenclature has come up. The v02ms program now uses the same algorithm for generating channel names as used by CGS.

Standardization Over the past 18 months, the CISON has begun to focus more on standardization of software, rather than calibration of software. As a result, the CISON is beginning to leverage software resources across the

CISN partners. For example, the BSL and the USGS Menlo Park are planning to adopt large portions of the software running at the SCMC for the NCMC. The northern and southern California developers met for a two-day meeting in October 2004 to discuss plans for the joint software development. Examples of collaboration include the development of the CISN Messaging Service - software designed to replace the commercial `SmartSockets` package used in the initial development of `TriNet`, implementation of the `RequestCardGenerator` and `Jiggle` in northern California, and initial efforts to develop specifications for a magnitude coordinator.

3.9 CISN Display

CISN Display is an integrated Web enabled earthquake notification system, designed for emergency management 24/7 operations centers. The application provides users with maps of real-time seismicity, and automatically provides access to Web-related earthquake products such as ShakeMaps. CISN Display also offers an open source GIS mapping tool that allows users to plot freely available layers of public highways, roads and bridges, as well as private layers of organizational-specific infrastructure and facilities information.

Version 1.0 was released on Dec 8th, 2004. As part of the Version 1.0 release, the CISN has brought 2 additional servers online (for a total of 4) to provide reliable access to earthquake information.

As part of this release, the CISN has implemented a login service on the QuakeWatch servers. This change is to allow the CISN to manage system resources so that critical users in the emergency response community will have access to the data. In particular, because of this change, all Beta testers of CISN display should follow the steps for account registration to set up an account.

CISN Display is designed to provide earthquake information for emergency response. First-responders, organizations with critical lifelines and infrastructure, and emergency responders are invited to register for an account at <http://www.cisn.org/software/cisndisplay.htm>.

3.10 Earthquake Information Distribution

In response to a request from the PMG, USGS and OES management established an *Ad Hoc* panel in May 2003 to develop specifications for an earthquake information system and to review existing systems as well as systems under development. Lind Gee of the BSL and David Oppenheimer of the USGS were asked to co-chair this panel and to provide a written report within 90 days. The panel met on July 9-10th at the BSL and the report was published on September 16 (*Ad Hoc Panel on Earthquake Information Distribution*, 2003). The panel

reviewed the three major existing or planned distribution systems (QDDS, QuakeWatch, and ShakeCast) and noted that none of the systems addressed all the current needs for earthquake information distribution. In particular, firewalls are a growing problem for systems relying on socket-based connections. The panel recommended that a new system be developed, and outlined preliminary specifications for such as system.

Following the publication of the report, OES asked to BSL to write a proposal for the development of the Earthquake Information Distribution System or EIDS. OES approved the proposal and forwarded it to FEMA for review. FEMA agreed to provide \$100,000 toward the development of the system out of the 2002 Emergency Management Program Grant to the State of California.

The award from FEMA was combined with the OES funding of the CISN and the contract was received by UC Berkeley on May 13th, 2004. In parallel, Lind Gee and David Oppenheimer worked with the members of the *Ad Hoc* panel to develop detailed specifications – appropriate for a Request For Proposal or RFP – based on the September 2003 report. The specifications were completed in late June and submitted to UC Berkeley Purchasing on July 6, 2004. Unfortunately, the late award of the funding combined with the difficulties of issuing an RFP complicated efforts to award the funding in a timely fashion.

In mid-August, the BSL decided to proceed with a sole source award to Instrumental Software Technologies, Inc (ISTI). Paul Friberg of ISTI was one of two vendors who made presentations to the AdHoc Panel in July of 2003 regarding an earthquake information distribution system. On September 28, 2004 the BSL was notified that an extension to March 30, 2005 has been awarded by FEMA.

Over the last nine months, BSL have worked with ISTI on the development of the software. In particular, Pete Lombard has been involved in extensive testing of the EIDS software and documentation. The USGS is planning to hold a meeting in October 2005 to discuss the roll out of the EIDS software.

3.11 Outreach

There has been significant progress at www.cisn.org in FY04/05. Two years ago, the CISN shared the Web server at the Northern California Earthquake Data Center. With the purchase of new, dedicated Web computers, the CISN Web site is now supported by two servers located at Berkeley and Caltech. The Web servers are set up so that the load can be distributed between them, providing improved access during times of high demand.

With the increased robustness provided by the new servers, the CISN has begun to provide access to certain earthquake products directly from www.cisn.org. For example, ShakeMaps are now served directly from the

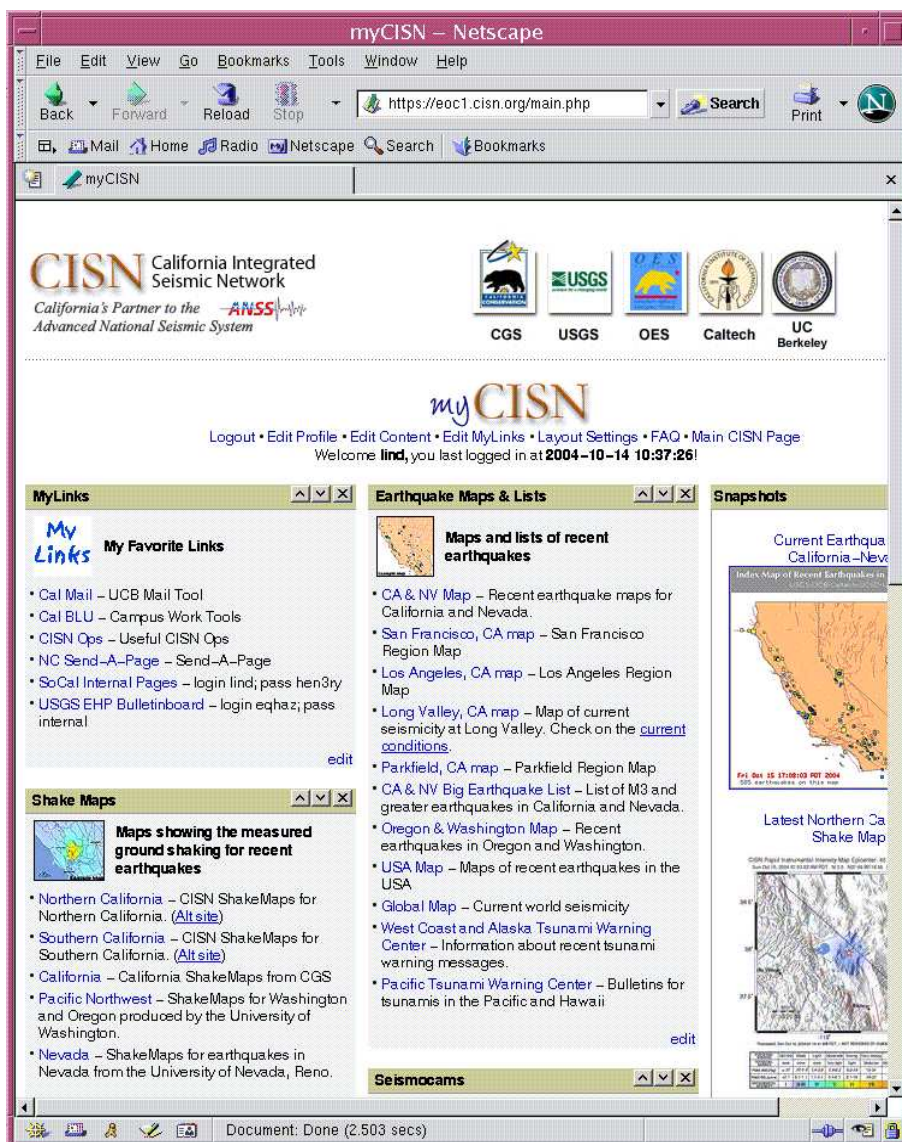


Figure 4.4: Screenshot of the myCISN Web site, as personalized for Lind Gee. The interface allows users to select and organize the earthquake information they want to see. New modifications under development also allow users to create a section of personalized links.

CISN Web site, in addition to being available from several USGS Web servers and the CGS.

In early December 2003, the CISN began offering a sign-up for earthquake notifications by email. Although both northern and southern California have offered individual sign-ups in the past, the new service provides uniform notification messages for earthquakes of M3.5 and higher in California. In addition, users can sign up to be notified when ShakeMaps are generated.

Design and content of <http://www.cisn.org> continues to evolve. The Web site is an important tool for CISN outreach as well as for communication and documentation among the CISN partners.

Also in FY03/04, the CISN established a Web site dedicated for emergency managers. Following a suggestion from the Advisory Committee, we have designed a Web site to provide personalized access to earthquake information. Known as “myCISN,” the Web site is available at eoc.cisn.org (Figure 4.4). Access to the Web site is limited to registered users in order to provide highly reliable access.

At present, “myCISN” is a single Web server located at UC Berkeley. However, modifications to the database are underway to allow for multiple servers in the future. A second computer was purchased with FY03/04 funds and will either be installed in Sacramento or in southern

California. During the past year, the CISN worked with ISTI to develop and test a plan for the deployment of multiple servers.

4. Acknowledgements

CISN activities at the BSL are supported by funding from the Governor's Office of Emergency Services.

Barbara Romanowicz and Lind Gee are members of the CISN Steering Committee. Lind Gee is a member of the CISN Program Management Committee and she leads the CISN project at the BSL. Doug Neuhauser is chair of the CISN Standards Committee, which includes Lind Gee and Pete Lombard as members.

Because of the breadth of the CISN project, many BSL staff have been involved including: John Friday, Lind Gee, Bill Karavas, Pete Lombard, Doug Neuhauser, Charley Paffenbarger, and Stephane Zuzlewski. Lind Gee contributed to this chapter. Additional information about the CISN is available through reports from the Program Management Committee.

5. References

Ad Hoc Panel on Earthquake Information Distribution (L. Gee and D. Oppenheimer, chairs), Requirements for an Earthquake Information Distribution System, http://www.cisn.org/ahpeid/ahpeid_final.pdf, 2003.

Gee, L., D. Dreger, G. Wurman, Y. Gung, B. Uhrhammer, and B. Romanowicz, A Decade of Regional Moment Tensor Analysis at UC Berkeley, *EOS Trans. AGU*, 84(46), Fall Meet. Suppl., Abstract S52C-0148, 2003.

Gee, L., D. Oppenheimer, T. Shakal, D. Given, and E. Hauksson, Performance of the CISN during the 2003 San Simeon Earthquake, http://www.cisn.org/docs/CISN_SanSimeon.pdf, 2004a.

Gee, L., J. Polet, R. Uhrhammer, and K. Hutton, Earthquake Magnitudes in California, *Seism. Res. Lett.*, 75(2), 272, 2004b.

Hauksson, E., L. Gee, D. Given, D. Oppenheimer, and T. Shakal, Report to the CISN Advisory and Steering Committees, #5, <http://www.cisn.org/oes/2003.05.30.pdf>, 2003.

Hok, S., and D. J. Wald, Spatial Variability of Peak Strong Ground Motions: Implications for ShakeMap Interpolations, *EOS. Trans. AGU*, 84(46), F1121, 2003.

Kanamori, H., J. Mori, E. Hauksson, T. Heaton, L. Hutton, and L. Jones, Determination of earthquake energy release and M_L using TERRASCOPE, *Bull. Seis. Soc. Am.*, 83, 330-346, 1993.

Chapter 5

Northern Hayward Fault Network

1. Introduction

Complementary to the regional broadband network, a deployment of borehole-installed, wide-dynamic range seismographic stations is being established along the Hayward Fault and throughout the San Francisco Bay toll bridges network. This network is a cooperative development of the BSL and the USGS, with support from USGS, Caltrans, EPRI, the University of California Campus/Laboratory Collaboration (CLC) program, LLNL, and LBNL (Figure 5.1 and Table 5.1). Efforts at ongoing development of the network have also recently been enhanced through coordinated efforts with the Mini-PBO project (Chapter 8, which is partially funded by NSF and by the member institutions of that project).

The purpose of the network is threefold: 1) to lower substantially the threshold of microearthquake detection, 2) to increase the recorded bandwidth for events along the Hayward fault, and 3) to obtain bedrock ground motion signals at the bridges from small earthquakes for investigating bridge responses to stronger ground motions. A lower detection threshold increases the resolution of the fault-zone seismic structure; allows seismologists to monitor the spatial and temporal evolution of seismicity at magnitudes down to $M \sim -1.0$, where earthquake rates are many times higher than those captured by surface sites; allows researchers to look for pathologies in seismicity patterns that may be indicative of the nucleation of large damaging earthquakes; and allows scientists to investigate fault and earthquake scaling, physics and processes in the San Francisco Bay Area. This new data collection will also contribute to improved working models for the Hayward fault. The bedrock ground motion recordings are also being used to provide input for estimating the likely responses of the bridges to large, potentially damaging earthquakes. Combined with the improved Hayward fault models, source-specific response calculations can be made as well.

The Hayward Fault Network (HFN) consists of two parts. The Northern Hayward Fault Network (NHFN) is operated by the BSL and currently consists of 25 sta-

tions, including those located on Bay Area bridges and at borehole sites of the Mini-PBO (MPBO) project. This network is considered part of the BDSN and uses the network code BK. The Southern Hayward Fault Network (SHFN) is operated by the USGS and currently consists of 5 stations. This network is considered part of the NCSN and uses the network code NC. This chapter is primarily focused on the NHFN and activities associated with the BSL operations.

2. NHFN Overview

The five MPBO sites have 3-component borehole geophone packages. All the remaining HFN sites have six-component borehole sensor packages. The packages were designed and fabricated at LBNL's Geophysical Measurement Facility by Don Lippert and Ray Solbau, with the exception of site SFAB. For the HFN sites, three channels of acceleration are provided by Wilcoxon 731A piezoelectric accelerometers and three channels of velocity are provided by Oyo HS-1 4.5 Hz geophones. Velocity measurements for the MPBO sites are provided by Mark Products L-22 2 Hz geophones (Table 5.2). The 0.1-400 Hz Wilcoxon accelerometers have lower self-noise than the geophones above about 25-30 Hz, and remain on scale and linear to 0.5 g. In tests performed in the Byerly vault at UC Berkeley, the Wilcoxon is considerably quieter than the FBA-23 at all periods, and is almost as quiet as the STS-2 between 1 and 50 Hz.

Sensors are generally installed at depths of about 100 m, but several sites have sensors emplaced at depths of over 200 m and the Dumbarton bridge sites have sensors at multiple depths (Table 5.1). During initial stages of the project, the NHFN sensors provided signals to on-site Quanterra Q730 and RefTek 72A-07 data loggers.

Today, twelve of the NHFN sites currently have Quanterra data loggers with continuous telemetry to the BSL. Similar to BDSN sites, these stations are capable of on-site recording and local storage of all data for more than one day and have batteries to provide backup power. Signals from these stations are digitized at a variety of data rates up to 500 Hz at 24-bit resolution (Table 5.3). In

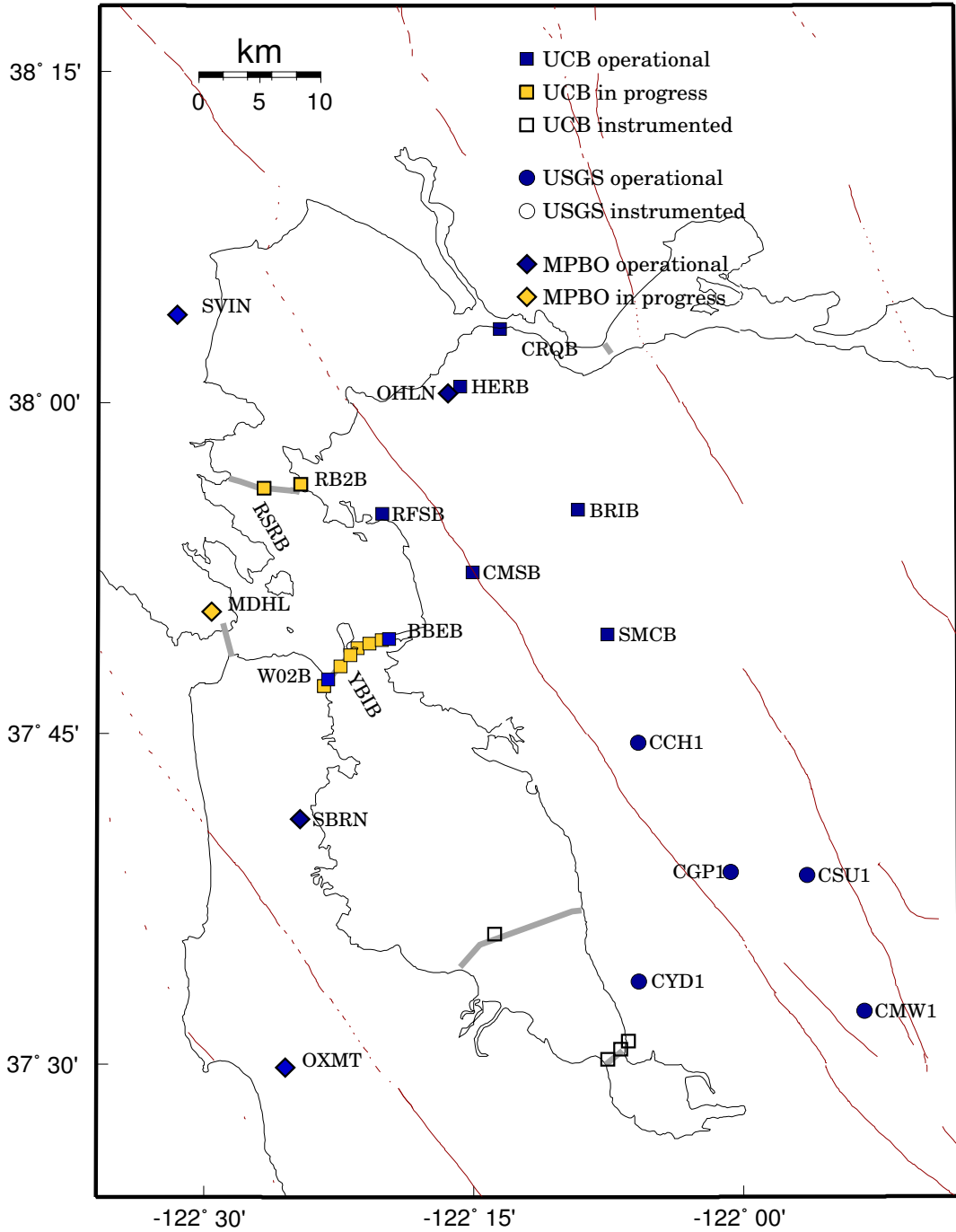


Figure 5.1: Map showing the locations of the HFN stations operated by the BSL (NHFN - squares) and the USGS (SHFN - circles) and Mini-PBO stations (diamonds) in the San Francisco Bay Area. Operational sites are filled, while sites in progress are grey. Other instrumented boreholes are indicated as open symbols.

contrast to the BDSN implementation, the NHFN data loggers employ casual FIR filters at high data rates and acausal FIR filters at lower data rates. Because of limitations in telemetry bandwidth and disk storage, 8 of these sites transmit triggered data at 500 sps, using the Murdock, Hutt, and Halbert (MHH) event detection algorithm (Murdock and Hutt, 1983), and continuous data at reduced rates (100, 20 and 1 sps) to the BSL, while the four MPBO sites transmit continuous data at 100 sps (one MPBO site does not have telemetry yet).

The remaining 12 sites of the NHFN have in the past recorded data using RefTek data loggers. These sites do not have continuous telemetry for acquisition and required visits from BSL staff for data recovery. Collection of data from these sites has been discontinued, but efforts are underway to upgrade them with Quanterra Q4120 data loggers and continuous telemetry.

Signals from the 5 SHFN stations are digitized by Nanometrics data loggers at 100 sps and transmit continuous data to Menlo Park by radio. These digital data streams are processed by the Earthworm system with the NCSN data and waveforms are saved when the Earthworm detects an event.

Experience has shown that the MHH detector does not provide uniform triggering across the NHFN on the smallest events of interest. In order to insure the recovery of 500 sps data for these earthquakes, a central-site controller has recently been implemented at the BSL using the 500 sps vertical component geophone data for event detection. Originally the 100 sps vertical component geophone data was used for event detection but the bandwidth proved to be inadequate for detection of the smaller events where most of the seismic wave energy was at frequencies above 40 Hz. Triggers from this controller are being used to recover the 500 sps data from the NHFN data loggers.

Data from the NHFN and SHFN are archived at the NCEDC. At this time, the tools are not in place to archive the Hayward fault data together. The NHFN data are archived with the BDSN data, while the SHFN are archived with the NCSN data (Chapter 11). However, the new central-site controller will provide the capability to both include SHFN data in the event detection and extract SHFN waveforms for these events in the future.

As originally planned, the Hayward Fault Network was to consist of 24 to 30 stations, 12-15 each north and south of San Leandro, managed respectively by UCB and USGS. This is not happening quickly, although west of the fault, Caltrans has provided sites along the Bay bridges. This important contribution to the Hayward Fault Network has doubled the number of sites with instrumentation. At times, Caltrans provides holes of opportunity away from the bridges (e.g., HERB), so we have plans for additional stations that will bring the network geometry to a more effective state for imaging and

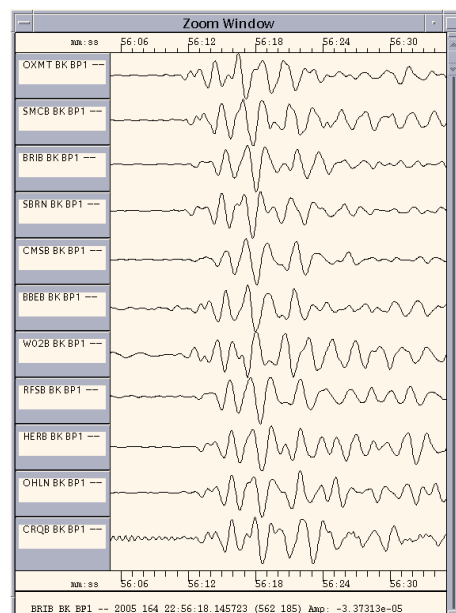


Figure 5.2: Plot of the P-wave waveforms, recorded by the NHFN/MPBO borehole stations, for a major intermediate focus Chilean earthquake (2005/06/13; 22:44 UT; 116 km deep; M_w 7.8; 8460 km S51E of Berkeley). The waveform data were deconvolved to ground velocity, 0.3-5.0 Hz band pass filtered to enhance the P-wave signal and normalized prior to plotting. For comparison, the traces are plotted in order of distance. The waveforms are highly similar at all stations except W02B where there the trace is inverted.

real-time monitoring of the fault.

As a check on the calibration and an example of the capabilities of a borehole installed network, we compare the bandpass filtered (0.3-5 Hz) ground velocity data recorded at NHFN and MPBO stations for a M 7.8 intermediate focus teleseism that occurred in Chile at a depth of 116 km in Figure 5.2.

3. 2004-2005 Activities

In addition to routine maintenance, operations and data collection; activities of the NHFN project over the past year have also included numerous efforts at network expansion, quality assurance, performance enhancement and catalog development.

Code	Net	Latitude	Longitude	Elev (m)	Over (m)	Date	Location
CRQB	BK	38.05578	-122.22487	-25.0	38.4	1996/07 - current	CB
HERB	BK	38.01250	-122.26222	-25.0	217.9	2000/05 - current	Hercules
BRIB	BK	37.91886	-122.15179	219.7	108.8	1995/07 - current	BR, Orinda
RFSB	BK	37.91608	-122.33610	-27.3	91.4	1996/01 - current	RFS, Richmond
CMSB	BK	37.87195	-122.25168	94.7	167.6	1994/12 - current	CMS, Berkeley
SMCB	BK	37.83881	-122.11159	180.9	3.4	1997/12 - current	SMC, Moraga
SVIN	BK	38.03325	-122.52638		158.7	2003/08 - current	MPBO, St. Vincent's school
OHLN	BK	38.00742	-122.27371		196.7	2001/07 - current	MPBO, Ohlone Park
MDHL	BK	37.84227	-122.49374		160.6	in progress	MPBO, Marin Headlands
SBRN	BK	37.68562	-122.41127		157.5	2001/08 - current	MPBO, San Bruno Mtn.
OXMT	BK	37.498	-122.425		194.2	2003/12 - current	MPBO, Ox Mtn.
BBEB	BK	37.82167	-122.32867		150.0	2002/05 - current	BB, Pier E23
E17B	BK	37.82086	-122.33534		160.0	1995/08 - current *	BB, Pier E17
E07B	BK	37.81847	-122.34688		134.0	1996/02 - current *	BB, Pier E7
YBIB	BK	37.81420	-122.35923	-27.0	61.0	1997/12 - current *	BB, Pier E2
YBAB	BK	37.80940	-122.36450		3.0	1998/06 - current *	BB, YB Anchorage
W05B	BK	37.80100	-122.37370		36.3	1997/10 - current *	BB, Pier W5
W02B	BK	37.79120	-122.38525		57.6	2003/06 - current	BB, Pier W2
SFAB	BK	37.78610	-122.3893		0.0	1998/06 - current *	BB, SF Anchorage
RSRB	BK	37.93575	-122.44648	-48.0	109.0	1997/06 - current *	RSRB, Pier 34
RB2B	BK	37.93	-122.41		133.8	2003/07 - current *	RSRB, Pier 58
SM1B	BK	37.59403	-122.23242		298.0	not recorded	SMB, Pier 343
DB3B	BK	37.51295	-122.10857		1.5	1994/09 - 1994/11	DB, Pier 44
					62.5	1994/09 - 1994/09	
					157.9	1994/07 - current *	
DB2B	BK	37.50687	-122.11566			1994/07 - current *	DB, Pier 27
					189.2	1992/07 - 1992/11	
DB1B	BK	37.49947	-122.12755		0.0	1994/07 - 1994/09	DB, Pier 1
					1.5	1994/09 - 1994/09	
					71.6	1994/09 - 1994/09	
					228.0	1993/08 - current *	
CCH1	NC	37.7432	-122.0967	226		1995/05 - current	Chabot
CGP1	NC	37.6454	-122.0114	340		1995/03 - current	Garin Park
CSU1	NC	37.6430	-121.9402	499		1995/10 - current	Sunol
CYD1	NC	37.5629	-122.0967	-23		2002/09 - current	Coyote
CMW1	NC	37.5403	-121.8876	343		1995/06 - current	Mill Creek

Table 5.1: Stations of the Hayward Fault Network. Each HFN station is listed with its station code, network id, location, operational dates, and site description. The latitude and longitude (in degrees) are given in the WGS84 reference frame. The elevation of the well head (in meters) is relative to the WGS84 reference ellipsoid. The overburden is given in meters. The start dates indicate either the upgrade or installation time. The abbreviations are: BB - Bay Bridge; BR - Briones Reserve; CMS - Cal Memorial Stadium; CB - Carquinez Bridge; DB - Dumbarton Bridge; MPBO - mini-Plate Boundary Observatory RFS - Richmond Field Station; RSRB - Richmond-San Rafael Bridge; SF - San Francisco; SMB - San Mateo Bridge; SMC - St. Mary's College; and, YB - Yerba Buena. The * for stations indicates that the stations are not currently recording data. RSRB is shut down while Caltrans is retrofitting the Richmond-San Rafael bridge (as of April 19, 2001) and YBIB has been off-line since August 24, 2000 when power cables to the site were shut down. Other off-line stations are in the process of being upgraded as funding for equipment becomes available. The table also includes 2 MPBO stations which became operational in the last 2 years, and 3 MPBO borehole sensors that have recently been installed.

3.1 Station Maintenance

Shown in Figure 5.3 are power spectral density (PSD) distributions of background noise for a sample of 8 NHFN

land and bridge site stations. In general, background noise levels of the borehole HFN stations is more variable and generally higher than that of the Parkfield HRSN

Site	Geophone	Accelerometer	Z	H1	h2	Data logger	Notes	Telem.
CRQB	Oyo HS-1	Wilcoxon 731A	-90	251	341	Q4120		FR
HERB	Oyo HS-1	Wilcoxon 731A	-90	TBD	TBD	Q4120		FR
BRIB	Oyo HS-1	Wilcoxon 731A	-90	79	349	Q4120	Acc. failed, Dilat.	FR
RFSB	Oyo HS-1	Wilcoxon 731A	-90	256	346	Q4120		FR
CMSB	Oyo HS-1	Wilcoxon 731A	-90	19	109	Q4120		FR
SMCB	Oyo HS-1	Wilcoxon 731A	-90	76	166	Q4120	Posthole	FR
SVIN	Mark L-22		-90	298	28	Q4120	Tensor.	FR/Rad.
OHLN	Mark L-22		-90	313*	43*	Q4120	Tensor.	FR
MDHL	Mark L-22		-90	TBD	TBD	None at present	Tensor.	
SBRN	Mark L-22		-90	347	77	Q4120	Tensor.	FR
OXMT	Mark L-22		-90	163	253	Q4120	Tensor.	FR
BBEB	Oyo HS-1	Wilcoxon 731A	-90	TBD	TBD	Q4120	Acc. failed	Radio
E17B	Oyo HS-1	Wilcoxon 731A	-90	TBD	TBD	None at present		
E07B	Oyo HS-1	Wilcoxon 731A	-90	TBD	TBD	None at present		
YBIB	Oyo HS-1	Wilcoxon 731A	-90	257	347	None at present	Z geop. failed	FR/Rad.
YBAB	Oyo HS-1	Wilcoxon 731A	-90	TBD	TBD	None at present		
W05B	Oyo HS-1	Wilcoxon 731A	-90	TBD	TBD	None at present		
W02B	Oyo HS-1	Wilcoxon 731A	-90	TBD	TBD	Q4120		Radio
SFAB	None	LLNL S-6000	TBD	TBD	TBD	None at present	Posthole	
RSRB	Oyo HS-1	Wilcoxon 731A	-90	50	140	None at present	2 acc. failed	FR
RB2B	Oyo HS-1	Wilcoxon 731A	-90	TBD	TBD	None at present	1 acc. failed	
SM1B	Oyo HS-1	Wilcoxon 731A	-90	TBD	TBD	None at present		
DB3B	Oyo HS-1	Wilcoxon 731A	-90	TBD	TBD	None at present	Acc. failed	
DB2B	Oyo HS-1	Wilcoxon 731A	-90	TBD	TBD	None at present		
DB1B	Oyo HS-1	Wilcoxon 731A	-90	TBD	TBD	None at present	Acc. failed	
CCH1	Oyo HS-1	Wilcoxon 731A	-90	TBD	TBD	Nanometrics HRD24	Dilat.	Radio
CGP1	Oyo HS-1	Wilcoxon 731A	-90	TBD	TBD	Nanometrics HRD24	Dilat.	Radio
CSU1	Oyo HS-1	Wilcoxon 731A	-90	TBD	TBD	Nanometrics HRD24	Dilat.	Radio
CYD1	Oyo HS-1	Wilcoxon 731A	-90	TBD	TBD	Nanometrics HRD24	Dilat.	Radio
CMW1	Oyo HS-1	Wilcoxon 731A	-90	TBD	TBD	Nanometrics HRD24	Dilat.	Radio

Table 5.2: Instrumentation of the HFN as of 06/30/2005. Every HFN downhole package consists of co-located geophones and accelerometers, with the exception of MPBO sites. 6 HFN sites also have dilatometers (Dilat.) and the 5 MPBO sites have tensor strainmeters (Tensor.) 12 NHFN sites have Quanterra data loggers with continuous telemetry to the BSL. The remaining sites are being upgraded to Quanterra data loggers. The 5 SHFN sites have Nanometrics data loggers with radio telemetry to the USGS. The orientation of the sensors (vertical - Z, horizontals - H1 and H2) are indicated where known or identified as "to be determined" (TBD). The azimuths of the horizontal component geophones have a 180 degree ambiguity owing to the dead vertical component geophone.

borehole stations (Figure 6.2). This is due in large part to the significantly greater level of cultural noise in the Bay Area, and to the fact that noise reduction efforts on the much more recently installed NHFN stations are still underway. For example the two noisiest stations (i.e. BBEB and W02B) are located on the Bay Bridge which is currently undergoing earthquake retrofit and east span reconstruction. These stations have also only recently come back on-line with upgraded infrastructure and instrumentation, so the full complement of noise reduction modifications have not yet been implemented.

On average the MPBO NHFN sites are more consistent and quieter (Figure 8.4). This is due in large part to the greater depth of the MPBO sensors, the locations of

MPBO stations in regions of generally less industrial and other cultural noise sources, and possibly to the absence of powered sensors (i.e. accelerometers) in their borehole sensor packages.

One of the most pervasive problems at NHFN stations equipped with the Q4120 data loggers is power line noise (60 Hz and its harmonics at 120, 180, and 240 Hz). This noise reduces the sensitivity of the MHH detectors. Whenever a NHFN station is visited, the engineer at the site and a seismologist at the BSL work together to expedite the testing process, especially when attempting to identify and correct ground-loop faults which generally induce significant 60, 120, 180, and 240 Hz seismic signal contamination due to stray power line signal pickup, gen-

Sensor	Channel	Rate (sps)	Mode	FIR
Accelerometer	CL?	500.0	T	Ca
Accelerometer	HL?	100.0	C	Ca
Accelerometer	BL?	20.0	C	Ac
Accelerometer	LL?	1.0	C	Ac
Geophone	DP?	500.0	T	Ca
Geophone	EP?	100.0	C	Ca
Geophone	BP?	20.0	C	Ac
Geophone	LP?	1.0	C	Ac

Table 5.3: Typical data streams acquired at each NHFN site, with channel name, sampling rate, sampling mode and FIR filter type. C indicates continuous; T triggered; Ca causal; and Ac acausal. The 100 sps channels (EP & HL) are only archived when the 500 sps channels are not available.

erally inductively coupled and aggravated by the presence of ground loops.

Below is a synopsis of maintenance efforts performed over the past year for several NHFN stations that gives some idea of the ongoing maintenance and performance enhancing measures that we are continuing to implement.

Geophone Calibrations

Comparisons of the inferred ground accelerations generated by local earthquakes, from co-sited HFN geophone and accelerometer pairs, shows that the waveforms generally are quite coherent in frequency and phase response but that their inferred ground accelerations differ significantly. At times the amplitudes differ by up to a factor of 2 while the times of the peak amplitudes are identical. This implies that the free period and damping of the geophones are well characterized and also that the generator constant is not accurate (assuming that the corresponding ground accelerations inferred from the accelerometers are accurate).

Generally speaking, the accelerometers, being an active device, are more accurate and also more stable than the geophones so it is reasonable to assume that the most likely reason for the difference is that the assumed generator constants for the geophones are not accurate. *Rodgers et al.* (1995) describe a way to absolutely calibrate the geophones in situ and to determine their generator constant, free period and fraction of critical damping. The only external parameter that is required is the value of the geophones inertial mass.

We have built a calibration test box which allows us to routinely perform the testing described by *Rodgers et al.* whenever site visits are made. The box drives the signal coil with a known current step and rapidly switches the signal coil between the current source and the data logger input. From this information, expected and actual sensor response characteristics can be compared and corrections

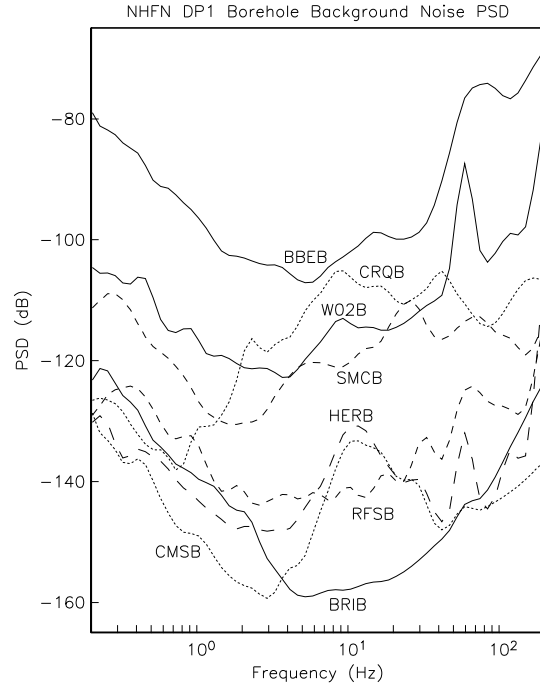


Figure 5.3: Plot showing the HFN.BK.DP1 background noise, PSD, for 8 of the NHFN stations. Plotted are the background low-noise PSD estimates. Ten minutes of .BK.DP1 data starting at 2005.268.0900 (2 AM PDT) were used in the analysis. Note that there is considerable variation in the general level and structure of the individual station background noise PSD estimates. Some of the stations show peaks at 60 Hz and its harmonics while others have a high average background level. The two bridge sites, BBEB and W02B are the noisiest while land site BRIB in Briones Regional Park (well away from the heavy cultural noise of the more populated region of the Bay Area) is the quietest. Two stations, CMSB and HERB show a peak in the 20-30 Hz range. The peak at CMSB is probably due to excitation of modes in the open bore hole and the peak at HERB is due to excitation of the local structure by the adjacent railway line and highways 4 and 80. The three stations in the middle of the group (RFSB, SMCB and CRQB) are responding to the local cultural noise. There are numerous ongoing experiments at the Richmond Field Station which are affecting the noise level at RFSB, CRQB is sited near a sewage treatment plant and the Carquinez bridge, and SMCB is currently only installed at post hole depth (3.5 m) on the St. Mary's campus.

applied. Also, changes in the sensor response over time can be evaluated so that adjustments can be made and pathologies arising in the sensors due to age can be identified. Once a geophone is absolutely calibrated, we can

also check the response of the corresponding accelerometer.

We are now performing the initial calibration tests and response adjustments for all NHFN stations as sites are visited for routine maintenance. We also plan a scheduled re-test of all sites to monitor for sensor responses changes through time.

NHFN Station Maintenance Synopsis

The NHFN station hardware has proven, on average, to be quite reliable. The following stations were visited to perform various maintenance and/or repair operations.

BBEB: Ran radio tests on Wilan link to Space Sciences Lab at 18 dBm and at maximum power (23 dBm) to ascertain effect on dropped packets. At 24 dBm power, the throughput was 6 times higher than at 18 dBm power and the number of dropped packets reduced from 4.6

BRIB: Numerous frame relay telemetry problems were encountered during August and September and the station was visited several times to troubleshoot and correct the problem.

CMSB: Quanterra hung after 8/17 reboot. The power was manually recycled and the Quanterra came back up.

CRQB: Quanterra hung after 8/17 reboot. The power was manually recycled and the Quanterra came back up and was functioning normally.

HERB: Velocity channel was found in September to not be responsive to events. The problem was traced to a blown fuse in the power system although it is unclear as to how that problem effected the responsiveness of the velocity channel.

RFSB: Visited station several times to repair frame relay and power supply problems.

SMCB: Quanterra hung after 8/17 reboot. The power was manually recycled and the Quanterra came back up.

W02B: Telemetry link went down in October and again in December due to an antenna problem.

3.2 New Installations

San Francisco-Oakland Bay Bridge

The infrastructure at seven stations along the San Francisco-Oakland Bay Bridge (SFAB, W02B, W05B, YBAB, E07B, E17B, and BBEB) was upgraded with the installation of weatherproof boxes, power, and telemetry in anticipation of installing Q4120 data loggers and telemetering the data back to Berkeley. BBEB was brought on-line in May of 2002, and W02B in June of 2003.

Land Sites

Agreements with Caltrans and St. Mary's College have been made to replace the post hole installation at St. Mary's College (SMCB) with a deep borehole installation. The hole is to be drilled by Caltrans as a hole of

opportunity when the schedule of a Caltrans drilling crew has an opening. The site has been reviewed by UCB, Caltrans and St. Mary's College personnel, and we are now in the drilling queue. Depending on the geology at borehole depth, this site may either become a MPBO site (w/o accelerometers) or a standard land site installation including both geophones and accelerometers.

Caltrans has also provided funding for instrumentation of several other land sites which we will install as future Caltrans drill time becomes available. Currently we are considering sites for these additional holes-of-opportunity at Pt. Pinole, on Wildcat Mtn. in the North Bay. We are in the process of obtaining permission from the East Bay Regional Park District (EBRPD) to site a HFN station at the Point Isabel Regional Shoreline.

Mini-PBO

The stations of the Mini-PBO project (Chapter 8) are equipped with borehole seismometers. As these stations have become operational, they augment HFN coverage (Figure 5.1). In the last year, SVIN and SBRN have added coverage to the north bay and east side of the south bay, respectively.

3.3 Data Analysis and Results

Combined Catalog

We are building a HF-specific data archive from the existing waveform data that have been collected by the heterogeneous set of recording systems in operation along the Hayward fault (i.e. the NHFN, SHFN, NCSN, and BDSN continuous and triggered waveforms). Recently we have taken the NHFN triggers collected during operations between 1995.248 and 1998.365 (recorded on portable RefTek recorders) and origin times from the Northern California catalog for this time period and undertaken a massive association of event and trigger times. The purpose of the effort is to compile a relatively uniform catalog of seismic data to low magnitudes and extending back in time to the beginning of reliable HFN data collection. The process has reduced nearly a million individual time segments to 316 real events along the Hayward fault during the period—an increase in the number of events of a factor of about 2.5 to 3 over the Northern California catalog alone in the same area.

Event Detection

As noted in the Introduction, one of the purposes of the HFN is to lower the threshold of microearthquake detection. Towards this goal, we have been developing new algorithms: a pattern recognition approach to identify small events, a phase onset time detector with sub-sample timing resolution, and a phase coherency method for single component identification of highly similar events.

Pattern Recognition: In order to improve the detection and analysis of small events (down to $M_L \sim -1.0$), some specialized algorithms are being developed. The Murdock-Hutt detection algorithms used by MultiSHEAR, which basically flags an event whenever the short-term average exceeds a longer-term average by some threshold ratio, is neither appropriate for nor capable of detecting the smallest seismic events. One solution is to use a pattern recognition approach to identify small events associated with the occurrence of an event that was flagged by the REDI system. Tests have indicated that the pattern recognition detection threshold is $M_L \sim -1.0$ for events occurring within ~ 10 km of a NHFN station. The basic idea is to use a quarter second of the initial P-wave waveform as a master pattern to search for similar patterns that occur within \pm one day of the master event. Experimentally, up to six small CMSB recorded events, at the $M_L \sim -1.0$ threshold and occurring within \pm one day of a master pattern, have been identified.

The pattern recognition method is CPU intensive, however, and it will require a dedicated computer to handle the pattern recognition tasks. To expedite the auto-correlation processing of the master pattern, an integer arithmetic cross-correlation algorithm has been developed which speeds up the requisite processing by an order of magnitude.

Phase Onset Time Detection: The phase onset time detector makes use of the concept that the complex spectral phase data, over the bandwidth of interest (i.e., where the SNR is sufficiently high), will sum to a minimum at the onset of an impulsive P-wave. The algorithm searches for the minimum phase time via phase shifting in the complex frequency domain over the bandwidth where the SNR is above 30 dB to identify the onset time of the seismic phase. The algorithm requires that the recorded waveforms be deconvolved to absolute ground displacement. This implicitly requires that any acausality in the anti-aliasing filtration chain, such as the FIR filters used in the BDSN Quanterra data loggers, be removed. The algorithm typically resolves P-wave onset times to one-fiftieth of the sample interval or better.

Phase Coherency: A spectral phase coherency algorithm was developed to facilitate high resolution quantification of the similarities and differences between highly similar Hayward fault events which occur months to years apart. The resolution of the complex spectral phase coherency methodology is an order of magnitude better than the cross correlation method which is commonly used to identify highly similar events with resolution of order a few meters. This method, originally developed using NHFN borehole data, is now being applied as well to data from another borehole network (the HRSN) to provide more rapid and objective identification of the large fraction (approx. 40%) of characteristically repeat-

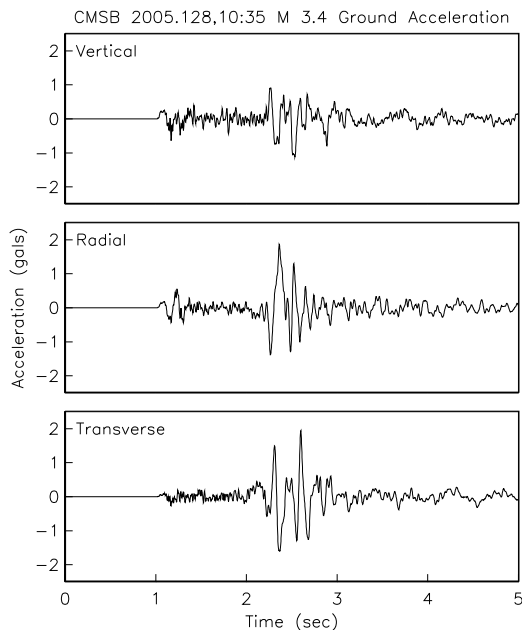


Figure 5.4: Plot showing the absolute ground accelerations recorded at CMSB, the 167 m deep borehole station at the Cal Memorial Stadium, for a M_L 3.4 earthquake at a hypocentral distance of 6.8 km. The horizontal traces have been rotated to radial and transverse and the observed peak ground ground acceleration is 2.44 gals (or 26,650 counts on the CMSB data logger. The sampling rate is 500 Hz and the bandwidth, limited by the FIR anti-aliasing filters in the data logger, is 200 Hz.

ing microearthquakes that occur at Parkfield, CA.

Berkeley Local Earthquake

At 10:35 UT on May 5, 2005, a M_L 3.4 earthquake occurred 4.6 km S29°E of CMSB at a depth of 5 km. The CMSB recording of this event demonstrates the signal-to-noise ratio and signal bandwidth that can be achieved using modern low-noise borehole implanted accelerometers of an NHFN station and its capacity for providing high-resolution registration of a local earthquake. The absolute ground accelerations observed at CMSB are shown in Figure 5.4. Given the observed M_L 3.4 magnitude and corresponding peak ground acceleration of 26,650 counts or 2.44 gal for this event and the effective acceleration clipping level of 196 gals for the CMSB hardware, the upper limit on the magnitude clipping level is estimated to be M_L 5.3 ($3.4 + \log_{10}(196/2.44)$) for a local earthquake.

The corresponding vertical component (CL1) acceleration spectra shown in Figure 5.5 demonstrates the signal-

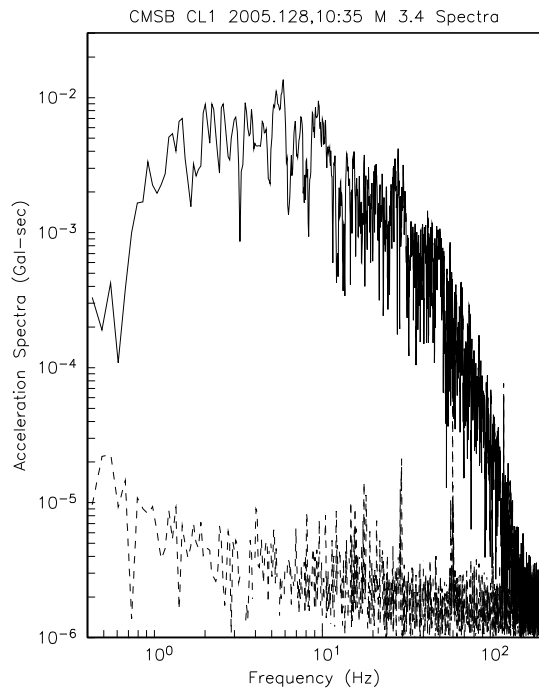


Figure 5.5: Plot showing the vertical component absolute ground acceleration spectra recorded at CMSB for a M_L 3.4 local earthquake (solid line) and the corresponding pre-event noise spectra dashed line).

to-noise ratio and signal bandwidth that can be achieved using modern low-noise borehole emplaced accelerometers. The signal bandwidth is 200 Hz and the SNR is above 50 dB in the 1-50 Hz band and the SNR is above 0 dB up to 170 Hz.

4. Acknowledgements

Thomas V. McEvelly, who passed away in February 2002, was instrumental in developing the Hayward Fault Network, and without his dedication and hard work the creation and continued operation of the NHFN would not have been possible.

Under Bob Nadeau's, Bob Uhrhammer's and Doug Dreger's general supervision, Rich Clymer, Doug Neuhauser, Bill Karavas, John Friday, and Rick Lellingner all contribute to the operation of the NHFN. Bob Nadeau and Bob Uhrhammer contributed to the preparation of this chapter.

Partial support for the NHFN is provided by the USGS through the NEHRP external grant program. Expansion of the NHFN has been made possible through generous funding from Caltrans, with the assistance of Pat Hipley. Larry Hutchings of LLNL has been an important collaborator on the project.

5. References

Rogers, P.W., A.J. Martin, M.C. Robertson, M.M. Hsu, and D.B. Harris, Signal-Coil Calibration of Electromagnetic Seismometers, *Bull. Seism. Soc. Am.*, 85(3), 845-850, 1995.

Murdock, J., and C. Hutt, A new event detector designed for the Seismic Research Observatories, *USGS Open-File-Report 83-0785*, 39 pp., 1983.

Chapter 6

Parkfield Borehole Network (HRSN)

1. Introduction

The operation of the High Resolution Seismic Network (HRSN) at Parkfield, California began in 1987, as part of the U.S. Geological Survey initiative known as the Parkfield Prediction Experiment (PPE) (*Bakun and Lindh, 1985*).

Figure 6.1 shows the location of the network, its relationship to the San Andreas fault, sites of significance from previous and ongoing research using the HRSN, double-difference relocated earthquake locations from 1987-1998, routine locations of seismicity from August 2002 to July 2003, nonvolcanic tremor locations from January 2001 through April 2005, and the epicenter of the 1966 and 2004 M6 earthquakes that motivated much of the research. The HRSN records exceptionally high-quality data, owing to its 13 closely spaced three-component borehole sensors (generally emplaced in the extremely low attenuation and background noise environment at 200 to 300 m depth (Table 6.1), its high-frequency wide bandwidth recordings (0-100 Hz), and its low magnitude detection threshold (below magnitude -1.0).

Several aspects of the Parkfield region make it ideal for the study of small earthquakes and nonvolcanic tremors and their relationship to tectonic processes and large earthquakes. These include the fact that the network spans the expected nucleation region of a repeating magnitude 6 event and a significant portion of the transition from locked to creeping behavior on the San Andreas fault, the availability of three-dimensional P and S velocity models (*Michelini and McEvilly, 1991*), the existing long-term HRSN seismicity catalogue that is complete to very low magnitudes and that includes at least half of the M6 seismic cycle, a well-defined and simple fault segment, the existence of deep nonvolcanic tremor (NVT) activity, and a homogeneous mode of seismic energy release as indicated by the earthquake source mechanisms (over 90% right-lateral strike-slip).

In a series of journal articles and Ph.D. theses, we have presented the cumulative, often unexpected, results of U.C. Berkeley's HRSN research efforts

(see: http://www.seismo.berkeley.edu/seismo/faq/parkfield_bib.html). They trace the evolution of a new and exciting picture of the San Andreas fault zone responding to its plate-boundary loading, and they are forcing new thinking on the dynamic processes and conditions within the fault zone at the sites of recurring small earthquakes and deep nonvolcanic tremors.

The Parkfield area has also become an area of focus of the EarthScope Project (<http://www.earthscope.org>) through the San Andreas Fault Observatory at Depth (SAFOD) experiment (<http://www.icdp-online.de/sites/sanandreas/news/news1.html>). SAFOD is a comprehensive project to drill into the hypocentral zone of repeating $M \sim 2$ earthquakes on the San Andreas Fault at a depth of about 3 km. The goals of SAFOD are to establish a multi-stage geophysical observatory in close proximity to these repeating earthquakes, to carry out a comprehensive suite of down-hole measurements in order to study the physical and chemical conditions under which earthquakes occur and to exhume rock and fluid samples for extensive laboratory studies (*Hickman et al., 2004*).

2. HRSN Overview

2.1 1986 - 1998

Installation of the HRSN deep (200-300m) borehole sensors initiated in 1986 and recording of triggered 500 sps earthquake data began in 1987. The HRSN sensors are 3-component geophones in a mutually orthogonal gimbaled package. This ensures that the sensor corresponding to channel DP1 is aligned vertically and that the others are aligned horizontally. In November 1987, the Varian well vertical array was installed and the first VSP survey was conducted, revealing clear S-wave anisotropy in the fault zone (*Daley and McEvilly, 1990*). During 1988, the original 10 station network was completed, which included a deep (572 m) sensor from the Varian well string. Data from network stations was telemetered into a central detection/recording system operating in triggered mode. Also in 1988, the Varian string system was slaved for about two years to the Vibroseis

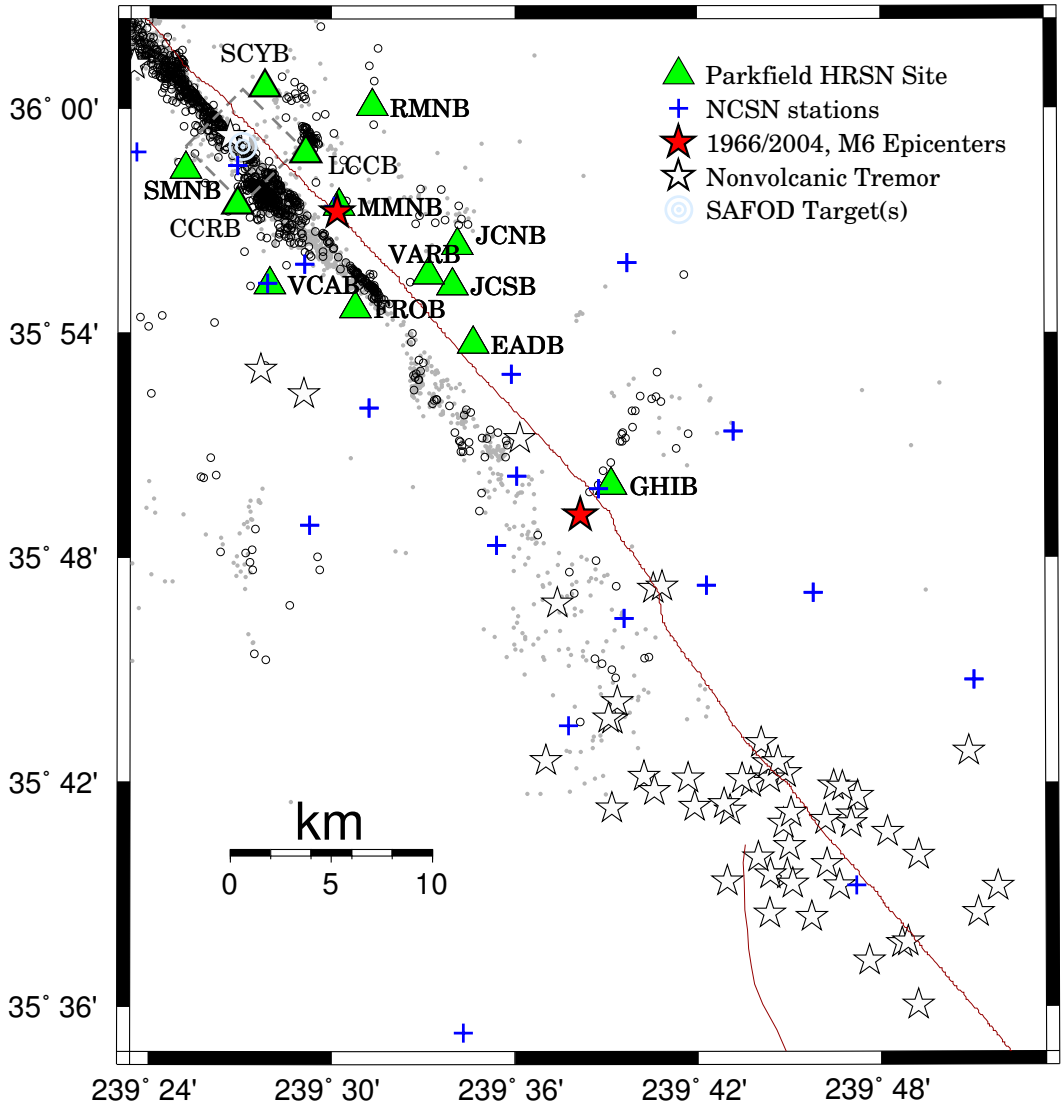


Figure 6.1: Map showing the San Andreas Fault trace and locations of the 13 Parkfield HRSN stations, the repeating M2 SAFOD targets (a 4 km by 4 km dashed box surrounds the SAFOD zone), and the epicenters of the 1966 and 2004 M6 Parkfield main shocks. Also shown are locations of the recently discovered nonvolcanic tremors, routine locations of earthquakes recorded by the expanded and upgraded 13 station HRSN (small open circles) and locations of events recorded by the earlier vintage 10 station HRSN relocated using an advanced 3-D double-differencing algorithm (gray points) applied to a cubic splines interpolated 3-D velocity model (*Michelini and McEvilly, 1991*).

control signals, allowing simultaneous recording of vibrator signals on both systems. For several years beginning in 1991, low-gain event recorders (from PASSCAL) were installed at several of the sites to extend the dynamic range from about M_L 1.5 to about M_L 4.5.

The data acquisition system operated quite reliably until late 1996, when periods of unacceptably high down time developed. During this period, as many as 7 of the remote, solar-powered telemetered stations were occasionally down simultaneously due to marginal solar generation capacity and old batteries, and recording system outages of a week or more were not uncommon. In July 1998, the original data acquisition system failed permanently. This system was a modified VSP recorder acquired from LBNL, based on a 1980- vintage LSI-11 cpu and a 5 MByte removable Bernoulli system disk with a 9-track tape drive, configured to record both triggered microearthquake and Vibroseis data (Vibroseis discontinued in 1994, *Karageorgi et al.*, 1997). The system was remote and completely autonomous, and data tapes were mailed about once a month to Berkeley for processing and analysis. The old system also had a one-sample timing uncertainty and a record length limitation because the tape write system recovery after event detection was longer than the length of the record, leaving the system off-line after record termination and until write recovery was completed.

2.2 1998 - 1999

In December 1998, the original HRSN acquisition system was replaced by 10 stand-alone PASSCAL RefTek systems with continuous recording. To process these data, development of a major data handling procedure will be required in order to identify the microearthquakes down to $M = -1$, since continuous telemetry to the Berkeley Seismological Laboratory (BSL) and application of a central site detection scheme was not an option at that time.

In July 1999, the network was reduced to four RefTeks at critical sites that would ensure continuity in monitoring at low magnitudes and the archive of characteristic events for studying the evolution of their recurrence intervals. Properties of the 10 original sites are summarized in Table 6.2.

2.3 Upgrade and SAFOD Expansion

Thanks to emergency funding from the USGS NEHRP, we replaced the original 10-station system with a modern 24-bit acquisition system (Quanterra 730 4-channel digitizers, advanced software using flash disk technology, spread-spectrum telemetry, Sun Ultra 10/440 central processor at the in-field collection point, with 56K frame-relay connectivity to Berkeley) in 2001. The new system is now online and recording data continuously at a

Sensor	Channel	Rate (sps)	Mode	FIR
Geophone	DP?	250.0	T and C	Ca
Geophone	BP?	20.0	C	Ac

Table 6.3: Data streams currently being acquired at each HRSN site. Sensor type, channel name, sampling rate, sampling mode, and type of FIR filter are given. C indicates continuous; T triggered; Ac acausal; Ca causal. “?” indicates orthogonal vertical and 2 horizontal components.

central site located on California Department of Forestry (CDF) fire station property in Parkfield.

We have also added three new borehole stations, with NSF support, at the NW end of the network as part of the SAFOD project to improve resolution of the structure, kinematics and monitoring capabilities in the SAFOD drill-path and target zones. Figure 6.1 illustrates the location of the drill site, the new borehole sites, and locations of earthquakes recorded by the initial and upgraded/expanded HRSN.

The three new SAFOD stations have a similar configuration as the original upgraded 10 station network and include an additional channel for electrical signals. Station descriptions and instrument properties are summarized in Tables 6.1 and 6.2. All HRSN Q730 data loggers employ FIR filters to extract data at 250 and 20 Hz (Table 6.3).

The remoteness of the drill site and new stations required an installation of an intermediate data collection point at Gastro Peak, with a microwave link to the CDF facility. The HRSN stations use SLIP to transmit TCP and UDP data packets over bidirectional spread-spectrum radio links between the on-site data acquisition systems and the central recording system at the CDF. Six of the sites transmit directly to a router at the central recording site. The other seven sites transmit to a router at Gastro Peak, where the data are aggregated and transmitted to the central site over a 4 MBit/second digital 5.4 GHz microwave link. All HRSN data are recorded to disk at the CDF site.

The upgraded and expanded system is compatible with the data flow and archiving common to all the elements of the BDSN/NHFN and the NCEDC, and is providing remote access and control of the system. It is also providing data with better timing accuracy and longer records, which are to eventually flow seamlessly into NCEDC. The new system also solves the problems of timing resolution, dynamic range, and missed detections, in addition to providing the added advantage of conventional data flow (the old system recorded SEG Y format).

Because of limitations in bandwidth, a modified version of the REDI system (this report) is used to detect events in the HRSN data, extract waveform triggers, and

Site	Net	Latitude	Longitude	Surf. (m)	Depth (m)	Date	Location
EADB	BP	35.89525	-120.42286	466	245	01/1988 -	Eade Ranch
FROB	BP	35.91078	-120.48722	509	284	01/1988 -	Froelich Ranch
GHIB	BP	35.83236	-120.34774	400	63	01/1988 -	Gold Hill
JCNB	BP	35.93911	-120.43083	527	224	01/1988 -	Joaquin Canyon North
JCSB	BP	35.92120	-120.43408	455	155	01/1988 -	Joaquin Canyon South
MMNB	BP	35.95654	-120.49586	698	221	01/1988 -	Middle Mountain
RMNB	BP	36.00086	-120.47772	1165	73	01/1988 -	Gastro Peak
SMNB	BP	35.97292	-120.58009	699	282	01/1988 -	Stockdale Mountain
VARB	BP	35.92614	-120.44707	478	572	01/1988 - 08/19/2003	Varian Well
VARB	BP	35.92614	-120.44707	478	298	08/25/2003 -	Varian Well
VCAB	BP	35.92177	-120.53424	758	200	01/1988 -	Vineyard Canyon
CCRB	BP	35.95718	-120.55158	595	251	05/2001 -	Cholame Creek
LCCB	BP	35.98005	-120.51424	640	252	08/2001 -	Little Cholame Creek
SCYB	BP	36.00938	-120.53660	945	252	08/2001 -	Stone Canyon

Table 6.1: Stations of the Parkfield HRSN. Each HRSN station is listed with its station code, network id, location, date of initial operation, and site description. The latitude and longitude (in degrees) are given in the WGS84 reference frame, the surface elevation (in meters) is relative to mean sea level, and the depth to the sensor (in meters) below the surface. Coordinates and station names for the 3 new SAFOD sites are given at the bottom.

Site	Sensor	Z	H1	H2	RefTek 24	RefTek 72-06	Quanterra 730
EADB	Mark Products L22	-90	170	260	01/1988 - 12/1998	12/1998 - 07/1999	03/2001 -
FROB	Mark Products L22	-90	338	248	01/1988 - 12/1998	12/1998 - 07/1999	03/2001 -
GHIB	Mark Products L22	90	failed	unk	01/1988 - 12/1998	12/1998 - 07/1999	03/2001 -
JCNB	Mark Products L22	-90	0	270	01/1988 - 12/1998	12/1998 - 06/2001	03/2001 -
JCSB	Geospace HS1	90	300	210	01/1988 - 12/1998	12/1998 - 07/1999	03/2001 -
MMNB	Mark Products L22	-90	175	265	01/1988 - 12/1998	12/1998 - 06/2001	03/2001 -
RMNB	Mark Products L22	-90	310	40	01/1988 - 12/1998	12/1998 - 07/1999	03/2001 -
SMNB	Mark Products L22	-90	120	210	01/1988 - 12/1998	12/1998 - 06/2001	03/2001 -
VARB	Litton 1023	90	15	285	01/1988 - 12/1998	12/1998 - 07/1999	03/2001 -
VCAB	Mark Products L22	-90	200	290	01/1988 - 12/1998	12/1998 - 06/2001	03/2001 -
CCRB	Mark Products L22	-90	N45W	N45E	-	-	05/2001 -
LCCB	Mark Products L22	-90	N45W	N45E	-	-	08/2001 -
SCYB	Mark Products L22	-90	N45W	N45E	-	-	08/2001 -

Table 6.2: Instrumentation of the Parkfield HRSN. Most HRSN sites have L22 sensors and were originally digitized with a RefTek 24 system. After the failure of the WESCOMP recording system, PASSCAL RefTek recorders were installed. In July of 1999, 6 of the PASSCAL systems were returned to IRIS and 4 were left at critical sites. The upgraded network uses a Quanterra 730 4-channel system. For the three new stations (bottom) horizontal orientations are approximate (N45W and N45E) and will be determined more accurately as available field time permits.

transmit the waveform segments to the BSL. However, the December 22, 2003 San Simeon earthquake and its aftershocks sent the HRSN into nearly continuous triggering. As a result, BSL staff disabled the transmission of triggered data.

At present, all continuous 20 sps data streams and 7 vertical component channels at 250 sps are telemetered to the BSL and archived on the NCEDC in near-real-time. All continuous 250 sps data are migrated periodically from HRSN computer in Parkfield to DLT tape. These tapes are then mailed periodically to the BSL and then are processed for archiving at the NCEDC.

A feature of the new system that has been particularly useful both for routine maintenance and for pathology identification has been the Internet connectivity of the central site processing computer and the station data loggers with the computer network at BSL. Through this connection, select data channels and on-site warning messages from the central site processor are sent directly to BSL for evaluation by project personnel. If, upon these evaluations, more detailed information on the HRSN's performance is required, additional information can also be remotely accessed from the central site processing computer at Parkfield. Analysis of this remotely acquired information has been extremely useful for trouble shooting by allowing field personnel to schedule and plan the details of maintenance visits to Parkfield. The connectivity also allows certain data acquisition parameters to be modified remotely when needed, and commands can be sent to the central site computer and data loggers to modify or restart processes when necessary.

The network connectivity also allows remote monitoring of the background noise levels being recorded by the HRSN stations. For example, shown in Figure 6.2 are power spectral density plots of background noise for vertical components of the 7 HRSN stations that are most critical for monitoring seismicity in the region containing SAFOD. The PSD analysis gives a rapid assessment of the HRSN seismometer responses across their wide bandwidth. By routinely generating these plots with data telemetered from Parkfield, changes in the seismometer responses, often indicating problems with the acquisition system, can be easily identified, and corrective measures can then be planned and executed on a relatively short time-frame.

3. 2004-2005 Activities

It has been an exceptionally busy year for Berkeley's HRSN project with the 28 September 2004 repeat of the long awaited M6 Parkfield earthquake (*Langbein et al., 2005*), the discovery of nonvolcanic tremor activity (*Nadeau and Dolenc, 2005*; research report ??) and the ongoing SAFOD project (all in addition to the routine operations, maintenance and enhancement of California's

first and longest operating borehole seismic network).

3.1 Operations and Maintenance

Routine maintenance tasks required this year to keep the HRSN in operation, include cleaning and replacement of corroded electrical connections, grounding adjustments, cleaning of solar panels, re-seating, resoldering and replacement of faulty pre-amp circuit cards, the testing and replacement of failing batteries, and insulation and painting of battery and data logger housings to address problems with low power during cold weather.

Remote monitoring of the networks health using the Berkeley Seismological Laboratory's SeisNetWatch software are also performed to identify both problems that can be resolved over the Internet (e.g. rebooting of data acquisition systems due to clock lockups) and more serious problems requiring field visits.

Over the years, such efforts have paid off handsomely by providing exceptionally low noise recordings (Figure 6.2) of very low amplitude seismic signals produced by microearthquakes (even below magnitude -1.0) and non-volcanic tremors.

3.2 Enhancing HRSN Performance

Detection, monitoring, and high-resolution recording of low-amplitude nonvolcanic tremors and earthquakes down to the smallest possible magnitude with the highest possible signal-to-noise (especially in the region of SAFOD drilling) are major objectives of the HRSN data collection effort. The minimization of data loss due to station outages and data-dropouts is critical to these objectives.

Over the past several years we have had a serious decline in the robustness of the power system components (primarily the aging solar panels and batteries that have been in use since initiation of the network in 1987) of the network. Simultaneous outages at multiple stations are now becoming an all too frequent occurrence and are seriously affecting efforts to monitor tremor and micro-and repeating earthquake activity in the Parkfield area.

For example, during the winter of late 2004/early 2005, monitoring for nonvolcanic tremor activity using a standard detection set of 8 HRSN channels revealed significant (and sometimes catastrophic) gaps in the data. Figure 6.3 illustrates the seriousness of the problem with an example from tremor monitoring during periods of overcast weather. During the 7 day period shown, all 8 stations used for monitoring tremor activity were out simultaneously for over 50% of the time. The remaining 50% of the time, outages occurred for at least some of these 8 stations, resulting in significantly degraded capability for unambiguous detection of the low-amplitude tremor activity.

As suspected, further investigation, both remotely and on site, showed that these gaps occurred due to insuffi-

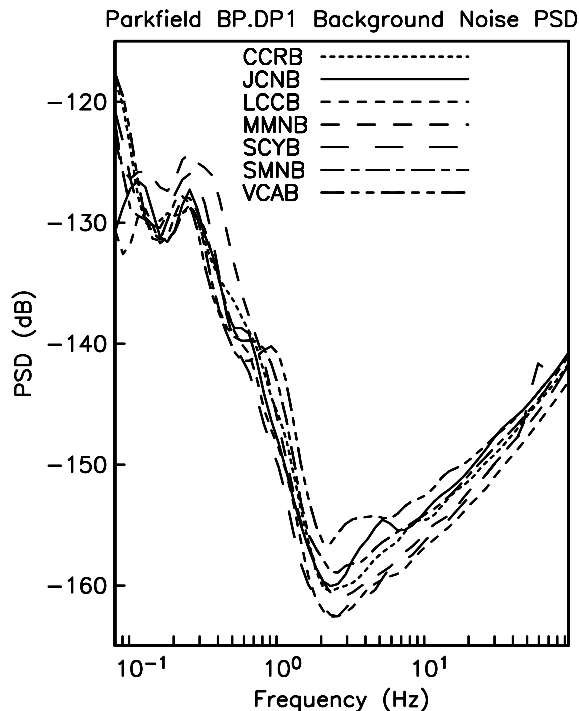


Figure 6.2: Background noise PSD plot for the seven continuously telemetered BP.DP1 data streams from Parkfield. The data are 20 minute samples starting at 2003.225.0900 (2 AM PDT). The plots show the background noise PSD as a function of frequency for the highest available sampling rate (250 sps) vertical component data which are continuously telemetered to Berkeley. Note the relatively low PSD levels and the overall consistency for all the HRSN stations. The 2 Hz minimum in the PSD plots for the HRSN sensor arises due to the 2 Hz sensors used at these sites. Below 2 Hz, noise levels rise rapidly and the peak at 3 sec (.3 Hz) is characteristic of teleseismic noise observed throughout California. In the 2 to 5 Hz range, VCAB and JCNB have historically shown higher background noise which is believed to result from excitation modes in the local structure. A small 60 Hz blip can be seen in the SCYB curve due to its close proximity to a power-line.

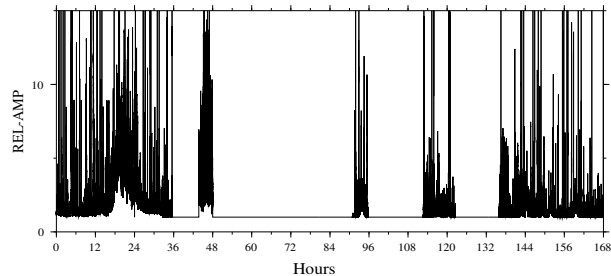


Figure 6.3: Stacked root-mean-square seismograms for the 8 stations of the HRSN used in monitoring tremor activity. Shown are 7 days of data starting at Hour 00 (UTC) of day 7 of 2005. Times when relative RMS amplitudes (REL-AMP) are 1.0 indicate periods when all 8 stations were out simultaneously.

cient battery re-charge at many of the network’s stations, which are remote solar powered installations. In previous years, similar but less severe data gaps have occurred during the winter months and have been attributed to overcast skies during the rainy season. Last winters exceptionally heavy rainy season exacerbated the outage problem to an intolerable level, and to avoid a potential repeat of the situation, efforts are now underway to refurbish and upgrade the solar power systems.

More specifically, the following steps are being taken: 1) replacement of the oldest batteries and switching of the remaining old batteries to the less power consuming pre-amplifiers; 2) improvement of the wiring scheme along the lines suggested by the solar power representative; 3) upgrade/replacement of solar panels. (Solar panels degrade at $\sim 1\%$ per year, and newer versions have improved output. Since the installation of the HRSN over 18 years ago, the same size/format panel has gone from 40 watts to 55). This is a relatively easy field task, and should gain us 20-30% capacity at each site.

Among the three newer sites (CCRB, SCYB, LCCB), both the batteries and solar panels are relatively new. Nonetheless, stations CCRB and LCCB both had some outages last winter, which is most likely explained by the limited sunlight in these areas due to hilly terrain. We plan, therefore, to add one more solar panel at each of these sites to enhance their power system robustness.

3.3 SAFOD Collaboration

An intensive and ongoing effort by the SAFOD target event location working group is underway with the following goals: 1) the characterization of the detailed velocity and seismicity structure in the crustal volume containing the SAFOD main hole and 2) to determine the most accurate estimates of the absolute locations of SAFOD’s target events. The HRSN data play a key role in this effort by providing low noise and high sensitivity

seismic waveforms from active and passive sources and by providing a backbone of earthquake and tremor detection and waveforms from the numerous microearthquakes and tremors that are occurring in the general vicinity of SAFOD.

In a special section of Geophysical Research Letters from May of 2004, several papers make significant use of the HRSN data for characterizing the SAFOD area and illustrate the role that the HRSN data have played in the SAFOD effort over the past year (e.g., *Oye et al.*, 2004; *Roecker et al.*, 2004; *Thurber et al.*, 2004; *Nadeau et al.*, 2004).

In addition to the data collection, Berkeley’s other contributions also include detailed monitoring of the repeating M2 SAFOD target sequences, and in particular, this year, their evolving pattern of behavior following the 28 September 2004, M6 Parkfield earthquake (Figure 6.4).

3.4 Data Processing

Monitoring the evolution of nonvolcanic tremors and microseismicity, particularly in the SAFOD drilling and target zone, is a primary objective of the HRSN project. In addition, the continued analysis of the HRSN data for determining detailed seismic structure, for the study of similar and characteristic microearthquake systematics, for estimation of deep fault slip rate evolution, and for various studies of fault zone and earthquake physics is also of great interest to seismologists. Before advanced studies of the Parkfield microseismicity can take place, however, initial processing, analysis, and routine cataloging of the earthquake data must be done. An integral part of this process is quality control of the processed data, including a final check of the routine catalog results.

The numerous and ongoing aftershocks from the December 2003 M6.5 San Simeon and Sept. 2004 M6.0 Parkfield earthquakes (Figure 6.5) have seriously complicated the tasks of initial processing, analysis, and location of the routine event catalog, calling for a significant revision of the “traditional” processing scheme we have used since 1987. Due to the severely limited resources available for reviewing, picking, and locating the tens of thousands of very small microearthquakes that have been detected by the HRSN since the San Simeon and Parkfield quakes, we have opted to focus on cataloging a critical subset of the data (i.e., the similar and characteristically repeating earthquakes). These subsets of data have found particular utility for a variety of applications, and because of their unique properties, these data lend themselves particularly well to automated processing.

Most of our efforts during 2000-2002 were spent on implementing the emergency upgrade and SAFOD expansion of the HRSN. Routine processing of the data collected during that period was deferred until after upgrade and installation efforts were completed. In 2003,

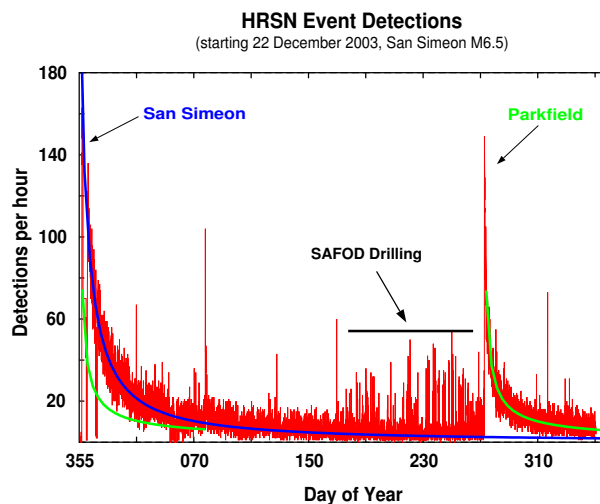


Figure 6.5: Shown are the number of HRSN triggers per hour for a period beginning with the San Simeon earthquake and continuing through several months after the Parkfield earthquake. For comparison, before these two large events, the average number of hourly HRSN triggers was less than 0.5 (i.e., about 10 per day). “Eyeball” fits of the decay curves for both events are also shown. The cumulative number of HRSN triggers in the first 5 months following San Simeon exceeded 70,000 and trigger levels continued to be over 150 triggers per day through to the Parkfield quake. In the first month following the Parkfield quake over 40,000 triggers were recorded. Extrapolation of the decay curve indicates that daily trigger levels will not return to near pre-San Simeon levels until well into 2007. At the same time, funding to support analyst’s time for routine processing and cataloging of the events has virtually dried-up, requiring the development and implementation of a new scheme for cataloging events.

• The SAFOD magnitude 2 target quakes continue to repeat

- Stress from the Parkfield M6 **did not** terminate the sequences.
- Stress from the M6 **did** shorten their recurrence times.
- The shortening implies ~ 8 cm of afterslip surrounding the M2 targets for the 71 days after the M6

Conclusions:

- 1) The M2 quakes remain viable targets for SAFOD.
- 2) Continued shorter than average recurrence times for future target quakes is expected due to ongoing afterslip from the M6.

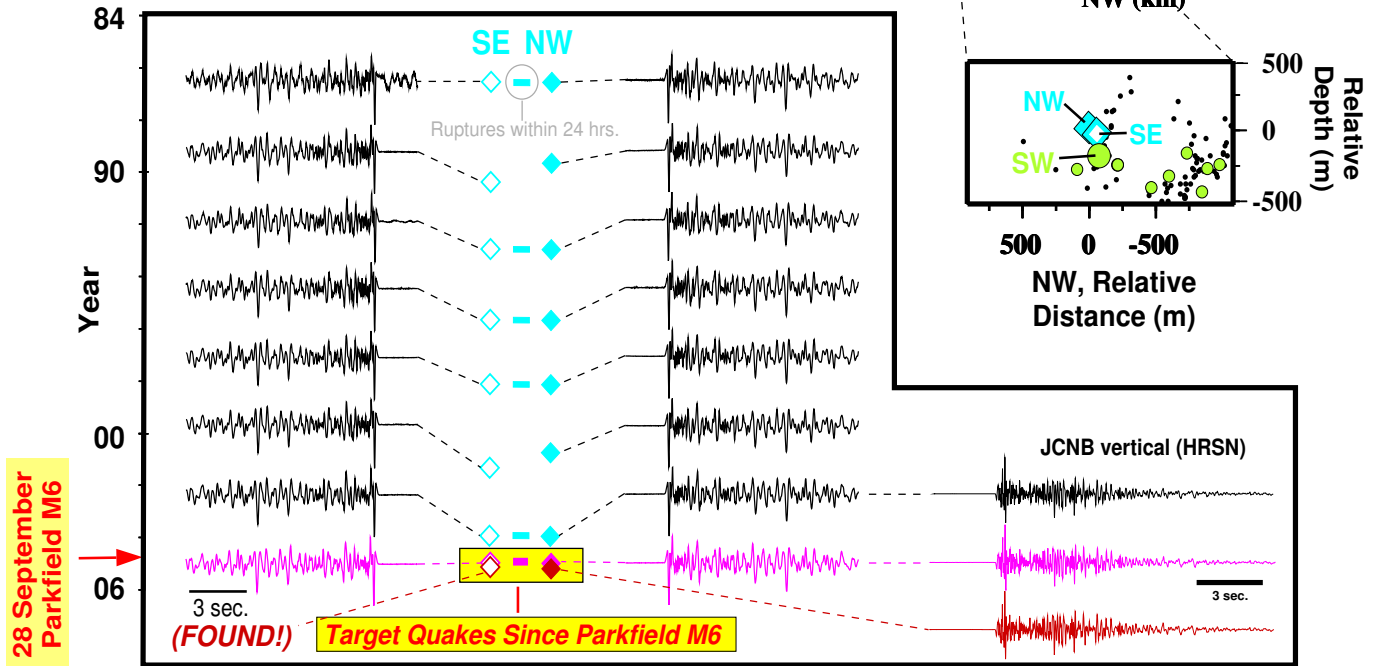


Figure 6.4: Upper right panel shows a 40 km along fault depth section of the San Andreas Fault that includes the epicenters of the 1966 and 2004 Parkfield M6 earthquakes (box and star respectively), HRSN catalog locations of seismicity in the region preceding the 2004 M6 event (black points) and the region containing the SAFOD target sequences of repeating M2 earthquakes (small box). Zoom box of the SAFOD region shows that the SAFOD target region actually contains numerous sites of repeating microearthquakes (circles and diamonds). The diamonds labeled NW and SE are the two primary M2 sequences being considered as targets for close-in monitoring and eventual penetration. Large circle labeled SW is also an ~ M2 repeating site that lies ~ 2-300 meters to the southwest of the primary targets and lies between the SAFOD drill site and the primary targets. Lower panel shows waveforms from the target sequence events occurring since 1984 and into the period immediately following the Parkfield mainshock. Waveforms on the left are from surface NCSN station PCA (VHZ channel) and the three on the right are from the HRSN. The much higher sampling rate and borehole sensors of the HRSN are critical in identifying and discriminating between repeats of the primary targets that are located only ~ 70 m apart and whose waveforms among the NCSN recordings are virtually indistinguishable. Both the primary target (NW and SE) and SW sequences experienced several repeats during the year following the 2004 M6 (for comparison, prior to the M6 the recurrence times of sequence members was generally once every ~ 3 years). During January of 2005 (between SAFOD's Phase 1 and Phase 2 drilling periods) a string of seismic sensors was deployed down the SAFOD hole and recorded one of the post-M6 SE sequence repeats. This close-in information in conjunction with recordings from the HRSN, NCSN, the temporary PASO deployment and the SAFOD pilot hole string led to some surprises regarding the accuracy of the absolute location estimates for the primary target sequences, and provided critical information for guiding drilling during phase 2 in the summer of 2005.

we began in earnest the task of routine processing of the ongoing data that was being collected. Our initial focus was on refining and developing our processing procedures to make the task more efficient and to ensure quality control of the processed catalogs. We also began working back in time to fill in the gap that developed during the deferment period. Because routine processing of the post-San Simeon and Parkfield data is effectively impossible at this time due to the overwhelming number of aftershocks, we have suspended our efforts at routine processing the ongoing data using the our existing procedures and have instead focused on development of an automated processing scheme for the similar and repeating events.

The basic scheme that we are now developing for processing these events involves first the compilation of a set of reference event waveforms, picks, and magnitudes. Using the continuous HRSN data now being collected and archived, waveform segments from the reference event catalog are then automatically scanned through the continuous data using cross-correlation sweeps to find waveform matches indicating the time of occurrence of a similar event. In the process a cross-correlation time alignment for the event is also obtained for each station. Following this initial sweep, the time alignments are used automatically to compile event triggered (snippet) data from the continuous records and phase specific cross-correlation alignments are automatically made to obtain fine scale P and S phase picks. These picks are then used to obtain catalog locations, and low-amplitude spectral ratios of the aligned waveforms with the reference event are then made automatically to obtain seismic moment and magnitude estimates.

Data Flow

Initial Processing. Continuous data streams on all 38 HRSN components are recorded at 20 and 250 sps on disk on the local HRSN computer at the CDF facility. The 20 sps data are transmitted continuously to the Berkeley Seismological Laboratory (BSL) over a frame-relay link and then archived at the NCEDC. In addition, the vertical component channels for the 7 stations critical to resolving seismicity in the SAFOD area are also being transmitted continuously to the BSL at 250 sps over the frame relay-circuit for purposes of quality control and fine tuning the triggering algorithm for the detection of the smallest possible events around SAFOD. These telemetered 250 sps data are archived on disk for only about 1 week at the BSL and are then deleted. When the local HRSN computer disk space is full, the continuous 250 sps data on the HRSN local computer are migrated onto DLT tape, and the tapes sent to Berkeley for long-term storage and for upload to disc into the NCEDC archive.

Shortly after being recorded to disk on the central site HRSN computer, event triggers for the individual

station data are determined, and a multi-station trigger association routine then processes the station triggers and identifies potential earthquakes. For each potential earthquake that is detected, a unique event identification number (compatible with the NCEDC classification scheme) is assigned. Prior to San Simeon earthquake of December 22, 2003, 30 second waveform segments were then collected for all stations and components and saved to local disk as an event gather, and event gathers were then periodically telemetered to BSL and included directly into the NCEDC earthquake database (dbms) for analysis and processing.

Because of its mandate to detect and record very low magnitude events in the Parkfield area, the HRSN is extremely sensitive to changes in very low amplitude seismic signals. As a consequence, in addition to detecting very small local earthquakes at Parkfield, the HRSN also detects numerous regional events. Since the beginning of the network's data collection in 1987, the local and regional events were discriminated based on analyst assessment of S-P times, and only local events with S-P times less than ~ 2.5 sec at the first arriving station were picked and located as part of the HRSN routine catalog.

Following the occurrence of the M6.5 San Simeon earthquake on December 22, of 2003, our long-standing data handling procedure was no longer viable due to the enormous rate of San Simeon aftershock detections (Figures 6.5) In the first 5 months following the mainshock, over 70,000 event detections were made by the HRSN system (compared to a yearly average detection rate of 6000 prior to San Simeon), and spot checks of the continuous 20 sps data revealed that the overwhelming majority of these detections resulted from seismic signals generated by San Simeon's aftershocks.

Data from the California Integrated Seismic Network (CISN) show that there were $\sim 1,150$ San Simeon aftershocks with magnitudes > 1.8 occurring in the week following the mainshock. During this same period, the number of event detections from the HRSN was $\sim 10,500$ (compared to an average weekly for the year prior to San Simeon of 115 detections/per week). This suggests that the HRSN is detecting San Simeon aftershocks well below magnitude 1, despite the network's ~ 50 km distance from the mainshock.

The dramatic increase in event detections vastly exceeded the HRSN's capacity to process both the continuous and triggered event waveform data. To prevent the loss of seismic waveform coverage, processing of the triggered waveform data has been suspended to allow archiving of the 250 sps continuous data to tape to continue uninterrupted. Cataloging of the event detection times from the modified REDI real-time system algorithm is also continuing, and the 250 sps waveform data is currently being periodically uploaded from the DLT tapes onto the NCEDC for access to the research research com-

munity, and its NCEDC accessibility will also play a vital role in the automated similar event catalog processing that we are currently developing.

4. Acknowledgements

Thomas V. McEvilly, who passed away in February 2002, was the PI on the HRSN project for many years. Without his dedication, the creation of the HRSN would not have been possible. Under Bob Nadeau's and Doug Dreger's general supervision, Rich Clymer, Bob Uhrhammer, Doug Neuhauser, Don Lippert, Bill Karavas, John Friday, and Pete Lombard all contribute to the operation of the HRSN. Bob Nadeau prepared this chapter. During this reporting period, operation, maintenance, and data processing for the HRSN project was supported by the USGS, through grants: 04HQGR0085 and 05HQGR0080.

5. References

- Bakun, W. H., and A. G. Lindh, The Parkfield, California, prediction experiment, *Earthq. Predict. Res.*, *3*, 285-304, 1985.
- Daley, T.M. and T.V. McEvilly, Shear wave anisotropy in the Parkfield Varian Well VSP, *Bull. Seism. Soc. Am.*, *80*, 857-869, 1990.
- Hickman, S., M.D. Zoback and W. Ellsworth, Introduction to special section: Preparing for the San Andreas Fault Observatory at Depth, *Geophys. Res. Lett.*, *31*, L12S01, doi:10.1029/2004GL020688, 2004.
- Karageorgi, E., R. Clymer and T.V. McEvilly, Seismological studies at Parkfield. II. Search for temporal variations in wave propagation using Vibroseis, *Bull. Seism. Soc. Am.*, *82*, 1388-1415, 1992.
- Karageorgi, E., R. Clymer and T.V. McEvilly, Seismological studies at Parkfield. IV: Variations in controlled-source waveform parameters and their correlation with seismic activity, 1987-1994, *Bull. Seismol. Soc. Am.*, *87*, 39-49, 1997.
- Langbein, J., R. Borchardt, D. Dreger, J. Fletcher, J.L. Hardebeck, M. Hellweg, C. Ji, M. Johnston, J.R. Murray, R. Nadeau M.J. Rymer, and J.A. Treiman, Preliminary Report on the 28 September 2004, M 6.0 Parkfield, California Earthquake, *Seismo. Res. Lett.*, *76*, 10-26, 2005.
- Michelini, A. and T.V. McEvilly, Seismological studies at Parkfield: I. Simultaneous inversion for velocity structure and hypocenters using B-splines parameterization, *Bull. Seismol. Soc. Am.*, *81*, 524-552, 1991.
- Nadeau, R.M. and D. Dolenc, Nonvolcanic Tremors Deep Beneath the San Andreas Fault, *SCIENCE*, *307*, 389, 2005.
- Nadeau, R.M., A. Michelini, R.A. Uhrhammer, D. Dolenc, and T.V. McEvilly, Detailed kinematics, structure and recurrence of micro-seismicity in the SAFOD target region, *Geophys. Res. Lett.*, *31*, L12S08, doi:10.1029/2003GL019409, 2004.
- Oye, V., J.A. Chavarria and P.E. Malin, Determining SAFOD area microearthquake locations solely with Pilot Hole seismic array data, *Geophys. Res. Lett.*, *31*, L12S10, doi:10.1029/2003GL019403, 2004.
- Roecker, S., C. Thurber and D. McPhee, Joint inversion of gravity and arrival time data from Parkfield: New constraints on structure and hypocenter locations near the SAFOD drillsite, *Geophys. Res. Lett.*, *31*, L12S04, doi:10.1029/2003GL019396, 2004.
- Thurber, C., S. Roecker, H. Zhang, S. Baher and W. Ellsworth, Fine-scale structure of the San Andreas fault zone and location of the SAFOD target earthquakes, *Geophys. Res. Lett.*, *31*, L12S02, doi:10.1029/2003GL019398, 2004.

Chapter 7

Bay Area Regional Deformation Network

1. Introduction

The Bay Area Regional Deformation (BARD) network of continuously operating Global Positioning System (GPS) receivers monitors crustal deformation in the San Francisco Bay area (“Bay Area”) and northern California (Murray *et al.*, 1998). It is a cooperative effort of the BSL, the USGS, and several other academic, commercial, and governmental institutions. Started by the USGS in 1991 with 2 stations spanning the Hayward fault (King *et al.*, 1995), BARD now comprises more than 70 permanent stations (Figure 7.1, Tables 7.1 and 7.2). The principal goals of the BARD network are: 1) to determine the distribution of deformation in northern California across the wide Pacific–North America plate boundary from the Sierras to the Farallon Islands; 2) to estimate three-dimensional interseismic strain accumulation along the San Andreas Fault (SAF) system in the Bay Area to assess seismic hazards; 3) to monitor hazardous faults and volcanoes for emergency response management; and 4) to provide infrastructure for geodetic data management and processing in northern California in support of related efforts within the surveying and other interested communities.

Among others, BARD includes 14 stations near Parkfield along the central San Andreas Fault, and 17 near the Long Valley caldera near Mammoth. The BSL maintains 22 stations [including 2 with equipment provided by Lawrence Livermore National Laboratory (LLNL) and UC Santa Cruz]. Other stations are maintained by the USGS (Menlo Park and Cascade Volcano Observatory), LLNL, Stanford Linear Accelerator, UC Davis, UC Santa Cruz, Hat Creek Radio Observatory, U. Wisconsin, Haselbach Surveying Instruments, East Bay Municipal Utilities District, the City of Modesto, the National Geodetic Survey, Thales, Inc., and the Jet Propulsion Laboratory. Many of these stations are part of larger networks devoted to real-time navigation, orbit determination, and crustal deformation.

Between 1993 and 2001, the BSL acquired 29 Ashtech Z-12 and Micro-Z receivers from a variety of funding sources, including from federal (NSF and USGS), state

(CLC), and private (EPRI) agencies. The network enhances continuous strain measurements in the Bay Area and includes several profiles between the Farallon Islands and the Sierra Nevada in order to better characterize the larger scale deformation field in northern California (Figure 7.1). Five sites have been equipped as part of the NSF-funded Mini-PBO project to establish collocated GPS, and borehole strainmeter and seismometer observatories in the Bay Area (see Chapter 8).

The number of continuous GPS stations in northern California is significantly increasing with over 250 new site installations planned by 2008 as part of the Plate Boundary Observatory (PBO) component of the NSF-funded Earthscope project. UNAVCO and researchers from BARD and the other regional networks, such as SCIGN, BARGEN, and PANGA, are funded by NSF to fold operation and maintenance of about 200 existing stations, which constitute the PBO Nucleus network, into the PBO array by 2008. Two BSL-maintained stations (SUTB and MUSB) are included in the PBO Nucleus network. The other BSL stations are either collocated with seismic instrumentation or are located near the San Andreas Fault where real-time processing of the GPS data for earthquake notification is a high priority. Another 23 northern California stations, including most of the Parkfield network, will be included in the PBO Nucleus, and we are working closely with UNAVCO to facilitate their transition to UNAVCO control.

Today, raw and RINEX data files from the BSL stations and the other stations run by BARD collaborators are archived at the BSL/USGS Northern California Earthquake Data Center (NCEDC) data archive maintained at the BSL (Romanowicz *et al.*, 1994). The data are checked to verify their integrity, quality, completeness, and conformance to the RINEX standard, and are then made accessible, usually within 2 hours of collection, to all BARD participants and other members of the GPS community through Internet, both by anonymous FTP and by the World Wide Web (<http://www.ncedc.org/bard/>).

Many of the BARD sites are classified as CORS stations by the NGS, and are used as reference stations by

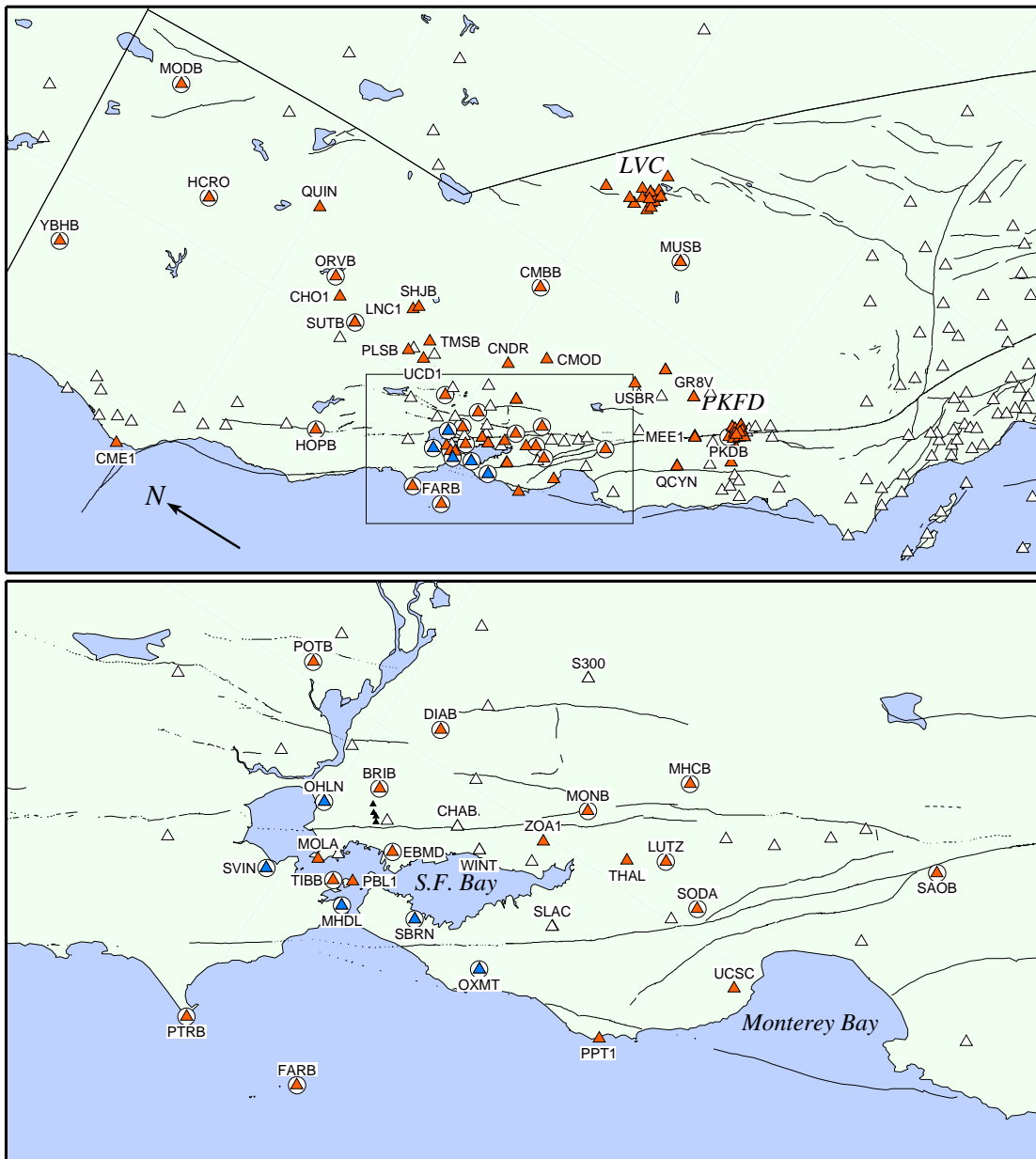


Figure 7.1: Operational BARD stations (dark triangles) in northern California (top) and in the San Francisco Bay area (bottom), including an 18-station network near the Long Valley Caldera (LVC) and a 14-station network near Parkfield (PKFD). In the oblique Mercator projection expected Pacific–North America relative plate motion is parallel to the horizontal. Circled stations use continuous real-time telemetry. The small black triangles near BRIB are the experimental L1 stations. Light triangles are PBO and Nucleus (previously existing continuous stations now part of PBO) stations operating in July 2005.

Code	Latitude	Longitude	Start	Receiver	Maint.	Telem.	Location
BRIB	37.91940	-122.15255	1993.58	A-Z12	BSL	FR	Briones Reservation, Orinda
CMBB	38.03418	-120.38604	1993.92	A-Z12	BSL	FR	Columbia College, Columbia
DIAB	37.87858	-121.91563	1998.33	A-Z12	BSL	FR	Mt. Diablo
FARB	37.69721	-123.00076	1994.00	A-Z12	BSL	R-FR/R	Farallon Island
HOPB	38.99518	-123.07472	1995.58	A-Z12	BSL	FR	Hopland Field Station, Hopland
LUTZ	37.28685	-121.86522	1996.33	A-Z12	BSL	FR	SCC Comm., Santa Clara
MHCB	37.34153	-121.64258	1996.33	A-Z12	BSL	FR	Lick Obs., Mt. Hamilton
MODB	41.90233	-120.30283	1999.83	A-Z12	BSL	NSN	Modoc Plateau
MOLA	37.94657	-122.41992	1993.75-2002.22	T-SSE	BSL		Pt. Molate, Richmond
MONB	37.49892	-121.87131	1998.50	A-Z12	BSL	FR	Monument Peak, Milpitas
MUSB	37.16994	-119.30935	1997.83	A-Z12	BSL	R-Mi-FR	Musick Mt.
OHLN	38.00742	-122.27371	2001.83	A-uZ	BSL	FR	Ohlone Park, Hercules
ORVB	39.55463	-121.50029	1996.83	A-Z12	BSL	FR	Oroville
OXMT	37.49936	-122.42432	2004.12	A-uZ	BSL	FR	Ox Mt., Half Moon Bay
PKDB	35.94524	-120.54155	1996.67	A-Z12	BSL	FR	Bear Valley Ranch, Parkfield
POTB	38.20258	-121.95560	1998.92-2005.12	A-Z12	BSL	FR	Potrero Hill, Fairfield
PTRB	37.99640	-123.01490	1998.58	A-Z12	BSL	R-FR	Point Reyes Lighthouse
SAOB	36.76530	-121.44718	1997.58	A-Z12	BSL	FR	San Andreas Obs., Hollister
SBRN	37.68622	-122.41044	2003.18	A-uZ	BSL	FR	San Bruno Mt., Brisbane
SODB	37.16640	-121.92552	1996.33	A-Z12	BSL	R-FR	Soda Springs, Los Gatos
SUTB	39.20584	-121.82060	1997.33	A-Z12	BSL	R-FR	Sutter Buttes
SVIN	38.03318	-122.52632	2003.89	A-uZ	BSL	R-FR	St. Vincents, San Rafael
TIBB	37.89087	-122.44760	1994.42	A-Z12	BSL	R	Tiburon
YBHB	41.73166	-122.71073	1996.75	A-Z12	BSL	FR	Yreka Blue Horn Mine, Yreka
CAND	35.93935	-120.43370	1999.33	A-Z12	USGS	R-FR	Cann, Parkfield
CARH	35.88838	-120.43082	2001.58	A-Z12	USGS	R-FR	Carr Hill 2, Parkfield
CARR	35.88835	-120.43084	1989.00-2003.31	A-Z12	JPL		Carr Hill, Parkfield
CRBT	35.79161	-120.75075	2001.67	A-Z12	USGS	R-FR	Camp Roberts, Parkfield
HOGS	35.86671	-120.47949	2001.50	A-Z12	USGS	R-FR	Hogs, Parkfield
HUNT	35.88081	-120.40238	2001.58	A-Z12	USGS	R-FR	Hunt, Parkfield
LAND	35.89979	-120.47328	1999.33	A-Z12	USGS	R-FR	Lang, Parkfield
LOWS	35.82871	-120.59428	2001.58	A-Z12	USGS	R-FR	Lowes, Parkfield
MASW	35.83260	-120.44306	2001.58	A-Z12	USGS	R-FR	Mason West, Parkfield
MIDA	35.92191	-120.45883	1999.75	A-Z12	USGS	R-FR	Mida, Parkfield
MNMC	35.96947	-120.43405	2001.58	A-Z12	USGS	R-FR	Mine Mt., Parkfield
POMM	35.91991	-120.47843	1999.75	A-Z12	USGS	R-FR	Pomm, Parkfield
RNCH	35.89999	-120.52482	2001.58	A-Z12	USGS	R-FR	Ranchita, Parkfield
TBLP	35.91741	-120.36034	2001.67	A-Z12	USGS	R-FR	Table, Parkfield

Table 7.1: Currently operating stations of the BARD GPS network maintained by the BSL and by the BSL/USGS/SCIGN in the Parkfield region. Receivers: A = Ashtech, T = Trimble. See Table 3.2 for telemetry codes and for BSL sites collocated with seismic stations. Data from other agencies retrieved or pushed by FTP or from the Web.

the surveying community. We coordinate efforts with surveying community at meetings of the Northern California GPS Users Group and the California Spatial Reference Center. Data and ancillary information about BARD stations are also made compatible with standards set by the International GPS Service (IGS), which administers the global tracking network used to estimate precise orbits and has been instrumental in coordinating the efforts of other regional tracking networks. The

NCEDC also retrieves data from other GPS archives, such as at SIO, JPL, and NGS, in order to provide a complete archive of all high-precision continuous GPS measurements collected in northern California.

2. 2004-2005 Activities

The typical configuration of a BSL continuous GPS station installation has been described in detail in pre-

Code	Latitude	Longitude	Start	Receiver	Maint.	Location
CHAB	37.72412	-122.11931	1992.00	A-Z12	USGS	Chabot, San Leandro
WINT	37.65264	-122.14056	1992.00	A-Z12	USGS	Winton, Hayward
EBMD	37.81501	-122.28380	1999.18	T-SSi	EBMUD	EBMUD, Oakland
QUIN	39.97455	-120.94443	1992.68	Rogue	JPL	Quincy
S300	37.66642	-121.55815	1998.48	T-SSi	LLNL	Site 300, Livermore
HCRO	40.81563	-121.46915	2003.50	T-SSi	HCRO	Hat Creek Radio Obs.
CHO1	39.43264	-121.66496	1999.50	A-Z12	NGS	Chico
CME1	40.44177	-124.39633	1995.74	A-Z12	NGS	Cape Mendocino
CMOD	37.64130	-121.99997	2000.76	T-SSi	City	Modesto
CNDR	37.89641	-121.27849	1999.27	A-Z12	NGS	Condor, Stockton
PBL1	37.85306	-122.41944	1995.50-2004.19	A-Z12	NGS	Point Blunt, Angel Island
PPT1	37.18167	-122.39333	1996.00	A-Z12	NGS	Pigeon Point
SLAC	37.41652	-122.20426	2002.34	Leica	SLAC	Stanford Linear Accel. Center
SUAA	37.42691	-122.17328	1994.30-2003.10	A-Z12	SU	Stanford University
THAL	37.35149	-121.93549	2003.00	A-uZ	Thales	Thales, Inc., Santa Clara
UCD1	38.53624	-121.75123	1996.38	T-SSi	UCD	UC Davis
UCSC	36.99279	-122.05219	2000.31-2002.67	T-SSi	UCSC	UC Santa Cruz
ZOA1	37.54305	-122.01594	2002.50	Novatel	FAA	Fremont
GR8V	36.39901	-120.41577	2003.04	T-5700	UWisc	San Andreas Creeping Segment
MEE1	36.18690	-120.75860	2003.02	T-5700	UWisc	San Andreas Creeping Segment
MEE2	36.18052	-120.76684	2003.03	T-5700	UWisc	San Andreas Creeping Segment
QCYN	36.16116	-121.13748	2003.05	T-5700	UWisc	San Andreas Creeping Segment
USBR	36.84257	-120.43567	2004.30	T-SSi	CVWD	Central Valley
CCID	36.73901	-120.35657	2004.30	T-NetRS	CVWD	Mendota, Central Valley
LNC1	38.84651	-121.35023	2003.51	A-Z12	NGS	Lincoln
PLSB	38.68530	-121.76150	2004.14	Leica	Haselbach	Woodland
SHJB	38.81418	-121.29606	2003.22	Leica	Haselbach	Rocklin
TMSB	38.57078	-121.54922	2003.22	Leica	Haselbach	West Sacramento
BALD	37.78330	-118.90130	1999.67	A-ZFX	CVO	Bald Mt., LVC
CA99	37.64460	-118.89670	1999.67	A-ZFX	CVO	Casa 1999, LVC
CASA	37.64464	-118.89666	1993.00	Rogue	JPL	Casa Diablo, LVC
DDMN	37.74430	-118.98120	1999.67	A-ZFX	CVO	Deadman Creek, LVC
DECH	38.05150	-119.09060	2001.58	A-ZFX	CVO	Dechambeau Ranch, LVC
HOTK	37.65860	-118.82130	2001.67	A-Z12	CVO	Hot Creek, LVC
JNPR	37.77170	-119.08470	1997.81	A-Z12	USGS	Juniper, LVC
KNOL	37.65912	-118.97917	1998.58	A-ZFX	CVO	Knolls, LVC
KRAC	37.71330	-118.88050	2001.67	A-Z12	CVO	Krakatoa-USGS, LVC
KRAK	37.71313	-118.88114	1994.73-2004.04	Rogue	JPL	Krakatoa, LVC
LINC	37.63719	-119.01729	1998.67	A-Z12	CVO	Lincoln, LVC
MINS	37.65376	-119.06090	1995.92	A-Z12	USGS	Minaret Summit, LVC
MWTP	37.64052	-118.94473	1998.58	A-ZFX	CVO	Mammoth Water Treat Plant, LVC
PMTN	37.83130	-119.05690	1999.67	A-Z12	CVO	Panorama Mt., LVC
RDOM	37.67707	-118.89794	1998.58	A-ZFX	CVO	Resurgent Dome, LVC
SAWC	37.68990	-118.95310	2000.65	A-ZFX	CVO	Saw, LVC
TILC	37.61890	-118.86280	2000.65	A-Z12	CVO	Tilla, LVC
WATC	37.66440	-118.65390	2001.67	A-Z12	CVO	Waterson, LVC

Table 7.2: Currently operating stations of the BARD GPS network maintained by other agencies and by the USGS Cascade Volcano Observatory (CVO) in the Long Valley caldera region. Other agencies include: EBMUD = East Bay Mun. Util. Dist., UCD = UC Davis, SU = Stanford Univ., UCSC = UC Santa Cruz, UWisc = U. of Wisconsin, City = City of Modesto (see also Table 2.1). Data from other agencies retrieved or pushed by FTP or from the Web.

vious annual reports. We here provide a brief description and highlight some of the recent changes. During July 2004–June 2005, we performed maintenance and improved telemetry at existing BARD stations, assisted with the transfer of several stations to PBO control, and prepared for a new station installation in the Marin Headlands.

2.1 BARD Stations

Each BSL BARD station uses a low-multipath choking antenna, most of which are mounted to a reinforced concrete pillar approximately 0.5–1.0 meter above local ground level. The reinforcing steel bars of the pillar are drilled and cemented into rock outcrop to improve long-term monument stability. A low-loss antenna cable is used to minimize signal degradation on the longer cable setups that normally would require signal amplification. Low-voltage cutoff devices are installed to improve receiver performance following power outages. Most use Ashtech Z-12 receivers that are programmed to record data once every 30 seconds and observe up to 12 satellites simultaneously at elevations down to the horizon. The antennas are equipped with SCIGN antenna adapters and hemispherical domes, designed to provide security and protection from weather and other natural phenomena, and to minimize differential radio propagation delays. The BSL acquired 7 Ashtech MicroZ-CGRS (uZ) receivers with NSF funding for the Mini-PBO project. These receivers, designed for continuous station applications, use less power (5.6 W) than the Z-12 receivers due to the lack of an interactive screen, provide better remote receiver control, and can support serial telemetry in both native raw format and the receiver independent BINEX format.

Data from most BSL-maintained stations are collected at 30-second intervals and transmitted continuously over serial connections (Table 7.1). Station TIBB uses a direct radio link to Berkeley, and MODB uses VSAT satellite telemetry. Most stations use frame relay technology, either alone or in combination with radio telemetry. Fourteen GPS stations are collocated with broadband seismometers and Quanterra data loggers (Table 3.2). With the support of IRIS we developed software that converts continuous GPS data to MiniSEED opaque blockettes that are stored and retrieved from the Quanterra data loggers (*Perin et al.*, 1998), providing more robust data recovery from onsite disks following telemetry outages.

Data from DIAB, MONB, OHLN, OXMT, SBRN, SVIN, and TIBB in the Bay Area, and 13 stations in the Parkfield region (all but PKDB), are now being collected at 1-second intervals. All high-rate observations collected by these stations are currently available from the NCEDC. Collecting at such high-frequency (for GPS) allows dynamic displacements due to large earthquakes to be better measured; however, this 30-fold increase

in data can pose telemetry bandwidth limitations. We are planning to convert additional stations to 1-second sampling where possible during the next year. In the Bay Area, we have converted stations that have sufficient bandwidth and are currently assessing bandwidth issues at other stations. Prior to the September 28, 2004 M6 Parkfield earthquake, data from the Parkfield stations were collected on an on-site computer, written to removable disk once per month, and sent to SOPAC for long-term archiving (decimated 30-sec data is acquired daily via the BSL frame relay circuit). In response to the earthquake, we modified the procedures to download 1-second data converted to compact RINEX format at hourly intervals, which does not significantly impact the telemetry bandwidth.

The BSL also acquired several Wi-Lan VIP 110-24 VINES Ethernet bridge radios. These 2.4 GHz spread spectrum radios use a tree structure to create a distributed Ethernet backbone with speeds up to 11 Mbps. Each system uses a directional antenna to talk to its “parent” in the tree, and an omni-directional antenna to talk to its children, if multiple, or a directional antenna if it has only 1 child. These radios offer several advantages over the Freewave radios used at other sites, including TCP/IP Ethernet control, higher bandwidth, and greater flexibility for setting up networks. We installed a set of Wi-Lan radios at the SVIN Mini-PBO station to transmit data from the site to the frame relay circuit, and are assisting EBMUD in converting their continuous station to real-time telemetry using Wi-Lan radios.

2.2 Station Maintenance

In February 2005, we terminated operations of the Potrero Hills site POTB, which had been operating since December 1998, as well as the collocated seismic instrumentation, due to the transfer of property ownership. The operations of BARD stations at Chabot (CHAB) maintained by the USGS, and SLAC maintained by the Stanford Linear Accelerator were transferred to the Plate Boundary Observatory in May 2005. The SLAC receiver replaced the nearby SUAA receiver that Stanford formally stopped maintaining during this last year. As part of our collaboration with the Hat Creek Radio Observatory, we swapped the HCRO GPS receiver several times during the year to facilitate their use of RTK instrumentation. HCRO will transfer to the PBO network in Fall 2005. We are currently planning to install a new GPS station as part of the completion of the Marin Headlands (MHDL) Mini-PBO station in Fall 2005, which has been awaiting the establishment of AC power.

We improved data telemetry at several stations during the last year. Replacement of a corroded cable allowed data from BRIB to be telemetered via the collocated Quanterra data logger. The Cylink radios used for FARB was replaced with a Wi-Lan radio as part of a

reconfiguration of the telemetry paths through UC San Francisco rather than Mount Tamalpais. As part of this reconfiguration and coincident with the replacement of a badly rusted antenna mast, the Freewave radio path at PTRB was adjusted to pass through UCSF, although data recovery was hampered for several months by problems with an improperly oriented radio antenna.

We also performed routine maintenance at several sites during the year, including replacement of cables and batteries at the GRIZ and VOLM L1-profile stations, and replacement of a failing Ashtech Z-12 receiver at YBHB November 2004. Several Ashtech uZ receivers have also failed by progressively recording few and fewer satellites, first at OXMT in 2003, then at OHLN in August 2004, and more recently at SVIN. Ashtech believes that a bad capacitor was installed in this series of receivers. These receivers will be repaired in Fall 2005.

3. Data Analysis and Results

We use the GAMIT/GLOBK software developed at MIT and SIO to process data from the BARD and other nearby continuous GPS networks. Recent improvements to GAMIT/GLOBK include better accounting of ocean-tide effects, estimating gradients in atmospheric variations, and applying elevation-dependent weighting to the data observables. We process data from more than 70 stations within hours of the completion of the day using rapid or predicted orbits. We have also reprocessed older data from the present to 1991 using improved orbits, and combined these solutions with global IGS solutions provided by SOPAC. Data from over 20 IGS fiducial sites located in North America and Hawaii are included in the solutions to help define a global reference frame.

The estimated relative baseline determinations typically have 1–3 mm long-term scatter in the horizontal components and the 5–10 mm scatter in the vertical. Average velocities for the longest running BARD stations relative to stable North America during 1993–2004 are shown in Figure 7.2, with 95% confidence regions assuming white noise. Also shown are preliminary velocities determined for the PBO and PBO Nucleus networks during 2004–2005.5. In a study using only the continuous GPS stations in northern California and Nevada (*Murray and Segall, 2001*), we found that the northern Sierra Nevada–Central Valley is tectonically stable with 3 mm/yr right-lateral shear across the Walker Lane–Mt. Shasta seismicity trend. Deformation along the coast in central California is dominated by the active SAF system, which accommodates about 35 mm/yr of right-lateral shear. Our recent Bay Area Velocity Unification (BÄVÜ) study combines survey-mode and continuous GPS solutions into a self-consistent velocity field in the San Francisco Bay area and develops a three-dimensional block model appropriate for the complex fault geometries (*d’Alessio et al.,*

2005). This study finds interseismic rates on faults that are consistent with geologic estimates, undetectable San Andreas Fault-normal compression in the Bay Area, and evidence for up to 5 mm/yr right-lateral shear deformation just east of the central San Andreas Fault.

Transient signals have been observed on BARD stations from at least 3 earthquakes in northern California, including the August 1998 M_w 5.1 San Juan Bautista earthquake (*Uhrhammer et al., 1999*), and the December 2003 M_w 6.5 San Simeon earthquake (*Rolandone et al., 2004; Murray et al., 2004*). The long-anticipated 28 September 2005 M_w 6.0 Parkfield significantly displaced all the continuous BARD stations in the Parkfield region, many of which collect at 1-second sampling intervals, allowing very accurate discrimination between coseismic and postseismic displacements. Significant postseismic displacements have been observed at all the stations within 30 km of the fault, most exceeding the coseismic displacements (Figures 7.3 and 7.4). At CARH, which is located between two strands of the San Andreas fault, the postseismic displacements towards the southeast are opposite in direction to the northwest coseismic displacement. Together with creepmeters and borehole strainmeters, the 2004 Parkfield earthquake was one of the most well recorded earthquakes using geodetic data (*Langbein et al., 2005*). Preliminary results from our investigations of finite-fault rupture models for the Parkfield earthquake from inversions of seismic and geodetic data (*Dreger et al., 2005*) are presented in the research section (13.2.).

4. Real-Time Processing

We are developing real-time analysis techniques that will enable rapid determinations (within minutes) of deformation following major earthquakes to complement seismological information. We use GAMIT/GLOBK processing techniques to estimate independent hourly solutions at the several cm-level horizontal precision and during the past year established an extension of the REDI system where estimates of postseismic positions are attempted when 10 minutes of data become available following an earthquake (*Murray et al., 2002*). We currently process 1-hour data batches available within 20 minutes of measurement from more than 20 continuously telemetered BSL and other stations providing hourly data. The hourly solutions have higher scatter than the 24-hour solutions (3–10 mm in the horizontal and 10–30 mm in the vertical), but our simulations suggest that displacements 3–5 times these levels should be reliably detected, and that the current network should be able to resolve the finite dimensions and slip magnitude of a M7 earthquake on the Hayward Fault.

We are testing a relatively new component of GAMIT that uses Kalman filtering techniques and improved am-

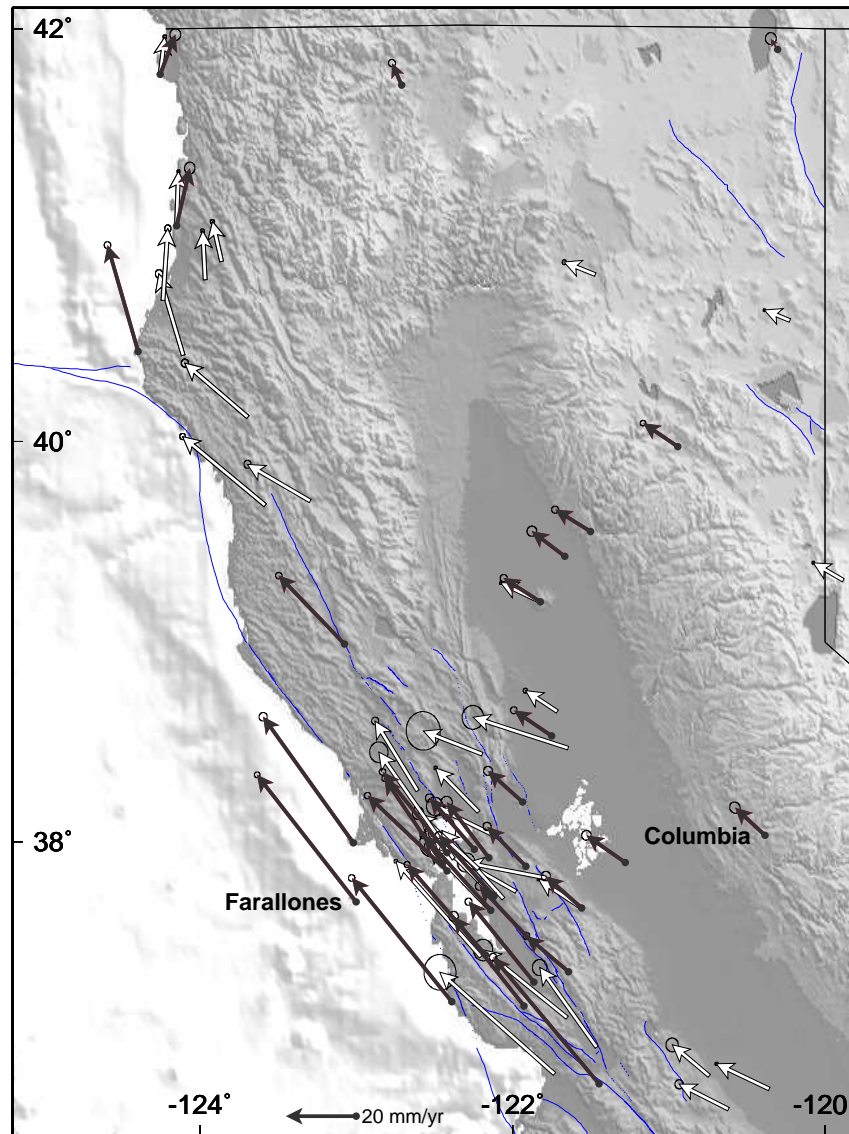


Figure 7.2: Velocities relative to stable North America for the BARD stations derived from 1993–2005 data (dark arrows) and for the PBO and Nucleus stations from 2004–2005.5 (white arrows). Ellipses show 95% confidence regions, assuming white noise only. The 35 mm/yr motion between Columbia and the Farallones is primarily due to shear across the San Andreas fault system.

ambiguity resolution methods to provide higher-precision kinematic positions. We are testing these rapid processing techniques to estimate higher frequency 1-Hz GPS displacements, which have been used to detect surface from large earthquakes and can potentially add valuable information about the seismic source. We are also developing methods to rapidly estimate finite-source models from coseismic GPS displacements and to use these

models to predict strong-ground motions and improve ShakeMap depictions of these motions as rapidly as possible after an earthquake. The first step of this project has been the development of a new methodology to improve prediction of strong ground motion from a simple uniform-slip geodetic model of the source. This methodology is based on a simple assumption that the large slip should take longer to terminate. We use well known scal-

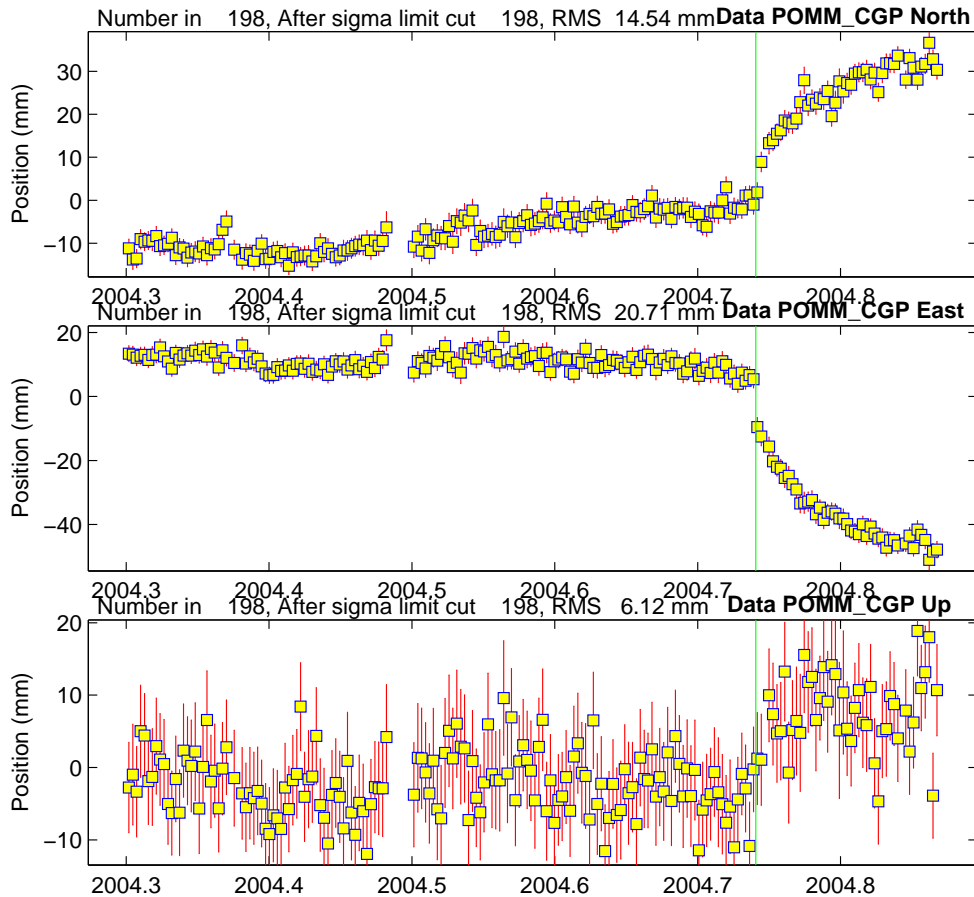


Figure 7.3: Daily position timeseries for POMM, a continuous GPS station located close to the epicenter of the 28 September 2004 Parkfield earthquake. The coseismic displacement, based on one-second solutions, is about 24 mm to the primarily to the west. The postseismic deformation after one-month is about 61 mm to the northwest. Most sites in the continuous network show significant levels of postseismic deformation following an exponential or logarithmic variation in displacement.

ing relations between stress drop and slip velocity to develop a spatio-temporal slip model. We have tested this model on the 1992 Northridge earthquake and found that the predicted ground motions agree well with observed motions and with other models derived from combinations of seismic and geodetic data (*Rhie et al.*, 2005).

5. Acknowledgements

Mark Murray oversees the BARD program. Wade Johnson, Rich Clymer, Cedric de La Beaujardiere, Bill Karavas, John Friday, and Doug Neuhauser contributed to the operation of the BARD network.

6. References

Bürgmann, R., D. Schmidt, R.M. Nadeau, M. d’Alessio, E. Fielding, D. Manaker, T. V. McEvelly, and

M. H. Murray, Earthquake potential along the northern Hayward fault, California, *Science*, 289, 1178–1182, 2000.

d’Alessio, M. A., I. A. Johanson, R. Bürgmann, D. A. Schmidt, and M. H. Murray, Slicing up the San Francisco Bay Area: Block kinematics from GPS-derived surface velocities, *J. Geophys. Res.*, 110, B06403, doi:10.1029/2004JB003496, 2005.

Dreger, D. S., L. Gee, P. Lombard, M. H. Murray, and B. Romanowicz, Rapid finite-source analysis and near-fault strong ground motions: Application to the 2003 Mw 6.5 San Simeon and 2004 Mw 6.0 Parkfield earthquakes, *Seismol. Res. Lett.*, 76(1), 40–48, 2005.

King, N. E., J. L. Svarc, E. B. Fogleman, W. K. Gross, K. W. Clark, G. D. Hamilton, C. H. Stiffler, and J. M. Sutton, Continuous GPS observations across the Hayward fault, California, 1991–1994, *J. Geophys. Res.*, 100, 20,271–20,283, 1995.

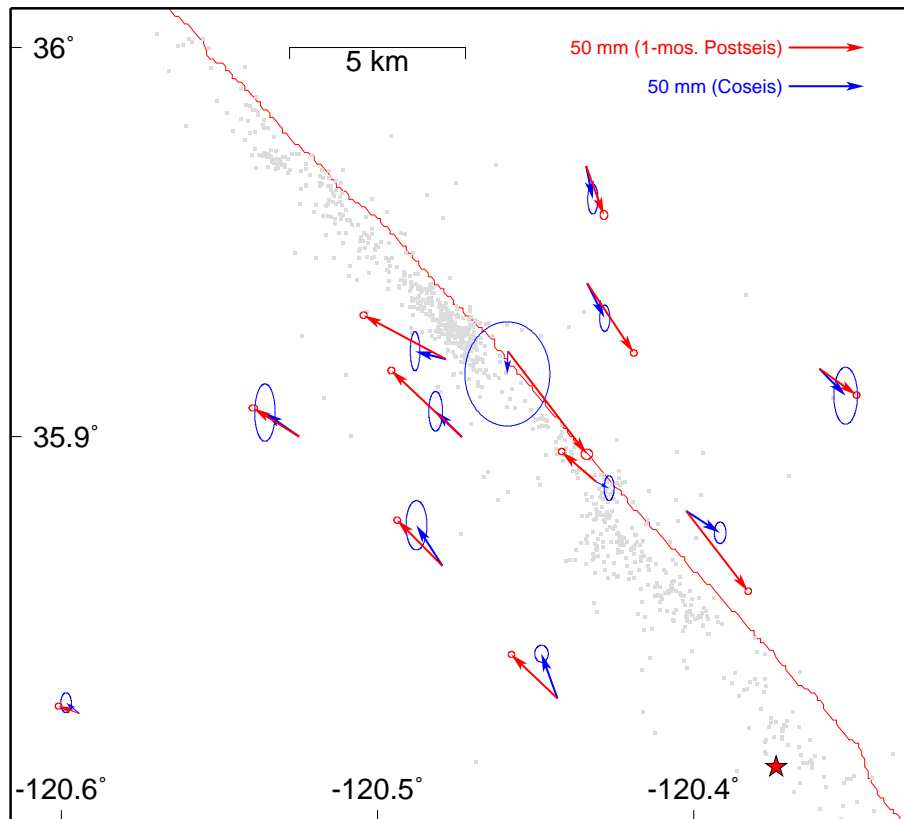


Figure 7.4: Coseismic and postseismic deformation of the 28 September 2004 Parkfield earthquake, which ruptured a 25 km section of the fault within the network (star, epicenter; gray circles, aftershocks). Coseismic are from one-second solutions, and postseismic are from daily solutions one-month following the earthquake.

Langbein et al. (M. H. Murray, contributor), Preliminary report on the 28 September 2004, M 6.0 Parkfield, California earthquake, *Seismol. Res. Lett.*, 76(1), 10–26, 2005.

Murray, M. H., and P. Segall, Continuous GPS measurement of Pacific–North America plate boundary deformation in northern California and Nevada, *Geophys. Res. Lett.*, 28, 4315–4318, 2001.

Murray, M. H., R. Bürgmann, W. H. Prescott, B. Romanowicz, S. Schwartz, P. Segall, and E. Silver, The Bay Area Regional Deformation (BARD) permanent GPS network in northern California, *EOS Trans. AGU*, 79(45), Fall Meeting Suppl., F206, 1998.

Murray, M., Neuhauser D., Gee, L., Dreger, D., Basset, A., and Romanowicz, B., Combining real-time seismic and geodetic data to improve rapid earthquake information, *EOS. Trans. AGU*, 83(47), G52A-0957, 2002.

Murray, M.H., D.C. Agnew, R. Bürgmann, K. Hurst, R.W. King, F. Rolandone, J. Svarc, GPS Deformation measurements of the 2003 San Simeon earthquake, *Seism. Res. Lett.*, 75, 295, 2004.

Perin, B. J., C. M. Meertens, D. S. Neuhauser, D. R. Baxter, M. H. Murray, and R. Butler, Institutional

collaborations for joint seismic and GPS measurements, *Seismol. Res. Lett.*, 69, 159, 1998.

Rhie, J., D. Dreger, and M. H. Murray, A prediction of strong ground motions from geodetic data for PGV ShakeMaps, *Geophys. Res. Lett.*, in prep., 2005.

Rolandone, F., I. Johanson, and R. Bürgmann, Geodetic observations of the M6.5 San Simeon earthquake with focus on the response of the creeping segment of the San Andreas fault, *Seism. Res. Lett.*, 75, 293, 2004.

Romanowicz, B., B. Bogaert, D. Neuhauser, and D. Oppenheimer, Accessing northern California earthquake data via Internet, *EOS Trans. AGU*, 75, 257–260, 1994.

Uhrhammer, R., L. S. Gee, M. Murray, D. Dreger, and B. Romanowicz, The M_w 5.1 San Juan Bautista, California earthquake of 12 August 1998, *Seismol. Res. Lett.*, 70, 10–18, 1999.

Chapter 8

Plate Boundary Deformation Project

1. Introduction

The Integrated Instrumentation Program for Broadband Observations of Plate Boundary Deformation, commonly referred to as “Mini-PBO”, is a joint project of the BSL, the Department of Terrestrial Magnetism at Carnegie Institution of Washington (CIW), the IGPP at UC San Diego (UCSD), and the U.S. Geological Survey (USGS) at Menlo Park, Calif. It augments existing infrastructure in central California to form an integrated pilot system of instrumentation for the study of plate boundary deformation, with special emphasis on its relation to earthquakes. This project was partially funded through the EAR NSF/IF program with matching funds from the participating institutions and the Southern California Integrated Geodetic Network (SCIGN).

Because the time scales for plate boundary deformation range over at least 8 orders of magnitude, from seconds to decades, no single technique is adequate. We have initiated an integrated approach that makes use of three complementary and mature geodetic technologies: continuous GPS, borehole tensor strainmeters, and interferometric synthetic aperture radar (InSAR), to characterize broadband surface deformation. Also, ultrasensitive borehole seismometers monitor microearthquake activity related to subsurface deformation.

The project has three components: 1) the installation of broadband deformation stations in the San Francisco Bay area; 2) the installation of GPS stations in the Parkfield region; and 3) support for skeletal operations of a 5-m X-band SAR downlink facility in San Diego to collect and archive radar data, and develop an online SAR database for WInSAR users. The BSL has participated in the first two of these components. Additional details about the Parkfield GPS stations, installed in 2001 to link the BARD network in central and northern California to the SCIGN network in southern California and currently operating in real-time streaming mode with instantaneous position analysis, are provided in the BARD chapter of this report. The remainder of this chapter describes San Francisco Bay area broadband deformation station component of this project.

The broadband deformation stations augment existing instrumentation along the Hayward and San Andreas faults in the San Francisco Bay area (Figure 8.1). During July 2001 to August 2002, five boreholes were drilled and equipped with tensor strainmeters and 3-component L22 (velocity) seismometers (Table 8.1). These were the first deployments of a new type of strainmeter developed by CIW that use 3 sensing volumes placed in an annulus with 120-degree angular separation (Figure 8.2, which allows the 3-component horizontal strain tensor to be determined. All of the stations include pore pressure sensors and 2-component tiltmeters. Four of the stations now are equipped with GPS receivers recording at 1 sample per second and Quanterra recording systems that provide 100-Hz seismic and strainmeter data. The GPS antennas at these stations are mounted at the top of the borehole casings to achieve stable compact monuments. These stations complement existing Bay Area stations of the BARD continuous network, the BDSN and HFN seismic networks, and borehole dilatometers along the southern Hayward fault and in the San Juan Bautista region.

Although the EarthScope project decided not to install the CIW hydraulic strainmeter systems due to logistical considerations, many of the techniques developed during this project have been adopted for use in the Plate Boundary Observatory strainmeter network, including the compact GPS antenna mount.

2. Mini-PBO Station Configuration

The general configuration of borehole instrument installation at each Mini-PBO station is shown in Figure 8.3. A 6.625” steel casing was cemented into a 10.75” hole to 500-650’ depth to prevent the upper, most unconsolidated materials from collapsing into the hole. Below this depth a 6” uncased hole was drilled to the target region for the strainmeter and seismometer packages. Coring, in order to identify the region with the most competent rock for the strainmeter, was attempted with only moderate success at a few of the holes and was not attempted at

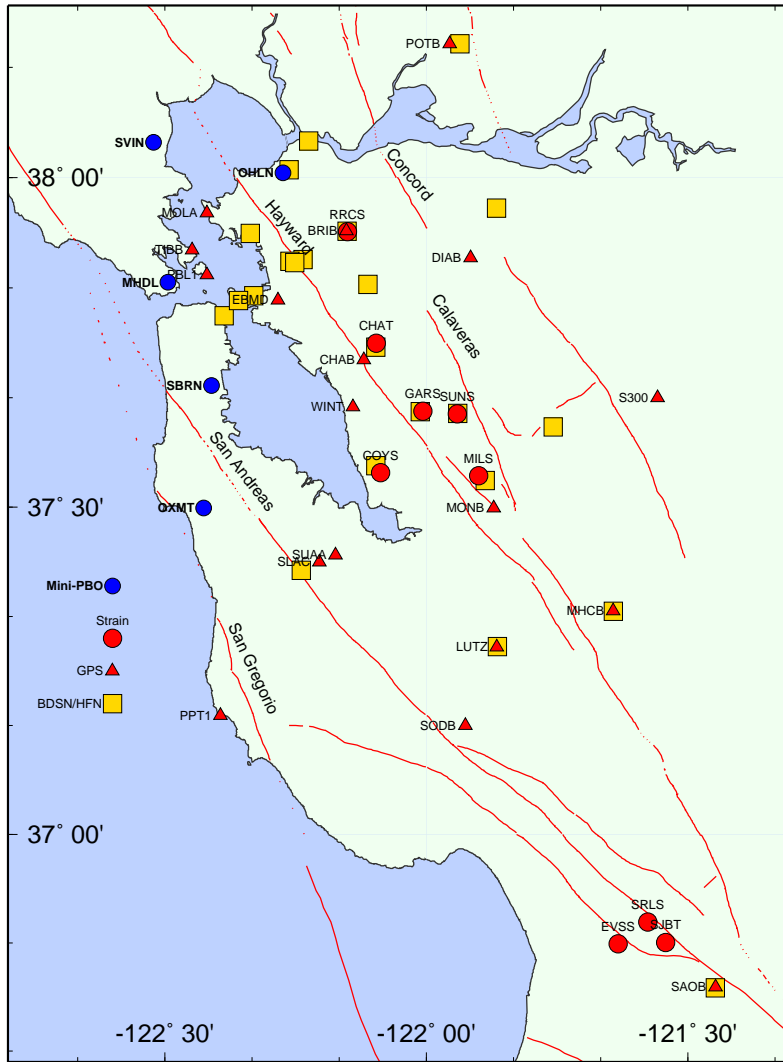


Figure 8.1: Map of San Francisco Bay and San Juan Bautista area with existing borehole strainmeter and continuous GPS stations. The 5 new Mini-PBO stations (blue) complement the existing configuration of BARD GPS (red triangles) and borehole strainmeter sites (red circles) and BDSN and borehole HFN seismic stations (yellow).

Code	Latitude	Longitude	Installed	Strainmeter depth (ft)	Seismometer depth (ft)	Location
OHLN	38.00625	-122.27299	2001/07/16	670.5	645.5	Ohlone Park, Hercules
SBRN	37.68622	-122.41044	2001/08/06	551.5	530.0	San Bruno Mtn. SP, Brisbane
OXMT	37.49936	-122.42431	2002/02/06	662.7	637.3	Ox Mtn., Half Moon Bay
MHDL	37.84227	-122.49374	2002/08/06	520.6	489.2	Golden Gate NRA, Sausalito
SVIN	38.03318	-122.52632	2002/08/29	527.0	500.0	St. Vincent CYO School, San Rafael

Table 8.1: Operating stations of the Mini-PBO network. Strainmeter installation date is given. Depth to tensor strainmeter and 3-component seismometers in feet. High-frequency seismic and strainmeter data, and 1-Hz GPS data are available at all sites except MHDL.

St. Vincents. We found that video logs provided a reasonable substitute. The target region of each hole was

filled with a non-shrink grout into which the strainmeter was lowered, allowing the grout to completely fill the in-

ner cavity of the strainmeter within the annulus formed by the sensing volumes to ensure good coupling to the surrounding rock.

The 3-component seismometer package was then lowered to just above the strainmeter, on a 2" PVC pipe, and neat cement was used to fill the hole and PVC pipe to entirely enclose the package. The pipe above this depth was left open for later installation of the pore pressure sensor. To allow water to circulate into the pipe from the surrounding rock for the pore pressure measurements, the steel casing was perforated, a sand/gravel pack was emplaced, and a PVC screen was used at this depth. At each hole, the casing was then cemented inside to about 200', and outside to about 20' depth. A 12" PVC conductor casing was cemented on the outside from the surface to 20' to stabilize the hole for drilling and to provide an environmental health seal for shallow groundwater flow. The annulus between the 12" conductor casing and the 6.625" steel casing was cemented to about 10' depth and above was left decoupled from the upper surface to help minimize monument instability for the GPS antenna mounted on top of the steel casing.

The BSL developed a GPS mount for the top of the borehole casings to create a stable, compact monument. This design will be used at the more than 140 PBO strainmeter stations to be installed over the next 5 years. The antennas, using standard SCIGN adapters and domes for protection, are attached to the top of the 6-inch metal casing, which will be mechanically isolated from the upper few meters of the ground. The casing below this level is cemented fully to the surrounding rock. The GPS mount design consists of two 11-inch diameter stainless steel flanges. The lower slip- and- weld type flange is welded onto the top of the borehole casing providing a level surface for the second flange. The upper blind-type flange, to which the 1 1/4" stainless steel pipe used to connect to the SCIGN DC3 adaptor is attached, is bolted to the lower flange and includes two offset stainless steel dowels to insure precise self-centering alignment. During the period July 2003–June 2004, the BSL completed the installation of GPS systems using the borehole mount at St. Vincents School for Boys (SVIN) near San Rafael and at the Ox Mt site (OXMT) near Half Moon Bay.

Two-component tiltmeters were installed at all the stations by the USGS in 2003. Data from these sensors are recorded at 10-minute intervals and telemetered using the GOES system. Pore pressure sensors are also installed at all the stations and data are recorded at 1 Hz on the Quanterra dataloggers, except at Marin Headlands, where 10-minute interval data are also recorded on the Zeno datalogger.

The 1-Hz GPS, and 100-Hz strainmeter and seismometer data is acquired on Quanterra data loggers and continuously telemetered by frame relay to the BSL. Low frequency (600 second) data (including strainmeters, for re-

dundancy) is telemetered using the GOES system to the USGS. All data is available to the community through the Northern California Earthquake Data Center (NCEDC) in SEED format, using procedures developed by the BSL and USGS to archive similar data from 139 sites of the USGS ultra-low-frequency (UL) geophysical network, including data from strainmeters, tiltmeters, creep meters, magnetometers, and water well levels.

The BSL is supervising GPS, power, frame relay telemetry, and Quanterra 4120 datalogger installation and maintenance at all the broadband deformation stations. Power, telemetry, and dataloggers are currently installed at all stations except MHDL, where we are waiting for PG&E to install the power drop. Telemetry at SVIN was established in June 2003 using Wi-LAN radios, a new type of radio that the BSL is currently beginning to adopt. These radios act as Ethernet bridges, providing superior access to console control on the Quanterras. The radios can also provide a spanning tree network structure for a regional wireless network, which allows greater flexibility for future network installations. We will use Wi-LAN radios at MHDL as well to provide a link between the borehole site and the frame-relay network interface circuit, which is located about 0.5 miles from the site.

2.1 2004-05 Activities

The BSL and USGS are addressing minor problems at the stations. Highly correlated low-amplitude noise had contaminated the seismic and strain channels at several of the stations, mostly due to electrical ground loop issues. Replacement of strainmeter electronics boxes and moving the placement of some cables resolved many of the problems although minor issues remain at OHLN, which continues to be contaminated by 600-second frequency noise due to the satellite data transmission. The USGS replaced the tiltmeter at SVIN in September 2004, recorded 24 hours of downhole thermister data in October 2004, repressurized the pore pressure packer at SVIN and installed a thermister at SBRN in December 2004. PG&E has scheduled work to install the AC power at MHDL in Fall 2005, after which we will complete the installation of the fifth Mini-PBO station.

3. Broadband Deformation Data

The borehole seismic packages provide good signal to noise characteristics compared to the NHFN stations due to their relatively deep installation. The systems have the best signal to noise near their 2-Hz characteristic frequency. The deepest installation at OXMT has the lowest noise at higher frequencies (Figure 8.4). We are considering adding a pre-amplifier to these systems to improve their signal-to-noise characteristics, since microseismic noise typically found around 0.1 Hz is not evident on most of the sites. These stations currently sample at

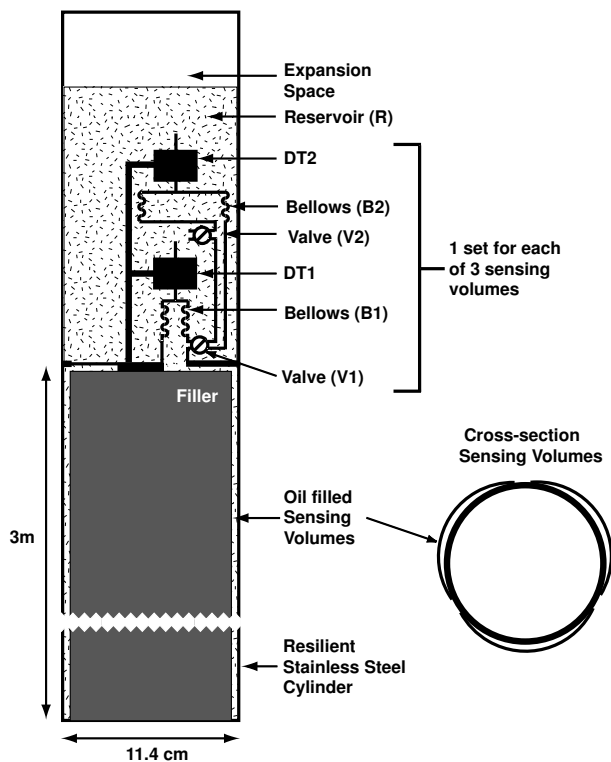


Figure 8.2: Tensor strainmeter diagram. These instruments are a modification of hydraulic sensing dilatometer design to achieve a volume strain sensitivity of 10^{*-12} with constant frequency response from 0 to more than 10 Hz and a dynamic range of about 130 dB. The design incorporates a second bellows- DT- valve sub- system which provides extended dynamic range, complete preservation of baseline during required instrumental resets, and redundant sensing electronics. Figure courtesy A. Linde (USGS).

100-Hz, so they miss some of the seismic energy at high frequencies that are observed on the 500-Hz Parkfield borehole stations. Analysis of GPS observations show that the short-term daily repeatabilities in the horizontal components are about 0.5-1 mm, and annual signals with about 1 mm amplitude. These values are similar to those obtained with more typical monuments, such as concrete piers or braced monuments.

The tensor strainmeters appear to faithfully record strain signals over a broad frequency range, except at the longest periods where the strains show a long-term exponential signal. This large signal is most likely due to cement hardening effects and re-equilibration of stresses in the surrounding rock in response to the sudden appearance of the borehole. These effects can last for many years and are the principal reason that borehole strainmeters cannot reliably measure strain at periods greater than a few months.

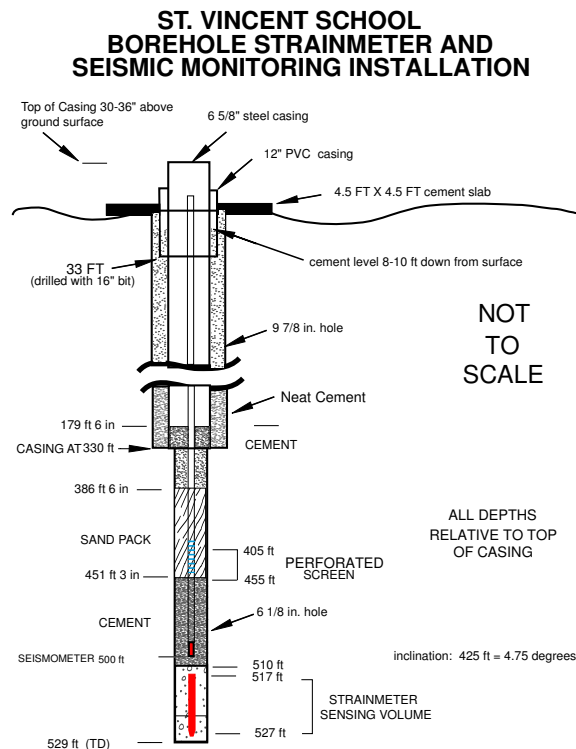


Figure 8.3: The Mini-PBO borehole configuration at St. Vincents, showing the emplacement of the strainmeter and seismometer instruments downhole. The GPS receiver is mounted on the top. Figure courtesy B. Mueller (USGS).

At periods around 1 day, tidally induced strains are the dominant strain signal. Since the response of the strainmeter volumes is difficult to estimate independently, theoretically predicted Earth tides are typically used to calibrate the strainmeters. Figure 8.5 shows the approximate microstrain of the OHLN strainmeter over a several month period interval, and some of the steps required to clean the data, including removing the tides and atmospheric pressure effects. The remaining signal is highly correlated with rainfall, indicating the extent that hydrologic events can affect strain. The proximity of the strainmeters to the San Francisco Bay complicates the determinations of theoretical tides due to ocean and bay loading effects, a problem that has not been resolved for all the strainmeters, particularly for OHLN, which exhibits a physically unrealistic negative M2 tide.

At higher frequencies, strains due to seismic events are also well recorded. The December 26, 2004 M=9 Great Sumatra earthquake excited free oscillations of the Earth that were measurable on the Mini-PBO strainmeters and nearby dilatometers in California. Figure 8.6 shows a preliminary comparison of observed and theoretical normal modes measured at 4 stations. In this band, a num-

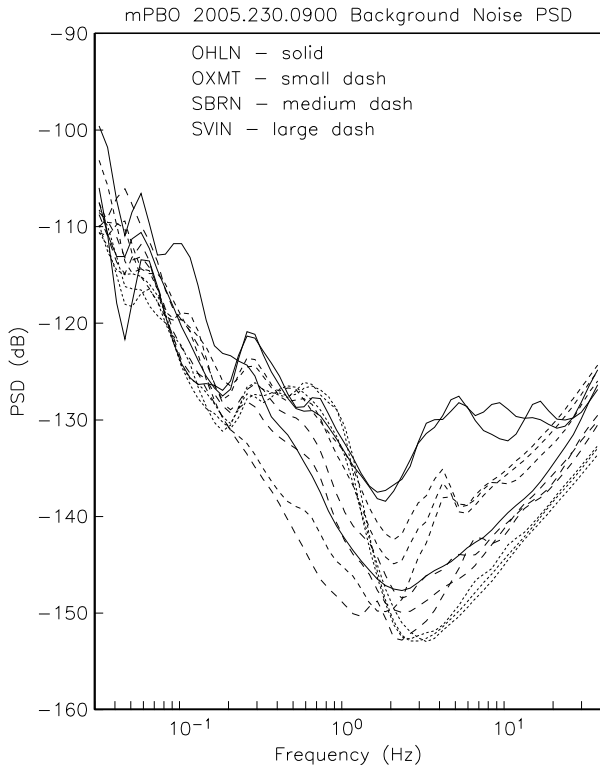


Figure 8.4: Representative background noise measured by the borehole seismic packages at the completed 4 Mini-PBO stations. Three components (vertical plus two horizontal) are shown for each station. The systems have the best signal to noise ratio near their 2-Hz characteristic frequency.

ber of normal modes ($0S_4$, $0S_5$, $0S_7$, $2S_4$, $0S_8$, $2S_5$, $0S_9$, and $0S_{10}$) are clearly observed. We are improving our strainmeter data editing techniques to remove high-rate atmospheric effects over long time intervals, which should improve resolution of the normal mode peaks.

We are also examining the strain data for other types of transient behavior, such as episodic creep or slow earthquake displacements. These multiparameter stations are providing a prototype for more than 140 planned borehole strainmeter, seismometer, and GPS stations in Cascadia and along the San Andreas fault as part of the Plate Boundary Observatory.

4. Acknowledgements

This project is sponsored by the National Science Foundation EAR/IF program with matching funds from the participating institutions and the Southern California Earthquake Center (SCEC) (PI Romanowicz).

Under Mark Murray's supervision, André Basset, Bill Karavas, John Friday, Dave Rapkin, Doug Neuhauser, Tom McEvelly, Wade Johnson, and Rich Clymer have

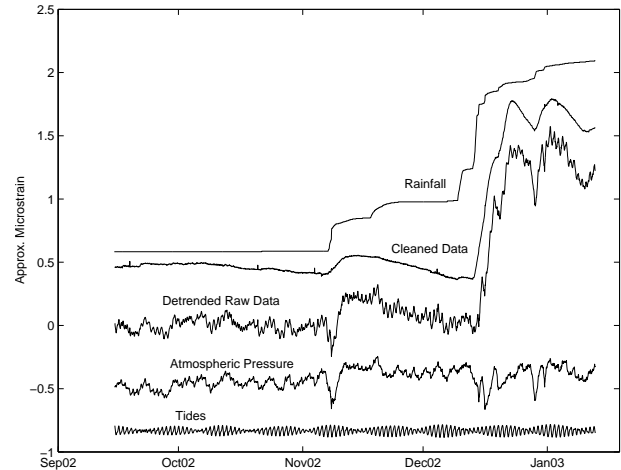


Figure 8.5: Four-month subset of OHLN strainmeter data, detrended to flatten the first 50 days (middle trace), decomposed using BAYTAP-G into tidal, atmospheric pressure, and "cleaned" data components (with arbitrary vertical offsets). The remaining large strain signals in the cleaned data are highly correlated with rainfall and therefore are likely non-tectonic in origin.

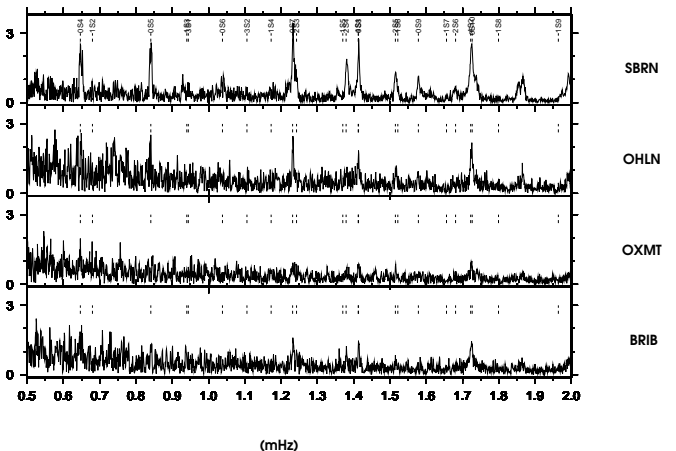


Figure 8.6: Normal modes in the 0.5 to 2.0 mHz band measured on Mini-PBO strainmeters and the BRIB dilatometer following the 2004 M9 Sumatra earthquake. The time window began 8 hours before the event and spans 200 hours. Tides have been removed, but not atmospheric effects, which may account for the higher background noise levels. *Figure courtesy of Aimin Cao.*

contributed to the BSL component of the Mini-PBO project. Several USGS colleagues, especially Malcolm Johnston, Bob Mueller, and Doug Myren, played critical roles in the drilling and instrument installation phases.

Chapter 9

Data Acquisition and Quality Control

1. Introduction

Stations from nearly all networks operated by the BSL transmit data continuously to the BSL facilities on the UC Berkeley campus for analysis and archive. In this chapter, we describe activities and facilities which cross-cut the individual networks described in Chapters 3 - 8, including the facilities in McCone Hall, procedures for data acquisition and quality control, sensor testing capabilities and procedures, and a collaborative experiment in early warning.

While some of these activities are continuous from year to year, we have identified changes or activities which are specific to 2004-2005.

2. McCone Hall Facilities

The routine data acquisition, processing, and archiving activities of the BSL are carried out in McCone Hall. The BSL facilities in McCone are designed to provide air conditioning, 100-bit switched network, and reliable power with UPS and generator.

Because of the mission-critical nature of the automated earthquake processing, most computer systems operated by the BSL run on circuits with both UPS and generator power. Air conditioning is provided through both "building air" and two additional AC units.

2.1 Power

Over the years, the BSL has experienced problems with the McCone generator system, including a failure in 1999 due to a combination of a weakened power system and a leak in the water pump. In the 2001-2002 Annual Report, we described the failure of the McCone and Byerly generators during the March 7, 2002 campus-wide power outage.

While the failure of the generator at Byerly Vault was traced to PPCS human error (the generator had been left in a mode where it would not automatically start when power was lost), the failure of the McCone generator was due to poor maintenance. Similar to the situation in

1999, it failed due to problems in the power system combined with a leak in the water pump.

In the fall of 2002, BSL staff met with Eric Haemer, Sara Shirazi, and several others from PPCS to discuss maintenance and routine load testing of the McCone generator. As a result, the McCone generator is scheduled for quarterly load tests and bi-monthly run tests.

2.2 Air Conditioning

In parallel with power problems, the BSL has faced cooling problems in room 237 in the past year. As with power, the growth of the computing systems in the past year has led to an increased heat load. This came to a crisis during the fall of 2002, with peak temperatures in the computer room exceeded 85° when the AC unit failed. After consideration of several options, the BSL decided to add an additional AC unit to room 237. The new unit (which is not supported by UPS/generator power) has helped keep systems running, although the BSL held a summit with PPCS staff in February 2004 to review ongoing cooling problems. As a result, PPCC worked with the contractor to install a larger impeller on the chilled water circulation pump. This has increased the cooling capacity of our dry cooler on the roof. In addition, PPCS has been coming by more regularly to inspect the filters on the unit.

2.3 New Facilities

The BSL is actively working with the campus to relocate the critical operations of data acquisition, processing, archiving, and data distribution to a more robust facility than McCone Hall. With assistance from the Office of the Vice Chancellor for Research, the BSL has been granted space in 2195 Hearst, a recently completed building on the Oxford Tract. 2195 Hearst was constructed to current seismic codes, and the hardened campus computer facility within was designed with special attention for post-earthquake operations. The computer center contains state-of-the art seismic bracing, UPS power and air conditioning with generator backup, and extensive security and equipment monitoring.

BDSN and REDI Telemetry and Data Flow

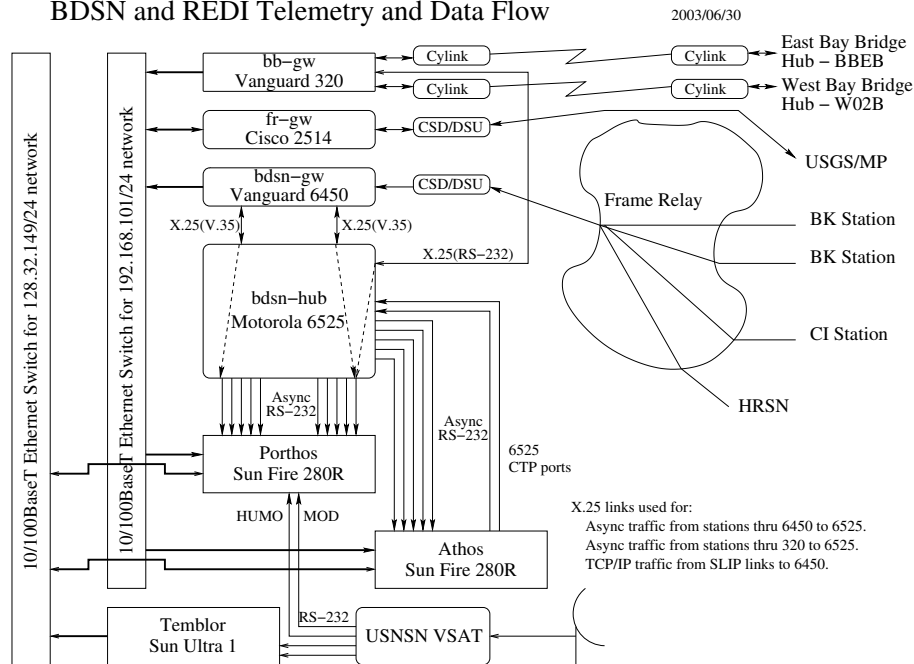


Figure 9.1: Data flow from the BDSN, NHFN, MPBO, HRSN, and BARD network into the BSL central processing facility.

During 2004-2005, the BSL began to relocate equipment to the new facilities in 2195 Hearst. Overall, the BSL plans to move all of its data acquisition, real-time earthquake processing computers and data archive and distribution computers to the new facility. This also involves moving all telemetry equipment (5 T1s lines, dedicated leased phone circuit to our paging service, dialin/dialout modems, as well as various radio and VSAT communication equipment) to the new location. As of June 30, 2005, the data archiving system and half of the real-time acquisition and earthquake processing computers had been relocated to 2195 Hearst, and the private network used for seismic data acquisition and earthquake processing was temporarily bridged between McCone Hall and 2195 Hearst using an encrypted tunnel across the campus backbone network. [The remainder of the data acquisition and processing systems were moved on September 16, 2005 along with the 5 T1 circuits and associated routers].

3. Data Acquisition

Central-site data acquisition for the BDSN/NHFN/MPBO is performed by two computer systems located at the BSL (Figure 9.1). These acquisition systems are also used for the Parkfield-Hollister electromagnetic array and for the BARD network. A third system is used primarily as data exchange system with the USNSN and receives a feed from CMB, HUMO,

MOD, SAO, and WDC from the the NSN VSAT. This system also transmits data to the USNSN from HOPS, CMB, SAO, WDC, and YBH. Data acquisition for the HRSN follows a more complicated path, as described in Chapter 6.

3.1 Comserv

The BSL uses the `comserv` program for central data acquisition, which was developed by Quanterra. The `comserv` program receives data from a remote Quanterra data logger, and redistributes the data to one or more `comserv` client programs. The `comserv` clients used by REDI include `datalog`, which writes the data to disk files for archival purposes, `cdafill`, which writes the data to the shared memory region for REDI analysis, and other programs such as the seismic alarm process, the DAC480 system, and the feed for the Memento Mori Web page (Figure 9.2).

The two computers that perform data acquisition also serve as REDI processing systems. In order to facilitate REDI processing, each system maintains a shared memory region that contains the most recent 30 minutes of data for each channel used by the REDI analysis system. All REDI analysis routines first attempt to use data in the shared memory region, and will only revert to retrieving data from disk files if the requested data is unavailable in the shared memory region.

Most stations transmit data to only one or the other

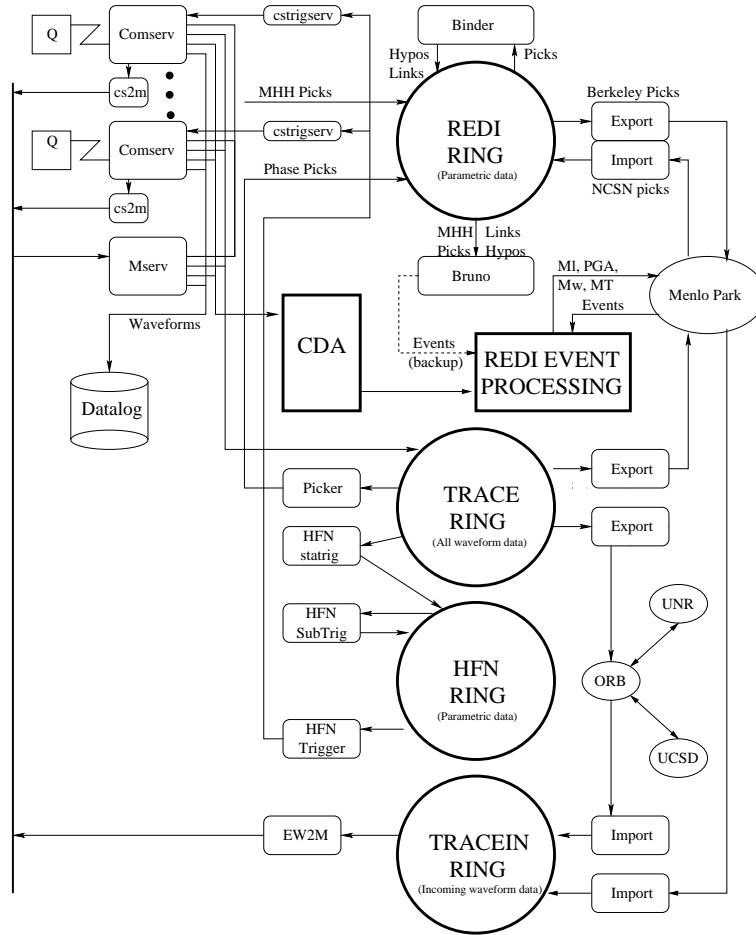


Figure 9.2: Dataflow in the REDI processing environment, showing waveform data coming in from the Quanterra data loggers (Q) into **comserv**. From **comserv**, data are logged to disk (via **datalog**), distributed to other computers (**mserv**), fed into the CDA for REDI processing, and spooled into a trace ring for export.

of the two REDI systems. The **comserv** client program **cs2m** receives data from a **comserv** and multicasts the data over a private ethernet. The program **mcast**, a modified version of Quanterra's **comserv** program, receives the multicast data from **cs2m**, and provides a **comserv**-like interface to local **comserv** clients. This allows each REDI system to have a **comserv** server for every station.

We have extended the multicasting approach to handle data received from other networks such as the NCSN and UNR. These data are received by Earthworm data exchange programs, and are then converted to MiniSEED and multicast in the same manner as the BSL data. We use **mserv** on both REDI computers to receive the multicast data, and handle it in an identical fashion to the BSL MiniSEED data.

3.2 BH Sampling Rate

The BSL converted most - but not quite all - of the BDSN BH data streams from 20 samples per second to 40 samples per second at the beginning of the GMT day on June 15, 2004 (day 167). This change affects: BDM, BKS, BRIB (broadband sensor only), CMB, CVS, FARB, HOPS, HUMO, JCC, JRSC, MHC, MNRC, MOD, ORV, PACP, PKD, POTR, RFSB (surface strong-motion only), SAO, SCCB, WDC, and YBH. Stations BRK, KCC, and WENL were converted at the beginning of day 168.

This change in sampling rate was made in order to be consistent with the USArray specifications. At this time, we do not intend to change the sampling rate of the BP channels associated with the BSL borehole networks - the NHFN, MPBO, and HRSN.

4. Seismic Noise Analysis

BSL seismic data are routinely monitored for state-of-health. An automated analysis is computed weekly to characterize the seismic noise level recorded by each broadband seismometer. The estimation of the Power Spectral Density (PSD) of the ground motion recorded at a seismic station provides an objective measure of background seismic noise characteristics over a wide range of frequencies. When used routinely, the PSD algorithm also provides an objective measure of seasonal and secular variation in the noise characteristics and aids in the early diagnoses of instrumental problems. A PSD estimation algorithm was developed in the early 1990's at the BSL for characterizing the background seismic noise and as a tool for quality control. As presently implemented, the algorithm sends the results via email to the engineering and some research staff members and generates a bargraph output which compares all the BDSN broadband stations by components. A summary of the results for 2004-2005 is displayed in Figure 3.3. Other PSD plots for the NHFN, HRSN, and MPBO are shown in Figures 5.3, 6.2, and 8.4 respectively.

Four years ago, we expanded our use of the weekly PSD results to monitor trends in the noise level at each station. In addition to the weekly bar graph, additional figures showing the analysis for the current year are produced. These cumulative PSD plots are generated for each station and show the noise level in 5 frequency bands for the broadband channels. These cumulative plots make it easier to spot certain problems, such as failure of a sensor. In addition to the station-based plots, a summary plot for each channel is produced, comparing all stations. These figures are presented as part of a noise analysis of the BDSN on the WWW at <http://www.seismo.berkeley.edu/seismo/bdsn/psd/>.

The PSD algorithm has been documented in previous annual reports.

4.1 PDF Noise Analysis

In addition to the PSD analysis developed by Bob Uhrhammer, the BSL has implemented the Ambient Noise Probability Density Function (PDF) analysis system developed by Dan McNamara and Ray Buland (2004). This system does its noise analysis over all the data of a given time period (week or year), including earthquakes, calibration pulses, and cultural noise. This is in contrast to Bob Uhrhammer's PSD analysis which looks at only the quietest portion of data within a day or week. Pete Lombard of the BSL has extended the McNamara code to cover a larger frequency range and to support the many different types of sensors employed by the BSL. Besides the originally supported broadband sensors, our PDF analysis now includes surface and borehole accelerometers, strain meters, and electric and mag-

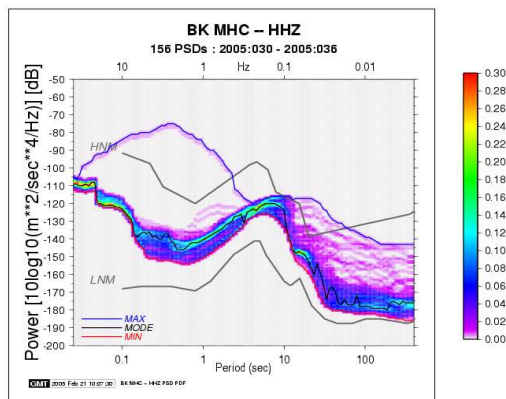


Figure 9.3: Noise analysis results for the week of 01/30/05 at BDSN station MHC, on the HHZ component. Prominent features in the figure are the Alum Rock earthquake (2005/02/05, 18:43 UTC; M_L 4.4; and a prominent noise spike near 30 HZ, probably due to rotating machinery nearby to the station at the Mount Hamilton Observatory.

netic field sensors. These enhancements to the PDF code, plus a number of bug fixes, were provided back to the McNamara team for incorporation in their work. The results of the PDF analysis are presented on the web at <http://moho/seismo/PDF/>. Figure 9.3 shows the noise analysis results for a typical week.

5. Sensor Testing Facility

The BSL has set up an instrumentation test facility in the Byerly Seismographic Vault in order to systematically determine and to compare the characteristics of up to eight sensors at a time. The test equipment consists of an eight-channel Quanterra Q4120 high-resolution data logger and a custom interconnect panel that provides isolated power and preamplification when required to facilitate the connection and routing of signals from the sensors to the data logger with shielded signal lines. Upon acquisition of the 100 samples-per-second (sps) data from the instruments under test, PSD analysis and spectral phase coherency analysis are used to characterize and compare the performance of each sensor. Tilt tests and seismic signals with a sufficient signal level above the background seismic noise are also used to verify the absolute calibration of the sensors. A simple vertical shake table is used to access the linearity of a seismic sensor.

The sensor testing facility of the BSL is described in detail in the 2001-2002 Annual Report.

Instruments tested during the past year included functional testing of a Streckeisen STS-2, an Episensor FBA-ES-T, a Guralp CMG-3T, a horizontal STS-1 and com-

parison testing of a pair of Metrozet accelerometers.

5.1 Functional Tests

A Streckeisen STS-2 broadband seismometer (s/n 50205) and an Episensor FBA-ES-T (s/n 1557) were installed for testing. We found that both sensors were operating within their nominal specifications. These sensors were subsequently installed at FARB.

On September 24, the ex-FARB Guralp CMG-3T s/n T393 was installed for testing. We found that all three components exhibited highly correlated broadband noise which indicated that there is a common mode internal noise source present in the Guralp electronics.

On January 10, a horizontal STS-1 (s/n 39010) and its electronics box were installed for testing. This sensor is scheduled to replace the failing E-component sensor at MOD. We found that this sensor was operating within its nominal specifications.

On April 6, a pair of three-component Metrozet accelerometers were installed for long term testing and comparison with the BKS FBA-23 accelerometer recordings.

5.2 Comparison Tests

The goal of comparison testing is to determine the calibration, coherency, and background noise PSD characteristics of the sensors being tested. Metrozet approached the BSL with a request to install a pair of Metrozet strong motion accelerometers in a seismically quiet vault for testing. We agreed, on the condition that Metrozet perform the bulk of the comparison analysis, and on April 6, a pair of three-component Metrozet accelerometers were installed for long term testing and comparison with the BKS FBA-23 accelerometer recordings.

A comparison of the strong motion waveforms recorded by the two Metrozet sensors and the co-sited BKS FBA-23, for a recent ML 3.0 earthquake (2005.267.1125) which occurred 5.3 km SSE of BKS at a depth of 5.4 km, are shown in Figure 9.4. The raw data, without deconvolving the instrument response, have been low-pass filtered at 20 Hz for the comparison and the data are plotted on a relative scale.

The corresponding waveforms from all three sensors shown in Figure 9.4 are visually highly similar and there are no offsets or other aberrant behavior in the Metrozet signals. Comparing the signal levels from the Metrozet sensors in counts with the corresponding ground accelerations inferred from the BKS FBA-23, we find that the sensitivity of the Metrozet sensor coupled to the Q4120 data logger is nominally 43.6x the sensitivity of the FBA-23 coupled to the Q680 data logger or 2.30 million counts/(m/s²).

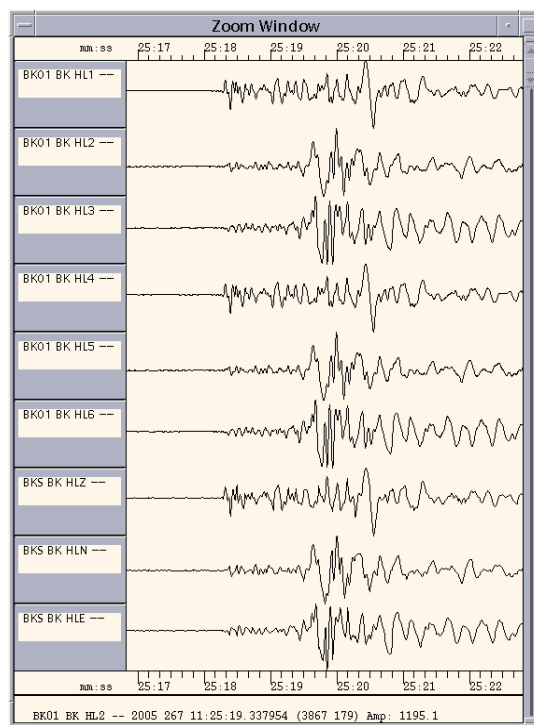


Figure 9.4: Comparison of the acceleration signals recorded by the two three-component Metrozet accelerometers and the BKS FBA-23 three-component accelerometer.

6. Acknowledgements

Doug Neuhauser, Bob Uhrhammer, Lind Gee, Pete Lombard, and Rick McKenzie are involved in the data acquisition and quality control of BDSN/NHFN/MBPO data. Development of the sensor test facility and analysis system was a collaborative effort of Bob Uhrhammer, Tom McEvelly, John Friday, and Bill Karavas. IRIS and DTRA provided, in part, funding and/or incentive to set up and operate the facility and we thank them for their support. Bob Uhrhammer, Lind Gee, and Doug Neuhauser contributed to the preparation of this chapter.

7. References

- McNamara, D. and R. Buland, *Bull. Seism. Soc. Am.*, 94, 4, 2004.
- Scherbaum, Frank. Of Poles and Zeros: Fundamentals in Digital Seismology, Volume 15 of Modern Approaches in Geophysics, G. Nolet, Managing Editor, Kluwer Academic Press, Dordrecht, xi + 257 pp., 1996.
- Tapley, W. C. and J. E. Tull, SAC - Seismic Analysis Code: Users Manual, *Lawrence Livermore National Laboratory*, Revision 4, 388 pp., March 20, 1992.

Chapter 10

Northern California Earthquake Monitoring

1. Introduction

Routine analysis of the data produced by BSL networks begins as the waveforms are acquired by computers at UC Berkeley, and ranges from automatic processing for earthquake response to analyst review for earthquake catalogs and quality control.

Over the last 10 years, the BSL has invested in the development of the hardware and software necessary for an automated earthquake notification system (*Gee et al.*, 1996; 2003a). The Rapid Earthquake Data Integration (REDI) project is a research program at the BSL for the rapid determination of earthquake parameters with three major objectives: to provide near real-time locations and magnitudes of northern and central California earthquakes, to provide estimates of the rupture characteristics and the distribution of ground shaking following significant earthquakes, and to develop better tools for the rapid assessment of damage and estimation of loss. A long-term goal of the project is the development of a system to warn of imminent ground shaking in the seconds after an earthquake has initiated but before strong motions begin at sites that may be damaged.

In 1996, the BSL and USGS began collaboration on a joint notification system for northern and central California earthquakes. The current system merges the programs in Menlo Park and Berkeley into a single earthquake notification system, combining data from the NCSN and the BDSN.

Today, the BSL and USGS system forms the Northern California Management Center (NCMC) of the California Integrated Seismic Network (Chapter 4).

2. Northern California Management Center

The details of the Northern California processing system and the REDI project have been described in past annual reports. In this section, we will describe how the Northern California Management Center fits within the

CISN system, detail recent developments, and discuss plans for the future development.

Figure 4.3 in Chapter 4 illustrates the NCMC as part of the the CISN communications ring. The NCMC is a distributed center, with elements in Berkeley and Menlo Park. The 35 mile separation between these two centers is in sharp contrast to the Southern California Management Center, where the USGS Pasadena is located across the street from the Caltech Seismological Laboratory. As described in Chapter 4, the CISN partners are connected by a dedicated T1 communications link, with the capability of falling back to the Internet. In addition to the CISN ring, the BSL and the USGS Menlo Park have a second dedicated communication link to provide bandwidth for shipping waveform data and other information between their processing systems.

Figure 10.1 provides more detail on the current system at the NCMC. At present, two Earthworm-Earlybird systems in Menlo Park feed two “standard” REDI processing systems at UC Berkeley. One of these systems is the production or paging system; the other is set up as a hot backup. The second system is frequently used to test new software developments before migrating them to the production environment. The Earthworm-Earlybird-REDI systems perform the standard detection, location, estimation of M_d , M_L , and M_w , as well as processing of ground motion data. The computation of ShakeMaps is also performed on two systems, one in Menlo Park and one in Berkeley, as described below. An additional system performs finite-fault processing and the computation of higher level ShakeMaps.

The dense network and Earthworm-Earlybird processing environment of the NCSN provides rapid and accurate earthquake locations, low magnitude detection thresholds, and first-motion mechanisms for smaller quakes. The high dynamic range data loggers, digital telemetry, and broadband and strong-motion sensors of the BDSN and REDI analysis software provide reliable magnitude determination, moment tensor estimation, peak ground motions, and source rupture charac-

Northern California Management Center Current Implementation

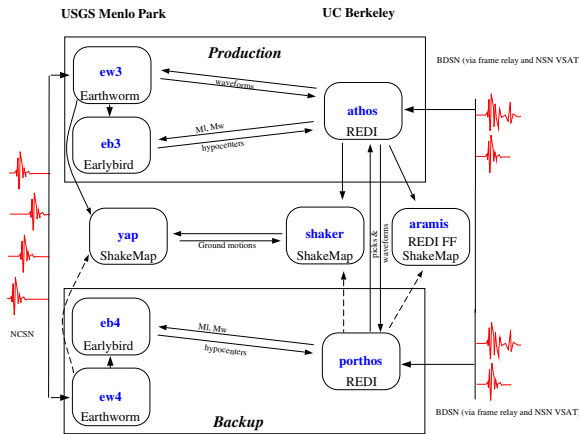


Figure 10.1: Detailed view of the current Northern California processing system, showing the two Earthworm-Earlybird-REDI systems, the two ShakeMap systems, and the finite-fault system.

teristics. Robust preliminary hypocenters are available about 25 seconds after the origin time, while preliminary coda magnitudes follow within 2-4 minutes. Estimates of local magnitude are generally available 30-120 seconds later, and other parameters, such as the peak ground acceleration and moment magnitude, follow within 1-4 minutes (Figure 10.2).

Earthquake information from the joint notification system is distributed by pager/cellphone, e-mail, and the WWW. The first two mechanisms “push” the information to recipients, while the current Web interface requires interested parties to actively seek the information. Consequently, paging and, to a lesser extent, e-mail are the preferred methods for emergency response notification. The *recenteqs* site has enjoyed enormous popularity since its introduction and provides a valuable resource for information whose bandwidth exceeds the limits of wireless systems and for access to information which is useful not only in the seconds immediately after an earthquake, but in the following hours and days as well.

3. 2004-2005 Activities

3.1 System Development

As part of ongoing efforts to improve the monitoring systems in northern California, the BSL and the USGS Menlo Park have started to develop the next generation of the northern California joint notification system or the Northern California Seismic System (NCSS).

Figure 10.1 illustrates the current organization of

the two systems. As described above, an Earthworm/Earlybird component is tied to a REDI component and the pair form a single “joint notification system.” Although this approach has functioned reasonably well over the last eight years, there are a number of potential problems associated with the separation of critical system elements by ~35 miles of San Francisco Bay.

Recognizing this, we intend to redesign the Northern California operations so that a single independent system operates at the USGS and at UC Berkeley. In FY01/02, our discussions proceeded to the stage of establishing specifications and determining the details required for design. In the last year, however, most of the development effort focused on CISM activities, and specific plans for the “next generation” Northern California system were put on hold. This enforced wait provided the opportunity for some ideas to mature and the current plans for the NCMC are somewhat different from those envisioned in 2001.

The current design draws strongly on the experience in Southern California for the development of TriNet (Figure 10.3), with some modifications to allow for local differences (such as very different forms of data acquisition and variability in network distribution). In addition, the BSL and the USGS want to minimize use of proprietary software in the system. The TriNet software uses three forms of proprietary software: Talerian Smart Sockets (TSS) for inter-module communication via a “publish and subscribe” method, RogueWave software for database communication, and Oracle as the database management system. As part of the development of the Northern California Earthquake Data Center, the USGS and BSL have worked extensively with Oracle databases and extending this to the real-time system is not viewed as a major issue. However, we did take the opportunity to review options for replacing Smart Sockets and RogueWave with Southern California, resulting in joint agreement on replacement packages and shared development effort.

In the last three years, BSL staff, particularly Pete Lombard, have become extremely familiar with portions of the TriNet software. We have begun to adapt the software for Northern California, making adjustments and modifications along the way. For example, Pete Lombard has adapted the TriNet magnitude module to northern California, where it is running on a test system. Pete made a number of suggestions on how to improve the performance of the magnitude module and has worked closely with Caltech and the USGS/Pasadena on modifications. One of the recent discoveries with the magnitude module was related to differences in time references as implemented in the database schema.

Last year, the BSL and the USGS Menlo Park undertook the effort to develop and test a design to exchange “reduced amplitude timeseries.” One of the im-

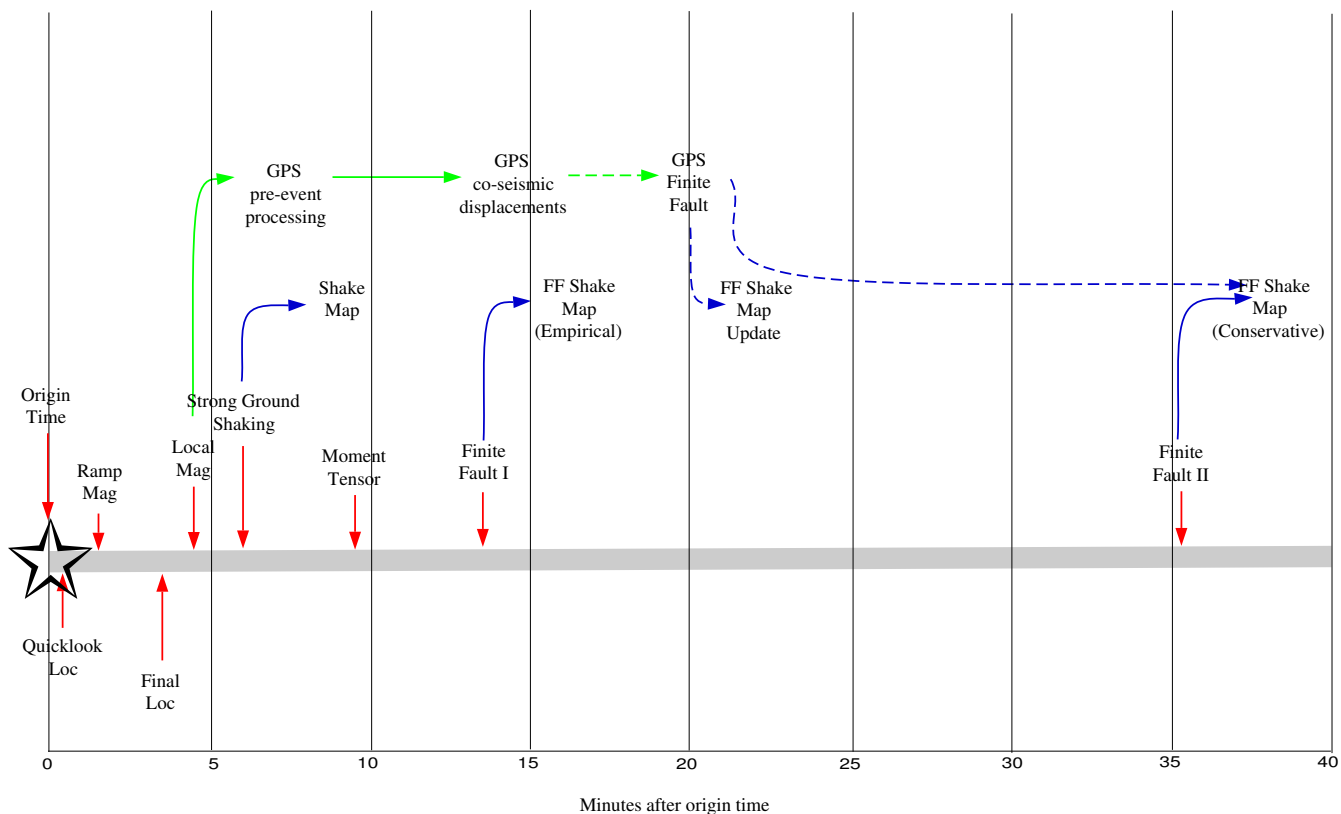


Figure 10.2: Illustration of the current (solid lines) and planned/proposed (dotted lines) development of real-time processing in northern California. The Finite Fault I and II are fully implemented within the REDI system at UC Berkeley and are integrated with ShakeMap. The resulting maps are still being evaluated and are not currently available to the public.

portant innovations of the TriNet software development was the concept of continuous processing (*Kanamori et al., 1999*), where waveform data are processed to produce Wood Anderson synthetic amplitudes and peak ground motions constantly. A program called *rad* produces a reduced timeseries, sampled every 5 secs, and stores it in a memory area called an “Amplitude Data Area” or ADA. Other modules can access the ADA to retrieve amplitudes to calculate magnitude and ShakeMaps as needed. In the the past year, the BSL and the USGS Menlo Park have collaborated to establish the tools for the ADA-based exchange. As part of the software development in northern California, a number of modules have been developed.

During 2004-2005, effort turned more toward the goal of retiring *CUSP* - the system used by the USGS Menlo Park to time earthquakes. *CUSP* was initially developed in Southern California during the late 1970s - early 1980s and has been used for a number of years in Northern

California. However, the *CUSP* system is becoming increasingly outdated.

The NCMC has developed a plan to retire *CUSP*, based on the implementation of some components of the Southern California system. Over the past year, BSL staff have worked to implement the *RequestCardGenerator* (a module that decides which channels to archive, given a particular earthquake), a waveform archiving module, and *Jiggle* (the earthquake timing interface). The NCMC and SCMC collaborated on modifications to *Jiggle* for use in Northern California such as the computation of M_d . The goal is to have a test system up and running with the next year.

Also during the past year, Northern and Southern California developers spent two days in Pasadena discussing issues of joint interest.

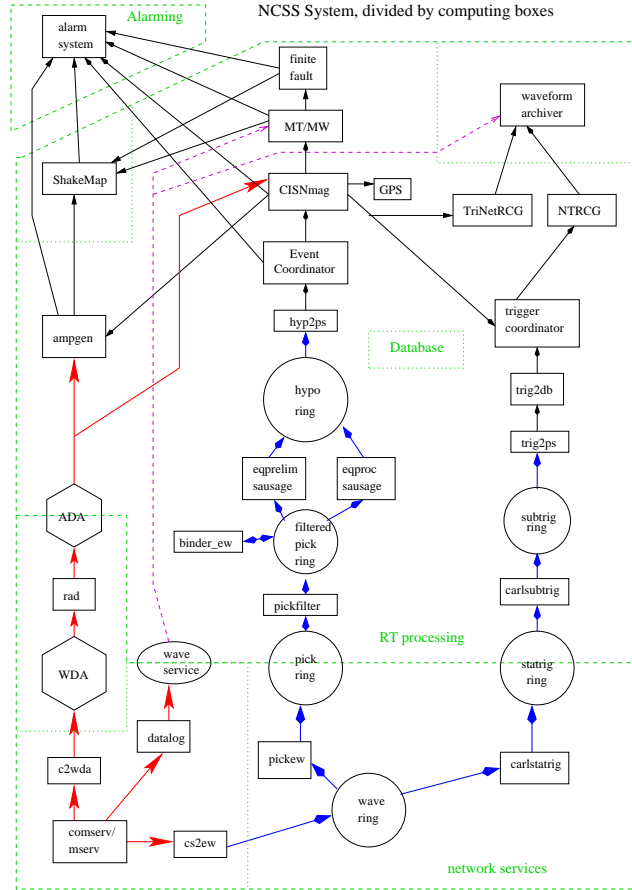


Figure 10.3: Schematic diagram of the planned NCSS system. The design combines elements of the Earthworm, TriNet, and REDI systems

3.2 M_w

The REDI system has routinely produced automatic estimates of moment magnitude (M_w) for many years. However, these estimates were not routinely used as the “official” magnitude until after the 05/14/2002 Gilroy earthquake (M_w 4.9, M_L 5.1), motivated by the complications created by the publication of multiple magnitudes.

In last year’s annual report, we discussed the issue of when to report M_w . As currently implemented, solutions that meet a minimum quality criterion are automatically reported (a variance reduction of 40% or higher). This criterion appears to work very well and screens out events contaminated by teleseisms. Over the last few years, nearly all events over 4.5 have met this criterion, as have a number of events in the M3.5-4.5 range.

As part of the effort to establish a statewide magnitude reporting hierarchy, we have looked more closely at the estimates of M_w (Gee *et al.*, 2003b; 2004b) and the

comparison between M_w and M_L .

Two methods of determining regional moment tensor (RMT) solutions have been automated as part of the REDI system - the complete waveform modeling technique (CW) of Dreger and Romanowicz (1994) and the surface wave inversion (SW) of Romanowicz *et al.* (1993). Comparison between the CW method and other regional moment tensor studies in northern California and the western United States show excellent agreement in the estimate of seismic moment and M_w . Over 128 events, the average difference in M_w is 0.002 magnitude units.

4. Routine Earthquake Analysis

In fiscal year 2004-2005, nearly 16,000 earthquakes were detected by the automatic systems in northern California. This compares with over 12,000 in 2003-2004 and 8,300 events in 2002-2003. The increase in the number of events can be attributed to the 2003 San Simeon and

2004 Parkfield earthquakes, both of which have had energetic aftershock sequences. Of those 15,000+ events, over 450 had preliminary magnitudes greater than 3. Fifty-five events had M_L greater than 4. The largest event recorded by the system was the M_w 7.1 event offshore of Crescent City (the largest event in the network was the Mw 6.0 Parkfield event).

As described in the 2003-2004 Annual Report, the BSL staff are no longer reading BDSN records for local and regional earthquakes (as of March 2004). This decision was based in part to reduce duplication of effort between Berkeley and Menlo Park.

The BSL continues to focus on the unique contributions that can be made from the broadband network. From July 2004 through June 2005, BSL analysts reviewed nearly 58 earthquakes in northern California and adjoining areas of magnitude 3.5 and higher. Reviewed moment tensor solutions were obtained for 65 events (through 6/30/2005). Figure 10.4 and Table 10.1 display the earthquakes located in the BSL catalog and the moment tensor solutions.

4.1 Seismic Background Noise PSD in Northern and Central California

The density and distribution of broadband seismic stations sited in Northern and Central California has increased over the past year due the installation of USArray transportable broadband seismic stations. One design goal of the transportable network is to complement the existing BDSN broadband stations and cover the region with an average interstation spacing of ~ 70 km. Our motivation for characterizing the seismic background noise PSD level observed at the transportable stations is, in part, that we would like to occupy the best sites after the transportable array moves out of the region, in order to improve the coverage of the BDSN network.

PSD algorithm

We have been characterizing the vertical and horizontal seismic background noise levels observed in Northern and Central California via Power Spectral Density (PSD) analysis of the seismic background signals recorded by the BDSN broadband seismic stations (BK network) and by the USArray broadband seismic stations (TA network). Two frequency bands, the 1-5 Hz short-period (SP) band and the 30-60 second long-period (LP) band, are analyzed to characterize the background noise in the seismic bands of interest particularly for the study of the seismic signals from local and regional seismic events.

The PSD algorithm uses a statistical approach to robustly estimate the background noise PSD. The PSD estimates are reported in dB relative to $1 \text{ (m/s}^2\text{)}^2/\text{Hz}$. The input time series is parsed into eight (possibly overlapping) time series and each of the resulting time series are appropriately windowed prior to calculating their PSD

estimates. For short time series, less than 1.5 hours in length, the time series are detrended and sine tapered while for longer time series the dominant semi-diurnal gravitational tide signal is also removed to avoid biasing the long-period PSD estimates. The PSD estimates are smoothed and reported at twenty logarithmically spaced intervals per decade in period.

Owing to the statistical nature of the PSD algorithm, it is required that the time series to be processed contain at least 65,635 (216) contiguous samples. Shorter time series are not processed and a warning is issued. The PSD algorithm can process data with a wide variety of sampling rates (from < 0.01 sps to > 500 sps). A typical usage with broadband data is for the time series to contain one day of continuous LH (1 sps) data (86,400 samples), say. Since the sensor transfer function representation in the SEED data volume for a typical inertial seismometer does not include the static component of the response, the background noise PSD estimates for periods longer than approximately an hour will be biased high; and hence, they will be unreliable.

The PSD code distribution along with examples of its usage are available via the Web at <http://seismo.berkeley.edu/algorithms/>.

Seismic Background Noise Analysis

We acquired SEED data volumes containing a network day (2005.268) of 1 Hz three-component broadband data from the TA transportable network (27 stations) and from the BK permanent network (26 stations). This data was used to characterize the seismic background noise in the 30-60 second LP band. We also acquired SEED data volumes containing two network hours (2005.268.0000-0200) of 40 Hz three-component broadband data from the TA transportable network and from the BK permanent network (day 2005.268.0000-0200). This data was used to characterize the seismic background noise in the 1-5 Hz SP band.

The observed vertical-component LP (30-60 second period) seismic background noise PSD is shown in Figure 10.5 and the corresponding horizontal-component noise is shown in Figure 10.6. The spread between the quietest and noisiest stations on the vertical-component is ~ 20 dB with only four stations in the two noisiest levels. The spread between the quietest and noisiest stations on the horizontal-component is ~ 30 dB with 19 stations (36%) in the two noisiest levels. The stations with the low observed seismic noise levels are generally sites on bed rock or in hard rock mines and remote from cultural noise sources. The stations with high horizontal-component PSD noise levels are generally sites with either thick alluvial deposits or high ambient cultural noise levels.

The observed vertical-component SP (1-5 Hz) seismic background noise PSD is shown in Figure 10.7 and the corresponding horizontal-component noise is shown in Fig-

Location	Date	UTC Time	Lat.	Lon.	MT Depth	M_l	M_w	Str.	Dip	Rake	Mo
Newport, OR	07/12/2004	16:45:00.0	44.332	-124.520	21	4.9	4.8	81	87	-175	1.54e23
San Simeon	07/13/2004	23:45:45.0	35.700	-121.059	5	4.1	4.1	123	51	105	1.51e22
Lakeview, OR	07/22/2004	20:26:27.0	42.212	-120.283	8	4.3	4.6	176	64	-101	8.08e22
San Simeon	07/27/2004	03:38:17.0	35.718	-121.053	5	3.9	3.7	117	53	98	3.69e21
Pinnacles	07/31/2004	10:35:54.0	36.641	-121.259	11	3.6	3.5	231	85	18	1.86e21
Newport, OR	08/19/2004	06:06:03.0	44.665	-124.300	24	4.7	4.6	159	87	8	7.96e22
Pinnacles	08/30/2004	04:30:57.0	36.578	-121.179	11	4.0	4.0	49	89	-4	1.00e22
San Simeon	08/31/2004	00:40:18.0	35.674	-121.117	5	4.0	3.8	114	53	63	6.29e21
Pinnacles	08/31/2004	09:12:27.9	36.589	-121.184	11	3.9	3.9	53	85	-11	6.58e21
Bodie	09/18/2004	07:08:00.0	37.990	-118.692	5	4.1	4.1	57	82	37	1.69e22
Bodie	09/18/2004	12:39:20.0	37.993	-118.719	5	3.6	3.6	342	72	-156	1.71e21
Bodie	09/18/2004	23:02:17.0	38.009	-118.679	8	5.4	5.5	239	89	-23	1.67e21
Bodie	09/18/2004	23:43:31.0	38.009	-118.668	5	5.3	5.4	53	88	10	1.27e24
Bodie	09/19/2004	06:58:04.0	38.008	-118.679	11	3.9	3.9	340	77	163	9.26e21
Bodie	09/20/2004	16:51:04.0	38.029	-118.644	5	4.9	4.8	244	84	-19	1.57e23
San Juan Bautista	09/22/2004	10:57:35.0	36.803	-121.535	11	3.8	3.7	53	86	-25	3.90e21
Coalinga	09/26/2004	15:54:05.0	36.155	-120.654	5	3.7	3.7	119	51	103	4.11e21
Parkfield	09/28/2004	17:15:24.0	35.815	-120.374	8	6.0	6.0	48	82	-13	9.97e24
Parkfield	09/28/2004	17:24:15.0	35.806	-120.349	5	4.7	4.7	330	83	-167	1.45e23
Parkfield	09/28/2004	19:31:27.0	35.839	-120.387	8	4.0	4.1	56	90	-11	1.38e22
Parkfield	09/29/2004	17:10:04.0	35.953	-120.502	11	5.2	5.1	236	87	6	4.45e23
Keene	09/29/2004	22:54:54.0	35.389	-118.621	11	5.0	5.0	295	89	-169	4.02e23
Parkfield	09/30/2004	18:54:28.0	35.984	-120.550	11	5.1	4.9	232	89	7	2.66e23
Templeton	10/02/2004	12:22:09.0	35.542	-120.813	8	4.3	4.1	120	48	109	1.50e22
Bodie	10/09/2004	03:45:48.0	37.980	-118.659	11	4.7	4.6	93	86	10	7.61e22
Bodie	10/10/2004	14:03:22.0	37.963	-118.661	8	3.5	3.6	185	79	164	3.19e21
Bodie	10/20/2004	11:35:15.0	38.039	-118.608	5	4.1	4.0	250	84	-45	1.13e22
Bodie	10/20/2004	12:03:11.0	38.039	-118.612	8	3.9	3.6	46	90	40	3.18e21
Gilroy	10/25/2004	19:55:38.0	39.967	-121.599	5	3.9	3.7	213	81	10	4.27e21
Geysers	10/29/2004	18:02:55.0	38.819	-122.793	5	3.8	3.8	16	56	-107	6.57e21
Parkfield	11/19/2004	02:56:00.0	35.862	-120.408	8	3.8	3.7	145	87	174	4.17e21
Pinnacles	11/24/2004	02:06:04.0	36.607	-121.209	8	4.5	4.4	222	85	6	4.18e22
Pinnacles	11/24/2004	05:23:40.0	36.600	-121.202	11	3.5	3.7	48	88	-23	3.87e21
Parkfield	11/29/2004	01:54:14.0	35.944	-120.492	8	4.2	4.2	52	85	-17	2.30e22
Willow Creek	12/05/2004	01:48:04.0	40.740	-123.802	21	3.9	4.3	181	49	-75	2.72e22
Blue Lake	12/12/2004	09:13:33.0	40.697	-123.867	27	4.1	4.3	53	72	-10	5.47e22
Pinnacles	12/15/2004	04:16:52.0	36.635	-121.253	14	3.9	3.8	227	86	14	5.11e21
Geysers	12/27/2004	10:36:23.0	38.747	-122.727	5	4.3	4.3	111	48	-72	3.13e22
Avenal	01/28/2005	13:03:26.0	36.047	-120.037	8	3.9	3.8	293	46	102	6.59e21
Alum Rock	02/05/2005	18:43:30.0	37.395	-121.487	14	4.4	4.1	333	90	-178	1.47e22
Parkfield	02/08/2005	22:00:48.0	35.952	-120.506	14	3.5	3.6	57	89	6	2.52e21
Toms Place	03/13/2005	22:09:12.0	37.453	-118.840	8	4.2	4.0	11	90	12	1.32e22
Petrolia	03/18/2005	07:23:58.0	40.370	-124.984	18	4.4	5.0	186	78	30	3.03e23
Parkfield	03/26/2005	04:36:48.0	35.838	-120.388	8	3.6	3.7	138	87	164	4.00e21
Mettler	04/16/2005	19:18:13.0	35.027	-119.178	11	5.1	4.6	249	63	80	1.05e23
Ferndale	04/28/2005	18:31:20.0	40.594	-125.580	14	3.8	4.0	110	87	-177	1.15e22
Green Valley	05/08/2005	08:43:55.0	38.378	-122.166	8	4.2	4.2	171	78	167	2.01e22
Piedmont	05/08/2005	10:35:55.0	37.840	-122.222	5	3.4	3.3	37	80	-28	1.07e21
Geysers	05/09/2005	22:37:39.0	38.786	-122.753	5	4.2	4.4	161	84	-168	3.76e22
Burney	05/10/2005	20:21:10.0	40.946	-121.757	8	4.5	4.5	152	58	-124	5.52e22
Parkfield	05/16/2005	07:24:37.0	35.928	-120.478	11	4.7	4.5	318	86	-169	6.64e22
Anza	06/12/2005	15:41:46.0	33.53	-116.58	14	5.2	5.2	304	65	174	6.48e23
Mendocino	06/15/2005	02:50:54.0	41.328	-125.868	21	0.0	7.0	225	85	13	3.79e26
Mendocino	06/15/2005	06:27:05.0	40.823	-126.489	21	4.6	4.7	207	84	-7	1.09e23
Mendocino	06/15/2005	07:14:11.0	40.905	-126.392	24	4.6	4.7	207	70	23	1.16e23
Yucaipa	06/16/2005	20:53:25.0	34.058	-117.007	11	5.3	4.9	309	48	140	2.42e23
Mendocino	06/17/2005	06:21:41.0	40.758	-126.595	21	6.6	6.7	105	80	170	1.06e26
Tahoe Vista	06/26/2005	18:45:57.0	39.310	-120.067	11	5.2	4.8	230	86	-14	1.78e23

Table 10.1: Moment tensor solutions for significant events from July 1, 2004 to June 30, 2005 using a complete waveform fitting inversion. Epicentral information from the UC Berkeley/USGS Northern California Management Center. Moment is in dyne-cm and depth is in km.

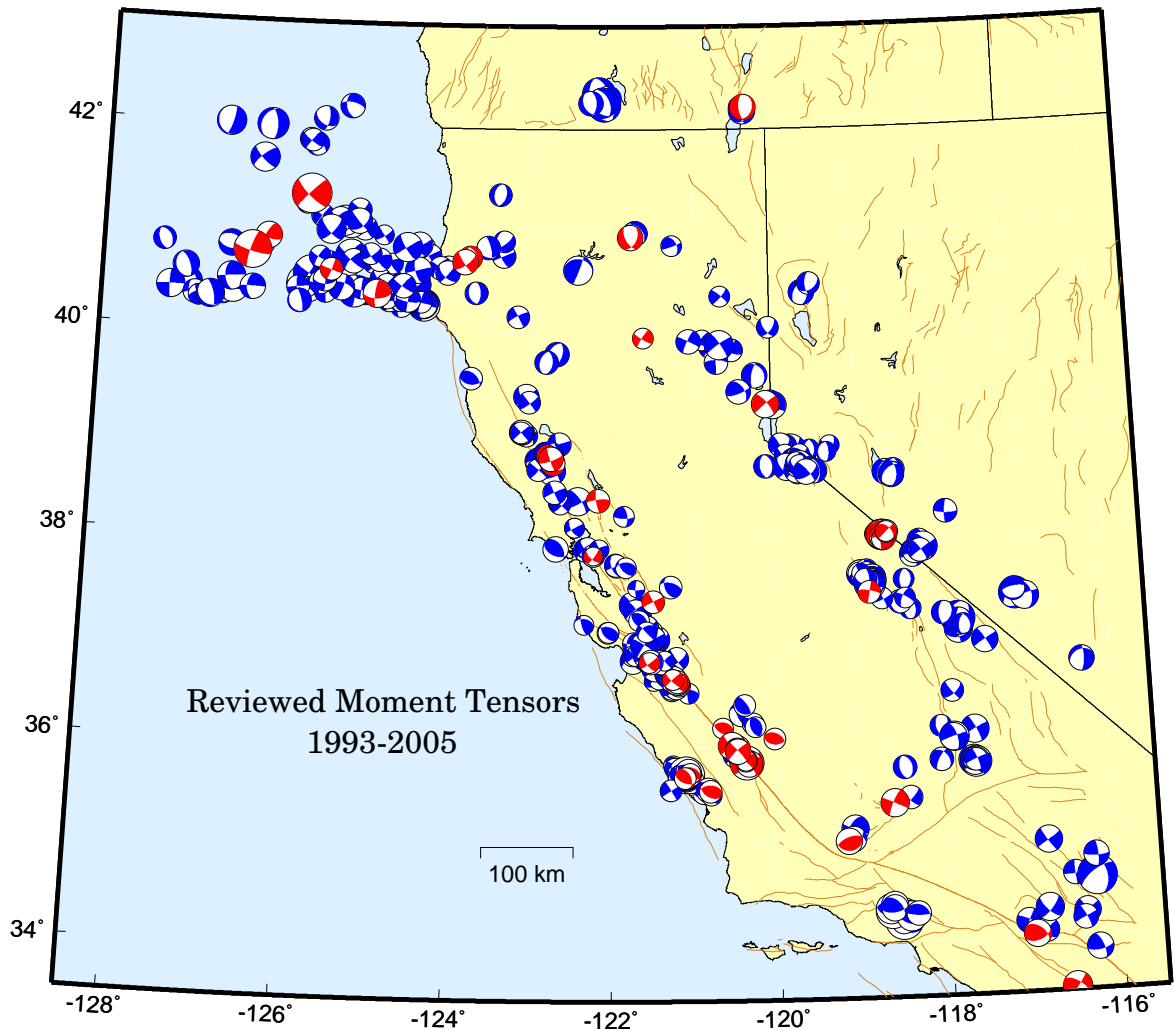


Figure 10.4: Map comparing the reviewed moment tensor solutions determined by the BSL in the last 12 years (blue) and those from the last fiscal year (red).

ure 10.8. The spread between the quietest and noisiest stations on the vertical-component is ~ 50 dB with nine stations in the two noisiest levels. The spread between the quietest and noisiest stations on the horizontal-component is likewise ~ 50 dB with 10 stations in the two noisiest levels. The stations with high horizontal-component PSD noise levels are generally either sites with thick alluvial deposits or high ambient cultural noise levels.

4.2 Teleseisms

In addition to the routine analysis of local and regional earthquakes, the BSL also processes teleseismic earthquakes. Taking advantage of the ANSS catalog, an-

alysts review teleseisms of magnitude 5.8 and higher. All events of magnitude 6 and higher are read on the quietest BDSN station, while events of magnitude 6.5 and higher are read on the quietest station and BKS. Earthquakes of magnitude 7 and higher are read on all BDSN stations. The phase and amplitude data are provided to the NEIC, along with the locations and magnitudes, as contributions to the global catalogs, such as that of the ISC.

5. Acknowledgements

Lind Gee leads the development of the REDI system and directs the routine analysis. Peter Lombard and

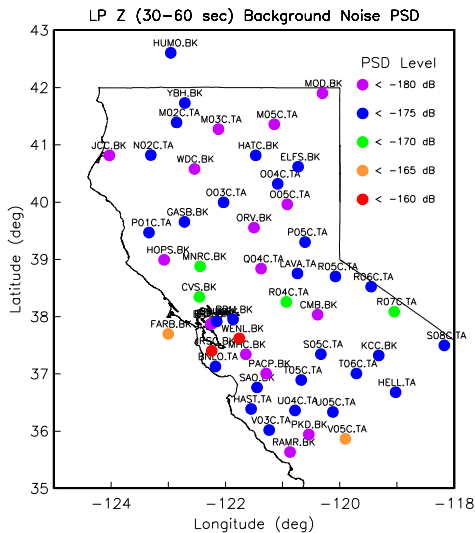


Figure 10.5: Results of seismic background noise PSD analysis of the vertical-component LP (30-60 second) observed at BK and TA network stations in Northern and Central California.

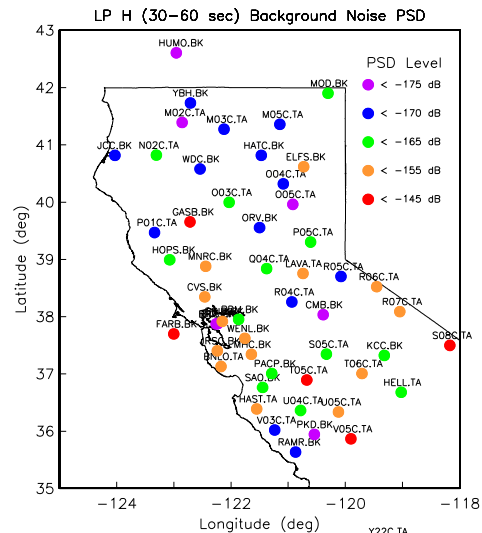


Figure 10.6: Results of seismic background noise PSD analysis of the horizontal-component LP (30-60 second) observed at BK and TA network stations in Northern and Central California.

Doug Neuhauser contribute to the development of software. Rick McKenzie, Doug Dreger, Dennise Templeton, Peggy Hellweg, and David Dolenc contribute to the routine analysis. Lind Gee, Doug Neuhauser, Bob Uhrhammer and Dennise Templeton contributed to the writing of this chapter.

Partial support for the develop of the REDI system is provided by the USGS.

The facilities of the IRIS Data Management System, and specifically the IRIS Data Management Center, were used by Bob Uhrhammer for access to the TA network (USArray) waveform and metadata required in the noise comparison study.

6. References

Dehlinger, P., and B. Bolt, Earthquakes and associated tectonics in a part of coastal central California, *Bull. Seis. Soc. Am.*, *77*, 2056-2073, 1987.

Dreger, D., Lombard, P., Boatwright, J., Wald D., and L. Gee, Finite source models of the December 22, 2003 San Simeon earthquake and applications to ShakeMap (abstract), *Seismol. Res. Lett.*, *75*, 293, 2004.

Dreger, D., and B. Romanowicz, Source characteristics of events in the San Francisco Bay region, *USGS Open*

File Report 94-176, 301-309, 1994.

Dziewonski, A.M., T.-A. Chou and J.H. Woodhouse, Determination of earthquake source parameters from waveform data for studies of global and regional seismicity, *J. Geophys. Res.*, *86*, 2825-2852, 1981.

Earthquake Engineering Research Institute, Preliminary observations on the December 22, 2003, San Simeon earthquake, http://www.eeri.org/lfe/usa_san_simeon.html, 2004.

Gee, L., D. Oppenheimer, T. Shakal, D. Given, and E. Hauksson, Performance of the CISN during the 2003 San Simeon Earthquake, http://www.cisn.org/docs/CISN_SanSimeon.pdf, 2004a.

Gee, L., J. Polet, R. Uhrhammer, and K. Hutton, Earthquake Magnitudes in California, *Seism. Res. Lett.*, *75(2)*, 272, 2004b.

Gee, L., D. Neuhauser, D. Dreger, M. Pasyanos, R. Uhrhammer, and B. Romanowicz, The Rapid Earthquake Data Integration Project, *Handbook of Earthquake and Engineering Seismology*, IASPEI, 1261-1273, 2003a.

Gee, L., D. Dreger, G. Wurman, Y. Gung, B. Uhrhammer, and B. Romanowicz, A Decade of Regional Moment Tensor Analysis at UC Berkeley, *Eos Trans. AGU*, *84(46)*, Fall Meet. Suppl., Abstract S52C-0148, 2003b.

Gee, L., D. Neuhauser, D. Dreger, M. Pasyanos, B. Ro-

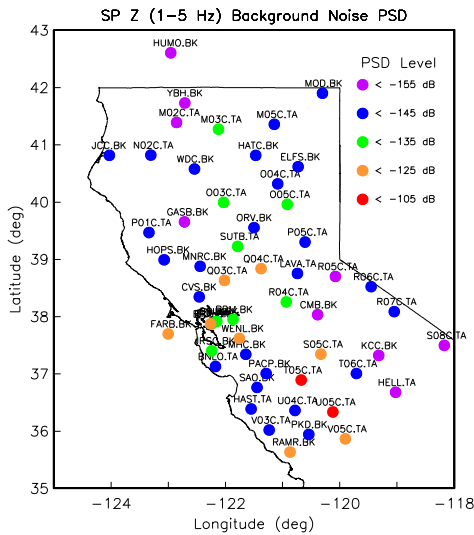


Figure 10.7: Results of seismic background noise PSD analysis of the vertical-component SP (1-5 Hz) observed at BK and TA network stations in Northern and Central California.

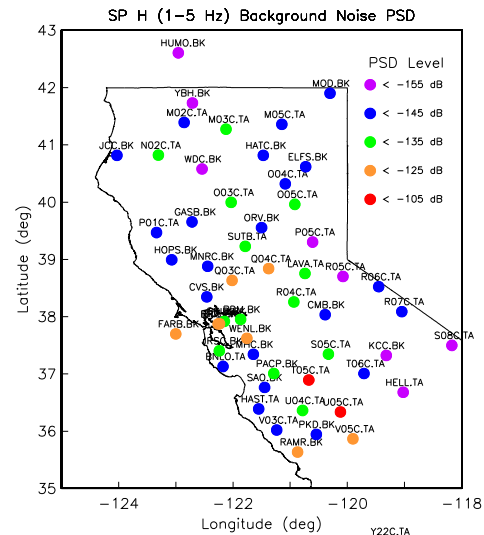


Figure 10.8: Results of seismic background noise PSD analysis of the horizontal-component SP (1-5 Hz) observed at BK and TA network stations in Northern and Central California.

manowicz, and R. Uhrhammer, The Rapid Earthquake Data Integration System, *Bull. Seis. Soc. Am.*, 86, 936-945, 1996.

Hardebeck, J., Boatwright, J., Dreger, D., Goel, R., Graizer, V., Hudnut, K., Ji, C., Jones, L., Langbein, J., Lin, J., Roeloffs, E., Simpson, R., Stark, K., Stein, R., and J. Tinsley, Preliminary report on the 22 December 2003 M6.5 San Simeon, California, earthquake, *Seismol. Res. Lett.*, 75, 155-172, 2004.

Ichinose, G., J. Anderson, K. Smith, and Y. Zeng, Source parameters of eastern California and western Nevada earthquakes from regional moment tensor solutions, *Bull. Seis. Soc. Am.*, 93, 61-84, 2003.

Ritsema, J., and T. Lay, Long-period regional waveform moment tensor inversion for earthquakes in the western United States, *J. Geophys. Res.*, 100, 9853-9864, 1995.

Romanowicz, B., D. Dreger, M. Pasyanos, and R. Uhrhammer, Monitoring of strain release in central and northern California using broadband data, *Geophys. Res. Lett.*, 20, 1643-1646, 1993.

Pasyanos, M., D. Dreger, and B. Romanowicz, Toward real-time estimation of regional moment tensors, *Bull. Seis. Soc. Am.*, 86, 1255-1269, 1996.

Thio, H. K., and H. Kanamori, Moment-tensor inver-

sions for local earthquakes using surface waves recorded at TERRAScope, *Bull. Seis. Soc. Am.*, 85, 1021-1038, 1995.

Chapter 11

Northern California Earthquake Data Center

1. Introduction

The Northern California Earthquake Data Center, a joint project of the Berkeley Seismological Laboratory (BSL) and the U.S. Geological Survey at Menlo Park, serves as an online archive for various types of digital data relating to earthquakes in central and northern California. The NCEDC is located at the Berkeley Seismological Laboratory, and has been accessible to users via the Internet since mid-1992.

The primary goal of the NCEDC is to provide a stable and permanent archival and distribution center of digital geophysical data for networks in northern and central California. These data include seismic waveforms, electromagnetic data, GPS data, strain, creep, and earthquake parameters. The seismic data comes principally from the Berkeley Digital Seismic Network (BDSN) operated by the Seismological Laboratory, the Northern California Seismic Network (NCSN) operated by the USGS, the Berkeley High Resolution Seismic Network (HRSN) at Parkfield, the EarthScope USArray Transportable Array stations in northern California, the various Geysers networks, and selected stations from adjacent networks such as the University of Nevada, Reno network and the Southern California Seismic Network (SCSN). GPS data are primarily from the Bay Area Regional Deformation (BARD) GPS network and the USGS/Menlo Park GPS surveys. The collection of NCSN digital waveforms dates from 1984 to the present, the BDSN digital waveforms date from 1987 to the present, and the BARD GPS data date from 1993 to the present. The BDSN includes stations that form the specialized Northern Hayward Fault Network (NHFN) and the MiniPBO (MPBO) borehole seismic and strain stations in the SF Bay Region.

2. 2004-2005 Activities

By its nature, data archiving is an ongoing activity. In 2004-2005, the NCEDC continued to expand its data holdings and enhance access to the data. Projects and

activities of particular note include:

- Archiving data from EarthScope USArray (network TA) stations for northern California.
- Developing software and procedures, and purchasing hardware to support the archiving of continuous NCSN seismograms from tapes for 2001-2005, and to initiate the archiving of future continuous NCSN seismograms.
- Resumed work on the Northern California Seismicity Project.
- Relocated the NCEDC data archive and distribution hardware to a new state-of-the-art co-location facility in a new seismically braced building on the Berkeley campus.

These activities and projects are described in detail below.

3. Data Collections

The bulk of the data at the NCEDC consists of waveform and GPS data from northern California. Figure 11.1 shows the relative proportion of each data set at the NCEDC. The total size of the datasets archived at the NCEDC is shown in Table 11.1. Figure 11.2 shows the geographic distribution of data archived by the NCEDC.

3.1 BDSN/NHFN/MPBO Seismic Data

The archival of current BDSN (Chapter 3), NHFN (Chapter 5), and Mini-PBO (Chapter 8) (all stations using the network code BK) seismic data is an ongoing task. These data are telemetered from more than 42 seismic data loggers in real-time to the BSL, where they are written to disk files. Each day, an extraction process creates a daily archive by retrieving all continuous and event-triggered data for the previous day. The daily

Volume of Data archived at the NCEDC

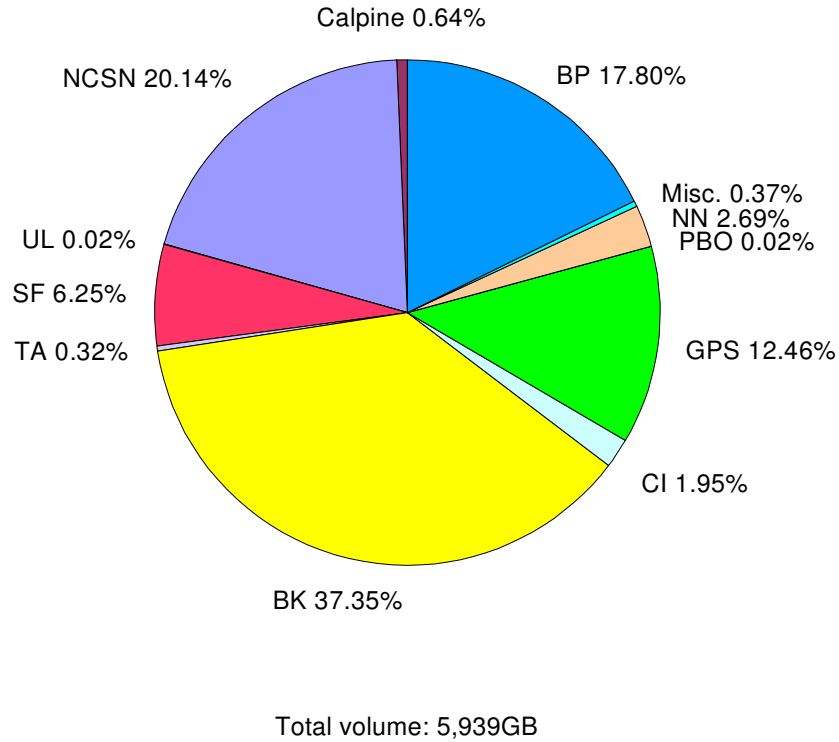


Figure 11.1: Chart showing the relative proportion of each data set at the NCEDC.

Data Type	GBytes
BDSN/NHFN/MPBO (broadband, electric and magnetic field, strain) waveforms	2,218
NCSN seismograms	1,196
Parkfield HRSN seismograms	1,057
BARD GPS (RINEX and raw data)	740
UNR Nevada seismograms	160
SCSN seismograms	116
Calpine/Unocal Geysers region seismograms	38
EarthScope SAFOD seismograms	372
EarthScope USArray seismograms	19
EarthScope PBO strain waveforms	1
USGS Low frequency geophysical waveforms	1
Misc data	22
Total size of archived data	5,939

Table 11.1: Volume of Data Archived at the NCEDC by network

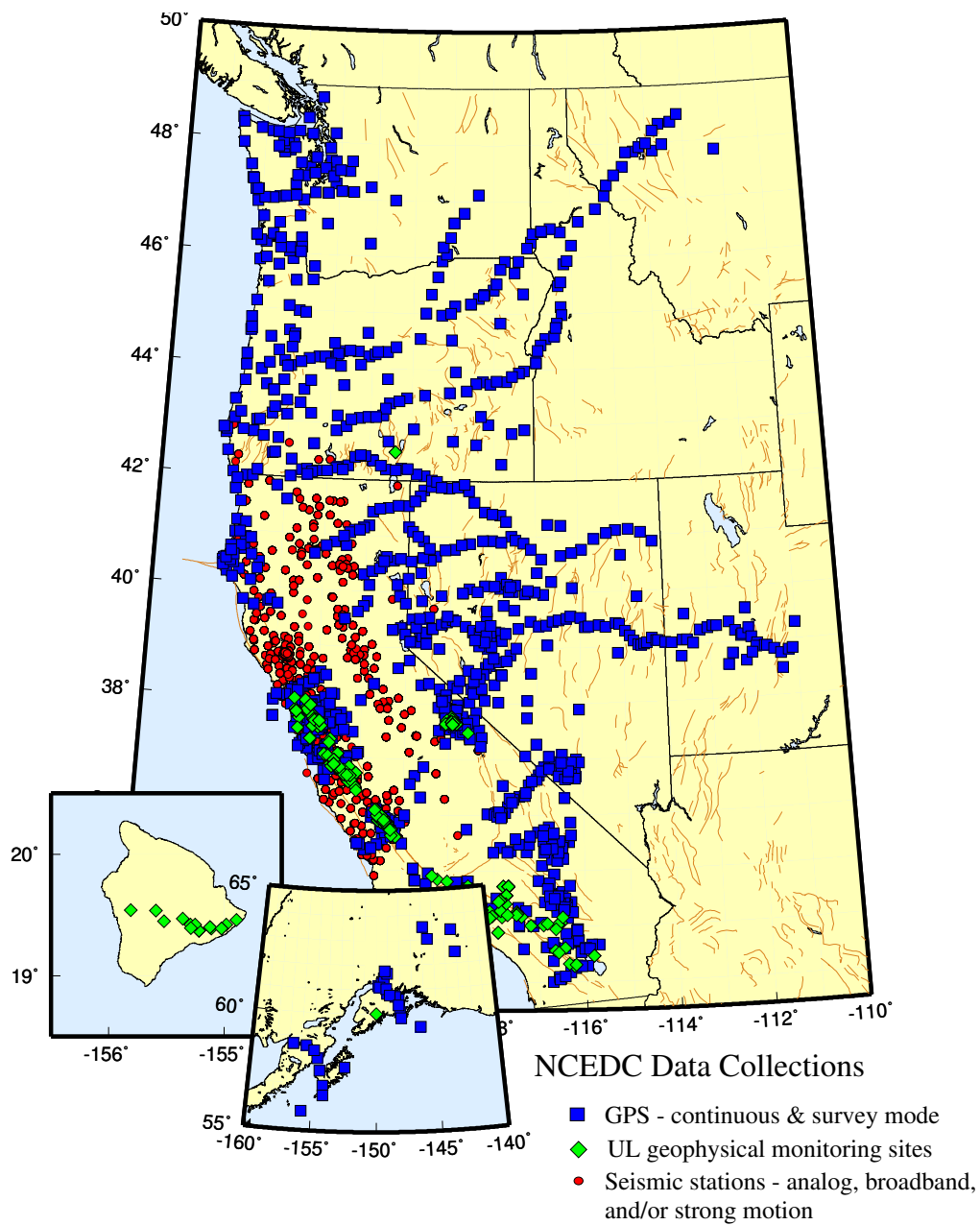


Figure 11.2: Map showing the location of stations whose data are archived at the NCEDC. Circles are seismic sites; squares are GPS sites; and diamonds are the locations of USGS Low-frequency experiments.

archive is run through quality control procedures to correct any timing errors, triggered data is reselected based on the REDI, NCSN, and BSL earthquake catalogs, and the resulting daily collection of data is archived at the NCEDC.

All data acquired from the BDSN/NHFN/MPBO Quanterra data loggers are archived at the NCEDC. The NCEDC has made an effort to archive older digital data, and the 16-bit BDSN digital broadband data from 1987-1991 have been converted to MiniSEED and are now online. In late June 2002, the NCEDC initiated a project to convert the remaining 16-bit BDSN data (MHC, SAO, and PKD1) from late 1991 through mid-1992 to MiniSEED. An undergraduate student was hired to read the old tapes and to work on the conversion. All remaining 20 Hz 16 bit BDSN data has been converted to MiniSEED, and we are working on the decimation procedures to create the 1 Hz data channels. Data acquired by portable 24-bit RefTek recorders before the installation of Quanterra data loggers at NHFN sites has not yet been converted to MiniSEED and archived. Figure 11.3 illustrates the data completeness level of the core BDSN stations.

In September 2004, we began to archive continuous high frequency data (80 Hz and 100 Hz) from all of the BDSN broadband, strong motion, and strainmeter sensors.

3.2 NCSN/SHFN Seismic Data

NCSN and SHFN waveform data are sent to the NCEDC via the Internet and/or private IP network. The NCSN event waveform files are automatically transferred from the USGS Menlo Park to the NCEDC as part of the routine analysis procedure by the USGS, and are automatically verified and archived by the NCEDC.

The NCEDC maintains a list of teleseismic events recorded by the NCSN, which is updated automatically whenever a new NCSN event file is received at the NCEDC, since these events do not appear in the NCSN catalog.

The NCSN operates a total of 15 continuously telemetered digital broadband stations: 11 stations in northwest California and southwest Oregon in support of the USGS/NOAA Consolidated Reporting of EarthquakeS and Tsunamis (CREST) system, two digital broadband stations in the Mammoth region, and two digital broadband stations in the Parkfield region. The NCEDC established procedures to create an archive of continuous data from these stations, in addition to the event waveform files. These data are currently sampled at 100 Hz and are archived continuously. At the USGS's request, the 3 component 500 Hz data from the Mammoth Deep Hole are also continuously archived.

In January 2005, in response to interest in non-volcanic tremors detected in northern and central California, we

started to archive continuous high frequency data from 21 additional NCSN stations in selected regions of northern California and Parkfield. In response to requests for additional continuous NCSN data, we received approval to rebudget funds to purchase disk and tape systems to support the reading and archiving of continuous waveforms from the entire NCSN from 2001 to the present, and to establish procedures for continuous archiving of current NCSN data. We are purchasing the require hardware, and will start reading the NCSN data tapes within the next month. We are working with the NCSN to provide reliable delivery of all current NCSN data channels to the NCEDC over the Internet for continuous archiving.

3.3 Parkfield High Resolution Seismic Network Data

Event seismograms from the Parkfield High Resolution Seismic Network (HRSN) from 1987 through June 1998 are available in their raw SEG Y format via NCEDC research accounts. A number of events have faulty timing due to the lack or failure of a precision timesource for the network. Due to funding limitations, there is currently no ongoing work to correct the timing problems in the older events or to create MiniSEED volumes for these events. However, a preliminary catalog for a significant number of these events has been constructed, and the catalog is available via the web at the NCEDC.

As described in Chapter 6, the original HRSN acquisition system died in late 1998, and an interim system of portable RefTek recorders were installed at some of the sites. Data from this interim system are not currently available online.

In 2000 and 2001, 3 new borehole sites were installed, and the network was upgraded to operate with Quanterra Q730 data loggers and digital telemetry. The upgraded acquisition system detected events using the HRSN stations and extracts waveforms from the HRSN PASO stations. The event waveform files were automatically transferred to the NCEDC, where they were made available to the research community via anonymous ftp until they are reviewed and permanently archived. In 2000-2003 the PASO array, a temporary IRIS PASSCAL broadband network with real-time telemetry, was installed in the Parkfield area and its recording system was housed at the HRSN recording site in Parkfield. During this time, the HRSN collected event data from both the HRSN and PASO array and provided this integrated data set to researchers in near-real-time.

The HRSN 20 Hz (BP) and state-of-health channels were archived continuously at the NCEDC. As an interim measure, the NCEDC also archived the continuous 250 Hz (DP) data channels through late 2002 in order to help researchers retrieve events that were not detected during the network upgrade.

The increased seismic activity related to the magnitude

BK Data Availability

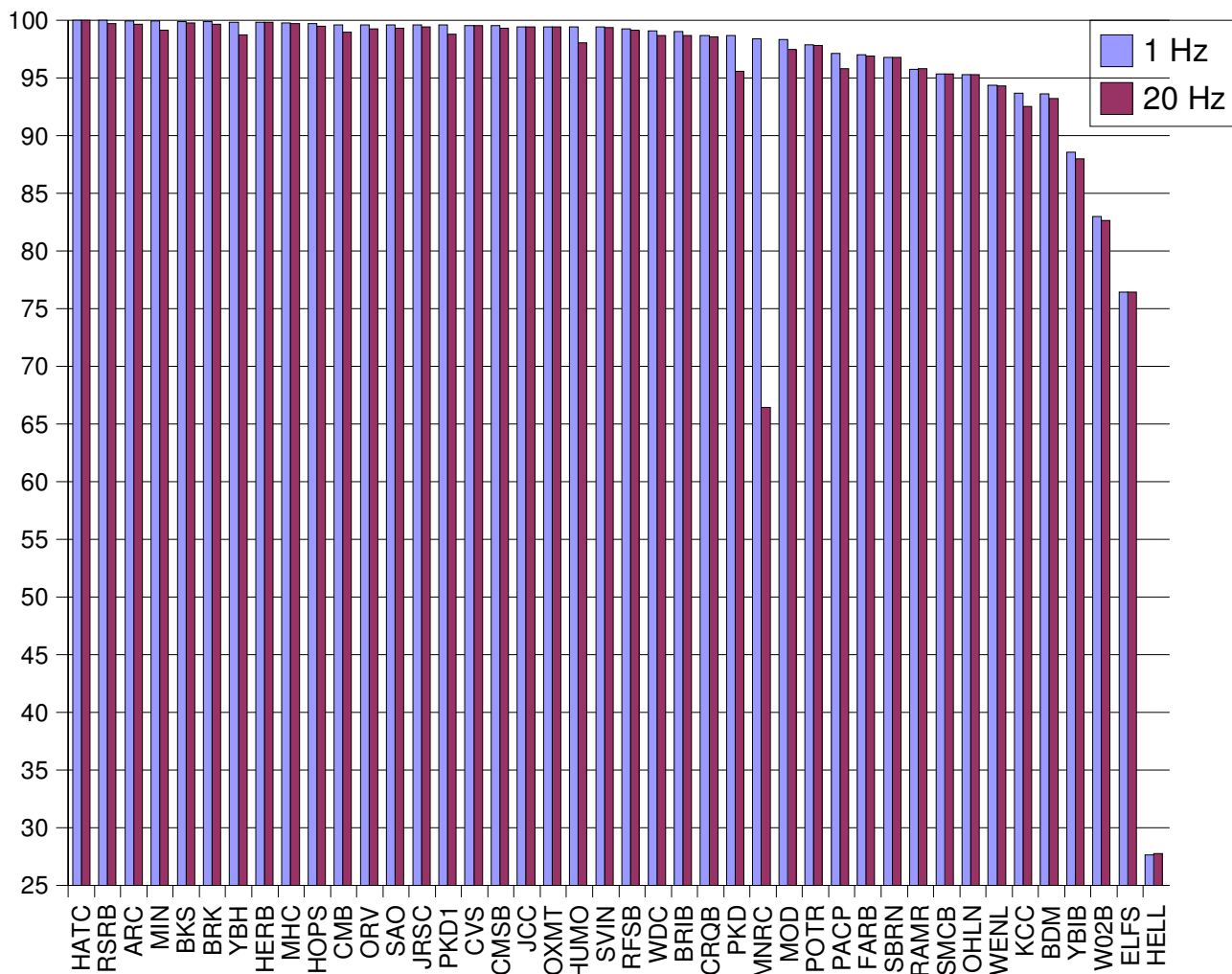


Figure 11.3: Chart showing the availability of BDSN/NHFN/MPBO (BK network) data at the NCEDC for the 1 Hz and 20 or 40 Hz channels from 01/01/1996 - 09/01/2005. The data availability from these networks is better than 95% at nearly all stations. Notable exceptions are ELFS and HELL (BDSN/USArray sites with problematic satellite telemetry), MNRC (operated for the first year with only dialup telemetry before the installation of continuous telemetry), YBIB (lost AC power before decommissioning the site), and W02B (experienced significant radio problems). In general, a difference between the 1 and 20 or 40 Hz data is indicative of one or more significant telemetry problems. Following a major telemetry outage, BSL staff will recover 1 Hz continuous data but only event data for the higher rate data channels.

6.5 earthquake in nearby San Simeon on December 22, 2003 drastically increased the number of triggers by the HRSN network. From December 2003 through August 2004, the HRSN had over 70,000 triggers. The 56Kb frame relay connection from Parkfield to UC Berkeley, which was installed to transmit continuous 20 Hz data, selected 250 Hz channels, and event triggered 250 Hz waveforms from the network, was saturated from the increased activity. The HRSN stopped telemetering the event-triggered waveforms, and the NCEDC started to archive continuous 20 and 250 Hz data from the entire network from tapes created at the HRSN operations center in Parkfield in order to preserve this unique dataset. The seismicity again increased after the magnitude 6.0 Parkfield earthquake on September 28, 2004. The NCEDC plans to continue archiving both the continuous 250 Hz and 20 Hz data streams for the foreseeable future.

3.4 EarthScope USArray Transportable Array

EarthScope began installing broadband stations for the Transportable Array component of USArray in California in 2005. The NCEDC started acquiring telemetered continuous data from the northern California and surrounding stations as they were installed, and is archiving these data to support users working with northern California seismic data. These data are made available to users using the same data request methods as all other continuous data waveform data at the NCEDC. The Transportable Array stations have a limited operational timespan of 18 to 24 months, after which they will be relocated to new sites across the country.

3.5 EarthScope SAFOD

In July 2002, scientists from Duke University successfully installed a three component 32 level downhole seismic array in the pilot hole at the EarthScope SAFOD site in collaboration with Steve Hickman (USGS), Mark Zoback (Stanford University) and the Oyo Geospace Engineering Resources International (GERI) Corporation. High frequency event recordings from this array has been provided by Duke University for archiving at the NCEDC. We converted data from the original SEG-2 format data files to MiniSEED, and have developed the SEED instrument responses for this data set. We are continuing to receive seismic data from the SAFOD Pilot Hole and Main Hole, and will make this data available as resources permit. We anticipate receiving funding from SAFOD in the future to cover the cost of archiving these data.

3.6 UNR Broadband data

The University of Nevada, Reno (UNR) operates several broadband stations in western Nevada and eastern California that are important for northern California earthquake processing and analysis. Starting in August 2000, the NCEDC has been receiving and archiving continuous broadband data from four UNR stations. The data are transmitted in real-time from UNR to UC Berkeley, where they are made available for real-time earthquake processing and for archiving. Initially, some of the stations were sampled at 20 Hz, but all stations are now sampled and archived continuously at 100 Hz.

The NCEDC installed Simple Wave Server (SWS) software at UNR, which provides an interface to UNR's recent collection of waveforms. The SWS is used by the NCEDC to retrieve waveforms from UNR that were missing at the NCEDC due to real-time telemetry outages between UNR and UC Berkeley.

3.7 Electro-Magnetic Data

The NCEDC continues to archive and process electric and magnetic field data acquired from data loggers at two sites (SAO and PKD). At PKD and SAO, 3 components of magnetic field and 2 or 4 components of electric field are digitized and telemetered in real-time along with seismic data to the Berkeley Seismological Laboratory, where they are processed and archived at the NCEDC in a similar fashion to the seismic data (Chapter ??).

The system generates continuous data channels at 40 Hz, 1 Hz, and .1 Hz for each component of data. All these data are archived and remain available online at the NCEDC. Using programs developed by Dr. Martin Fullerkrug at the Stanford University STAR Laboratory (now at the Institute for Meteorology and Geophysics at the University of Frankfurt), the NCEDC is computing and archiving magnetic activity and Schumann resonance analysis using the 40 Hz data from this dataset. The magnetic activity and Schumann resonance data can be accessed from the Web.

In collaboration with Dr. Simon Klemperer at Stanford University and Dr. Darcy McPhee at the USGS, the NCEDC is archiving similar continuous electric and magnetic field data from instruments co-located at the Stanford JRSC seismic station.

The NCEDC also archives data from a low-frequency, long-baseline electric field project operated by Dr. Steve Park of UC Riverside at site PKD2. These data are acquired and archived in an identical manner to the other electric field data at the NCEDC.

3.8 GPS Data

The NCEDC continues to expand its archive of GPS data through the BARD (Bay Area Regional Deformation) network of continuously monitored GPS receivers

in northern California (Chapter 7). The NCEDC GPS archive now includes 67 continuous sites in northern California. There are approximately 50 core BARD sites owned and operated by UC Berkeley, USGS (Menlo Park and Cascade Volcano Observatory), LLNL, UC Davis, UC Santa Cruz, Trimble Navigation, and Stanford. Data are also archived from sites operated by other agencies including East Bay Municipal Utilities District, the City of Modesto, the National Geodetic Survey, and the Jet Propulsion Laboratory.

In addition to the standard 15 second or 30 second continuous GPS datastream, the NCEDC is now archiving and distributing high-rate 1 Hz continuous GPS data from the 14 stations in Parkfield and selected BARD stations. These high-rate data are available via anonymous FTP from the NCEDC but are currently not included in the GPS Seamless Archive (GSAC), since the GSAC does not currently handle both high-rate and low-rate data from the same site and day.

The NCEDC continues to archive non-continuous survey GPS data. The initial dataset archived is the survey GPS data collected by the USGS Menlo Park for northern California and other locations. The NCEDC is the principal archive for this dataset. Significant quality control efforts were implemented by the NCEDC to ensure that the raw data, scanned site log sheets, and RINEX data are archived for each survey. All the USGS MP GPS data has been transferred to the NCEDC and virtually all the data from 1992 to the present has been archived and is available for distribution.

3.9 Geysers Seismic Data

The Calpine Corporation currently operates a micro-seismic monitoring network in the Geysers region of northern California. Prior to 1999 this network was operated by Unocal. Through various agreements, both Unocal and Calpine have released triggered event waveform data from 1989 through 2000 along with preliminary event catalogs for the same time period for archiving and distribution through the NCEDC. This dataset represents over 296,000 events that were recorded by Calpine/Unocal Geysers network, and are available via research accounts at the NCEDC.

The Lawrence Berkeley Laboratory (LBL), with funding from the California Energy Commission, operates a 22 station network in the Geysers region with an emphasis on monitoring seismicity related to well water injection. The earthquake locations and waveforms from this network are sent to the NCEDC, and the locations are forwarded to the NCSN so that they can be merged into the NCSN earthquake catalog. The LBL Geysers waveforms will be available at the NCEDC once the events have been merged into the NCSN catalog.

3.10 USGS Low Frequency Data

Over the last 27 years, the USGS at Menlo Park, in collaboration with other principal investigators, has collected an extensive low-frequency geophysical data set that contains over 1300 channels of tilt, tensor strain, dilatational strain, creep, magnetic field, water level, and auxiliary channels such as temperature, pore pressure, rain and snow accumulation, and wind speed. In collaboration with the USGS, we assembled the requisite information for the hardware representation of the stations and the instrument responses for many channels of this diverse dataset, and developed the required programs to populate and update the hardware database and generate the instrument responses. We developed the programs and procedures to automate the process of importing the raw waveform data and convert it to MiniSEED format.

We have currently archived timeseries data from 887 data channels from 167 sites, and have instrument response information for 542 channels at 139 sites. The waveform archive is updated on a daily basis with data from 350 currently operating data channels. We will augment the raw data archive as additional instrument response information is assembled by the USGS for the channels, and will work with the USGS to clearly define the attributes of the “processed” data channels.

3.11 SCSN/Statewide seismic data

Starting in 2004, the NCEDC started to archive broadband and strong motion data from 15 SCSN (network CI) stations that are telemetered to the Northern California Management Center (NCMC) of the California Integrated Seismic Network (CISN). These data are used in the prototype real-time state-wide earthquake processing system and also provide increased coverage for northern California events. Since the data are telemetered directly from the stations in real-time to both the SCSN and to the NCMC, the NCEDC archives the NCMC’s copy of the data to ensure that at least one copy of the data will be preserved.

3.12 Northern California Seismicity Project

The objective of Northern California Seismicity Project is to characterize the spatial and temporal evolution of the northern and Central California seismicity during the initial part of the earthquake cycle as the region emerges from the stress shadow of the great 1906 San Francisco earthquake. Although the current BSL catalog of earthquakes for the region appears to be a simple list of events, one must remember that it really is a very complex data set. The existing catalog is inhomogeneous in that it suffers from the three types of man-made seismicity changes, namely, detection changes, reporting changes, and magnitude shifts. The inherent catalog in-

homogeneity exists because the location and magnitude determination methodologies have changed as the instrumentation and computational capabilities improved over the past century. It is easy to misinterpret observed variations in seismicity if we do not understand these inherent limitations of the catalog. As a result, the northern and central California seismicity since 1906 is poorly understood.

Creation of a northern and central California catalog of seismicity that is homogeneous, that spans as many years as possible, and that includes formal estimates of the parameters and their uncertainty is a fundamental prerequisite for probabilistic studies of the seismicity. The existence of the invaluable BSL seismological archive, containing the original seismograms as well as the original reading/analysis sheets allows the application of modern analytical algorithms towards the problem of determining the source parameters of the historical earthquakes.

Our approach is to systematically re-analyze the data acquired from the reading/analysis sheet archive to develop a homogeneous catalog of earthquake location and local magnitude (ML) including formal uncertainties on all parameters which extends as far back in time as the instrumental records allow and which is complete above appropriate threshold magnitudes. We anticipate being able to compile a new catalog of location and ML which spans 1930 to the present and is which complete at the ML 3 threshold.

The locations and available magnitude estimates for all northern and central California earthquake epicenters, for which geographic coordinates were available, were transcribed to a computer readable flat file in 1964. This list of events subsequently became the origins of the current BSL historical seismicity catalog. BSL began routine computer transcription of the reading/analysis sheet data in 1984. The first NCSP task is to transcribe the 1983 and earlier data from the original reading/analysis sheets for northern and central California earthquakes to a computer readable flat files. We thus started by transcribing the data for 1983, and we have been working back in time. Several students have been working on the project this past year, and we are currently transcribing data from the early 1950's. As we work back in time, the task has become more time consuming. Two significant epochs have affected our transcription effort to date. First, the BSL began transmittal of the BSL locations and phase data for a subset of BSL stations to the ISC via teletype in 1964. We recovered this data from the ISC CD-ROM's and generated the relevant files to facilitate and expedite the transcription effort. Starting in 1950, the BSL bulletins contained all relevant phase onset and amplitude data for the determination of location and local magnitude, and only the location data were available in computer readable form. Thus, we have to transcribe all the available phase and amplitude data

on the reading/analysis sheets. To date, we have transcribed data for over 7,300 earthquakes with more than 132,000 phase readings and 31,000 amplitude readings.

3.13 Earthquake Catalogs

Northern California

Currently both the USGS and BSL construct and maintain earthquake catalogs for northern and central California. The "official" UC Berkeley earthquake catalog begins in 1910, and the USGS "official" catalog begins in 1966. Both of these catalogs are archived and available through the NCEDC, but the existence of 2 catalogs has caused confusion among both researchers and the public. The BSL and the USGS have spent considerable effort over the past years to define procedures for merging the data from the two catalogs into a single northern and central California earthquake catalog in order to present a unified view of northern California seismicity. The differences in time period, variations in data availability, and mismatches in regions of coverage all complicate the task.

Worldwide

The NCEDC, in conjunction with the Council of the National Seismic System (CNSS), produced and distributed a world-wide composite catalog of earthquakes based on the catalogs of the national and various U.S. regional networks for several years. Each network updates their earthquake catalog on a daily basis at the NCEDC, and the NCEDC constructs a composite world-wide earthquake catalog by combining the data, removing duplicate entries that may occur from multiple networks recording an event, and giving priority to the data from each network's *authoritative region*. The catalog, which includes data from 14 regional and national networks, is searchable using a Web interface at the NCEDC. The catalog is also freely available to anyone via ftp over the Internet.

With the demise of the CNSS and the development of the Advanced National Seismic System (ANSS), the NCEDC was asked to update its Web pages to present the composite catalog as a product of the ANSS. This conversion was completed in the fall of 2002. We continue to create, house, distribute, and provide a searchable web interface to the ANSS composite catalog, and to aid the regional networks in submitting data to the catalog.

4. Hardware and Software Systems

In 2005, the NCEDC relocated its archive and distribution system from McCone Hall to a new state-of-the-art computer facility in a new seismically braced building on the Berkeley campus. The facility provides seismically

braced equipment racks, gigabit ethernet network, air conditioning and power conditioning. The entire facility is powered by a UPS with generator backup.

The currently installed NCEDC facilities consist of a mass storage environment hosted by a Sun V240 host computer, a 100 slot LTO-2 tape library with two tape drives and a 20 TByte capacity, and 10 TBytes of RAID storage all managed with the SAM-FS hierarchical storage management (HSM) software. A dual processor Sun Ultra 60 provides Web services and research account access to the NCEDC, a dual Sun 280R processor provide data import and export services, and a Sun Ultra 450 computer is used for quality control procedures. Two AIT tape libraries will be used to read NCSN continuous data tapes. An 64-bit Linux system hosts a database dedicated to providing data to external users.

The hardware and software system is configured to automatically create multiple copies of each timeseries file. The NCEDC creates an online copy of each file on online RAID, a second copy on LTO-2 tape which is stored online in the tape library, and a third copy on LTO-2 tape which is stored offline and offsite. All NCEDC data is therefore online and rapidly accessible by users.

The NCEDC operates two instances of its Oracle database, one for internal operations, and one for external use for user data queries and data distribution programs. The databases are synchronized using multi-master replication.

5. Data Quality Control

The NCEDC developed a GUI-based state-driven system *CalQC* to facilitate the quality control processing that is applied to the continuously archived data sets at the NCEDC.

The quality control procedures for these datasets include the following tasks:

- data extraction of a full day of data,
- quickcheck program to summarize the quality and stability of the stations' clocks,
- determine if there is missing data for any data channel,
- provided procedures to retrieve missing data from the stations and incorporate it into the day's data,
- optional creation of multi-day timeseries plots for state-of-health data channels,
- optional timing corrections for data,
- optional extraction of event-based waveforms from continuous data channels,

- optional repacking of MiniSEED data,
- creating waveform inventory entries in the NCEDC database,
- publishing the data for remote access on the NCEDC.

CalQC uses previously developed programs to perform each function, but it provides a graphical point-and-click interface to automate these procedures, and to provide the analyst with a record of when each process was started, whether it executed correctly, and whether the analyst has indicated that a step has been completed. *CalQC* is used to process all data from the BDSN network, and all continuous data from the NCSN, UNR, SCSN, and HRSN networks that are archived by the NCEDC.

6. User Interface

6.1 SeismiQuery

We have ported and installed the IRIS *SeismiQuery* program at the NCEDC, which provides a common interface for querying attributes and available data for SEED format data, and have provided both IRIS and the SCEC Data Center with our modified version of *SeismiQuery*.

6.2 NetDC

In a collaborative project with the IRIS DMC and other worldwide datacenters, the NCEDC helped develop and implement *NetDC*, a protocol which will provide a seamless user interface to multiple datacenters for geophysical network and station inventory, instrument responses, and data retrieval requests. The *NetDC* builds upon the foundation and concepts of the IRIS *BREQ_FAST* data request system. The *NetDC* system was put into production in January 2000, and is currently operational at three datacenters worldwide – the NCEDC, IRIS DMC, and Geoscope. The *NetDC* system receives user requests via email, automatically routes the appropriate portion of the requests to the appropriate datacenter, optionally aggregates the responses from the various datacenters, and delivers the data (or ftp pointers to the data) to the users via email.

6.3 STP

In 2002, the NCEDC wrote a collaborative proposal with the SCEDC to the Southern California Earthquake Center, with the goal of unifying data access between the two data centers. As part of this project, the NCEDC and SCEDC are working to support a common set of 3 tools for accessing waveform and parametric data: *SeismiQuery*, *NetDC*, and *STP*.

The *Seismogram Transfer Program* or *STP* is a simple client-server program, developed at the SCEDC. Access to *STP* is either through a simple direct interface that is available for Sun or Linux platforms, or through a GUI Web interface. With the direct interface, the data are placed directly on a user's computer in several possible formats, with the byte-swap conversion performed automatically. With the Web interface, the selected and converted data are retrieved with a single ftp command. The *STP* interface also allows rapid access to parametric data such as hypocenters and phases.

The NCEDC has continued work on *STP*, working with the SCEDC on extensions and needed additions. We added support for the full SEED channel name (Station, Network, Channel, and Location), and are now able to return event-associated waveforms from the NCSN waveform archive.

6.4 EVT_FAST

In order to provide Web access to the NCSN waveform before the SEED conversion and instrument response for the NCSN has been completed, the NCEDC implemented *EVT_FAST*, an interim email-based waveform request system similar to the *BREQ_FAST* email request system. Users can email *EVT_FAST* requests to the NCEDC and request NCSN waveform data based on the NCSN event id. The NCSN waveform data is converted to either SAC ASCII, SAC binary, or AH format, and placed in the anonymous ftp directory so that users can retrieve the data. The *EVT_FAST* waveforms are currently named with the USGS's native NCSN channel names. We have just begun the work to provide *EVT_FAST* waveform data in SEED format with SEED channel names.

6.5 FISSURES

The *FISSURES* project developed from an initiative by IRIS to improve earth scientists' efficiency by developing a unified environment that can provide interactive or programmatic access to waveform data and the corresponding metadata for instrument response, as well as station and channel inventory information. *FISSURES* was developed using CORBA (Common Object Request Broker Architecture) as the architecture to implement a system-independent method for the exchange of this binary data. The IRIS DMC developed a series of services, referred to as the *Data Handling Interface (DHI)*, using the *FISSURES* architecture to provide waveform and metadata from the IRIS DMC.

The NCEDC has implemented the *FISSURES Data Handling Interface (DHI)* services at the NCEDC, which involves interfacing the DHI servers with the NCEDC database schema. We started with the source code for the IRIS DMC's DHI servers, which reduced significantly the implementation's time. We now have the waveform

and event *FISSURES* services running in demonstration mode at the NCEDC. These services interact with the NCEDC database and data storage system, and can deliver NCEDC event and channel metadata as well as waveforms using the *FISSURES* interfaces. We have installed the *FISSURES DHI* servers, and worked with the IRIS DMC in 2003-2004 to register with the *FISSURES* naming services which are run at both the IRIS DMC and the NCEDC.

6.6 GSAC

Since 1997, the NCEDC has collaborated with UNAVCO and other members of the GPS community on the development of the *GPS Seamless Archive Centers (GSAC)* project. This project allows a user to access the most current version of GPS data and metadata from distributed archive locations. The NCEDC is participating at several levels in the *GSAC* project: as a primary provider of data collected from core BARD stations and USGS MP surveys, and as a wholesale collection point for other data collected in northern California. We helped to define database schema and file formats for the *GSAC* project, and have produced complete and incremental monumentation and data holdings files describing the data sets that are produced by the BARD project or archived at the NCEDC so that other members of the *GSAC* community can provide up-to-date information about our holdings. Currently, the NCEDC is the primary provider for over 120,000 data files from over 1400 continuous and survey-mode monuments. The data holdings records for these data have been incorporated into the *GSAC* retailer system, which became publicly available in late 2002.

7. Database Development

Most of the parametric data archived at the NCEDC, such as earthquake catalogs, phase and amplitude readings, waveform inventory, and instrument responses, have been stored in flat text files. Flat files are easily stored and viewed, but are not efficiently searched. Over the last year, the NCEDC, in collaboration with the Southern California Earthquake Data Center (SCEDC) and the California Integrated Seismic Network (CISN), has continued development of database schemas to store the parametric data from the joint earthquake catalog, station history, complete instrument response for all data channels, and waveform inventory.

The parametric schema supports tables and associations for the joint earthquake catalog. It allows for multiple hypocenters per event, multiple magnitudes per hypocenter, and association of phases and amplitudes with multiple versions of hypocenters and magnitudes respectively. The instrument response schema represents

full multi-stage instrument responses (including filter coefficients) for the broadband data loggers. The hardware tracking schema will represent the interconnection of instruments, amplifiers, filters, and data loggers over time. This schema will be used to store the joint northern California earthquake catalog and the ANSS composite catalog.

The entire description for the BDSN/NHFN/MPBO, HRSN, and USGS Low Frequency Geophysical networks and data archive has been entered into the hardware tracking, SEED instrument response, and waveform tables. Using programs developed to perform queries of waveform inventory and instrument responses, the NCEDC can now generate full SEED volumes for these networks based on information from the database and the waveforms on the mass storage system.

During 2002-2003, the NCEDC and NCSN jointly developed a system consisting of an extensive spreadsheet containing per-channel information that describes the hardware of each NCSN data channel and provides each channel with a SEED-compliant channel name. This spreadsheet, combined with a limited number of files that describe the central-site analog digitizer, FIR decimation filters, and general characteristics of digital acquisition systems, allow the NCSN to assemble its station history in a format that the NCEDC can use to populate the hardware tracking and instrument response database tables for the NCSN.

During 2003-2004, the NCEDC and NCSN finalized the CUSP-to-SEED channel mapping for the NCSN waveform, and entered all of the hardware tracking and response information into the NCEDC database for the sites operated by the NCSN, and can now generate complete SEED responses for all of those data channels. There is, however, additional work that needs to be done in conjunction with contributing networks such as CA DWR, UNR, and SCSN to provide responses for shared stations.

The second part of this project is the conversion of the NCSN waveforms from their native CUSP format into MiniSEED, the standard NCEDC waveform format. Multiple problems needed to be addressed, such as ambiguous or erroneously labeled CUSP data channel, sensors that were recorded on multiple data channels, and ensuring that each distinct data channel is mapped to a distinct SEED channel name. The NCEDC developed programs to use the time-dependent NCSN instrument response spreadsheet and NCSN-supplied channel name transformation rules to determine the SEED channel naming, and to provide feedback to the NCSN on channel naming problems. In 2004, the NCEDC converted all the NCSN waveform data from the period 1984 through 2003 from CUSP format into MiniSEED format. We entered the waveform descriptors into the NCEDC database, and provided association information between

the NCSN event ids and the corresponding waveform data. We have converted all the NCSN archived waveforms from their initial CUSP format to MiniSEED, and convert all new incoming CUSP waveforms to MiniSEED as they are received at the NCEDC.

The NCEDC has developed XML import and export procedures to provide better maintenance of the hardware tracking information and resulting instrument responses for stations in our database. When changes are made to either existing hardware or to station configurations, we export the current view in XML format, use a GUI-based XML editor to easily update the information, and import the changes back into the database. When adding new stations or hardware, we can easily use information from existing hardware or stations as templates for the new information. This allows us to treat the database as the authoritative source of information, and to use off-the-shelf tools such as the XML editor and XML differencing programs as part of our database maintenance procedures.

We distributed all our programs and procedures for populating the hardware tracking and instrument response tables to the SCSN in order to help them populate their database.

During 2002-2003, the BSL had been processing events detected by the HRSN (BP) network. The waveform data and event parameters (picks and hypocenters) are stored in separate HRSN database tables, and will be merged with events from the NCSN when the NCSN catalog is migrated to the database. However, human event processing stopped after the San Simeon earthquake due to the rapid increase in seismicity related to that event.

Additional details on the joint catalog effort and database schema development may be found at <http://www.ncedc.org/db>

8. Data Distribution

The NCEDC continues to use the World Wide Web as a principal interface for users to request, search, and receive data from the NCEDC. The NCEDC has implemented a number of useful and original mechanisms of data search and retrieval using the World Wide Web, which are available to anyone on the Internet. All the documentation about the NCEDC, including the research users' guide, is available via the Web. Users can perform catalog searches and retrieve hypocentral information and phase readings from the various earthquake catalogs at the NCEDC via easy-to-use forms on the Web. In addition, users can peruse the index of available broadband data at the NCEDC, and can request and retrieve broadband data in standard SEED format via the Web. Access to all datasets is available via research accounts at the NCEDC.

The NCEDC acquired the internet domain name

`ncedc.org` this year to better represent the data center as a multi-institutional collaborative project. The NCEDC's new Web address is <http://www.ncedc.org/>.

The NCEDC hosts a web page that allows users to easily query the NCEDC waveform inventory, and generate and submit *NetDC* requests to the NCEDC. The NCEDC currently supports both the *BREQ_FAST* and *NetDC* request formats. As part of our collaboration with SCEDC, the NCEDC provided its *BREQ_FAST* and *NetDC* interface programs to SCEDC. The NCEDC also supports the SCEC *STP* data request interface, as well as the IRIS *FISSURES DHI* interfaces for waveforms, station meta-data, and event information.

The various earthquake catalogs, phase, and earthquake mechanism can be searched using NCEDC web interfaces that allow users to select the catalog, attributes such as geographical region, time and magnitude. The GPS data is available to all users via anonymous ftp. Research accounts are available to any qualified researcher who needs access to the other datasets that currently are not available via the Web.

The GPS data archived at the NCEDC is available over the Internet through the GSAC retailer system, which became publicly available in late 2002, as well as by anonymous FTP.

9. Acknowledgements

The NCEDC is a joint project of the BSL and the USGS Menlo Park and is partially funded by the USGS.

Doug Neuhauser is the manager of the NCEDC. Stephane Zuzlewski, Rick McKenzie, Mark Murray, and Lind Gee of the BSL and David Oppenheimer, Hal Macbeth, and Fred Klein of the USGS Menlo Park contribute to the operation of the NCEDC. Doug Neuhauser, Lind Gee, Stephane Zuzlewski, and Bob Uhrhammer contributed to the preparation of this chapter.

Chapter 12

Outreach and Educational Activities

1. Introduction

The BSL is involved in a variety of outreach activities, ranging from lectures and lab tours to educational displays and the development of classroom materials for K-12 teachers. We maintain an earthquake information tape (510-642-2160) and an extensive set of Web pages, providing basic earthquake and seismic hazard information for northern and central California.

2. Outreach Overview

2.1 Educational Displays

As part of the BSL's outreach activities, we have made REDI earthquake data available to a number of universities, colleges, and museums as educational displays. As noted above, this year marked the expansion of this program to the K-12 environment. Participating organizations receive a REDI pager and the Qpager software to display the earthquake information. The Qpager program maps the previous seven days of seismicity, with earthquake shown as a dot. The size of the dot indicates the magnitude of the event, while the color of the dot indicates its age. These educational displays have been installed at UC Berkeley (McCone Hall, Earthquake Engineering Research Center, LHS), California Academy of Sciences, CSU Fresno, CSU Northridge, CSU Sacramento, Caltech, College of the Redwoods, Fresno City College, Humboldt State University, San Diego State University, Sonoma State University, Stanford University (Blume Engineering Center, Department of Geophysics), UC Davis, UC Santa Cruz, UC San Diego, and USC. In a pilot project initiated two years ago, the San Francisco Unified School District has been given two pager systems for use in middle school classrooms.

In addition to the seismicity displays, the BSL provides local waveform feeds for helicorders at several visitor centers associated with BDSN stations (CMB and MHC). Organizations such as LHS, KRON, and KPIX receive feeds from BKS via dedicated phone lines for display, while the USGS Menlo Park uses data from CMB for display in the lobby of the seismology building. The

BSL has also loaned a seismometer and helicorder display to the San Leandro Unified School District for their use in science classes.

2.2 WWW

Over the last year, we have continued to expand our presence on the WWW. Our primary goal has been to provide a source of earthquake information for the public, although we also provide information about the networks, such as station profiles, which benefits the research community as well. We provide such information as seminar schedules, course advertisements, descriptions of operations and research, updates on recent earthquake activity, details on Bay Area seismicity and hazards, and links to other earthquake and earth science servers. We also use the WWW server for our own information distribution, with such details as the computing and operational resources, rosters, and schedules for various purposes.

2.3 Earthquake Research Affiliates Program

The UC Berkeley Earthquake Research Affiliates (ERA) Program is an outreach project of the BSL, the Department of Geology and Geophysics, and the Earthquake Engineering Research Center. The purpose is to promote the support of earthquake research while involving corporations and governmental agencies in academic investigation and education activities such as conferences and field trips. The ERA program provides an interface between the academic investigation and practical application of earthquake studies.

3. 2004-2005 Activities

3.1 Tours and Presentations

BSL staff spent considerable time with public relations activities during the past year. Several tours are given each month, with audiences ranging from middle-school students to scientists and engineers from China and Japan. The December 26, 2004 Sumatra earthquake and tsunami (and the March M8.7 aftershock) increased

interest in tours last year and the number of requests received by the BSL.

The BSL hosted several special groups during 2004-2005. Several large groups visited, including classes from the local Montessori School, Bret Harte Middle School, the Northern California Chapter of Phi Beta Kappa, and a number of home-schooled students. In addition to the tours, Drs. Romanowicz, Dreger, Gee, Hellweg, and Uhrhammer presented talks on earthquakes and related phenomena to public groups.

3.2 Open Houses

The BSL participated in *CalDay* this year. The attendance for the open house was quite good - visitors showed up before we opened the doors! The visitors learned about UC Berkeley's role in earthquake monitoring, watched a streaming feed of earthquake data, jumped up and down to "make a quake," played with the earthquake machine, made P and S-waves with springs, learned about earthquake preparedness, and were given sample seismograms. In addition, Drs. Bolt and Romanowicz gave lectures on *CalDay*.

Lawson Lecture

As part of the activities for the centennial of the great 1906 San Francisco earthquake and fire, the BSL established an annual lecture in 2003. The public lecture is held each April and focus on issues of earthquakes and society. This year was the third Lawson Lecture and Dr. Barbara Romanowicz gave an excellent presentation on *The 2004 Giant Earthquake and Tsunami: Observations and Lessons Learned*. If you missed the lecture, don't despair! A Web cast of the talk is available at http://www.seismo.berkeley.edu/seismo/news/lawson_lecture.html.

Putting Down Roots

One of the major activities associated with the 1906 Centennial is the publication of a booklet on earthquake preparedness. The last publication of this type in the Bay Area followed the 1989 Loma Prieta earthquake. *Putting Down Roots in Earthquake Country* is a collaborative effort among the American Red Cross, Association of Bay Area Governments, California Earthquake Authority, California Geological Survey, California Office of Emergency Services, Earthquake Engineering Research Center, San Francisco Office of Emergency Services and Homeland Security, Southern California Earthquake Center, Structural Engineers Association of Northern California, UC Berkeley, US Department of Homeland Security (FEMA), and the USGS. Publication of the booklet is expected in later this year, with additional releases scheduled for 2006. (*Putting Down Roots* was

released in September and is available on the Web at <http://pubs.usgs.gov/gip/2005/15/>.)

SSA 2006

The BSL will co-host the annual meeting of the Seismological Society of America (SSA), scheduled for 4/18/2006 - 4/22/2006, with the USGS. Plans are moving ahead to hold the *100th Anniversary Earthquake Conference* as a co-convened meeting by the SSA, the Earthquake Engineering Research Institute, and California Governor's Office of Emergency Services. The joint conference, which will be held in the Moscone convention center in San Francisco, will focus on what has been accomplished during the last century, showcasing best practices and research results in science, engineering, and emergency management.

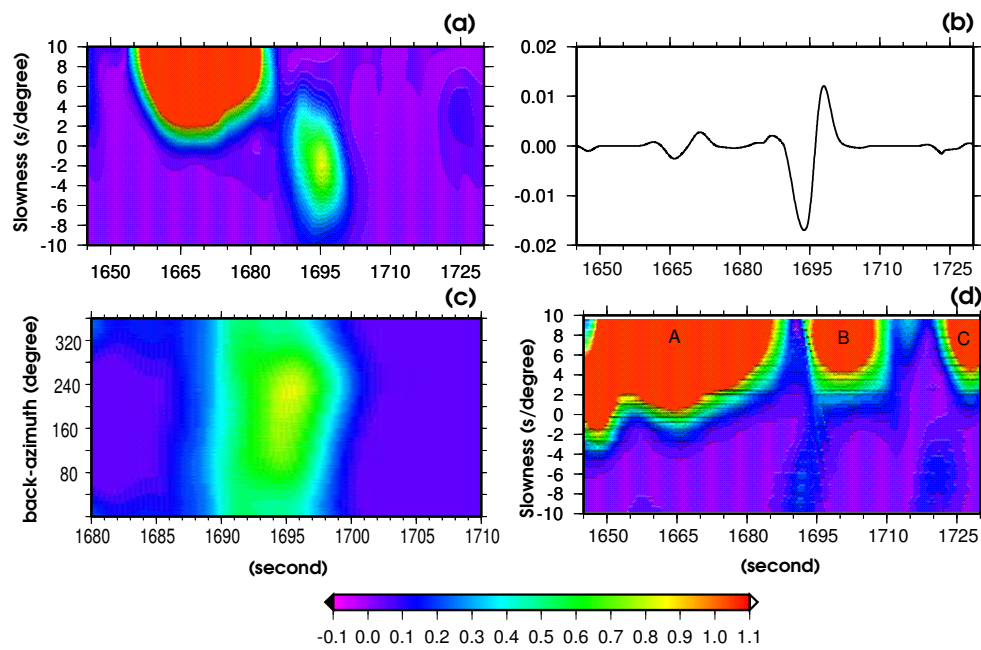
Lind Gee and Peggy Hellweg are on the Steering Committee for the anniversary conference and has been participating in monthly conference calls to plan for the meeting. In particular, there is much activity related to setting up the program, developing a realistic budget, and planning for special events such as a banquet celebrating the centennial of SSA. The development of the program is particularly exciting, as the conference is a unique gathering of people in earthquake-related fields. A plenary session is planned for each day, with presentations designed to cross disciplinary boundaries.

4. Acknowledgements

Lind Gee oversees the outreach activities at the BSL. Barbara Romanowicz, Peggy Hellweg, Bob Uhrhammer, Rick McKenzie, and many other faculty, staff, and students at the BSL contribute to the outreach activities. Lind Gee contributed to the preparation of this chapter.

Chapter 13

Research Studies



1. Nonvolcanic Tremors on the Central San Andreas Fault

Robert M. Nadeau, David Dolenc and Aurelie Guilhem

1.1 Introduction

Nonvolcanic tremor activity (i.e., long-duration seismic signals with no clear P or S waves (Figure 13.1) may provide important clues to the rheology and processes responsible for the nucleation and seismic cycles of large earthquakes. Prior to our research, nonvolcanic tremors had only been observed in subduction zones (i.e., thrust fault plate boundaries) (e.g., *Obara, 2002; Rogers and Dragert, 2003*), where fluids from subduction processes were believed to play an important role in generating these tremors.

In Cascadia, a significant correlation between subduction zone tremor activity and subseismogenic zone (i.e. beneath the upper ~ 15 km of Earth's crust where earthquakes occur) slow slip events (referred to as episodic tremor and slip (ETS, *Rogers and Dragert, 2003*)) has also been observed, suggesting that stress changes from ETS events increase stress and possibly trigger earthquakes in the shallower seismogenic fault zone.

1.2 SAF Tremors

Because subduction has not occurred along the central SAF for several million years, fluids from active subduction are not present, and nonvolcanic tremor activity was not expected along the the central SAF zone.

Recently, however, our detailed inspection of triggered event data from Berkeley's borehole High Resolution Seismic Network (HRSN) at Parkfield, California revealed tremor-like signals originating in the vicinity of Cholame (Figure 13.1) (*Nadeau and Dolenc, 2005*).

Following the methods of *Obara (2002)*, seismic data recorded continuously with 20 Hz sampling frequency by two stations of the Southern California Seismic Network (SCSN) (Figure 13.1) and with 250 Hz sampling by the HRSN were then used to analyze these events.

Within an ~ 15 km search radius centered ~ 5 km southeast of Cholame (Figure 13.1) and during a 3-year period from 23 December 2000 to 22 December 2003 (i.e., when the M6.5 San Simeon earthquake occurred), 110 tremor events lasting between 4 to 20 minutes were identified. Locations of the tremors indicate that within the search radius, the tremors were confined to an ~ 25 km segment of the SAF and occur at depths of between 20 to 40 km.

The depths, frequency content (generally 1 to 10 Hz), S-wave propagation velocity, and waveform character of the SAF tremors were similar to those of the subduction zone tremors; however, the SAF tremors are less frequent (fewer than 5 events in any 24 hour period), have shorter

duration (less than 20 minutes), have smaller peak amplitudes (comparable to M0.5 earthquakes), and release less energy (energy equivalents $< M1.5$).

Our discovery of these nonvolcanic tremors is important for three principal reasons: 1) they occur along a transform plate boundary (i.e., the SAF) in contrast to previous nonvolcanic tremors that occur only in subduction zones, 2) no obvious source for fluid re-charge exists in the area to aid in the genesis of the tremors and 3) the highest level of tremor activity in the region occurs beneath the inferred epicentral region (1) of the moment magnitude (M) ~ 7.8 1857 Fort Tejon earthquake whose rupture zone is currently locked.

This segment of the SAF has an estimated earthquake recurrence time of 140 years (+93, -69) (*WGCEP, 1995*), and it is now over 140 years since the Fort Tejon event. Because stress changes from ETS events may trigger large earthquakes (4), future increases in SAF tremor activity may signal periods of increased probability for the next large earthquake on the segment.

An apparent correlation between tremor and local micro-earthquake rates at Cholame (*Nadeau and Dolenc, 2005*) also suggests that deep deformation associated with the Cholame tremors (i.e., ETS) may also be stressing the shallower seismogenic zone in this area.

Further evidence for stress-coupling between tremor related deep deformation and shallower SAF earthquake activity is also seen in the correlation between stress release from the nearby 28 September 2004, M6 Parkfield earthquake and the evolution of tremor activity rates in the area (Figure 13.2)

1.3 Acknowledgements

Supported by U.S. Geological Survey award no. 04HQGR0085 and U.S. Department of Energy Office of Basic Energy Sciences contract no. DE-AC03-765F00098.

1.4 References

- Nadeau, R.M. and D. Dolenc, Nonvolcanic Tremors Deep Beneath the San Andreas Fault, *Science*, 307, 389, 2005.
- Obara, K., Nonvolcanic Deep Tremor Associated with Subduction in Southwest Japan, *Science*, 296, 1679-1681, 2002.
- Rogers, G. and H. Dragert, Episodic Tremor and Slip on the Cascadia Subduction Zone: The Chatter of Silent Slip, *Science*, 300, 1942-1943, 2003.

Location

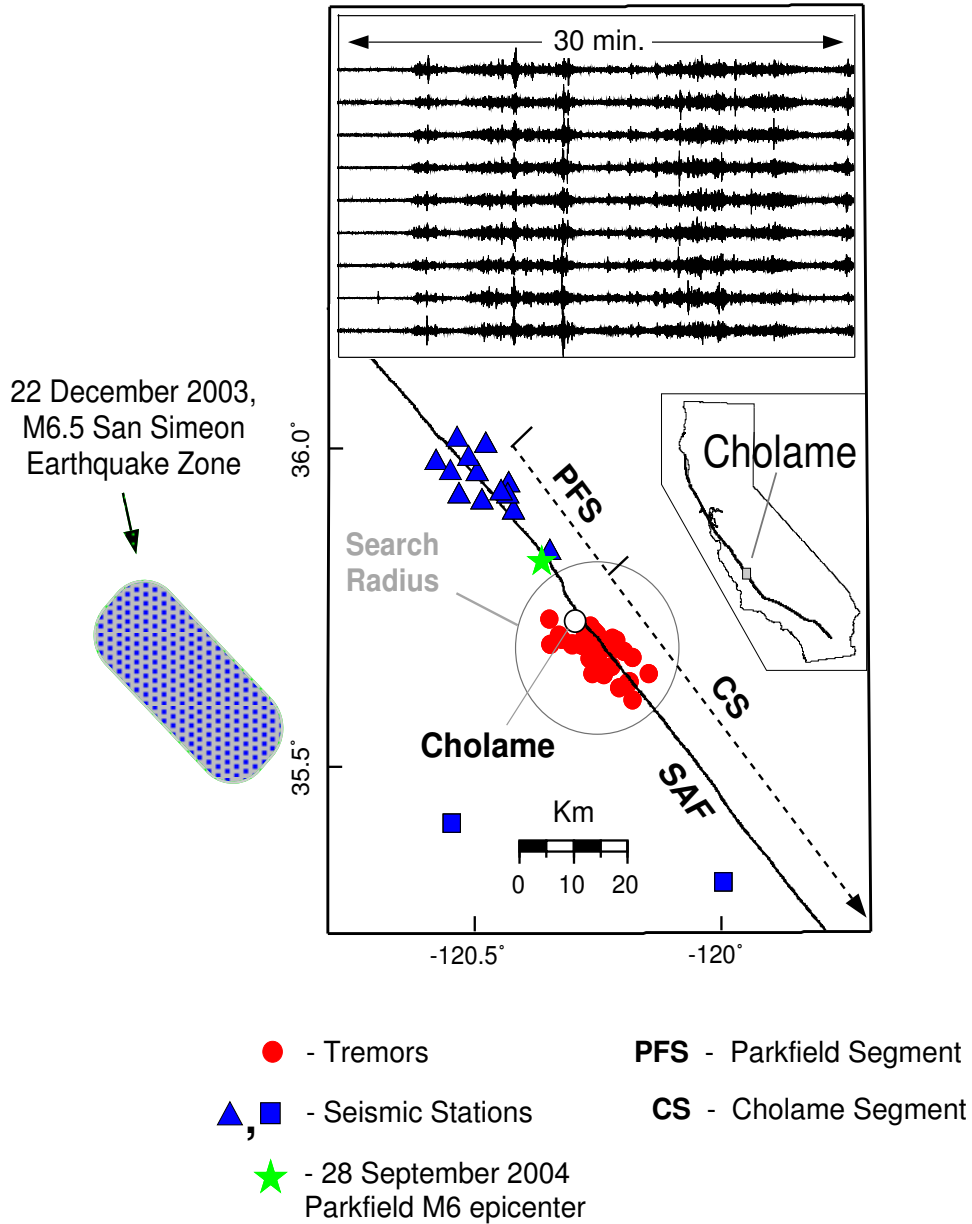


Figure 13.1: Thirty-four well-located tremors (small circles) along the northern Cholame Segment (CS) of the SAF. Triangles and squares are seismic stations of the HRSN and SCSN, respectively. Large circle is ~ 15-km-radius search zone. Star is the epicenter of the 28 September 2004, M6 Parkfield earthquake. (Inset, top) Horizontal component seismograms (3 to 8 Hz band-pass filtered) of two tremor events (ev1 and ev2) recorded by the stations with gray symbols. (Left) Approximate rupture zone of the 22 December 2003, M6.5 San Simeon Earthquake that occurred ~ 50 km to the west of the tremor zone. (Bottom inset) The location of Cholame, California.

Tremor Rate History

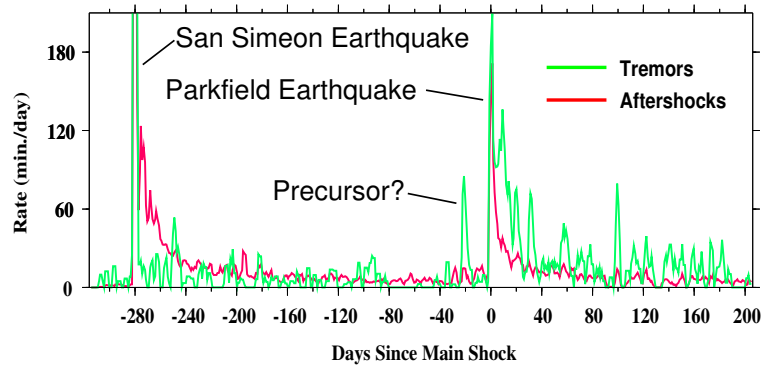


Figure 13.2: Activity rate history of nonvolcanic tremors (green) and microearthquakes (red) detected by the borehole High Resolution Seismic Network (HRSN) at Parkfield, CA. History spans 40 days prior to the San Simeon Earthquake through 200 days after the Parkfield mains shock. Tremor activity rates were not strongly influenced by the San Simeon event that occurred some 50 km to the west. However, the Parkfield earthquake whose epicenter occurred within about 10 km of the tremor zone had a strong impact. Parkfield aftershocks decayed much more rapidly than the tremor rate activity, suggesting some lag time between stress induced activity in the much deeper tremor zone relative to that in the seismogenic zone above. A precursory burst of tremor activity was also observed some 20 days prior to the Parkfield event. This is consistent with the observations of *Nadeau and Dolenc (2005)* which suggest a reciprocal stressing relationship in which stress changes associated with the tremor zone induce shallower earthquake activity with a lag time of a few weeks.

Working Group on California Earthquake Probabilities (WGCEP), Seismic hazards in southern California: probable earthquakes, 1994 to 2024, *Bull. Seism. Soc. Am.*, 85, 379-439, 1995.

2. Kinematic Modeling of the 2004 Parkfield Earthquake

Douglas Dreger, Mark Murray, Robert Nadeau, Peggy Hellweg, and Ahyi Kim

2.1 Introduction

The long-awaited Parkfield, California, earthquake occurred on September 28, 2004. This Mw 6.0 event was the latest in a series of moderate quakes (occurring approximately every 22 years) to strike the Parkfield segment of the San Andreas fault dating back to the nineteenth century. In anticipation of the repeat event a variety of geophysical instruments have been operating in Parkfield since the mid-1980s. Unfortunately, data from these instruments show no discernable precursory phenomena to the magnitude zero level (Langbein *et al.*, 2005). Nevertheless, the 2004 event was extremely well recorded by the seismic stations of the California Integrated Seismic Network, and continuous GPS sites, and therefore offers the best opportunity to date to learn about the physics of earthquake rupture. With the numerous near-fault stations from the USGS and CGS strong motion networks high resolution models of the kinematic rupture process are obtainable.

In this report we present our preliminary kinematic modeling results using local and regional seismic waveform data and the continuous GPS data.

2.2 Inversion Method

In our preliminary modeling we used 8 seismic stations located at distances from 3 to 328 km from the epicenter (Figure 13.3). The data was bandpass filtered between 0.02 to 0.3 Hz to emphasize the low frequency nature of the source process. The stations that were used provide excellent azimuthal coverage of the ruptured fault.

Seismic Green's functions were computed with an f - k integration code using the GIL7 velocity model, which has been found to be suitable for the California Coast Ranges (e.g. Pasyanos *et al.*, 1996).

In addition to the seismic data we used 11 coseismic displacement measurements from near-fault continuous GPS sites (Figure 13.4). The coseismic data was obtained from the 1-second solutions by averaging from 10 minutes before to 2-10 minutes after the event, effectively removing the post-seismic signal.

The GPS Green's functions were computed for an elastic half-space (Okada, 1992) representing the average of the elastic parameters in the upper 12 km of the GIL7 seismic velocity model.

We used the inversion method of *Hartzell and Heaton* (1983), and we performed inversions using each data set separately and combined. We performed inversions using a dipping fault (from the moment tensor solution) and a vertical fault from relocated aftershocks and modeling of

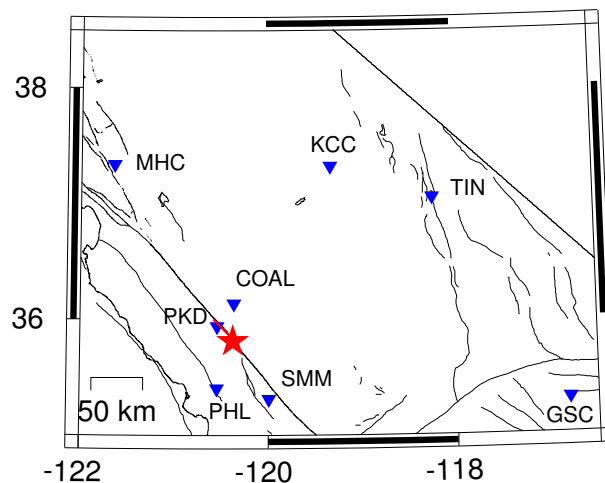


Figure 13.3: Location map. Seismic stations are shown as inverted triangles. The epicenter is shown as a star, and extent of fault model as a bold (red) line

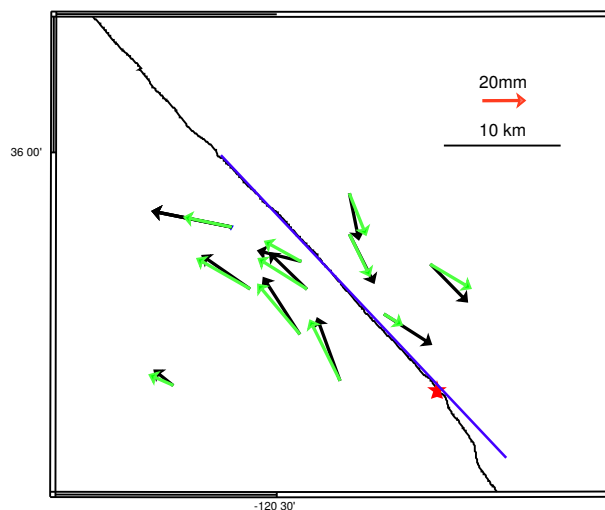


Figure 13.4: Observed GPS displacements (black) and predicted (green). The epicenter and assumed fault trace (blue line) are shown. The black line gives the distance scale, and the red arrow the GPS deformation scale.

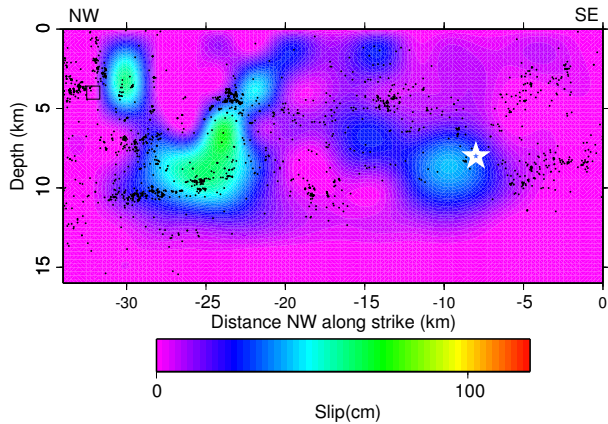


Figure 13.5: Smoothed slip distribution obtained from simultaneous inversion of seismic waveform and GPS data. The two deep asperities (5-12 km depth) are well constrained.

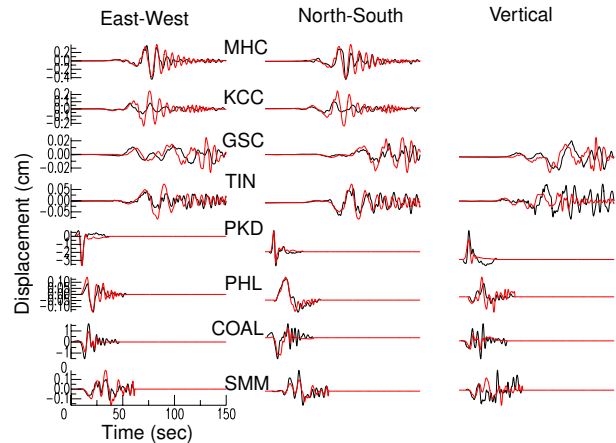


Figure 13.6: Observed (black) and predicted (red) displacement waveforms. The predicted waveforms are for the slip model shown in Figure 13.5

post-seismic deformation. These inversions showed that better fits were obtained with the vertical fault.

Inversions were performed with variable rake, however we found that it did not significantly improve fit so subsequent inversions assumed pure right-lateral slip.

Multiple time windows were used to model spatial variation in rupture velocity and rise time.

For the best fitting combined-data inversion result we obtained a scalar seismic moment of 1.17×10^{25} dyne cm, $M_w=6.0$, and rupture velocity of 3.0 km/s. The rise time is spatially variable, but is on average 1.2 seconds.

2.3 Slip Model

In Figure 13.5 the best-fitting combined-data inversion result is compared to double-difference relocated aftershocks (*Hardebeck personal communication, 2004*). The slip model shows an asperity located close to the hypocenter and another in the 12 to 5 km depth range about 20 km to the NW. The two deep patches of slip are well constrained by the seismic waveform and GPS data. The slip shallower than 5 km improves the fit to the GPS data, but is not well resolved.

Aftershocks tend to locate along the edges of the large slip patches in areas where the shear stress increased due to the fault rupture.

As shown in Figure 13.6 the kinematic slip model results in a very good level of fit to the seismic waveform data. The fit to the GPS data (Figure 13.4) is also good.

A surprising result is the NW rupture directivity. The directivity is well constrained by the regional seismic data. Inspection of the waveforms at the PKD and SMM stations (Figure 13.6) reveals significant differences in S-wave pulse width and amplitude that can only be explained by a NW propagating rupture. GPS data and

InSar inversion results (*Ingrid Johanson, personal communication, 2005*) similarly support the result that most of the mainshock slip was located NW of the epicenter. Interestingly strong motion stations to the SE have the largest peak values suggesting a component of SE-ward directivity (*Shakel et al., 2005*) that is not seen by the regional seismic waveform and the geodetic data sets. It is possible that the elevated strong ground motions SE of the epicenter are due to unaccounted for source process, and/or amplification effects due to the three-dimensional velocity structure of the San Andreas fault in this region (e.g. *Michael and Eberhart-Phillips, 1991; Eberhart-Phillips and Michael, 1993*). Our ongoing work is investigating both possibilities.

The slip in 2004 fills in the Parkfield segment that ruptured in 1934 and 1966, and therefore on this level the 2004 event is a typical repeat in the sequence of moderate Parkfield earthquakes. The 2004 rupture differs significantly however in that it nucleated at the SE end of the segment rupturing NW, while the two earlier events nucleated at the NW end rupturing SE (*Bakun and McEvilly, 1979*). This difference indicates that the actual triggering mechanism is very complex, and presently poorly understood. The 2004 event was possibly affected by a series of small events (M4-5) between 1992 to 1994, as well as the stress change caused by the nearby Mw6 Coalinga earthquake (*Toda and Stein, 2002*).

2.4 Ongoing Work

Our group is presently working on an updated kinematic rupture model for the 2004 earthquake by combining the GPS and regional waveform data set with the near-fault strong motion records and also the InSar-inferred deformation. This model will be used as a

boundary condition to calculate the stress change on the fault by solving the elasto-dynamic equations of motion using a finite-difference method (*e.g. Ide et al.*, 1997). The inferred stress change will be compared to observations of postseismic deformation and recurrence of characteristically repeating microearthquake sequences. Two of these sequences are the target sequences for the SAFOD deep borehole experiment.

Evidence of lateral velocity heterogeneity across the San Andreas fault (*Michael and Eberhart-Phillips*, 1991) might be an explanation for the elevated strong ground motions observed south of the epicenter. We will examine this possibility by performing finite-source simulations with 3D velocity structure to assess the impact of fault zone structure. In the longer term we will re-invert for kinematic slip parameters using 3D Green's functions.

The similarity and differences of the 2004 event to those that occurred in 1922, 1934, and 1966 is very important, and therefore we are also in the process of reexamining the historical records for these earlier Parkfield events. With the constrained slip model for the 2004 event we will simulate motions for the various narrow band instrument types in operation at the time of the previous Parkfield earthquakes to ascertain the amount of information these waveforms carry with respect to the kinematic source process.

2.5 References

Bakun, W.H., and T.V. McEvelly, Earthquakes near Parkfield, California: Comparing the 1934 and 1966 sequences, *Science*, 205, 1375-1377, 1979.

Dreger, D. S., L. Gee, P. Lombard, M. H. Murray, and B. Romanowicz (2004). Rapid Finite-Source Analysis and Near-Fault Strong Ground Motions Application to the 2003 Mw6.5 San Simeon and 2004 Mw6.0 Parkfield Earthquakes, *Seism. Res. Lett.*, 2005.

Eberhart-Phillips, D., and A.J. Michael, Three-dimensional velocity structure and seismicity in the Parkfield region, central California, *J. Geophys. Res.*, 98, 15,737-15,758, 1993.

Hartzell, S. H., and T. H. Heaton, Inversion of strong ground motion and teleseismic waveform data for the fault rupture history of the 1979 Imperial Valley, California, earthquake, *Bull. Seism. Soc. Am.*, 73, 1553-1583, 1983.

Ide, S., and M. Takeo, Determination of constitutive relations of fault slip based on seismic wave analysis, *Journ. Geophys. Res.*, 102, 27,379-27,391, 1997.

Langbein, J., D. Dreger, J. Fletcher, J.L. Hardebeck, M. Hellweg, C. Ji, M. Johnston, J. R. Murray, R.M. Nadeau, M. Rymer, Preliminary Report on the 28 September 2004, M 6.0 Parkfield, California Earthquake, *Seism. Res. Lett.*, 76, 10-26, 2005.

Michael, A. J., and Eberhart-Phillips, D. M., Relationships between Fault Behavior, Subsurface Geology, and

Three-Dimensional Velocity Models, *Science*, 253, 651-654, 1991.

Okada, Y., Internal deformation due to shear and tensile faults in a half-space, *Bull. Seism. Soc. Am.*, 82, 1018-1040, 1992.

Pasyanos, M.E., D.S. Dreger, and B. Romanowicz, Toward Real-Time Estimation of Regional Moment Tensors, *Bull. Seism. Soc. Amer.*, 86, 1255-1269, 1996.

Shakel, A., V. Graizer, M. Huang, R. Borchert, H. Haddadi, K. Lin, C. Stephens, and P. Roffers, Preliminary analysis of strong-motion recordings from the 28 September 2004 Parkfield, California, earthquake, *Seism. Res. Lett.*, 76, 27-39, 2005.

Toda, S., and R.S. Stein, Response of the San Andreas Fault to the 1983 Coalinga-Nunez Earthquakes: An application of interaction-based probabilities for Parkfield, *J. Geophys. Res.*, 107, doi:10.1029/2001JB000172, 16pp., 2002.

3. The Parkfield Earthquakes: Then and Now

Margaret Hellweg and Bernard Dost (Koninklijk Nederlands Meteorologisch Instituut)

3.1 Introduction

When, in 1966, an earthquake of magnitude 6 occurred on the San Andreas Fault near the town of Parkfield, in central California, it caused excitement among seismologists for two reasons. First, a number of new seismic stations had just been installed near the epicenter and had recorded the quake; and second, many residents and seismologists could recall similar earthquakes which had happened there in 1922 and 1934, and had been recorded at regional seismograph stations. With the data from the new stations, seismologists were able to determine that the 1966 event had started to the NW of the town of Parkfield and had ruptured the fault to the SE. *Bakun and McEvilly* (1979, 1984) compared seismograms from the 1922, 1934 and 1966 Parkfield earthquakes. They found similarities in waveforms of the 1922 and 1934 events as recorded by the Bosch-Omori seismograph at the seismograph station at the University of California, Berkeley (BRK), 265 km NW of the epicenter. For the 1934 and 1966 events, they compared and found similarities in records from Wood-Anderson seismographs at Mount Hamilton (MHC), 185 km NW of the event, and at Santa Barbara (SBC), 185 km to its SE. In addition, they looked at recordings of the surface waves for all three events from the Galitzin seismograph in the Netherlands at DBN, almost 10,000 km away. This was one of the few stations world-wide which had good recordings from the same instrument for all three earthquakes. Thus, *Bakun and McEvilly* (1979, 1984) suggested that these events could be members of a sequence of characteristic earthquakes. In 1985, based in part on the waveform similarities for these events, *Bakun and Lindh* (1985) proposed that another, similar earthquake might again happen in the same place, perhaps around 1988. As part of a prediction experiment (*Bakun and Lindh*, 1985), many instruments were installed around the town of Parkfield to record such a quake and to determine whether any precursors might be observed.

3.2 Comparing seismograms

Since 1966, seismological instrumentation has changed. Early earthquakes were recorded on paper or perhaps on film. Now, we use digital recordings from broadband seismometers. These modern systems have many advantages: we know the transfer function of the instrument and can recover the true ground motion; the dynamic range is large, so we can analyse both small and large signals; and the frequency band of observations is wide, so we can observe both high and low frequency signals.

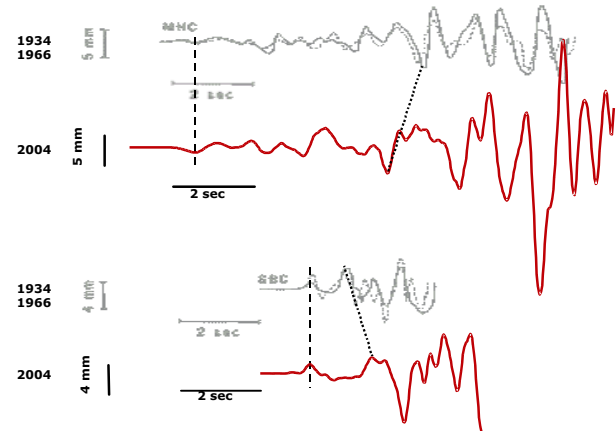


Figure 13.7: Comparison of the 2004 earthquake with events in 1966 (solid overplot) and 1934 (dashed overplot) for the stations MHC (top) and SBC (bottom). See text for details.

And finally, on September 28, 2004, another magnitude 6 earthquake occurred at Parkfield. Unlike the events in 1922, 1934 and 1966, this earthquake started well to the SE of the town of Parkfield, and ruptured NW. The rupture stopped about where the 1966 event had initiated (*Langbein et al*, 2005).

Fortunately, modern seismometers have been installed at the stations which *Bakun and McEvilly* (1979, 1984) used. We simulated the waveforms which would have been recorded for the 2004 Parkfield earthquake if old seismographs had still been running at the regional stations and at DBN.

At the regional stations, there are clear differences in the waveforms. These are probably related to the differences in the hypocenter and rupture direction of the 2004 event as compared to the earlier events. Figure 13.7 shows a comparison of P-wave records from the NS component of Wood-Anderson (WA) seismographs. The record for the 1934 is dashed and for 1966 solid (*Bakun and McEvilly*, 1979). These recordings are shown for the stations at MHC and SBA. Below each are WA traces for the 2004 event simulated from Berkeley Seismological Laboratory's station MHC and station SBA, which is a station of the Southern California Seismic Network operated by Caltech and the USGS. The records are on the

same scales and have been aligned on the P-wave. The WA records for the 2004 quake are clearly different from those of the earlier events. The Wood-Anderson amplitudes are proportionally larger at MHC than at SBC, and some phases arrive relatively earlier at MHC and later at SBC. These observations are consistent with NW rupture for the 2004 event, as compared to the SE rupture in 1966 and 1934.

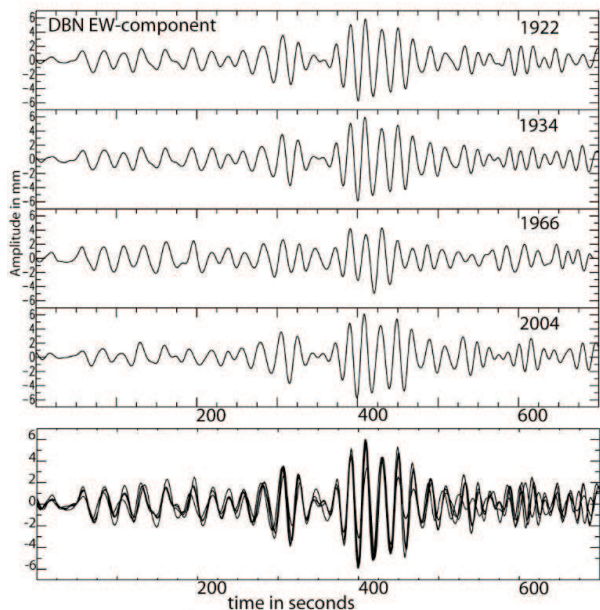


Figure 13.8: Comparison of the 2004 earthquake with the events in 1922, 1934 and 1966, as recorded at the teleseismic station DBN by a Galitzin seismograph. The amplitudes are given in mm recorded on the photographic paper. The records have been low pass filtered at 0.1 Hz. Below the seismograms for each event the recordings for the four events have been overplotted to emphasize their similarities.

Nearly 10,000 km from their epicenter, the events in 1922, 1934 and 1966 were recorded on light-sensitive paper by a set of horizontal Galitzin seismographs at De Bilt (DBN), the Netherlands. These seismographs were operated until 1994, when they were replaced by a 3-component, long period, digital seismometer, located at the same site. The modern instrument recorded the 2004 Parkfield earthquake.

In the records from DBN, there is some variation in the amplitudes of surface wave packets of the four events (Figure 13.8), although their phases seem to match quite well. For the comparison with the 2004 event, we have redigitized the photographic recordings of the horizontal components of the Galitzin seismographs for the 1922, 1934 and 1966 earthquakes. The waveform of the 2004 event closely resembles those of the 1922 and 1934 events.

The 1966 event deviates from the other three, especially for high frequencies. Amplitudes are comparable within the uncertainty in the gain, supporting the idea of a characteristic Parkfield earthquake (*Bakun and McEvilly, 1984*).

3.3 Perspectives

Before the 2004 event, the 1966 earthquake was the best-recorded of the Parkfield sequence. Stations of the Worldwide Standard Seismograph Network (WWSSN) were installed in the early 1960s, and recorded the 1966 earthquake at local, regional and teleseismic distances on paper records. The records were transferred to microchips (film), and recently some of them, including those from the Parkfield earthquake have been scanned as part of the Seismoarchives project at IRIS <http://www.iris.edu/data/SeismoArchives>. We plan to digitize these records from stations at all distances. Using rupture models for the 1966 and 2004 earthquakes, we will produce synthetic seismograms and compare them with the recordings for both events to investigate how well we can discriminate between these two very different rupture scenarios. Then, we will return to the even older data and apply what we have learned in order to better characterize this sequence of earthquakes.

3.4 References

- Bakun, W.H. and A.G. Lindh, The Parkfield, California, earthquake prediction experiment, *Science*, *229*, 619-624, 1985.
- Bakun, W.H., and T.V. McEvilly, Earthquakes near Parkfield, California: Comparing the 1934 and 1966 sequences, *Science*, *205*, 1375-1377, 1979.
- Bakun, W.H., and T.V. McEvilly, Recurrence models and Parkfield, California, earthquakes, *J. Geophys. Res.*, *89*, 3051-3058, 1984.
- Langbein, J., R. Borchardt, D. Dreger, J. Fletcher, J.L. Hardebeck, M. Hellweg, C. Ji, J. Johnston, J.R. Murray, R. Nadeau, M.J. Rymer, and J.A. Treiman, Preliminary report on the 28 September 2004, M 6.0 Parkfield, California earthquake, *Seismol. Res. Lett.*, *76*, 10-26, 2005.

4. A View of the 2004 Parkfield Earthquake from InSAR

Ingrid A. Johanson, Eric J. Fielding (JPL/Caltech), Roland Bürgmann

4.1 Introduction

The 2004 Parkfield earthquake was the long-awaited fulfillment of the USGS's Parkfield Prediction Experiment (*Bakun and Lindh, 1985, Bakun and McEvilly, 1984*). Since 1881 $M \sim 6$ earthquakes occurred near the town of Parkfield in Central California every ~ 20 years. After the event in 1966, the next earthquake was predicted to occur in 1988 ± 6 years. The years since the original prediction have seen the advent of space-based geodesy and now interferometric synthetic aperture radar (InSAR) data can now be added to the wealth of information on this earthquake. We present the results of a slip model encompassing the earthquake and two days of postseismic slip constrained by InSAR data from the ENVISAT satellite.

4.2 Interferogram processing

We use data from the European Space Agency's ENVISAT satellite, processed using ROLPAC software, developed at JPL. Phase unwrapping was performed by SNAPHU (*Chen and Zebker, 2001*) and was aided by a priori range change estimates from an inversion of GPS displacements during the interferogram time span. The contribution of topography to the interferogram phase was removed using a SRTM digital elevation model.

The ENVISAT satellite passed over the Parkfield area on September, 30 2004, two days after the Parkfield earthquake, on ascending track 435. We were able to make a pair with a previous ENVISAT acquisition from July 3, 2003. This interferometric pair is the most direct measure of the coseismic-only deformation field available using InSAR.

4.3 Data reduction

While the Parkfield earthquake has been highly anticipated, it is nonetheless a moderate sized event. As Figure 13.9 shows, the earthquake produced ground deformation resulting in 1 fringe (2π radians), corresponding to 28 mm of range change (change in distance between the ground and the satellite). This is comparable to the expected size of atmospheric errors in an interferogram (*Zebker et al., 1997*). The interferogram also displays ground deformation due to groundwater movement. The signal from the Paso Robles Basin to the southwest (circled in Figure 13.9) is particularly noticeable. We have pared the interferogram down to just the immediate vicinity of the Parkfield earthquake (dashed line in Figure 13.9) and removed areas affected by groundwater

induced vertical motion in the Paso Robles and Salinas basins and topography-correlated atmospheric errors to the East and South.

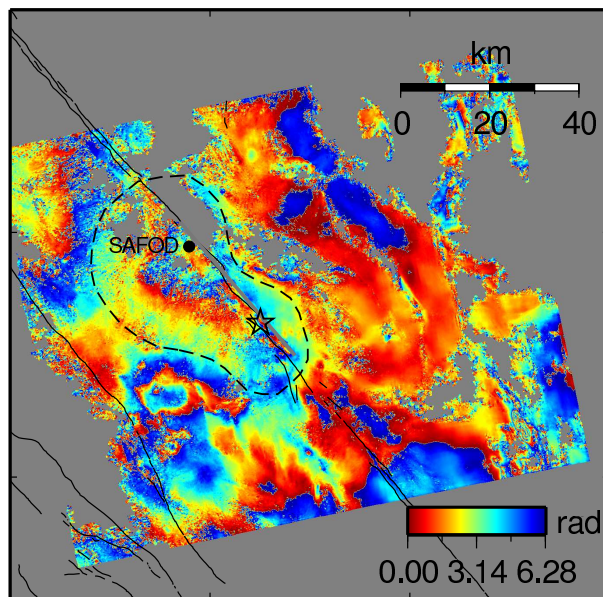


Figure 13.9: Interferogram from 7/3/2003 to 9/30/2004. Star is the epicenter of the 2004 Parkfield earthquake, dashed line borders area used in the inversion and dot is the location of the San Andreas Fault Observatory at Depth (SAFOD). Color scale is from 0 to 2π and repeats.

For the inversion, the geocoded and trimmed interferogram was sub-sampled on a grid with 1 km spacing. We correct our interferogram samples for coseismic and postseismic slip from the San Simeon earthquake and interseismic motion using an unpublished model based on GPS and InSAR and the model of Rolandone et al. (2004), respectively.

4.4 Model Results

The model plane is vertical with a strike of 319 degrees. We discretize the plane into 300 2 km x 1 km elements and perform a least squares inversion while seeking a smooth distribution of right-lateral slip. The results are shown in Figure 13.10. The slip model contains two high-slip asperities: one just above the hypocenter (red star in Figure 13.10) and a larger asperity to the northwest. Much of the slip in our model occurs within the area outlined by aftershocks as shown in Figure 13.10. Langbein et al. (2005) note that the relocated aftershocks occur

in the same clusters and streaks as the pre-earthquake background seismicity, including a streak which is visible in the aftershocks at about 5 km depth. One interpretation of microseismicity streaks is that they occur at the boundaries of creeping and locked asperities of the fault surface. Assuming that in an earthquake the strong asperity makes up its slip deficit by slipping more than the surrounding creeping sections, the microseismic streak would be expected to bound areas of high coseismic slip. The streak of aftershocks at 5 km depth occurs near the top of the northwest asperity, and could be interpreted as weakly bounding it.

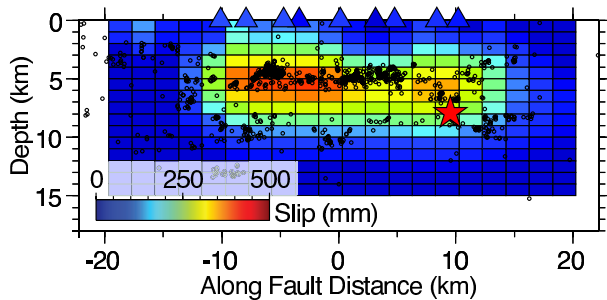


Figure 13.10: Results of inversion for slip during the 2004 Parkfield earthquake and two days of postseismic slip. Red star is earthquake hypocenter, black circles are double-difference relocated aftershocks (Langbein *et al.*, 2005), and colored triangles are surface offsets measured by creepmeters. X-axis datum is GPS station Carr Hill (CARH)

Creepmeter measured surface offsets are plotted as colored triangles in Figure 13.10 for comparison. Many of the creepmeters on the main SAF trace went off scale either during or soon after the earthquake. Between Sep. 30 and Oct. 2, these creepmeters were brought back on scale and an offset was manually measured. The triangles in Figure 13.10 represent the total creep measured when the creepmeters were brought back on scale. The top row of our model matches the overall magnitude and some of the features of the creepmeter surface slip distribution. Both show more surface slip 0-10 km north of Carr Hill than to the south.

The total moment of our model is 2.56×10^{18} Nm; equivalent to $M_w 6.2$. Seismic modelling of the coseismic rupture has estimated a moment magnitude $M_w 6.0$, which would require 1.32×10^{18} Nm ($M_w 6.0$) of the slip in our model to have occurred within the first two days of the postseismic period. An analysis of additional InSAR and GPS data spanning three months post-earthquake, suggests that 1.48×10^{18} Nm ($M_w 6.1$) of moment was subsequently released postseismically (Johanson *et al.*, submitted). Johanson *et al.* (submitted) find that aseismic slip could account for as much as 70% of the total

(coseismic and postseismic) moment release of the Parkfield earthquake.

4.5 Acknowledgements

This work was funded by SCEC and NSF grant EAR-0337308

4.6 References

- Bakun, W. H., and A. G. Lindh, The Parkfield, California, earthquake prediction experiment, *Science*, *229*, 619-624, 1985.
- Bakun, W. H., and T. V. McEvilly, Recurrence models and Parkfield, California, earthquakes. *Journal of Geophysical Research* *89*, 3051-3058, 1984.
- Chen, C. W., and H. A. Zebker, Two-dimensional phase unwrapping with use of statistical models for cost functions in nonlinear optimization, *J. Opt. Soc. Am. A Opt. Image Sci.*, *18*, 338-351, 2001.
- Johanson, I. A., E. J. Fielding, F. Rolandone, and R. Bürgmann, Coseismic and Postseismic Slip of the 2004 Parkfield Earthquake from Space-Geodetic Data, *Bull. Seismo. Soc. Am.*, submitted.
- Langbein, J., R. Borchardt, D. Dreger, J. Fletcher, J. L. Hardebeck, M. Hellweg, C. Ji, M. Johnston, J. R. Murray, and R. Nadeau, Preliminary Report on the 28 September 2004, M 6.0 Parkfield, California Earthquake, *Seismol. Res. Lett.*, *76*, 10-26, 2005.
- Rolandone, F., I. Johanson, R. Bürgmann, and D. Agnew, Variation in aseismic slip and fault normal strain along the creeping section of the San Andreas fault from GPS, InSAR and trilateration data, *Eos, Trans., AGU*, *85*, G32A-05, 2004.
- Zebker, H. A., P. A. Rosen, and S. Hensley, Atmospheric Effects in Interferometric Synthetic Aperture Radar Surface Deformation and Topographic Maps, *J. Geophys. Res.*, *102*, 7547-7563, 1997.

5. Frictional Afterslip Following the 2004 Parkfield, California Earthquake

Kaj M. Johnson, Roland Bürgmann, and Kristine Larson (University Colorado)

5.1 Introduction

The abundance of geodetic and seismic data recording postseismic deformation following the 2004 Parkfield earthquake provides an unprecedented opportunity to resolve frictional properties on the Parkfield section of the San Andreas fault. The Parkfield segment transitions between the locked section to the southeast that last ruptured in the 1857 Fort Tejon earthquake and the creeping section to the northwest. We develop 3D rate- and state-dependent friction models of afterslip following the 2004 earthquake to investigate the frictional behavior of the fault. It is assumed that the coseismic rupture occurred on an area of the fault surrounded by aseismic creep that accelerated after the earthquake. We estimate the distribution of coseismic slip, afterslip, and rate-state frictional parameters by inverting a two-step slip model. In the model we: 1) estimate the coseismic slip distribution from 1 Hz GPS data, and 2) use the corresponding coseismic shear stress change on the fault as input into a numerical afterslip model governed by rate-state friction. We find the rate-state frictional parameter A-B, which is an indicator of frictional stability, is in the range $10^{-4} - 10^{-3}$ at 50 MPa normal stress, about an order of magnitude lower than experimental values for granite at conditions well above or below the transition from potentially unstable (negative A-B) to nominally stable (positive A-B) friction. The estimate of A-B values fall within a wide range of experimental values reported for Serpentine which crops out along the San Andreas fault zone. The critical slip distance, d_c , which characterizes the distance over which strength breaks down during a slip event, is in the range 0.01-0.1 m, consistent with seismic estimates and a fault gouge thickness of 1-10 m. The afterslip model reproduces most features observed in the GPS time-series data including high surface velocities in the first few months after the earthquake and lower rates at later times, as well as the cumulative postseismic displacement. The model tends to under-predict the displacement data at later times, suggesting that perhaps the modeled afterslip period ends too quickly or an un-modeled deformation process dominates the signal at later times.

5.2 The model

To model afterslip at Parkfield we discretize a 65-km-long segment of the San Andreas fault into rectangular patches of uniform slip dislocations in a homogeneous elastic half-space. We assume the slip rate distribution

on the fault prior to the earthquake is that estimated by *Murray et al.* (2001) who inverted GPS velocities averaged over 1991-1998 for the interseismic slip rate. Also following *Murray et al.* (2001), we assume the fault is locked down to 15 km depth to the southeast of Parkfield, creeping at 25 mm/yr down to 15 km depth northwest of Parkfield, and creeping at 32 mm/yr everywhere below 15 km depth. These large creeping sections of the fault are assumed to extend infinitely along the strike of the San Andreas fault.

We envision that the area of the fault bounded by micro-seismicity (*Nadeau et al.*, 2005) is locked between earthquakes and is surrounded by aseismic fault creep. The locked part of the fault ruptures during the earthquake and creep in the surrounding areas accelerates to relax the coseismic stress load. We assume the coseismic stresses relax during afterslip according to the following Dieterich-Ruina formulation of rate-state friction, equations (1) and (2), together with the equation relating stress on the fault to slip

$$\tau = \sigma \{ \mu + A \ln(V/V^*) + B \ln(V^*\theta/d_c) \} \quad (13.1)$$

$$\frac{d\theta}{dt} = 1 - \frac{V\theta}{d_c} \quad (13.2)$$

where τ is shear stress on the fault, σ is the normal stress, V is sliding velocity, V^* is a reference velocity, μ is the nominal coefficient of friction at the steady reference velocity, θ is a state variable that evolves with time, A and B are laboratory-derived constants, and d_c is the so-called critical slip distance. d_c is interpreted as an indication of the size of asperity contacts and is thought of as the slip necessary to renew surface contacts. In this formulation, the state, θ , can be interpreted as the average asperity contact time because it increases linearly with time at zero slip velocity.

The conditions on stress and state before the earthquake are obtained from the interseismic slip rate distribution (*Murray et al.*, 2001) assuming steady state conditions ($d\theta/dt = 0$). The initial condition on stress immediately after the earthquake (the beginning of the afterslip period) is the pre-earthquake stress plus the stress change caused by the earthquake.

The objective is to invert GPS data with a forward model of the coseismic and postseismic processes to obtain estimates of the frictional parameters, A , B , and d_c . The two-step forward model produces a coseismic slip distribution and the resulting afterslip distribution that is driven by the coseismic stress change. In the first step,

we perform a linear slip inversion of the coseismic GPS data for the coseismic slip distribution. In the second step, we specify the rate-state friction parameters and initial conditions and solve for the evolution of afterslip as. σA , σB , and D_c vary linearly with depth.

5.3 Results

Figure 13.11 shows the best-fitting coseismic slip and afterslip distributions. The cumulative afterslip after 9 months is shown. The afterslip is largely localized within two patches. One patch is in the upper 5 km, just above the larger coseismic slip patch. The other patch of afterslip occurs above the hypocenter.

The fit to the GPS time-series is shown in Figure 13.12. The model reproduces the rapid postseismic velocities during the first 0.1-0.2 years and the less rapid velocities during the later time periods. There is a tendency for the model to under-fit the displacements at later times indicating that the model relaxes and returns to the pre-earthquake rate too quickly. This may indicate that another (un-modeled) deformation mechanism, such as deep distributed flow, may dominate the signal at later times.

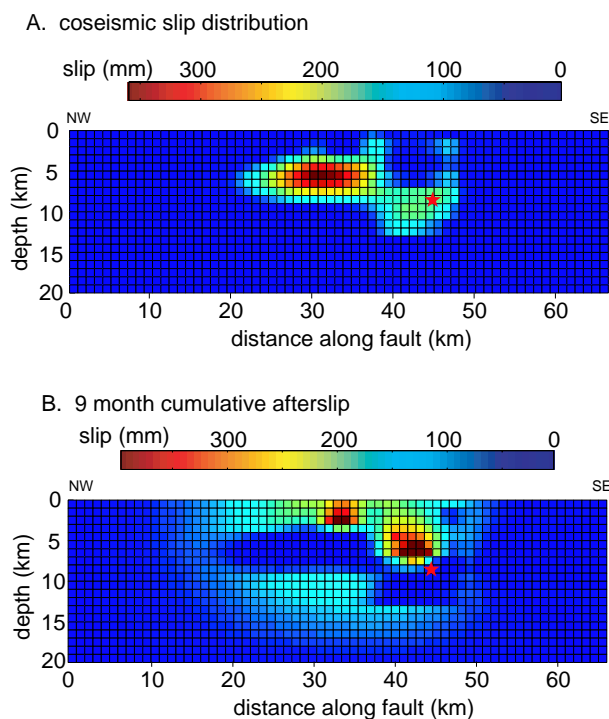


Figure 13.11: A. Best-fitting coseismic slip distribution and, B. corresponding 9-month cumulative rate-state afterslip.

Table 1 shows the approximate 95% confidence intervals on the frictional parameters. The values for A and B assume a uniform effective normal stress on the fault of

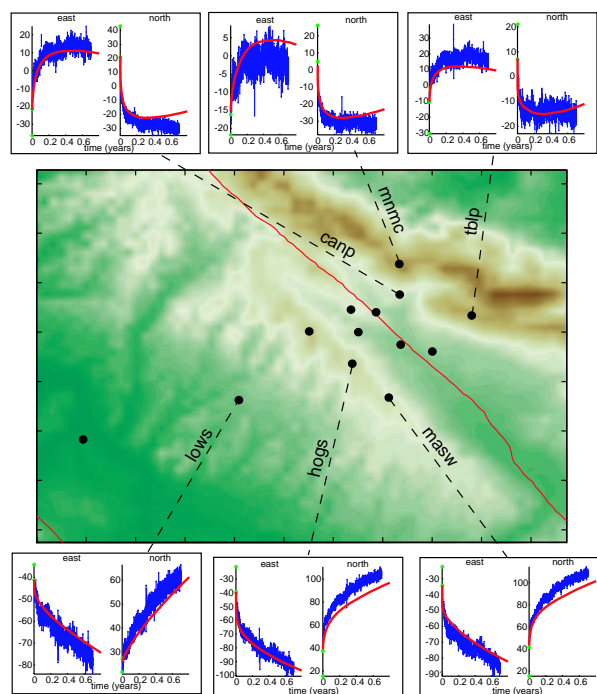


Figure 13.12: Fit to the postseismic GPS time series. Only a subset of data is shown because of space limitations. Data shown with 95% confidence error bars. Solid line is model. Vertical axis is displacement in mm.

50 MPa. The parameters vary linearly with depth, so we report the values at the center of the top and bottom rows of patches. A-B is on the order of 10^{-4} to 10^{-3} , which is about an order of magnitude lower than experimental values for granite at conditions well above or below the transition from potentially unstable (negative A-B) to nominally stable (positive A-B) friction. It is also an order of magnitude lower than an estimate from an afterslip inversion of the Tokachi-oki, Japan, earthquake (*Miyazaki et al.*, 2004). However, the estimated A-B values fall within a wide range of experimental values reported for Serpentine, which crops out along the San Andreas fault zone and is frequently mentioned as an important factor allowing for velocity-strengthening behavior of some faults (*Reinen et al.*, 1994). The low values of A-B might be indicative of a transition zone from velocity-weakening (negative A-B) to velocity-strengthening (positive A-B). Estimates of d_c are of the order 0.01-0.1 m, in reasonably good agreement with the seismic estimate near Parkfield (*Fletcher and Spudich*, 1998). The scaling relationship of *Marone and Kilgore* (1993) infers a fault gouge thickness of 1-10 meters.

5.4 Acknowledgements

This work is funded partially by NSF grant EAR-0309946.

Table 13.1: Table 1. 95% Confidence intervals on frictional parameters

parameter	top of fault	bottom of fault
A	0.0004-0.0052	0-0.024
B	0-0.0045	0-0.0468
A-B	0.0006-0.0018	0.0001-0.0021
d_c (meters)	0.020-0.250	0-0.650

5.5 References

Fletcher, J.B., and P. Spudich, Rupture characteristics of three $M \sim 4.7$ (1992-1994) Parkfield earthquakes, *Journal of Geophysical Research*, *103*, 835 - 854, 1998.

Marone, C., and B. Kilgore, Scaling of the critical slip distance for seismic faulting with shear strain in fault zones, *Nature*, *362*, 618-621, 1993.

Miyazaki, S., Segall, P., Fukuda, J., and T. Kato, Space time distribution of afterslip following the 2003 Tokachi-oki earthquake: Implications for variations in fault zone frictional properties, *Geophys. Res. Lett.*, *31*, doi: 10.1029/2003GL019410, 2004.

Murray, J.R., Segall, P., Cervelli, P., Prescott, W., and J. Svare, Inversion of GPS data for spatially variable slip-rate on the San Andreas fault near Parkfield, *Geophysical Research Letters*, *28*, 359 - 362, 2001.

Nadeau, R.M., Foxall, W., and T.V. McEvilly, Clustering and periodic recurrence of microearthquakes on the San Andreas fault at Parkfield, California, *Science*, *267*, 503 - 507, 1995.

Reinen, L.A., Weeks, J.D., and T.E. Tullis, The frictional behavior of Lizurdite and Antigorite Serpentinites: Experiments, constitutive models, and implications for natural faults, *Bulletin Seismological Society of America*, *143*, 317-358, 1994.

6. The Orinda Earthquake Sequence: Scaling of Small Earthquakes

Margaret Hellweg

6.1 Introduction

Does the faulting in large and small earthquakes involve different physical processes? This question remains open because of the pervasive difficulty in geophysics of performing controlled experiments. To find the answer, it is necessary, for example, to separate source from path and site effects in seismograms. A sequence of small earthquakes which occurred near Orinda, California, offers an opportunity to explore this question. This sequence occurred under Berkeley Seismological Laboratory's station BRIB (37.92 N, 122.15 W). At the surface are a broadband seismometer and an accelerometer. In addition to the surface installation, there is a borehole at the station equipped with a 3-component geophone and a 3-component accelerometer at a depth of 119 m. The sequence began on October 19, 2003, at 14:35:27 UTC, with an earthquake with M_d 2.5. The mainshock (MS) with M_L 3.5 followed about an hour later. In the next week and over the course of the next 3 months there were more than 4000 aftershocks ranging in magnitude from -2.5 to 3.4.

6.2 The largest events

The two largest earthquakes of the sequence were the mainshock on October 19, at 15:32 UTC with M_L 3.5, and an aftershock at 17:50 on October 20, with M_L 3.4 (Figure 13.13). For these two events one of the horizontal components of both the surface and the borehole seismometers was clipped. The black traces in Figure 13.13 show the seismometer records. Fortunately, the clipped component of the borehole seismometer coincides with the single functioning component of the borehole accelerometer. When the instrument response is removed from the accelerometer recording and the trace is integrated, it matches the corresponding component of the velocity sensor (gray traces in Figure 13.13). The offset traces at the beginning of the records in Figure 13.13A show a small event which occurred 1.5 s before the mainshock. These traces, scaled to be 100,000 times those for the mainshock, show some of the range of sizes of the events in this sequence. The large aftershock appears to be a double event (Figure 13.13B) with two clear P and two clear S phases.

6.3 Event magnitudes

How small are the smallest earthquakes in this sequence that we can see in the record? For most of the events, standard magnitudes cannot be determined:

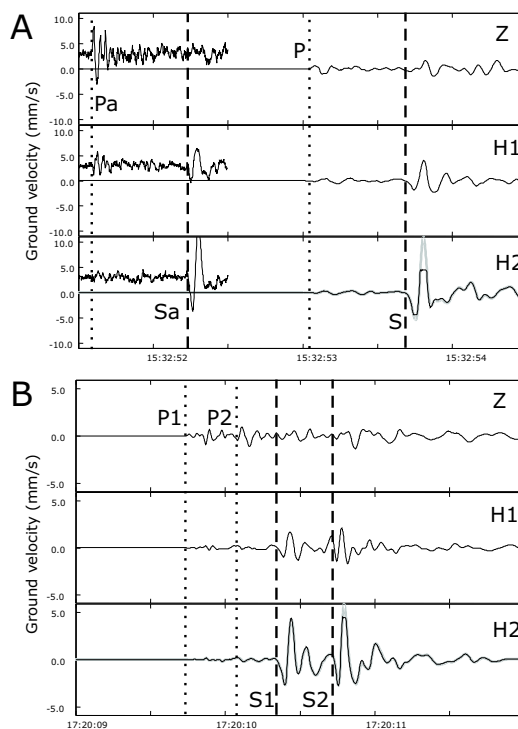


Figure 13.13: Seismograms of the mainshock (A) and largest aftershock (B). Z, H1 and H2 are the vertical and orthogonal horizontal components, respectively. The H2 geophone (black) was clipped for these two events, so the gray trace shows the instrument-corrected accelerometer record. Dotted and dashed lines show P- and S-arrivals, respectively. (A) About 1.5 s before the mainshock, a small event occurred. Its traces have been multiplied by 100,000. (B) The large aftershock appears to be a double-event. The P- and S-phases of the first and second event are indicated.

the events are too small to be recorded at other stations and, strictly speaking, the local magnitude scale is not defined for events so close to the recording station. To determine the magnitude threshold for the events, I calibrated a manual magnitude scale using events from the catalog. Following the definition of local magnitude (Richter, 1935), I measured the peak-to-peak amplitudes in the instrument-corrected velocity seismograms of the two horizontal components of the borehole velocity sensor and multiplied by the period and by the magnification of a Wood-Anderson instrument at that period. As the distances of these events from the station BRIB are all nearly the same, no distance correction is necessary.

Figure 13.14 shows a comparison between the catalog and manual magnitudes (gray dots). The line shows the least-squares regression between the catalog and manual magnitudes and allows the manual magnitudes to be projected to corresponding catalog magnitudes (black dots). The smallest events analysed correspond to M_L -1.5; however, there are still smaller events in the seismograms from the borehole geophone. No manual magnitudes have been determined for these tiny earthquakes yet, but the smallest events recorded at station BRIB are more than five units of magnitude smaller than the mainshock.

6.4 Perspectives

Many different interesting questions can be explored using this dataset. One of the most fundamental in terms of earthquake physics is the question of scaling: does the same thing happen in tiny events as in the large events which capture public attention. However, this sequence also offers a view into the relationship of mainshocks and aftershocks for small earthquakes. Normally, only a few aftershocks with magnitudes between 0.5 and 3.5 would make it into the catalog. For the Orinda MS, more than 4000 aftershocks have been recorded and are available for analysis. It should be possible to map their locations with respect to the MS, and perhaps determine its rupture surface independently. Other perspectives include investigations of the effects of path attenuation on the frequency content of small events.

6.5 References

Richter, C.F. An instrumental earthquake magnitude scale. *Bull. Seismo. Soc. Am.*, 25, 1-32, 1935.

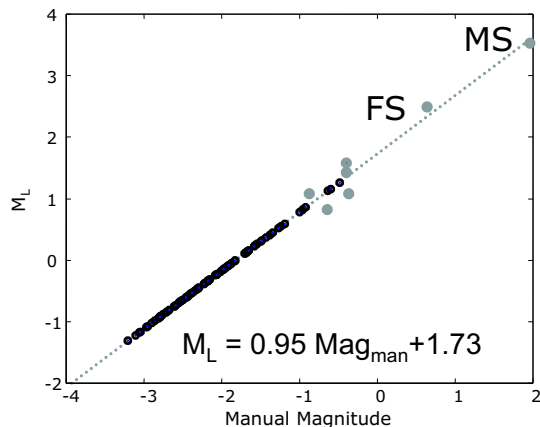


Figure 13.14: Magnitude calibration. Gray dots show the events from the Orinda sequence which are in the NCSN catalog. A least-squares regression (line) allows M_L to be determined for the many small events.

7. Inversion for the Velocity Structure of the Santa Clara Valley, California

David Dolenc, Doug Dreger, and Shawn Larsen (LLNL)

7.1 Introduction

In our previous work we investigated teleseismic, local, and microseism data recorded by the 41-station seismic array in the Santa Clara Valley (SCV) (Figure 13.15). We have found strong correlations between basin depth reported in the USGS 3D seismic velocity model (ver. 2) (*Jachens et al.*, 1997) and different relative measures of ground motion parameters such as teleseismic arrival delays, P-wave amplitudes, wave energy, local earthquake S-wave amplitudes, and periods of microseism horizontal to vertical spectral ratio peaks (*Dolenc et al.*, 2005; *Dolenc and Dreger*, 2005). The teleseismic, local earthquake, and microseism observations were also found to be strongly correlated with one another. The results suggested that all three datasets are sensitive to the basin structure (Figure 13.16) and could therefore be used together to improve the 3D velocity model.

7.2 Method

We started to develop a simultaneous inversion of the teleseismic, local, and microseism observations to refine the seismic velocity model within the SCV basins. To reduce the extremely large model space, we only invert for the velocity structure within the basins while the basin geometry, as defined in the USGS velocity model, is held fixed. The inversion is based on the approach described in *Aoi* (2002). We parameterize the velocity model in the basins and invert it by using teleseismic P-wave waveforms as well as additional relative parameters, such as teleseismic wave energy, local earthquake S-wave amplitude, and periods of microseism horizontal to vertical spectral ratio peaks. The model parameters are determined by the inversion with the constraint that the observation equation, which is nonlinear in the model parameters, is best satisfied in the sense of least squares. The observation equation is linearized by omitting higher order terms and solved iteratively by singular value decomposition. To solve the observation equation, synthetic waveforms as well as sensitivity functions (differential seismograms) are required. The 3D elastic finite-difference code (*Larsen and Schultz*, 1995) is used to calculate waveforms, and the sensitivity functions are obtained numerically by taking the difference of waveforms from perturbed and unperturbed models. The inversion is performed in the 0.1 to 1 Hz passband in which the SCV seismic experiment observations had a good signal to noise ratio.

We prepared four variations of the USGS model in the

basins: (1) laterally uniform velocity with a single vertical velocity gradient, (2) three regions of vertical velocity gradient distributed vertically, (3) six 1-km thick horizontal layers with constant velocities, and (4) multi-layered constant velocity slices draped over the basin geometry.

Because of the computational limitations, the slowest velocities in the models were increased to a minimum S-wave velocity of 1 km/s. The slowest P-wave velocity was 1.75 km/s. To model the plane wave from the teleseismic events, we used a disc of point sources in the deepest homogeneous layer of the velocity model, representing the upper mantle. To simulate the microseisms, we used a localized source of isotropic Rayleigh waves located offshore. The preliminary results of the f-k analysis of the observed and simulated microseisms display strong directionality in their propagation and localization of the source, which supports the use of the point source for microseisms.

Preliminary results show that the model parameters are iteratively modified and that the residuals between the data and synthetic seismograms are converging.

7.3 Conclusions

Previous results showed strong correlations between the SCV basin depth reported in the USGS 3D seismic velocity model and different relative measures of ground motion parameters observed for the teleseismic and local events, as well as microseisms. We are developing a simultaneous inversion of observations from the three datasets to refine the seismic velocity model in the SCV basins.

7.4 Acknowledgements

Part of this work was supported by the USGS grants 99HQGR0057 and 00HQGR0048. The Hellman Faculty Fund is acknowledged for partial support.

7.5 References

- Aoi, S., Boundary shape waveform inversion for estimating the depth of three-dimensional basin structures, *Bull. Seism. Soc. Am.* 92, 2410-2418, 2002.
- Dolenc D., D. Dreger, and S. Larsen, Basin structure influences on the propagation of teleseismic waves in the Santa Clara Valley, California, *Bull. Seismol. Soc. Am.*, 95, 1120-1136, 2005.
- Dolenc D. and D. Dreger, Microseisms observations in the Santa Clara Valley, California, *Bull. Seismol. Soc.*

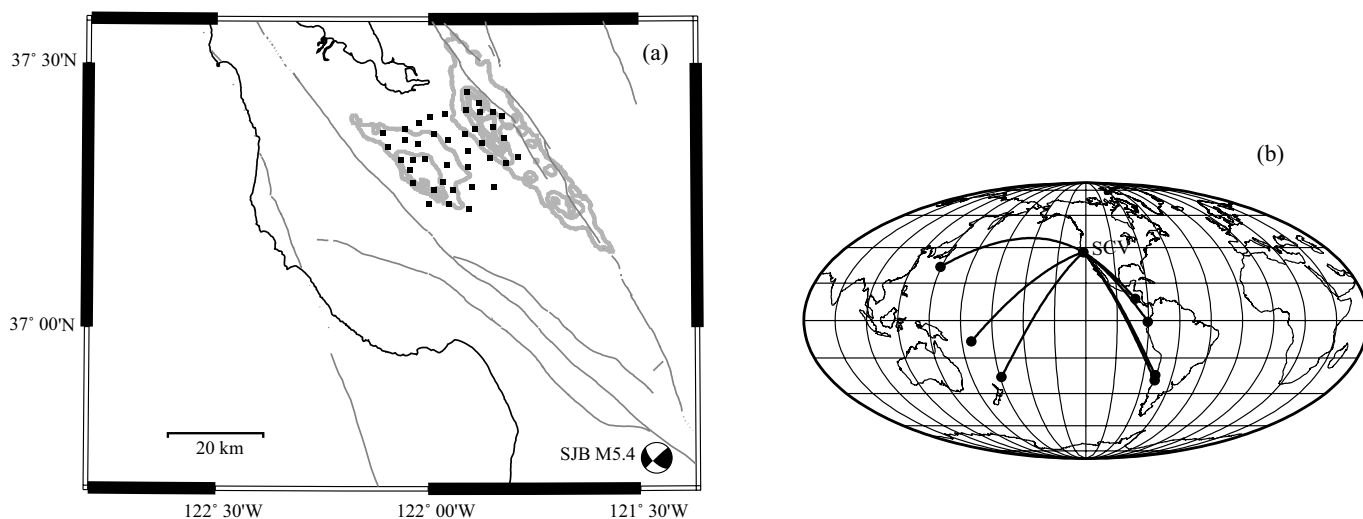


Figure 13.15: (a) Location of the SCV seismic array. Contours of the basins from the USGS model at 1km, 3 km, 5 km, and 6 km depth are shown in gray. Focal mechanism for the San Juan Bautista M_L 5.4 event is shown. (b) Locations of the teleseismic events used in the study.

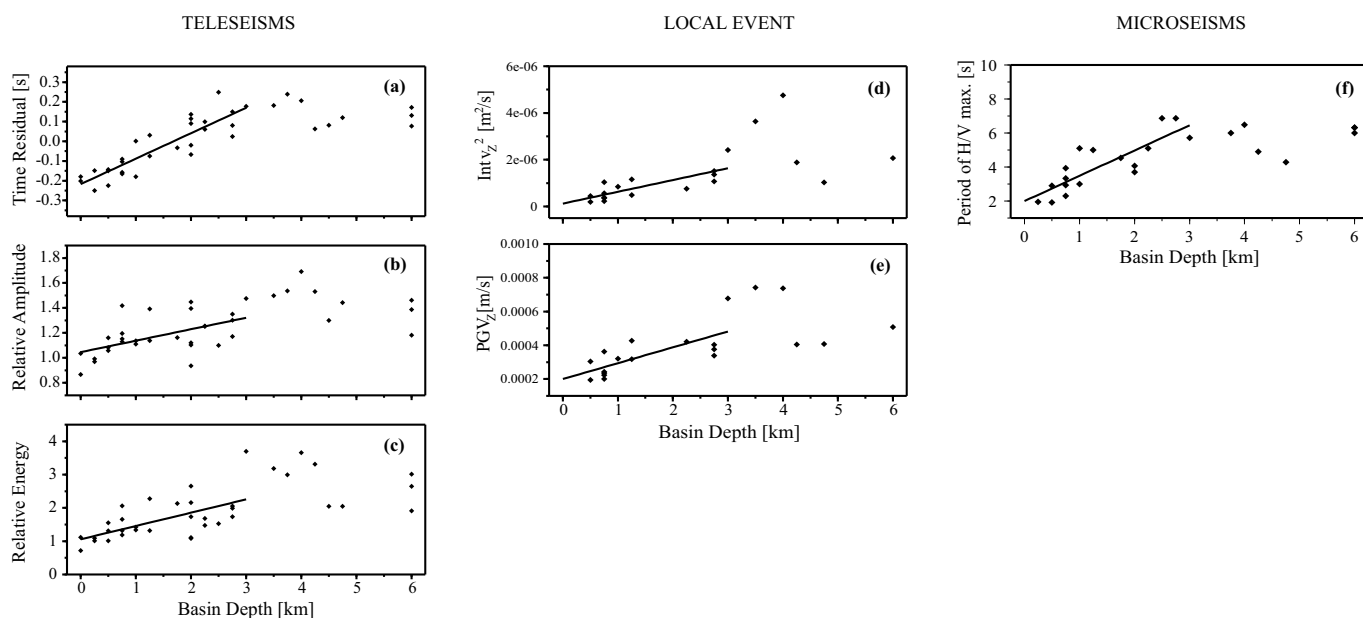


Figure 13.16: Correlations between different relative measures of ground motion parameters and USGS model basin depth. (a) Travel-time residuals, (b) relative amplitudes, and (c) average P-wave energy averaged over the teleseismic events shown in Figure 13.15b as a function of the USGS model basin depth. (d) Integrated squared vertical velocity and (e) vertical PGV measured for the San Juan Bautista event as a function of the USGS model basin depth. (f) Period of the microseisms H/V peak as a function of the USGS model basin depth.

Am., 95, 1137-1149, 2005.

Jachens, R. C., R. F. Sikora, E. E. Brabb, C. M. Wentworth, T. M. Brocher, M. S. Marlow, and C. W. Roberts, The basement interface: San Francisco Bay area, California, 3-D seismic velocity model, *EOS Trans. AGU* 78,

F436, 1997.

Larsen, S. and C. A. Schultz, ELAS3D: 2D/3D elastic finite-difference wave propagation code, *Technical Report No. UCRL-MA-121792*, 19 pp, 1995.

8. Analysis of Bridge Structures Crossing Fault Rupture Zones: Seismic Ground Motion Simulation

Douglas Dreger, Gabriel Hurtado (CEE) and Anil Chopra (CEE)

8.1 Introduction

Bridges that cross faults can be subjected to large dynamic and static ground motions. As there are very few actual ground motions recorded very close to ruptured faults ($< 100\text{m}$), ground motion simulation is the only viable way to obtain time histories for structural analysis. Professors Dreger (BSL) and Chopra (CEE) are collaborating on a Caltrans funded project investigating the response of bridges that cross faults with the objective of developing simplified methods that can be applied to bridge design. In this report the ground motion simulation part of the effort is described.

The bridges being considered have a minimum span of 30m, and therefore the simulation method must be capable of calculating seismic response time histories at this small distance from the fault. In addition, the method must accurately account for the near-fault source radiation pattern, far- and near-field seismic radiation, and have the ability to characterize motions for a broad range of fault types (e.g. vertical strike-slip and reverse faulting), as well as variable slip and full kinematic description of the rupture process. We must be able to accurately simulate the directivity effect as well as the sudden elastic rebound sometimes referred to as fling.

8.2 Simulation Method

The simulation method that we use is a 4th order accurate staggered-grid finite-difference code, e3d, developed at Lawrence Livermore National Laboratory (LLNL) (Larsen and Schultz, 1995). An advantage of this code is that it has been tested, and calibrated in a PEER/SCEC funded effort to validate numerical methods for ground motion simulation.

In addition, e3d simulates complete seismic waveforms in terms of near- intermediate- and far-field terms of the solution to the elasto-dynamic equation of motion. At such a close distance the fault all of these terms are important in strong ground motion generation.

We use a very fine model discretization of 20m. Motions at the closest stations to the fault (15m) are obtained by interpolation, and have been verified analytically for the strike-slip case. This high spatial resolution has the advantage that the kinematic source model also has high resolution producing a smooth evolution of the rupture front and the slip time function. The drawback of course is that it is computationally very expensive.

We simulate motions for a Mw6.5 earthquake using *Wells and Coppersmith* (1994) to estimate the fault

length and width. From the scalar seismic moment and the fault area the average slip is specified. We use *Somerville et al.*, (1999) to specify the slip rise time from the moment. Simulations have been performed for models ranging from a pure vertical strike-slip event to a 20-degree dipping thrust fault. We have tested rupture velocities of 70% and 140% (super-shear) of the shear wave velocity, although most of the simulations are for 80% of the shear wave velocity as is commonly reported in the literature for moderate earthquakes. We are in the process of setting up a distributed slip and variable rise time simulation to assess the effect of such source complexity on very near-fault strong ground motion.

The initial models are simplified greatly and using the finite-difference approach is "over-kill", but in the future we may consider more complex source functions and 3D fault structures such as velocity discontinuities across the fault or low-velocity fault gouge. It is desirable that the ground motion computation and the source resolution are at the same resolution, and in the future when comparisons are made with more complex models all of the ground motions will have been computed with the same theory and numerical algorithm.

The total model dimension is $50 \times 20 \times 15 \text{ km}^3$ and with the grid spacing of 20m this translates to 2.3 billion grid points, requiring 121.8 Gbytes of memory. The simulations were performed on a LLNL super computer.

8.3 Vertical Strike-Slip Results

Arrays of stations are located along the length of the fault. Subarrays 1 and 8 are located off the end of the fault. Subarrays 2 and 7 are at the two ends of the fault, subarrays 3-6 are along the fault trace. On each side of the fault the two closest stations are 15m from the fault. The hypocenter is located beneath subarray 3.

The displacement seismograms at the closest station to the fault for each subarray are shown in Figure 13.17. Static offsets are observed on the FP component at sites adjacent to the fault. The static offsets are due to the sudden elastic rebound of the fault and are sometimes referred to as fling. The static offset on one side of the fault shows one-half of the total differential motion across the fault. The sign of the static offset is opposite at the stations on the other side of the fault. The FP component static offsets are reduced in amplitude at the two sites at the end of the fault (subarrays 2 and 7). This is due to the elastic response of the medium around the fault in which "push" and "pull" quadrants result in deformation that

is not parallel to the fault strike. At these two sites, for the same reason, the FN component also shows a static offset. There are negligible static offsets at sites located off of the ends of the fault.

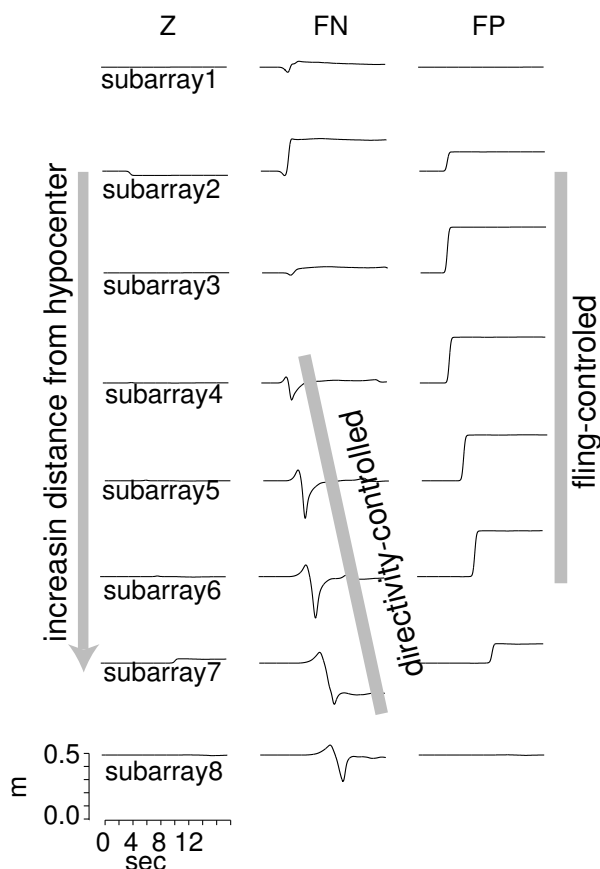


Figure 13.17: Comparison of three-component displacement records at subarrays 1-8 for the vertical strike-slip fault case. Rupture directivity is evident on the FN components. Constant amplitude static offsets are observed on the FP component for stations located along the fault.

The time from zero displacement to the final static value is controlled by the local slip rise time during rupture. In these simulations a constant average slip rise time from *Somerville et al.*, (1999) was assumed. At such close distance to the fault the corresponding velocity pulses are representative of the local slip velocity during rupture.

The FN component on the other hand only has dynamic pulse-like motions with no static offset (except for the two fault end cases already discussed). The FN component has the same amplitude on each side of the fault like the FP component, but in contrast it also has the same sign. The pulse amplitude is seen to steadily grow from subarray 3 to 6 due to directivity. At subarray 7 the FN amplitude is slightly reduced, and it remains large at

subarray 8 off of the end of the fault.

Because the fault is vertically dipping and the slip direction is horizontal the vertical motions are very weak in comparison to the two horizontal components. In the other simulations for different source and slip-direction geometries dynamic pulses and static offsets are observed on the vertical component.

In velocity the FN component becomes very pronounced, growing steadily in amplitude in the direction of rupture with maximum values on the order of 1 m/s. The velocity pulses have the same sign on each side of the fault. In contrast the FP (fling) velocity pulses along the fault have constant amplitude, but opposite sign on the two sides of the fault. The FP velocity pulses also have amplitude on the order of 1 m/s. The FP peak velocity close to the fault is controlled by the slip velocity on the fault. Slip velocity is proportional to stress drop and therefore for events with stress drop on the order 10 MPa the slip velocity is on the order of 1 m/s.

The magnitude of the directivity effect depends on how co-linear the strike and slip directions are. In the case of a vertical strike-slip fault the strike and rake are co-linear producing a maximum directivity effect. In the case of a reverse fault the rake is perpendicular to the strike and this produces a minimum directivity effect (except in the updip direction). The simulations for the other fault orientations clearly illustrate this point. Figure 13.17 also shows that the amount of directivity depends on distance from the epicenter to the station.

In general the simulations show that both static offsets and dynamic directivity-controlled pulses need to be considered on any of the three components to account for possible faulting variability. In fact, as the faulting style trends to dip-slip cases there is increased vertical motions and a transition of fling-controlled motions (static offsets) to the FN component, and directivity-controlled motions to the FP component. In oblique faulting cases it will be necessary to consider both dynamic pulses and static offsets in displacement on all three components.

8.4 References

Larsen, S. and C.A. Schultz (1995). ELAS3D: 2D/3D elastic finite-difference wave propagation code, *Technical Report No. UCRL-MA-121792*, 19 pp.

Somerville, P. G., K. Irikura, R. Graves, S. Sawada, D. Wald, N. Abrahamson, Y. Iwasaki, T. Kagawa, N. Smith, and A. Kowada (1999). Characterizing crustal earthquake slip models for the prediction of strong ground motion, *Seism. Res. Lett.*, 70, 59-80.

9. Investigation of Deep Earthquake Mechanics

Ahyi Kim and Douglas Dreger

9.1 Introduction

The mechanism of deep earthquakes in subducted oceanic lithosphere in the transition zone remains enigmatic, although there have been several studies about the mechanism for these events (e.g. *Seilver et al.*, 1995; *Raleigh and Patterson*, 1965; *Ogawa*, 1987; *Hobbs and Ord*, 1988). It is known that first motions from deep earthquakes show four-lobed radiation patterns typical of shallow shear dislocation (*Honda*, 1932). At such depth, because of tremendous pressure, frictional sliding similar to that for shallow events is not possible, yet they must have a separate mechanism that produces earthquake motions much like their shallow counterparts. Interpretation of constitutive relations for the deep-focus events is the one of the approaches to finding the mechanism for these events. For the great Bolivia earthquake, which occurred on June 9, 1994 with a moment magnitude of 8.2, *Kanamori et al.* (1998) argued that the source process was dissipative based on calculation of seismic efficiency from the observed low rupture velocity. In their paper they show that once rupture initiated, melting could occur, further reducing friction and promoting fault slip. In this study, using several large deep-focus earthquakes, we compute the dynamic and static stress change inferred from kinematic source models of deep-focus earthquakes to see if they have a more dissipative process on average than those of the shallow events, and to also see the range of variability of these parameters among the set of deep earthquakes that have reasonable set of models.

9.2 Data and Method

As a first step, we examined 2 deep-focus earthquakes, namely by the Bolivia (June 9, 1994 Mw8.2 623km) and Fiji earthquakes (March 9 1994 Mw7.6 563km). Kinematic models and other source parameters were determined by *Antolik* (1996). To examine the slip weakening constitutive relationship for deep-focus earthquakes, at first, we calculated, or collected from the literature information, about the seismic moment, the radiated seismic energy, faulting area, average slip, and static stress drop. Second, following the method of *Kanamori et al.* (1998), the possible temperature rises for all of the events were estimated using the parameters collected. To compute the temperature rise, it was necessary to assume the width of the shear zone, which was inferred from the rise time (e.g. *Kanamori et al.*, 1998), or the scaling of anti-crack width to shear-slip from laboratory measurements (e.g. *Bouchon and Ihmle*, 1999). The radiated energy, scalar seismic moment and stress drop were used to determine

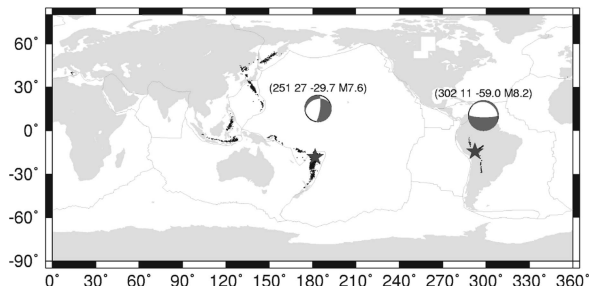


Figure 13.18: the location and moment tensor solution for the earthquakes. Bolivia earthquake occurred in the subducting Nazca plate. In this region, the deep earthquakes doesn't occur often, but they have very big magnitude when they occur. From the study of *Kanamori et al* (1998), Bolivia earthquake had the very high stress drop and Long risetime, and low seismic efficiency. On the other hand, For Fiji earthquake, which was occurred in the subducting Pacific plate. Most of the deep earthquakes occur in this region.

the seismic efficiency, which we correlated to independent observations of the rupture velocity in these events. From this analysis the events can be categorized in terms of the degree of their dissipative character. Third, to determine the temporal displacement and stress fields, we used the finite-difference method with a kinematic representation of the source process as a boundary condition (e.g. *Ide and Takeo*, 1997). We used kinematic models which have been well determined (*Antolik*, 1996). The finite-difference method is used to solve the equation of motion with an isotropic, linear-elastic stress constitutive relationship to determine the velocity/stress wavefield due to the prescribed finite-source slip. We used the absorbing boundary condition on all surfaces because all of the events are at great depth. The stress drop models obtained from this study were used to estimate the frictional energy and the possible temperature rise during faulting to assess whether frictional melting could have played a role in the other large deep earthquakes. For this analysis, we followed the method introduced in *Bouchon and Ihmle* (1999). The determined velocity/stress fields at the third step were used to examine the stress-slip constitutive relationship, the static stress drop, and the normal stress perturbation for each of the events. The magnitude of the dynamic shear and normal stress over the fault in advance of the rupture provides information on the level of deviatoric stress that triggers mecha-

nisms by which ruptures continue to grow; in the case of the Bolivia earthquake possibly outside the region of the metastable slab core.

9.3 Results

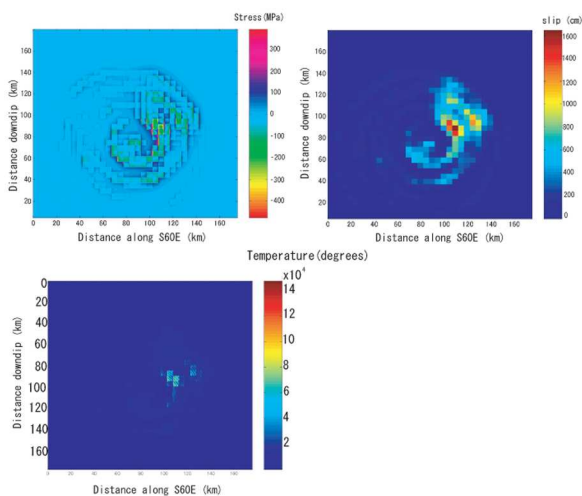


Figure 13.19: result for the Bolivia earthquake(Top right)slip distribution, (Top left)static stress distribution (bottom)possible temperature rise during the rupture.

Figure 2 shows the slip distribution, static stress change and possible temperature rise during the Bolivia earthquake. For the Bolivia earthquake, the source time function shows a large moment release 15 sec after initiation and as a result, the largest offset is not in the hypocenter region. The maximum stress change was 400Mpa, and the average stress was 21Mpa at the main rupture area, which is consistent with the result of static stress drop estimates (*Bouchon and Ihmle*, 1999). Using the stress distribution, we compute the possible temperature rise at each subfault. Taking into account the rock melting temperature of around 600 degrees, we found during the Bolivia earthquake, that melting likely occurred. The Fiji earthquake showed a factor of ten lower in temperature, but still was high enough to melt the surrounding rocks.

9.4 Conclusion

We examined the stress field and calculated the temperature increase for the Bolivia and Fiji earthquakes. For the thickness of the fault zone, assumed in both cases the temperature rise was high enough to melt the surrounding rocks. In our ongoing work, we are studying kinematic modeling, and the stress change of other large deep earthquakes.

9.5 References

Antolik, M.,D. Dreger, and B. Romanowicz, Rupture processes of large deep-focus earthquakes from inversion of moment rate functions, *Journ. Geophys. Res.*, *104*, 863-894, 1999.

Antolik, M., New results from studies of three outstanding problems in local, regional global seismology, Ph.D. Thesis, 311 pp., Univ. of Calif., Berkeley,1996.

Antolik, M., D. Dreger, and B. Romanowicz, Finite fault source study of the great 1994 deep Bolivia earthquake, *Geophys. Res. Lett.*, *23*, 1,589-1,592,1996.

Bouchon, M., and P. Ihmle, Stress drop and frictional heating during the 1994 deep Bolivia earthquake, *Geophys. Res. Lett.*, *26*, 3,521-3,524, 1999.

Green, H. W., and P. C. Burnley, A new self-organizing mechanism for deep-focus earthquakes, *Nature*, *341*, 733-737, 1989.

Hobbs, B. E., and A. Ord, Plastic instabilities: Implications for the origin of intermediate and deep focus earthquakes, *Journ. Geophys. Res.*, *93*, 10,521-10,540, 1988.

Honda, H., On the types of the seismograms and the mechanism of deep earthquake, 1932.

Ide, S., and M. Takeo, Determination of constitutive relations of fault slip based on seismic wave analysis, *Journ. Geophys. Res.*, *102*, 27,379-27,391, 1997.

Kanamori, H., D. L. Anderson, and T.H.Heaton, Frictional melting during the rupture of the 1994 Bolivian earthquake, *Science*, *279*, 839-842,1998.

McGuire, J. J., D. Wiens, P. Shore, and M. Bevis, The March 9, 1994 (Mw7.6) deep Tonga earthquake: Rupture outside the seismically active slab, *Journ. Geophys. Res.*, *102*, 15,163-15,182, 1997.

Ogawa, M., Shear instability in a viscoelastic material as the cause of deep-focus earthquakes, *Journ. Geophys. Res.*, *92*, 13,801-13,810, 1987.

Raleigh, C. B., and M. S. Patterson, Experimental deformation of serpentinite and tectonic implications, *Journ. Geophys. Res.*, *70*, 3,965-3,985,1965.

Silver, P. G., S. Beck, T. Wallace, and C. Meade, Rupture characteristics of the deep Bolivian earthquake of 9 June 1994 and the mechanism of deep-focus earthquake, *Science*, *268*, 69-73,1995.

10. ElarmS: A Methodology for Earthquake Early Warning

Richard M Allen

10.1 Introduction

The ElarmS methodology is designed to predict the distribution of peak ground shaking across the region affected by an earthquake before the beginning of significant ground motion at the epicenter. The method uses the first few seconds of the P-wave at the stations closest to the epicenter to estimate the magnitude of the earthquake. Attenuation relations provide the predicted distribution of ground shaking as a function of distance from the epicenter (Allen, 2004). The complete ElarmS system generates an "AlertMap" of predicted peak ground shaking. The first AlertMap is available 1 sec after the first P-wave trigger and is updated every second as additional data is gathered from stations further from the epicenter. More information about ElarmS is available at <http://www.ElarmS.org>.

10.2 Location and warning time

ElarmS uses the arrival times of P-waves to locate earthquakes. When the first station triggers, an event is located at that station with a depth typical of events in the region. The earthquake is then located between the first two, and then the first three stations to trigger. Once four stations have triggered a grid search method is used to locate the event, minimizing the misfit between predicted and observed arrival times. The warning time is defined as the remaining time until the onset of peak ground shaking and can be estimated given the origin time and location of the earthquake using S-wave arrival time curves. Offline testing of ElarmS using a dataset of 32 earthquakes in southern California shows that the first predictions of ground shaking are available before the S-arrival at the epicenter for 56% of earthquakes (Figure 13.20).

Warning time probability density functions have been calculated for northern California. These are based on the current distribution of broadband velocity and accelerometer stations across the region and the 35 earthquake rupture scenarios identified by the *Working Group on California Earthquake Probabilities* (2003). Figure 13.21 shows the probability that there will be an earthquake in the next 30 years for which there would be a given warning time for the city of San Francisco. These calculations show that it would be possible to provide warning for the vast majority of these damaging earthquakes. It also shows that for the most damaging events that cause ground shaking with $\text{MMI} > X$ in the city, it is more likely than not that there will be more than 20 sec warning.

10.3 Rapid magnitude estimation

The magnitude of an earthquake is rapidly estimated from the frequency content of the first four seconds of the P-wave arrival. The predominant period, τ_p , of the vertical component waveform is calculated using the method first described by Nakamura [1988]. The maximum τ_p observed within 4 sec, τ_p^{max} , has been measured for earthquakes $3.0 < M < 8.3$ from around the world and is found to scale with earthquake magnitude (Figure 13.22). The data shows no evidence to suggest that the scaling relation breaks down for the largest magnitude events with rupture durations greater than 4 sec.

The accuracy and timeliness of magnitude estimates are central to the usefulness of an early warning system. The accuracy of magnitude estimates are a function of the number of stations providing P-wave data. Datasets from both southern California and Japan show that using just the closest station to the epicenter the average magnitude error is ~ 0.75 magnitude units, once data from the closest 2 stations is available the error drops to ~ 0.6 , and to ~ 0.5 magnitude units once 4 stations provide data. The offline tests of 32 earthquakes from southern California show that magnitude estimates are available for 56% of earthquakes at the time of the S-arrival at the epicenter with an average magnitude error of 0.44 magnitude units (Figure 13.20a).

10.4 Distribution of ground shaking

Given the location and magnitude of an earthquake, the spatial distribution of peak ground shaking can be estimated using attenuation relations (e.g. Campbell, 1981; Joyner and Boore, 1981; Fukushima and Irikura, 1982; Abrahamson and Silva, 1997; Boore, et al., 1997; Campbell, 1997; Sadigh, et al., 1997; Field, 2000). Attenuation relations for small and large magnitude events have already been developed for southern California (Allen, 2004), and are under development for northern California.

ElarmS uses the attenuation relations in a two-stage process. One second after the first P-wave trigger the first estimate of magnitude is available and the attenuation relations provide PGA as a function of distance from the epicenter. The error in the PGA estimates as a function of time for the 32 earthquakes in the test dataset from southern California is shown in Figure 13.20b. As time progresses, the stations closest to the epicenter experience their PGA and this information is used to adjust the initial attenuation relation. The improvement in the PGA estimate is only marginal as shown in Figure

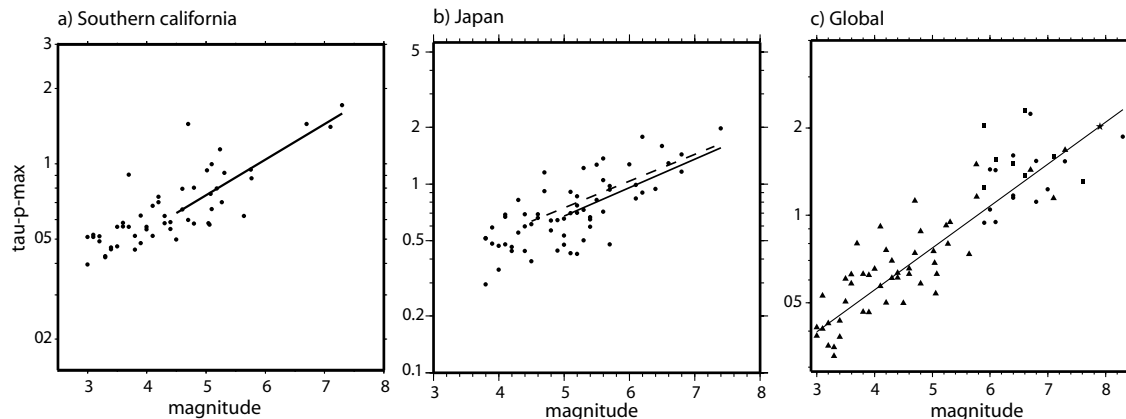


Figure 13.22: Scaling relation between event-averaged τ_p^{max} and magnitude. All data has been processed using the same recursive algorithms. A) Southern California earthquakes and best fit relation (solid line). From *Allen and Kanamori* (2003). B) Earthquakes in Japan and best fit relation (solid line). The dashed line is the best fit relation for California shown in A which is nearly identical. From *Lockman and Allen* (in review). C) Global compilation of earthquakes including southern California, Japan, Taiwan and the Denali earthquake. Waveforms are a mixture of accelerometers and broadband velocity instruments.

13.20c, but inclusion of PGA observations once available does remove outliers i.e. cases when the magnitude based estimate is very high or low.

10.5 Acknowledgements

This work was funded by the US Geological Survey NEHRP program, awards 03HQGR0043 and 05HQGR0074.

10.6 References

Abrahamson, N. A., and W. J. Silva, Empirical response spectral attenuation relations for shallow crustal earthquakes, *Seismo. Res. Lett.*, *68*, 94-127, 1997.

Allen, R. M., Rapid magnitude determination for earthquake early warning, in *The many facets of seismic risk*, edited by M. Pecce, et al., pp. 15-24, Universita degli Studi di Napoli "Federico II", Napoli, 2004.

Allen, R. M., and H. Kanamori, The potential for earthquake early warning in southern California, *Science*, *300*, 786-789, 2003.

Boore, D. M., W. B. Joyner, and T. E. Fumal, Equations for estimating horizontal response spectra and peak acceleration from western north american earthquakes; a summary of recent work, *Seismo. Res. Lett.*, *68*, 128-153, 1997.

Campbell, K. W., Near-source attenuation of peak horizontal acceleration, *Bull. Seism. Soc. Am.*, *71*, 2039-2070, 1981.

Campbell, K. W., Empirical near-source attenuation relationships for horizontal and vertical components of peak ground acceleration, peak ground velocity, and

pseudo-absolute acceleration response spectra, *Seismo. Res. Lett.*, *68*, 154-179, 1997.

Field, E. H., A modified ground-motion attenuation relationship for southern California that accounts for detailed site classification and a basin-depth effect, *Bull. Seismol. Soc. Am.*, *90*, S209-S221, 2000.

Fukushima, Y., and K. Irikura, Attenuation characteristics of peak ground motions in the 1995 hyogo-ken, *J. Phys. Earth*, *45*, 135-146, 1982.

Joyner, W. B., and D. M. Boore, Peak horizontal acceleration and velocity from strong-motion records including records from the 1979 imperial valley, California, earthquake, *Bull. Seismol. Soc. Am.*, *71*, 2011-2038, 1981.

Lockman, A., and R. M. Allen, Magnitude-period scaling relations for Japan and the Pacific Northwest: Implications for earthquake early warning, *Bull. Seismol. Soc. Am.* in review.

Nakamura, Y., On the urgent earthquake detection and alarm system (UrEDAS), *Proc. 9th World Conf. Earthquake Eng.*, *VII*, 673-678, 1988.

Sadigh, K., C. Y. Chang, J. A. Egan, F. Makdisi, and R. R. Youngs, Attenuation relationships for shallow crustal earthquakes based on California strong motion data, *Seismo. Res. Lett.*, *68*, 180-189, 1997.

Working Group on California Earthquake Probabilities, *Earthquake probabilities in the San Francisco Bay region: 2003 to 2031*, U.S. Geological Survey, 2003.

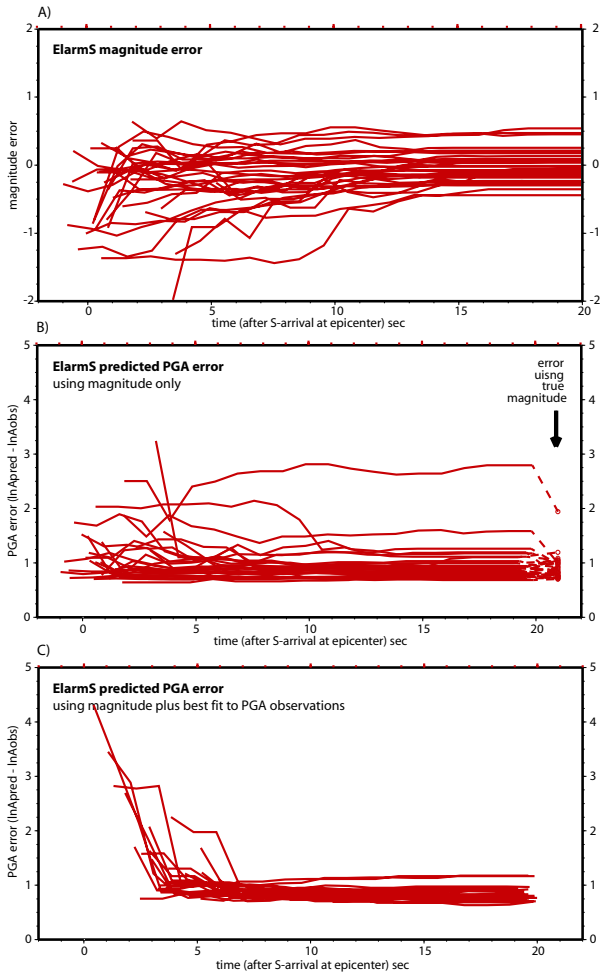


Figure 13.20: The results of testing ElarmS offline using a set of 32 earthquakes in southern California and the current distribution of stations. All panels show errors as a function of time with respect to the S-wave arrival at the epicenter which represents the earliest time of peak ground shaking during an earthquake. A) The error in the magnitude estimate. A magnitude estimate is available for 56% of earthquakes at the time of the S-arrival at the epicenter with an average magnitude error of 0.44 magnitude units. Within 5 sec magnitude estimates are available for 97% of events with an average error of 0.33. B) Average absolute error in PGA estimates at all stations. At the time of the S-arrival the average absolute error is 1.08. It drops to 1.00 within 5 sec, 0.98 within 10 sec, and reaches 0.95 at 15 sec. When the correct magnitude is used in the attenuation relations (i.e. removing the error in the ElarmS magnitude estimate), the error is 0.89, only slightly lower. C) Average error in PGA once available PGA observations are incorporated. The most important use of PGA observations is to remove outliers. The error in the PGA estimates is calculated in the usual way: the error is the natural logarithm of the predicted PGA minus the natural logarithm of the observed PGA for the event.

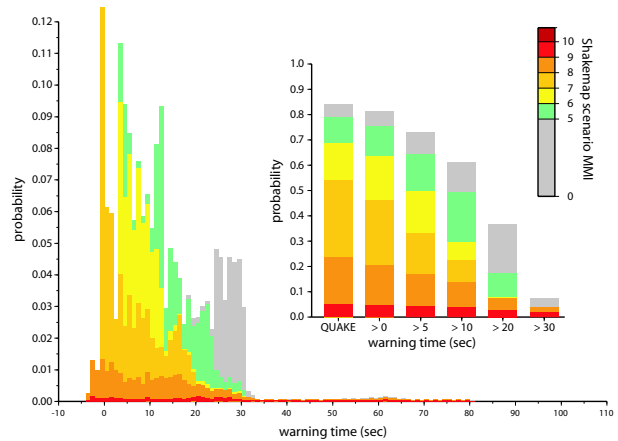


Figure 13.21: Earthquake early warning time probability density function for the city of San Francisco. Warning times were calculated for the 35 rupture scenarios identified by the *Working Group on California Earthquake Probabilities* (2003) and the probability of each rupture assigned to the warning time. Epicenters were distributed at 1 km intervals along the complete length of each rupture and the cumulative probability of all events set equal to the probability of the rupture scenario. The warning time is defined at the time at which 4 sec of the P-wave is available at 2 stations and a 2 sec delay for telemetry has been added. This distribution of warning times is based on the current distribution of stations with a moderate improvement to telemetry. The warning times are color coded by the predicted intensity of ground shaking in the city using the scenario ShakeMaps. The inset shows the probability of > 0, 5, 10, 20 and 30 sec warning along with the total probability of all 35 rupture scenarios (labeled QUAKE).

11. Northern California Seismicity Project

Robert A. Uhrhammer

11.1 Introduction

The Northern California Seismicity Project (NCSP) is a counterpart to the San Francisco Bay Region (SFBR) - Historical Earthquake Re-analysis Project (HERP) which has been reported upon in previous annual reports. The initial objective of this project which commenced in August, 2000, is to transcribe the pre-1984 data for $M_L \geq 2.8$ earthquakes which have occurred in Northern and Central California (NCC) (outside of the SFBR covered by HERP), from the original reading/analysis sheets, kept on store in the Berkeley Seismological Archives, to a computer readable format.

Characterization of the spatial and temporal evolution of NCSP seismicity during the initial part of the earthquake cycle as the region emerges from the stress shadow of the great 1906 San Francisco earthquake is the long term goal. The problem is that the existing BSL seismicity catalog for the SFBR, which spans most of the past century (1910-present), is inherently inhomogeneous because the location and magnitude determination methodologies have changed, as seismic instrumentation and computational capabilities have improved over time. As a result, NCC seismicity since 1906 is poorly understood.

Creation of a NCC seismicity catalog that is homogeneous, that spans as many years as possible, and that includes formal estimates of the parameters and their uncertainty is a fundamental prerequisite for probabilistic studies of the NCC seismicity. The existence of the invaluable BSL seismological archive, containing the original seismograms as well as the original reading/analysis sheets, coupled with the recently acquired BSL capability to scan and digitize historical seismograms at high resolution allows the application of modern analytical algorithms towards the problem of determining the source parameters of the historical SFBR earthquakes.

11.2 Background and Motivation

Although the 1910 to present BSL catalog of earthquakes for NCC appears to be a simple list of events, one must remember that it really is a very complex data set. It is easy to misinterpret observed variations in seismicity if we do not understand the limitations of this catalog. The existing 1910 to present BSL catalog of earthquakes for NCC is inhomogeneous in that it suffers from the three types of man-made seismicity changes identified by *Habermann, 1987*, namely detection changes, reporting changes, and magnitude shifts. The largest change in the detection capability of the BSL seismic station net-

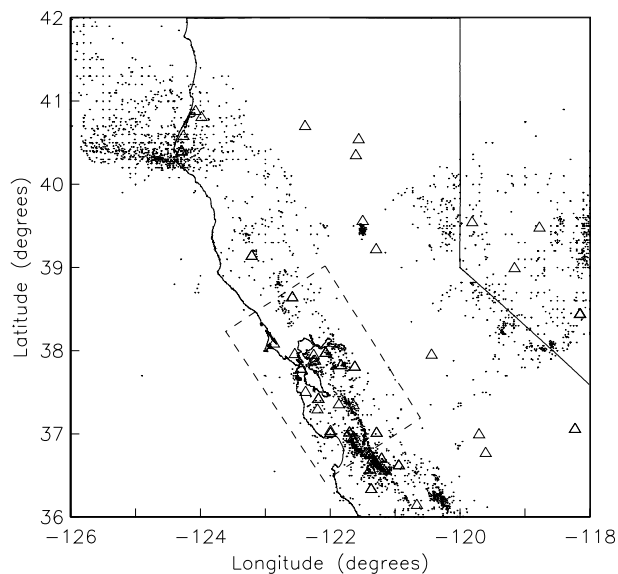


Figure 13.23: Map of the NCC Region showing the 1951-1983 $M_L \geq 2.9$ seismicity (small dots). The triangles are the seismic stations, operated by Berkeley and adjacent networks between 1951 and 1983, for which data are available. Events occurring in the dashed inset box were transcribed and analyzed as a part of the HERP project.

work occurred starting circa 1927 with the installation of the Wood-Anderson and Benioff seismometers at several sites in NCC (see Figure 13.23) and the resulting increase in sensitivity lowered the threshold for detection of NCC earthquakes by about 2 M_L units. The most significant reporting change occurred circa 1942 when the BSL began determining M_L for some earthquakes and by 1948 M_L was routinely determined and reported for all SFBR earthquakes listed in the BSL Bulletin (*Romney and Meeker, 1949*).

The lack of a homogeneous catalog of earthquake for the SFBR which spans most of the past century, the availability of the invaluable BSL seismological archive, the interest in the Working Group on California Earthquake Probabilities (WGCEP, 1999), the funding of an initial effort with support from the USGS-PG&E CRADA, and the purchase and loan of a high-resolution wide-format digitizer by the USGS, combine to provide both an incentive and a unique opportunity to systematically re-process, using modern algorithms, the BSL seismographic records and data for SFBR earthquakes and to produce a homogeneous catalog of earthquakes for the

region.

11.3 Current Effort

To expedite the transcription process, we converted all relevant available data from the online NCEDC event catalogs and the in-house phase data to a flat transcription file format for the years 1978 through 1983. We also acquired a copy of the International Data Center (ISC) CDROM which contains events and associated station data published in the ISC Bulletins from January 1964 through December 1977 (Version 1.2). This ISC data set includes event and station data contributed by Berkeley and the CDROM also contains a algorithm to search the database and extract and translate the ISC coded phase Berkeley data to a readable print format for years 1963 through 1977. This enabled us to start with transcription files that contained approximately half of the data that is on the original reading/analysis sheets for the years 1964 through 1983. The primary data from the original reading/analysis sheets, that was not included in this process, was the Wood-Anderson maximum trace amplitude data that is crucial for the determination of local magnitude.

During the past year six students worked on the process of transcribing the data from the original BSL reading/analysis sheets to computer readable form. They started by checking the transcription of the original reading/analysis sheets and locating the earthquakes from 1983 and they have been working back in time. Since none of the data on the pre-1964 reading/analysis sheets exists in a computer readable form, all data has to be transcribed and consequently it takes more time to transcribe each event. Currently they are currently transcribing reading/analysis sheet data from 1951 and they have processed reading/analysis sheets for over 4400 earthquakes which have occurred in NCC. Also, the pre-1951 reading/analysis sheets data do not contain Wood-Anderson maximum trace amplitude data which is used in the calculation of local magnitude so that the original Wood-Anderson seismograms with have to be retrieved from the archive and the amplitudes read. This quite labor intensive component of the project is planned for the coming year.

11.4 Acknowledgements

UC Berkeley students Vicky Chi Sum Chan, Jonathan Hsu, Rose Li, Sean Tsai, Noli Valera and visiting U Pennsylvania student Carmen Rodriguez participated in this project during the past year and we thank them for their efforts.

This project was partially supported by the USGS funding of the Northern California Earthquake Data Center.

11.5 References

Habermann, R. E., Man-made changes of seismicity rates, *Bull. Seism. Soc. Am.*, 77, 141-159, 1987.

Romney, C. F. and J. E. Meeker, Bulletin of the Seismographic Stations, *University of California Press*, 18, pp. 89, 1949.

12. Seismogram Scanning Project

Robert A. Uhrhammer

12.1 Introduction

This aim of Seismogram Scanning Project (SSP) is to scan selected analog seismograms kept on store in the Berkeley Seismological Laboratory (BSL) Seismogram Archive and generate digital image files for studying microseismic source areas and distribution in relation to wave climate. The Berkeley Seismogram Archive, where approximately 1.2 million analog seismograms dating back to 1910 are stored, contains seismograms recorded at the Berkeley seismic station, dating back to 1930, which are crucial for this project. This scanning project is being undertaken in collaboration with Dr. Peter Bromirski of the University of California, San Diego/Scripps Institution of Oceanography on his project funded by the California Department of Boating and Waterways. The corresponding digitization of the scanned seismograms is being done at the Scripps Institution of Oceanography.

12.2 Background and Motivation

The photographic and smoked paper seismograms kept on store in the BSL seismogram archive are gradually deteriorating over time and scanning of the seismograms into a computer readable format is essential if they are to be preserved for the future. BSL has a wide format scanner and whenever the opportunity and funding allows we make an effort to scan seismograms.

12.3 Current Effort

During the past year we have systematically scanned the November-March Berkeley vertical component Sprengnether seismograms for the winters of 1962 through 1991 and also the November-March Berkeley vertical component Wilip-Galitzin seismograms for the winters of 1930 through 1964 for a total of $\sim 10,000$ seismograms.

12.4 Digitization Procedure

Digitization of the photographic seismograms has two components. The seismograms are first scanned at a resolution of 400 dots per inch on an Contex Scanning Technology Ideal FSS 18000 DSP Full Scale Scanner using their interactive WIDEimage scanning software package (URL: <http://www.contex.com/software/wideimagenet/default.htm>). The scanned images are stored as Tag Image Format (TIF) bitmap image files. To substantially reduce the storage requirements a histogram analysis is employed to interactively set an appropriate thresh-

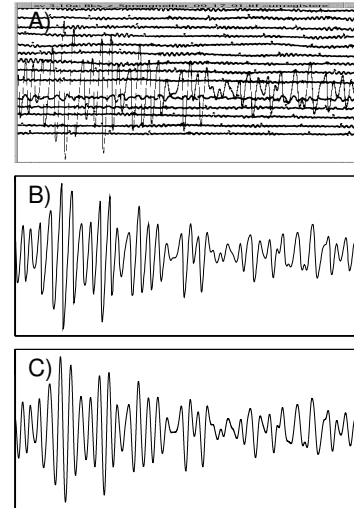


Figure 13.24: A comparison of: A) the scanned BKS Sprengnether Z-component seismogram; B) the corresponding digitized waveform, and; C) the corresponding waveform synthesized from the co-sited Streckeisen STS-1 broad band seismograph. The seismic signal is from a M 5.7 teleseism which occurred 4000 km SE of Berkeley (1991/09/18,09:48:13; 14.65N, 90.99W) in Guatemala. All three plots are at the same scale with the horizontal axis spanning 511.25 seconds and the vertical axis spanning 175 mm. That all three waveforms are highly similar is verification of the accuracy of the digitization procedure and the accuracy of the Sprengnether transfer function.

old and the scanned seismograms are stored as 1-bit resolution line-art images. The traces on the scanned seismogram image are then digitized at nominally 4 samples per second using the SeisDig software package (Bromirski and Chuang, 2003) available for download at URL: <http://www.ucsg.edu/~bromirski>. The resulting digitized seismogram has an amplitude resolution of 0.0635 mm (i.e. the pixel resolution and equivalent to a data logger sensitivity of 15748 DU/M) and a time resolution of 0.254 seconds for the SPR seismograms recorded at 15 mm/min and 0.127 seconds for the W-G seismograms recorded at 30 mm/min (also the pixel resolution). The effective dynamic range is approximately 64 dB ($20 \log_{10}(100\text{mm}/0.0635\text{mm})$). An example of a digitized SPR seismogram is shown in Figure 13.24.

12.5 Calibration of Wilip-Galitzin, Sprengnether and Streckeisen Seismographs

As seismic instrumentation has evolved, three different three-component set of long-period/broadband seismographs have been installed and operated, with overlapping intervals, at Berkeley since the 1930's. Wilip-Galitzin (W-G) seismographs were operated on the northern most seismic piers in the basement of Havi-land Hall on the Berkeley Campus (BRK) from August 28, 1930 until February 1, 1965. World Wide Standardized Station (WWSS) Sprengnether (SPR) long-period seismographs were operated in the Byerly Seismic Vault (BKS), located in Strawberry Canyon behind the Botanical Garden, from June 8, 1962 until September 30, 1991. Streckeisen (STS-1) broadband seismographs began recording in the Byerly Seismic Vault (BKS) on May 11, 1987 with a 16-bit PC-based recording system (*Bolt et al.*, 1988) and a 20 second pendulum configuration and by August 8, 1991 they had evolved into the current 24-bit Quanterra Q680 data logger and 360 second very-broadband (VBB) pendulum configuration. The W-G and SPR seismographs operated concurrently, but not co-sited, from June 8, 1962 until February 1, 1965. The SPR and STS-1 seismographs operated concurrently at BKS from August 8 until September 30, 1991. Comparison of selected seismograms from these intervals allow us to verify the calibration and response of these seismographs and to demonstrate that, within appropriate passbands, the earlier instrument seismograms can be reliably synthesized from later instrument seismograms and that absolute ground motions can be reliably estimated. An example of a SPR seismogram, synthesized from the corresponding STS-1 seismogram, is shown in Figure 13.24. A Streckeisen STS-2 seismograph has operated at BRK since January 1, 1993 and a comparison of selected seismograms from the BKS STS-1 and the BRK STS-2 is used to quantify differences in their site responses. A comparison of the responses of these seismographs is shown in Figure 13.25.

12.6 Acknowledgements

UC Berkeley students Amanda Austin and Kevin Lee participated in this project during the past year and we thank them for their efforts.

This project was funded by sub-award of the California Department of Boating and Waterways Contract 03-106-105.

12.7 References

Bolt, B. A., J. E. Friday and R. A. Uhrhammer, A PC-based Broadband Digital Seismograph Network, *Geophysical Journal*, 93, 565-573, 1998.

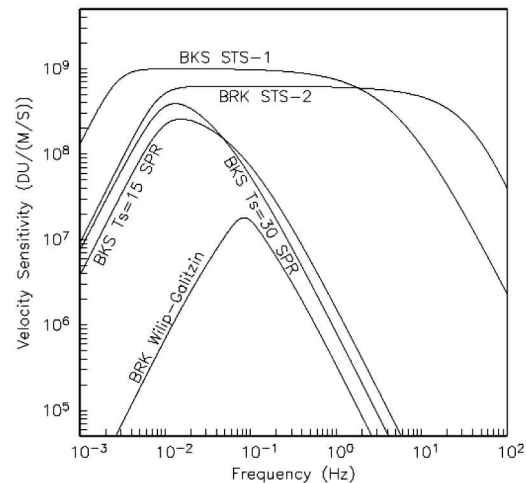


Figure 13.25: A comparison of the velocity responses of the BRK W-G and STS-2 and the BKS SPR and STS-1 seismographs operated at Berkeley. The W-G and SPR instruments recorded galvanometrically on photographic paper and the paper seismograms are scanned at a resolution of 400 dots per inch. The STS-1 and STS-2 instruments record digitally via a high-resolution data logger. The velocity sensitivity is given in digital units per meter per second (DU/(M/S)). Two responses are given for the SPR because its natural period (T_s) was changed from 30 seconds to 15 seconds on May 12, 1965.

Bromirski, P. D. and S. Chuang, SeisDig Software to Digitize Scanned Analog Seismogram Images: User's Manual, *Scripps Institution of Oceanography Technical Report*, Scripps Institution of Oceanography, Integrative Oceanography Division, UC San Diego, 28 pp., July 2, 2003.

13. Insight into the Origin of Earth's hum and Microseisms

Junkee Rhie and Barbara Romanowicz

13.1 Introduction

It is well understood that the background level of seismic noise is affected by fluid covers surrounding the solid Earth, such as the atmosphere and ocean. Microseism due to ocean waves is the most significant seismic noise at periods between 2 to 25 sec. For very long periods (> 1000 s), variations in atmospheric pressure affect more significantly the level of seismic noise with increasing period. Between the two period ranges, from 150 to 500 s, weak but dominant background noise is the continuous free oscillations of the Earth. [e.g. *Nawa, et al.*, 1998; *Suda et al.*, 1998]. The amplitude level of this excitation is very low and it can be only detected by stations with a quiet seismic environment or by stacking of several seismic records. Rhie and Romanowicz [2004] showed that the geographic locations of the sources generating ubiquitously propagating Rayleigh waves are mostly in the oceans and that infragravity waves may play an important role in the transfer of energy from the atmosphere to the solid Earth. The theoretical work explaining the oceanic origin of the continuous free oscillations followed, and demonstrated that infragravity waves have enough energy to generate continuous free oscillations. [*Tanimoto*, 2005]. Significant wave height measurements at buoys on the Pacific show significant correlations with the variations of seismic amplitude in the microseism band (2-25 s). An interesting observation is that the ocean measurements show a good correlation with the variation in the seismic amplitude in the hum band (150-500 s) as well. This observation may indicate that seismic excitations in both frequency bands, 2-25 s and 150-500 s, have the same source or similar generating mechanism, i.e. ocean waves propagating to the shore. However, long period energy propagates long distance more efficiently and is able to excite observable continuous free oscillations of the Earth.

13.2 Correlation between two arrays

Rhie and Romanowicz (2004) showed that there is a very good correlation between the variations in maximum stack amplitudes for two regional arrays at Japan (F-net) and California (BDSN) with common maximum amplitude on day 31 in 2000 at periods around 240 s. This correlation was explained by common sources generating long period surface wave energy over the ocean. Both seismic arrays detect maximum seismic energy arriving on day 31 and significant wave height measurements near the California and Japan coasts also show that wave heights were largest around day 31 in 2000.

We took time windows from 30 to 35 days in 2000 to compare the variations in seismic amplitudes for the two arrays. Stack amplitude functions as a function of time and back-azimuth are computed for both arrays and moving averages with the duration of 6 hours and shift of 1 hour are taken. Stack amplitude functions are computed by correcting for dispersion based on PREM. Gaussian filters with center period of 150 s and 240 s had been taken before the dispersion correction and stacking. The overall trends for both arrays and both frequency bands are consistent, but if we look more carefully, some differences emerge. For example, it is clear that onsets of first maxima on day 31 for F-net and BDSN have a time difference of about 0.5 days, which is too large to be explained by seismic wave propagation from one common source under the assumption of minor arc propagation. This indicates that both arrays detect elastic energy arrivals coupled at different geographic regions.

13.3 Correlation between ocean and seismic data

We collected significant wave height recordings measured at buoys deployed by National Ocean and Atmospheric Administration (NOAA) and Japan Meteorological Agency (JMA) on the Pacific for days of 30 through 35 in 2000. The significant wave heights are compared to the variations in the level of seismic amplitude at F-net and BDSN (Figure 13.26).

We computed maximum mean stack amplitude for center period of 240 s and compared the variations in amplitude with significant wave height measured at buoys placed close to the two arrays in Japan (F-net) and California (BDSN). Two significant wave height measurements in different parts of the Pacific show similar trends with two maxima on day 31 and 33. Rough comparison of the onsets of associated maxima in buoy and seismic data for the eastern Pacific shows that the maximum in the seismic data arrives later than that in buoy data on days 31 and 33. It indicates that seismic energy measured at the two arrays had been generated closer to the shore than the location of the buoys and the mechanism of generating continuous long period Rayleigh waves may be similar to the one for the microseisms at short periods. The significant wave heights measured at the buoys placed very close to the Californian coast (46027 in Figure 13.26) show much better agreement with the seismic data at BDSN. It is very difficult to determine similar trends of significant wave heights at eastern and western part of the Pacific are just local phenomena from

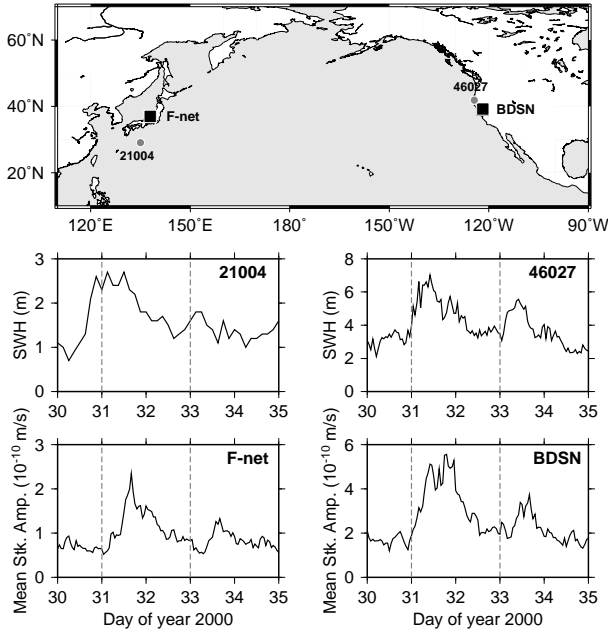


Figure 13.26: Significant wave heights at buoys (solid gray circles) near California and Japan coasts and mean stack amplitudes for two regional arrays (black squares)

separate ocean waves or basically initiated by one common origin. Considering long term correlation of seismic amplitudes for both arrays, we prefer one common atmospheric perturbation - that may be very spatially extended - which generates eastward and westward propagating ocean waves.

13.4 Cross continental propagation of surface wave energy

In the previous section, we showed there is very good correlation between ocean wave heights and seismic excitations. We believe that the energy in ocean waves is converted to elastic energy close to the coast and propagates over the array and this elastic energy can excite the continuous oscillations of the Earth. To confirm this hypothesis, we need to show the elastic energy generated from the ocean wave can propagate long distance to finally be able to excite normal modes of the Earth. We selected several high dynamic range, very broad band seismometers deployed in the United States and computed their power spectral densities at long periods between 50 to 350 s to check if there is similar trend we found in oceanic and seismic data near the coast of California (Figure 13.27). We can clearly see two large amplitude peaks in PSD on day 31 and 33 at all three stations (CMB, TUC, and HRV).

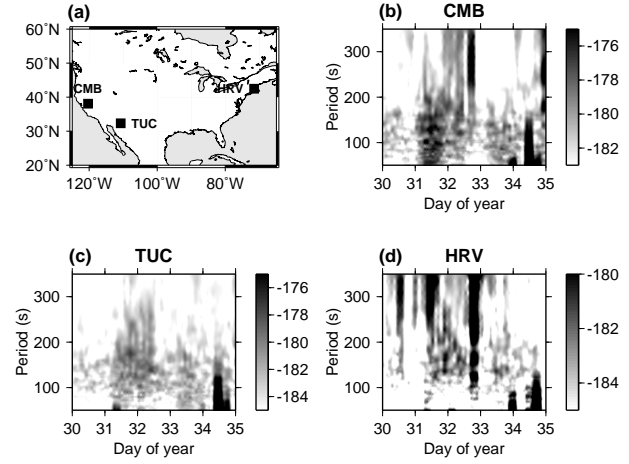


Figure 13.27: Power spectral densities at three stations. The unit for (b), (c) and (d) is $10 \times \log(m^2 s^{-4}) / Hz$.

13.5 Discussion

We showed that there is a good correlation between significant wave heights measured at buoys and the variation in seismic amplitudes at long periods. Also, this long period energy can propagate across the continent. This observation may indicate that interaction between ocean wave and sea floor near the coast generates not only short period seismic wave (microseisms) but also long period ones (the hum of the Earth).

13.6 Acknowledgements

We are thankful to Dr. Nozomu Takeuchi for making Japanese buoy data available.

13.7 References

- Nawa, K, N. Suda, Y. Fukao, T. Sato, Y. Aoyama, and K. Shibuya, Incessant excitation of the Earth's free oscillations, *Earth Planets Space*, 50, 3-8, 1998.
- Rhie, J. and B. Romanowicz, Excitation of Earth's continuous free oscillations by atmosphere-ocean-seafloor coupling, *Nature*, 431, 552-556, 2004.
- Suda, N. K. Nawa, and Y. Fukao, Earth's background free oscillations, *Science*, 279, 2089-2091, 1998.
- Tanimoto, T., The oceanic excitation hypothesis for the continuous oscillations of the Earth, *Geophys. J. Int.*, 160, 276-288, 2005.

14. Observations of Infragravity Waves at the Monterey Ocean Bottom Broadband Station (MOBB)

David Dolenc, Barbara Romanowicz, Debra Stakes (MBARI), Paul McGill (MBARI), and Doug Neuhauser

14.1 Introduction

The Monterey ocean bottom broadband station (MOBB) is a collaborative effort between the Monterey Bay Aquarium Research Institute (MBARI) and the Berkeley Seismological Laboratory (BSL). The MOBB is located 40 km offshore in the Monterey Bay, buried in the ocean floor at a water depth of 1000 m (*Romanowicz et al.*, 2003).

Infragravity waves are ocean surface waves with periods longer than the wind-driven waves and the swell. Their wave amplitudes in the deep water are small (< 1 cm) and they can be observed in the frequency band from 0.002 to 0.05 Hz. Infragravity waves have been identified as an important source of long-period noise at the ocean bottom (*Webb et al.*, 1991). Recently, they have also been proposed as a source of the Earth's continuous free oscillations (*Rhie and Romanowicz*, 2004; *Tanimoto*, 2005).

14.2 Observations

We computed power spectral density (PSD) for 1-hour long MOBB data segments and compared the results to the spectral wave density (SWD) measured at the nearby NOAA buoys. The SWD is computed at the buoys and measures energy of the ocean waves in m^2/Hz in the 0.01 Hz wide frequency bins that cover the 0.03 to 0.4 Hz range. The location of the buoys as well as comparison spectrograms for a 7-day period are shown in Figure 13.28. The infragravity peak can be observed in the PSD plot for the vertical MOBB channel (Figure 13.28, top panel). A rather sudden change of the infragravity peak width is indicated with a black line. The storm observed on day 344 was approaching from the WNW direction. Increased energy of the 10-20 s ocean waves on day 344 can therefore first be seen on buoy 46014, and last on buoy 46011. The arrival of these waves at buoy 46042 coincides with the increase of the infragravity signal on MOBB. This tells us that the infragravity waves observed at MOBB are primarily locally generated. The same can generally be observed throughout the deployment and for storms arriving from different azimuths.

14.3 Modulation of infragravity signal

The PSD for the vertical MOBB component for a 10-day period is shown in Figure 13.29b. As before, the strongest infragravity signal (days 18-20) coincides with the increased energy of 10-20 s ocean waves as recorded

at the local buoy 46042 (Figure 13.29f). In addition, two types of modulation of the infragravity peak can be observed (*Dolenc et al.*, 2005).

The modulation with a period equal to the diurnal tide and to a lesser extent the semidiurnal tide is best seen at the short-period end of the infragravity peak (30-40 s periods) as well as throughout the entire infragravity band. This modulation correlates with the amplitude of the ocean tides at MOBB, shown in Figure 13.29a.

Previous studies of the nonlinear interaction between short-period waves and currents (*Longuet-Higgins and Stewart*, 1960, 1964) found that the energy variations of the short-period waves correspond to work done by the currents against the radiation stress of the short-period waves. The magnitude of the energy exchange between the short-period waves and tidal current depends on the pattern of the tidal currents, but in simple situations, the energy of the short-period waves is in phase with the tidal elevations (*Longuet-Higgins and Stewart*, 1964). This agrees with our observations.

Another effect that the tides have on the generation of the infragravity waves is through different topography that is brought into play at the same water depth during different tide heights. The topography around MOBB is very complex and it is possible that already a small water depth change can significantly perturb the conditions for generation and reflection of infragravity waves.

We also observe a low-frequency modulation which is best seen as the variation of the period on the long-period side of the infragravity peak at which the infragravity peak rises above the noise from other sources (Figure 13.29b,c). First we compare this to the significant wave height measured at the local buoy 46042 (Figure 13.29d). The two agree well in the first half of the 10-day period, but then significant wave height has a peak in the second half of the day 25, when most of the wave energy was in the waves with periods shorter than 10 s (Figure 13.29f). Correlation between the period of the infragravity peak envelope and the significant wave height is shown in Figure 13.29g. Next, we looked at the correlation between the period of the infragravity peak envelope and the wave energy in individual frequency bins as observed at the local buoy. The best correlation was observed with the ocean waves with 14.3 s period for which the SWD is shown in Figure 13.29e,h. The correlation coefficient between the period of the infragravity peak envelope and the SWD observed in the individual bins at buoy 46042, as a function of the SWD bin period, is presented in

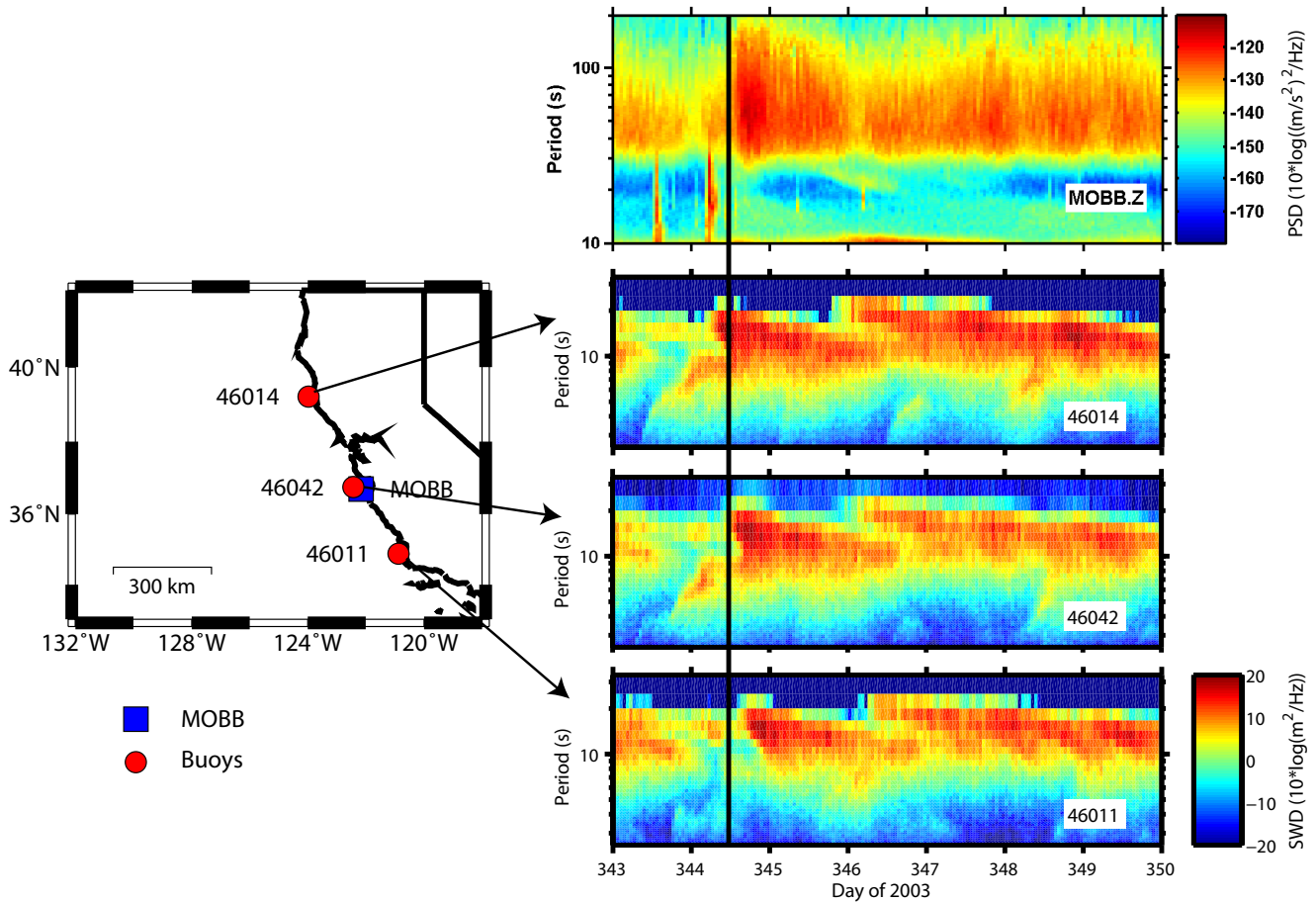


Figure 13.28: Left: The location of some of the NOAA buoys closest to the MOBB. Right: The power spectral density (PSD) for the vertical MOBB channel as a function of period and time (top). Bottom panels show the spectral wave density (SWD) calculated at 3 buoys. The vertical line indicates a sudden change of the infragravity peak width.

Figure 13.29i, and confirms that the infragravity peak long-period modulation correlates the strongest with the ocean wave energy at ~ 14 seconds.

A similar result can be obtained for other stormy periods at MOBB. This suggests that the short-period ocean waves are essential for the generation of the infragravity waves. It is interesting that the same period ocean waves are also the source of the microseisms noise, observed at the double frequency, at 6-7 s. This suggests that the generation mechanisms of infragravity waves and double frequency microseisms could be closely related.

14.4 Conclusions

Infragravity waves can be observed at the ocean bottom broadband seismic station MOBB. When compared to the energy of the short-period ocean waves recorded at the local buoys, infragravity waves in the longer than 20 s period band are found to be mainly locally generated from shorter period waves. Two types of modulation of the infragravity signal are observed. First, the entire in-

fragravity band is modulated in-phase with tides. It is possible that this is a result of the nonlinear exchange of energy between the short-period waves and tidal currents. Second, the low-frequency modulation of the observed infragravity peak is best correlated with the energy of the 14.3 s period ocean waves, suggesting a close relation of infragravity wave generation to that of double frequency microseisms.

14.5 Acknowledgements

The MOBB instrumentation, deployment, and maintenance were supported by the Lucile and David Packard Foundation funds to MBARI, the NSF Grant OCE9911392, and UC Berkeley funds to BSL.

14.6 References

Dolenc, D., B. Romanowicz, D. Stakes, P. McGill, and D. Neuhauser, Observations of infragravity waves at the Monterey ocean bottom broadband station

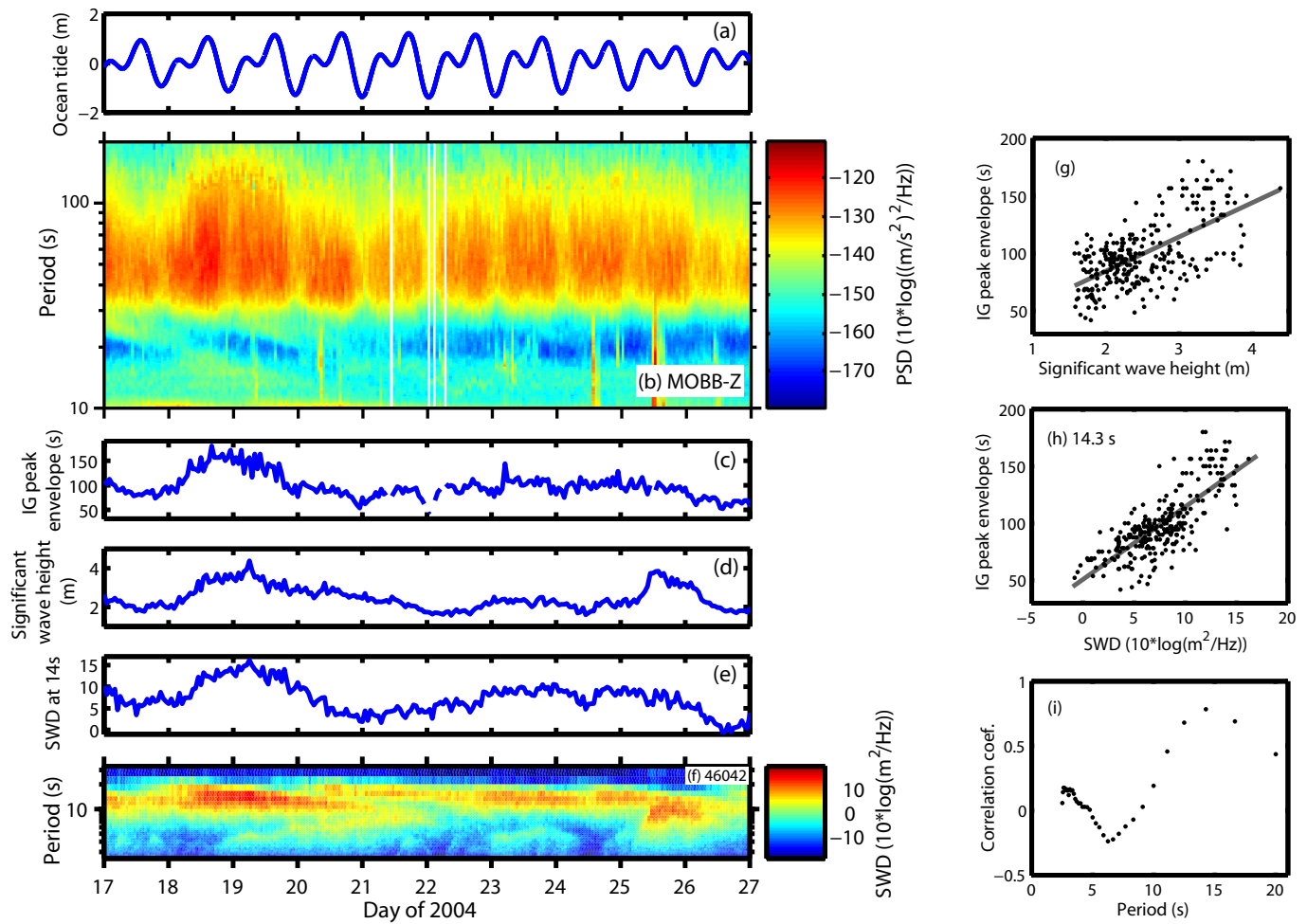


Figure 13.29: (a) Theoretical ocean tide at the MOBB location. (b) The power spectral density (PSD) for the vertical MOBB channel as a function of period and time. White lines indicate hours with some missing data. (c) The envelope of the infragravity peak presented in (b), taken at the long-period end, at the PSD value of -136 dB. (d) The significant wave height at the buoy 46042. (e) The spectral wave density (SWD) in the 14.3 s period bin at the buoy 46042. (f) The SWD at the buoy 46042 as a function of period and time. (g) The period of the infragravity peak envelope, taken at the long-period end, at the PSD value of -136 dB, as a function of the significant wave height as observed at the buoy 46042. Gray line shows best linear fit to the data. (h) The period of the infragravity peak envelope as a function of the SWD observed at the buoy 46042 in the 14.3 s period bin. Gray line shows best linear fit to the data. (i) The correlation coefficient between the period of the infragravity peak envelope and the SWD observed in the individual bins at buoy 46042, as a function of the SWD bin period.

(MOBB), *Geochem. Geophys. Geosyst.*, 6, Q09002, doi:10.1029/2005GC000988, 2005.

Longuet-Higgins, M. S. and R. W. Stewart, Changes in the form of short gravity waves on long waves and tidal currents, *J. Fluid Mech.*, 8, 565-583, 1960.

Longuet-Higgins, M. S. and R. W. Stewart, Radiation stresses in water waves; a physical discussion, with applications, *Deep-Sea Res.*, 11, 529-562, 1964.

Rhie, J. and B. Romanowicz, Excitation of Earth's continuous free oscillations by atmosphere-ocean-seafloor coupling, *Nature*, 431, 552-556, 2004.

Romanowicz, B., D. Stakes, R. Uhrhammer, P. McGill, D. Neuhauser, T. Ramirez, and D. Dolenc, The MOBB Experiment: A prototype permanent off-shore ocean bottom broadband station, *Eos Trans., AGU*, 84 (34), 325, 331-332, 2003.

Tanimoto, T., The oceanic excitation hypothesis for the continuous oscillation of the Earth, *Geophys. J. Int.*, 160, 276, 2005.

Webb, S. C., X. Zhang, and W. Crawford, Infragravity waves in the deep ocean, *J. Geophys. Res.*, 96, 2723-2736, 1991.

15. Seismic Imaging OF the Newberry Hotspot Track

Mei Xue and Richard M. Allen

15.1 Introduction

Located in the northwestern United States, the Newberry hotspot track, along the Oregon High Lava Plains (HLP), consists of a sequence of age-progressive silicic volcanic domes and lava flows, showing a monotonic age progression from east to west ending at the Newberry Caldera. While mantle plumes are often called upon to explain hotspot tracks, the Newberry hotspot track cannot be the product of plate motion over a stationary mantle source as its orientation is $\sim 120^\circ$ to plate motion, making it a good case study for alternative causal mechanisms of hotspot tracks. Four tectonic models have been proposed: (1) subduction counterflow (Draper, 1991; Jordan et al., 2004), (2) gravitational flow along lithospheric topography (Humphreys et al., 2000; Jordan et al., 2004), (3) lithospheric faulting (Rocchi et al., 2003), and (4) extension of Basin and Range (Christiansen et al., 2002). To study the Newberry track, the Oregon Array for Teleseismic Study (OATS) was installed in May 2003 and will operate until the spring of 2006 (Figure 13.30). Data is archived at DMC.

15.2 Shear-wave splits

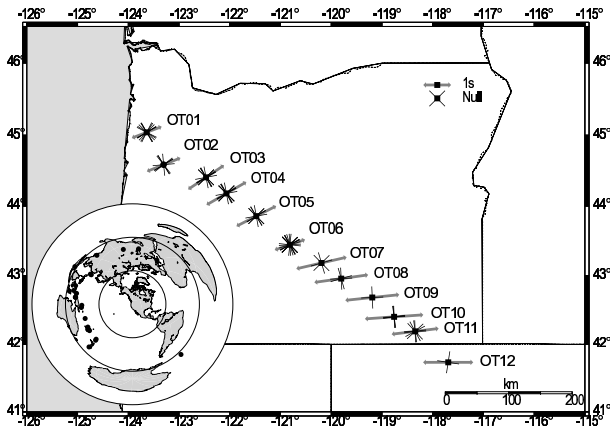


Figure 13.30: Splitting results across Oregon. The thick gray line indicates the result after stacking all useful events at each station. The line orientation gives the fast splitting direction, and its length is linearly proportional to splitting time. The thin black crosses indicate null results. Inset: Distribution of the 27 events used in the SKS splitting study.

To constrain the possible flow fields beneath the Newberry track, preliminary SKS splitting measurements were made for 27 events at 12 OATS stations. A grad-

ual rotation of fast direction is observed from ENE-WSW at the northwest end of the array to E-W to the southeast and the delay times average 1.65 sec (Figure 13.30). The SKS splits imply anisotropy primarily comes from asthenosphere and anisotropy orientation does not vary with depth beneath the track. Since the observed fast directions are not parallel to the Newberry track, and both the subduction counterflow model and the gravitational flow model require flow along the track, the lithospheric models are the most likely causal processes.

15.3 Teleseismic tomography results

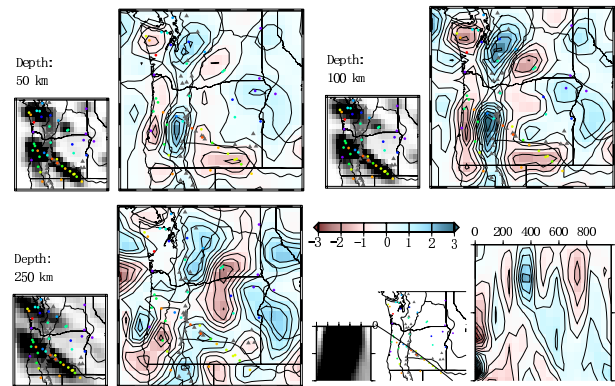


Figure 13.31: Ray density plots and horizontal slices through the Vs model at (a) 50 km depth, (b) 100 km depth and (c) 250 km depth. (d) shows vertical slice through the Vs model along the Newberry track with the ray density plot on the left, the map of cross-section in the middle, and the vertical slice on the right. The model grid spacing is 50 km in all three dimensions.

This study uses a total of 53 broad-band seismic stations, 12 from OATS, and others from nearby permanent networks (BK, CC, US, UO, UW, PN, IU, TA, LI) and temporary deployments (XJ, YC, YS). In this preliminary study, we inspect events with magnitude 6.0 and above from July 19th, 2003 to Nov. 11th, 2004. For the S wave velocity model, a total of 95 events with useable S and SKS phases were recorded at 45 stations, and a total number of 2148 rays were used in the Vs inversion. Our preliminary tomography results show large low velocity residuals all along the Newberry track to a depth ~ 150 km and no further continuation to the deep mantle (Figure 13.31). This suggests there is no migrating melt body in the asthenosphere beneath the region, and supports the conclusion from our SKS splitting analysis that

the Newberry track is more likely a result of lithospheric processes.

15.4 Conclusion

Preliminary results of SKS splitting and teleseismic tomography suggest a lithospheric origin for Newberry. First, there is no asthenospheric anomaly beneath the Newberry, instead low anomaly is beneath all of the HLP. Second, no flow observed in asthenosphere along the track.

15.5 Acknowledgements

This work was supported by the Graduate School of the University of Wisconsin-Madison. We thank Lee Powell, Neal Lord, Andrew Lockman, Robert Pyszalski, Bill Unger for helping installation of stations and collecting data.

15.6 References

Christensen, R.L., and R.S. Yeats, Post-Laramide geology of the U.S. Cordilleran region, in *The Cordilleran orogen: Conterminous U.S.*, edited by M.L. Zoback, pp. 261-406, Geological Society of America, Boulder, Colorado, 1992.

Christiansen, R.L., G.R. Foulger, and J.R. Evans, Upper-mantle origin of the Yellowstone Hotspot, *GSA Bulletin*, 114(10), 1245-1256, 2002.

Draper, D.S., Late Cenozoic Bimodal Magmatism in the Northern Basin and Range Province of Southeastern Oregon, *Journal of Volcanology and Geothermal Research*, 47(3-4), 299-328, 1991.

Humphreys, E.D., K.G. Dueker, D.L. Schutt, and R.B. Smith, Beneath Yellowstone: Evaluating plume and non-plume models using teleseismic images of the upper mantle, *GSA Today*, 10(12), 1-7, 2000.

Jordan, B.T., A.L. Grunder, R.A. Duncan, and A.L. Deino, Geochronology of age-progressive volcanism of the Oregon High Lava Plains: Implications for the plume interpretation of Yellowstone, *Journal of Geophysical Research*, 109 (B10202), doi:10.1029/2003JB002776, 2004.

Lawrence, R.D., Strike-Slip Faulting Terminates Basin and Range Province in Oregon, *Geological Society of America Bulletin*, 87(6), 846-850, 1976.

Macleod, N.S., G.W. Walker, and E.H. McKee, Geothermal significance of eastward increase in age of upper Cenozoic rhyolitic domes, in *Second United Nations Symposium on the Development and use of Geothermal Resources*, pp. 465-474, U.S. Government Printing Office, Washington D.C., 1976.

Pierce, K.L., and W.J. Morgan, The track of the Yellowstone hotspot: Volcanism, faulting, and uplift, in *Regional geology of eastern Idaho and western Wyoming*, edited by P. L.B., pp. 1-53, 1992.

Rocchi, S., F. Storti, V.G. Di, and F. Rossetti, *Intraplate strike-slip tectonics as an alternative to mantle plume activity, in Intraplate strike-slip deformation belts.*, edited by F. Salvini, Geological Society of London. London, United Kingdom, 2003.

16. Fluid-Influenced Faulting in the Long Valley Volcanic Region

Dennise C. Templeton and Douglas Dreger

16.1 Introduction

In volcanic areas, deviations from the usual double-couple (DC) model of shear faulting may be able to illuminate a link between the source process of an earthquake and fluids associated with the geothermal or magmatic system. These non-double-couple (non-DC) earthquakes have mechanisms vastly different from simple shear along a linear fault plane and are characterized by a compensated-linear-vector-dipole (CLVD) component, suggesting either fluid involvement or complex shear failure, and/or an isotropic component which describes volume changes in the source region.

In this study, we investigated the source kinematics of events greater than M3.5 occurring between 1993 - 2003 within a 100 km wide circular area centered at the Long Valley caldera, which includes the Mono-Inyo Craters to the north and the Sierra Nevada Block to the south, to identify events with significant coseismic volume changes. In this active geothermal and magmatic area, we treat coseismic volume changes as an indicator of fluid involvement at the source.

16.2 Data and Methodology

In this study we solved for four different source models: DC, deviatoric (DC+CLVD), DC+isotropic and the full moment tensor model (DC+CLVD+isotropic). The full moment tensor model can characterize source processes involving a combination of tensile and shear faulting (*Julian et al.*, 1998). The deviatoric moment tensor model describes volume conserving source processes which deviate from a simple DC mechanism. DC+isotropic source mechanisms have been used to describe combinations of near-simultaneous faulting near an underground explosion source (*Massé*, 1981). The pure DC model assumes that the earthquake source is best modeled as shear along a linear fault plane and a priori sets the CLVD and volumetric components to zero.

For the DC and DC+isotropic models, a grid search method iterating over strike, dip, rake, DC moment and isotropic moment, which is equal to zero in the pure DC case, was used to find the solution which best fit the observed three-component Berkeley Digital Seismic Network waveforms bandpass filtered between 0.02 and 0.05 Hz. For the deviatoric and full moment tensor models, the second rank symmetric seismic moment tensor is solved by linearly inverting complete three-component filtered broadband seismograms in the time domain using a weighted least squares approach. Green's functions for all four models were computed utilizing a frequency

wave-number integration method and the SoCal velocity model (*Dreger and Helmberger*, 1993) for source depths every 3 km between 2 - 17 km.

When testing more complex source models, the variance reduction usually increased with increasing complexity. F test statistics were performed to determine if the additional CLVD and/or volumetric components represented a true aspect of the source mechanism or if they were simply added non-physical parameters in the inversion.

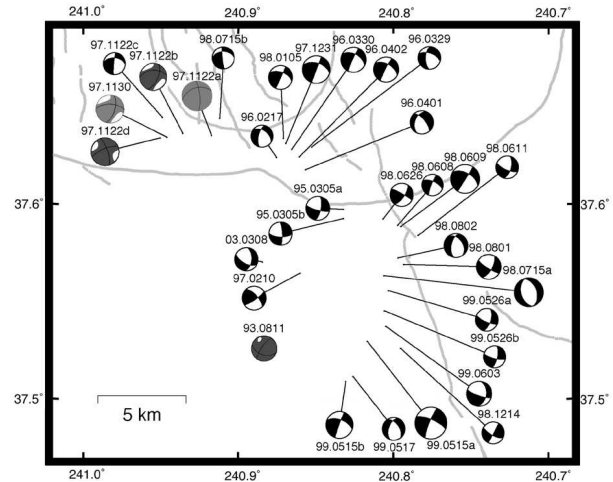


Figure 13.32: DC solutions shown in black. DC+isotropic solutions shown as dark gray. Full moment tensor solutions shown as light gray. Date of event shown as YY.MM.DD.

16.3 Results

Within the chosen space and time constraints, 33 high quality events are identified that have solutions with three or more stations in their inversion. Of these 33 events, 28 are best characterized using a simple DC model, four by a DC+isotropic source model, and one by a full moment tensor model. The isotropic components of the five non-DC events were between 27-48% of the total moment released for each event. All non-DC events are located either in the south moat of the caldera or in the Sierra Nevada block.

The first event with a significant volumetric component occurred on August 11, 1993 in the Sierra Nevada block during the Red Slate Mountain earthquake swarm. Previously, the only non-DC events to occur in this area

were a 1978 M5.8 event and two M6 1980 events (*Julian and Sipkin, 1985*). Event 93.08.11, however, did not occur along the same fault planes as these earlier events. Additionally, it is not known if the earlier non-DC components were due to fluid involvement or complex shear faulting.

The next four events with coseismic volume increases occurred in November 1997 in the south moat of the Long Valley caldera during a period of unrest at the peak of a large earthquake swarm. These south moat events had been previously identified as having significant volumetric components by *Dreger et al. (2000)* however, the current study investigates a wider range of possible source mechanisms. A previous study using a dense temporary seismic network operating during the summer of 1997 showed that most of 26 microearthquakes less than M3.1 were characterized by positive CLVD and isotropic components (*Foulger et al., 2004*). The difference in the total number of isotropic events between our two studies suggests that physical conditions which produce isotropic components are scale dependent, possibly in terms of the ability of individual high pressure reservoirs to sustain pressurization during the faulting process as the crack or fault grows larger.

We were not able to analyze the source process of earthquakes in or near the vicinity of the Mono-Inyo volcanic chain or Mammoth Mountain because events greater than M3.5 were not recorded during the time interval investigated by this study.

Pure DC events sometimes occurred close in space and time to events with significant non-DC components. For example, DC Event 97.11.22c occurred 10 minutes before non-DC Event 97.11.22d and was located just a few kilometers away from all four south moat non-DC events. In some cases, DC events determined by this study were located near previously identified fluid influenced microseismicity structures. For example, Events 97.12.31 and 98.01.05 occurred close in space to a microseismicity trend inferred to be a compensated tensile failure plane (*Foulger et al., 2004*). Thus, it appears that the factors necessary to produce isotropic components only coalesce and trigger non-DC events within a relatively small physical and temporal window in the Long Valley volcanic region.

16.4 Stability of Isotropic Component

We performed Jackknife tests on the four events with significant isotropic components that had four or more stations in their solution (Events 97.11.22a, 97.11.22b, 97.11.22d, and 97.11.30) to determine the likelihood of non-DC events incorrectly being identified as DC events. For all station combinations of three or more, we determined if the volumetric component was significant at or above the 95% significance level by using the F test statistic. All 52 combinations of four or more stations re-

covered the statistically significant isotropic component. For solutions with three stations, six iterations out of 60 failed to recover the isotropic component. It is reasonable to assume that significant isotropic components can be recovered with as few as three, but preferably with at least four, stations in the solution.

We also investigated the possibility of obtaining a spurious isotropic component due to poor data coverage. For this test, we took three high quality DC solutions (Events 97.12.31, 98.06.09, and 98.07.15) and performed Jackknife tests to see if any combination of three or more stations would result in a statistically significant isotropic component. Of 75 three station solutions, one returned a false positive. Of 65 four station solutions, three incorrectly determined that the event had a significant isotropic component. Five and six station solutions did not return false positives. Thus, we feel confident that the isotropic components of our non-DC events with at least five stations in their inversion are not due to poor data coverage. This test, however, casts a small amount of doubt as to the validity of non-DC Event 93.08.11 which has only three stations in its solution.

16.5 Acknowledgements

This research was supported by NSF through contract EAR-0087147.

16.6 References

- Dreger, D. S., H. Tkalic, and M. Johnston, Dilational processes accompanying earthquakes in the Long Valley Caldera, *Science*, 288, 122 - 125, 2000.
- Dreger, D. S., and D. V. Helmberger, Determination of source parameters at regional distances with three-component sparse network data, *J. Geophys. Res.*, 98, 8107 - 8125, 1993
- Foulger, G. R., B. R. Julian, D. P. Hill, A. M. Pitt, P. E. Malin, and E. Shalev, Non-double-couple microearthquakes at Long Valley caldera, California, provide evidence for hydraulic fracturing, *J. Volcanol. Geothermal Res.*, 132, 45 - 71, 2004.
- Julian, B. R., A. D. Miller, and G. R. Foulger, Non-double-couple earthquakes, 2, Theory, *Rev. Geophys.*, 36, 525 - 549, 1998.
- Julian, B. R., and S. A. Sipkin, Earthquake processes in the Long Valley Caldera area, California, *J. Geophys. Res.*, 90, 11,155 - 11,169, 1985.
- Massé, R. P., Review of seismic source models for underground nuclear explosions, *Bull. Seismol. Soc. Am.*, 71, 1249 - 1268, 1985.
- Templeton, D. C., and D. S. Dreger, Non-Double-Couple Earthquakes in the Long Valley Volcanic Region, *Bull. Seismol. Soc. Am.*, in press.

17. Measuring and Modeling Fluid Movements in Volcanoes: Insights from Continuous Broadband Seismic Monitoring at Galeras Volcano, Colombia

Margaret Hellweg, Douglas Dreger and Leigh House (Los Alamos National Laboratory)

17.1 Introduction

In July, 2004, after 11 years of relative quiescence, Galeras Volcano (Colombia) renewed its eruptive activity with a sequence of explosions and ash emissions. Initial evidence of the activity transition appeared in gas measurements from the instruments of the multiparameter station (Seidl et al, 2003, Faber et al, 2003) in early June, followed by a strong increase in the shallow seismic activity below the active cone on June 27 (Gómez et al, 2004). As is the case at many other volcanoes, the most clear evidence for the transition came in the form of seismic swarms, which included both volcano tectonic and long-period events, and tremor. Eruptive activity commenced with two brief episodes of ash emission, on July 16 and July 21. Since then, ash emissions and explosions have been intermittent. An episode lasting from August 11 - 19 began with a large explosion and released more ash than any individual episode from 1989 to 1993. Sudden deformation, as well as changes in the electric and magnetic fields at the crater electromagnetic (EM) station and the gas parameters, such as CO₂ concentration and fumarole temperature, accompanied the ash emissions on July 16 and July 21. While the EM and gas sensors were lost to ashfall by the end of July, monitoring continued via seismometers, tiltmeters and visual inspection.

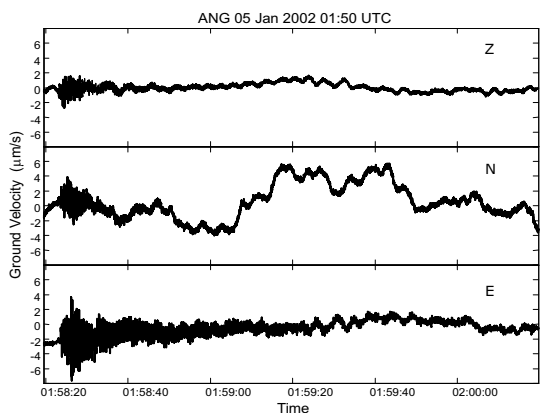


Figure 13.33: Raw velocity seismograms of a tornillo recorded with a broadband seismometer.

17.2 Tornillos and Explosions

We have been analysing tornillos, a particular type of seismic signal from Galeras, to learn about the movement of fluids in the volcanic system. In 1992 and 1993, tornillos occurred at Galeras prior to explosions (Narváez et al, 1997), so they have been considered a precursory signal. They are distinct seismic events with identifiable onsets and relatively long, gradually decaying event tails (codas) and their name comes from the resemblance of their shape on the seismic record to a screw (Figure 13.33). Ninety tornillos recorded at Galeras Volcano, Colombia, from December 1999, to December 2002, were not immediately associated with explosions. Then, no tornillos were observed from December 2002, until well after the beginning of eruptive activity, in September 2004 (Figure 13.34). As a class, the tornillos are complex, each having from one to 15 spectral peaks between 1 and 40 Hz. The peaks for frequencies which extend into the coda are extremely narrow, while those present only during the initial excitation are relatively broad. The frequency of the lowest spectral peak present in any of the tornillos recorded between December 1999, and December 2002, was higher than 1.6 Hz. In contrast, tornillos occurring after the eruption began included frequencies between 1.0 and 1.3 Hz.

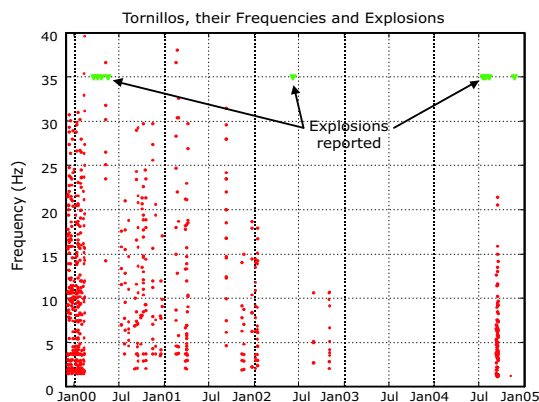


Figure 13.34: Occurrence of tornillos and their frequencies (dots). Triangles mark reported explosions.

Most analysis of tornillos has concentrated on the coda which gives them their name. However, each tornillo waveform is actually made up of three parts (Figure 13.35). In the high quality broadband recordings, the tornillos start with a very small, but clearly recognizable P-onset. This is followed about 0.25 s later by the arrival of wave energy on the horizontal traces, probably S-waves. This arrival becomes a complex wavepacket lasting between two and three seconds which then transitions into the coda. Preliminary comparisons of these wavepackets for many different tornillos suggest two things: that they can be classified into families, and that these families are only indirectly related to the exact frequency or family of frequencies present in the long-lasting coda into which they segue.

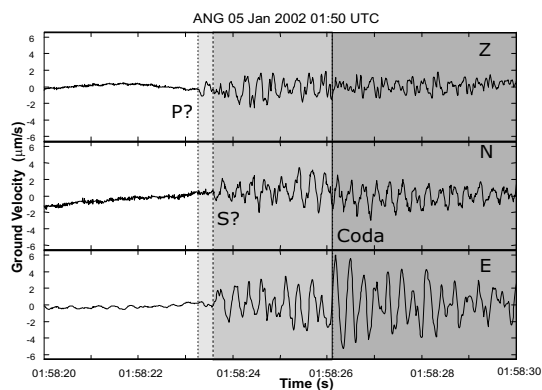


Figure 13.35: Displacement seismograms of the beginning of a tornillo. The first onset has polarization consistent with a P-wave, while the second onset is likely to be an S-wave. It is followed by a 2-3 s transition before the characteristic coda develops.

We are currently investigating and quantifying the characteristics of both the onsets and the intermediate wavepackets more thoroughly, as they bear important information about the mechanism which triggers a tornillo.

For the spectral peaks below 5 Hz, the polarization both remains constant during an individual tornillo, and varies little from one tornillo to the next. This suggests that tornillos are all generated within a limited volume of the volcanic edifice. The variation in the polarization at higher frequencies should allow us to constrain the size of this volume (Hellweg, 2003)..

17.3 Perspectives

Details in the tornillo onset and the intermediate wavepacket, and their relationships to the characteristics of the tornillo coda, are important factors which will enable us to derive a more thorough picture of what physical process in the volcano actually produces the tornillos. In particular, the tornillos associated with the recent activity give interesting clues: why are their frequencies lower and what governs the timing of their occurrence in the eruption sequence?

17.4 Acknowledgements

This project is funded by U.C. Berkeley - Los Alamos National Laboratory collaborative Institute for Geophysics and Planetary Physics Project number 04-1407. Tornillo data have been acquired as part of a cooperative project between the Bundesanstalt für Geowissenschaften und Rohstoffe (Germany) and the Instituto de Investigación e Información Geocientífica Minero-Ambiental y Nuclear (Colombia) on Multiparameter Monitoring of Volcanoes.

17.5 References

Faber, E., C. Morán, J. Poggenburg, G. Garzón, and M. Teschner, Continuous gas monitoring at Galeras Volcano, Colombia: First evidence, *J. Volc. Geotherm. Res.*, 25, 13-23, 2003.

Gómez, D., M. Hellweg, B. Buttkus, F. Böker, M.L. Calvache, G. Cortés, E. Faber, F. Gil Cruz, S. Greinwald, C. Laverde, L. Narváez, A. Ortega, H. Rademacher, G. Sandmann, D. Seidl, B. Silva and R. Torres, A volcano reawakens: Multiparameter observations of activity transition at Galeras Volcano (Colombia), *EOS Trans. AGU*, 85(47), *Fall Meet. Supp.*, Abstract V11B-1423, 2004.

Hellweg, M., The Polarization of Volcanic Seismic Signals: Medium or Source?, *J. Volc. Geotherm. Res.*, 128, 159-176, 2003.

Narváez, M.L., R.A. Torres, D.M. Gómez, G.P.J. Cortés, H.V. Cepeda, and J. Stix, Tornillo-type seismic signals at Galeras volcano, Colombia, 1992-1993. *J. Volcanol. Geotherm. Res.*, 77, 159-171, 1997.

Seidl, D., M. Hellweg, M. Calvache, D. Gómez, A. Ortega, R. Torres, F. Böker, B. Buttkus, E. Faber and S. Greinwald, The multiparameter-station at Galeras Volcano (Colombia): Concept and realization, *J. Volc. Geotherm. Res.*, 125, 1-12, 2003

Seidl, D. and M. Hellweg, Parametrization of multi-chromatic tornillo signals observed at Galeras Volcano (Colombia), *J. Volc. Geotherm. Res.*, 125, 171-189, 2003

18. Independent Okhotsk and Amurian Microplate Tectonics of Northeast Asia

Edwin (Trey) Apel, Roland Bürgmann, Misha Kogan (Columbia), and Robert King (MIT)

18.1 Introduction

The possible existence of independently rotating Okhotsk and Amurian microplates has been examined by many in an attempt to explain both seismological and geologic data in Northeast Asia (Cook *et al.*, 1986; Seno *et al.*, 1996). Geodetic measurements can be used to fully characterize the motion of tectonic plates; however, because most GPS sites in this region are in such close proximity to plate boundaries, previous attempts to firmly confirm or refute an independent Okhotsk plate have been inconclusive (Heki *et al.*, 1999; Steblou *et al.*, 2003). Independent Amurian plate motion is notably more difficult to constrain because of the uncertainty of the southwestern plate boundary and the sparsely spaced geodetic data.

Horizontal surface velocities of 122 GPS sites (82 from within the proposed Okhotsk and Amurian plate boundaries) constrain the plate kinematics of northeast Asia and allow for a rigorous test of the possibility of independent Okhotsk and Amurian plate motion. We use a block modeling approach to incorporate both rigid block rotation and near-boundary elastic strain accumulation effects in a formal inversion of the GPS velocities. Considered models include scenarios with and without independent microplates and a number of different plate boundary locations and locking depths.

18.2 GPS Velocities

The GPS velocities used in our inversion are from an updated velocity field of 151 global stations by (Steblov *et al.* 2003). We include data from additional campaign stations from central Sakhalin (Kogan *et al.*, 2003) and the Kamchatka peninsula (Bürgmann *et al.*, 2005), and from sites in northern Japan that are part of the continuous Japanese GSI network in our complete solution. These data were processed using GAMIT/GLOBK by Bob King at MIT and Misha Kogan at Columbia. Processing details can be found in (Steblov *et al.*, 2003).

In addition to our own analysis we integrate GPS-station velocities from published work in the region that help with defining the deformation patterns for the Baikal and central Amurian regions (Calais *et al.*, 2003). We also include selected stations from Zhang *et al.* (2004) that fell within or near the boundaries of the proposed Amurian microplate. These velocities were combined with our solutions by rotating them into a common reference frame. The sites selected for our inversion are shown in Figure 13.36 and Figure 13.37.

18.3 Blocks

We define our plates as rigid blocks on a spherical earth bounded by dislocations in an elastic halfspace and invert for poles and rates of rotation that minimize the misfit to the GPS velocities using an extension of the block modeling code by Meade and Hager (2005). The segments that bound the blocks represent uniformly slipping elastic dislocations locked to some specified depth. Because our inversion combines rigid block rotation with elastic strain accumulation effects, the parameterization of the block boundary geometry is critical. Geometry of the block boundaries is based heavily on seismicity and adopted from prior analyses (Bürgmann *et al.*, 2005) or adjusted as indicated by the geodetic data (Kogan *et al.*, 2003).

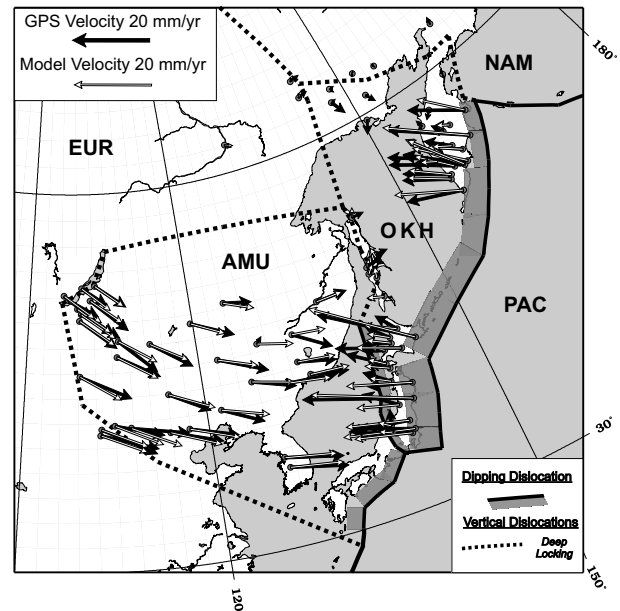


Figure 13.36: GPS velocities, in black, are shown in a fixed North American reference frame. Predicted model velocities from our 5-plate model are shown in white and show good fit to the data.

We invert the horizontal GPS velocities for poles of rotation constrained by the prescribed block geometry defined above. Systematic patterns in the residual velocities (observed minus predicted) are used as an indicator of where and how the model matches the observed surface velocities. Misfit statistics are used to formally evaluate

the statistical significance of the plate kinematic scenarios we test.

18.4 Results

Independent Okhotsk plate motion is tested using three main block configurations. In our 3-plate system we assume that the Okhotsk region is part of the North American plate and Amuria belongs to Eurasia. Our 4-plate model allows the Okhotsk block to rotate independently while the 5-plate model also includes an independently rotating Amurian block. Our inversions favor a scenario with independent Okhotsk plate motion but does not formally require it. The F-test statistic indicates that the improved fit is significant at 92% confidence. Independent Amurian plate motion is significant only at 69% confidence. The best fitting poles of rotation for our 5-plate model are shown in Figure 13.37.

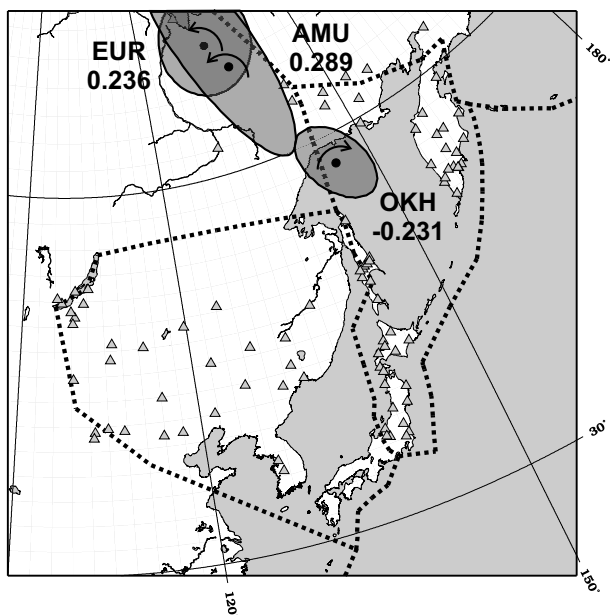


Figure 13.37: Poles of rotation for the Amurian, Okhotsk, and Eurasian plates. Error ellipses represent 95% confidence bounds. Triangles represent the locations of the GPS sites used in this study.

18.5 Discussion

The plate-motion parameters of independently rotating Okhotsk and Amurian plates are consistent with the style of active deformation inferred from focal mechanism solutions. For example, our inversions predict right-lateral motion in northern Sakhalin, oblique contraction in southern Sakhalin, and little to no active deformation in the sub-marine crust north of Sakhalin. Predicted opening in the Baikal region is also consistent with historical seismicity and active structures.

Subtle changes in block and segment geometry (e.g. dip) within or near subduction zones can cause significant changes in the estimated pole of rotation of the Okhotsk plate. This is due, in large part, to the close proximity of most GPS stations in northeast Asia to these plate boundaries, such as the Kamchatka-Kurile subduction zone. GPS velocities on the Kamchatka peninsula and in Japan capture a complex pattern associated with the heterogeneously locked subduction zone that may require more complex models. Additional blocks may also affect the determination of an independently rotating Okhotsk plate. Future work will examine the potential role of adjacent blocks such as the Philippine, Bering, northern Honshu, and Magadan blocks.

18.6 References

- Bürgmann, R., M. Kogan, G. Steblov, G. Hiley, V. Levin, and E. Apel, Interseismic coupling and asperity distribution along the Kamchatka subduction zone, *Journal of Geophysical Research*, 110, doi:10.1029/2005JB003648, 2005.
- Calais, E., M. Vergnolle, V. Sankov, A. Lukhnev, A. Miroshnitchenko, S. Amarjargal, and J. Deverchere, GPS measurements of crustal deformation in the Baikal-Mongolia area (1994-2002): Implications for current kinematics of Asia, *Journal of Geophysical Research*, 108(B10), 2003.
- Cook, D. B., K. Fujita, and C. A. McMullen (1986), Present-day plate interactions in northeast Asia - North-American, Eurasian, and Okhotsk plates, *Journal of Geodynamics*, 6(1-4), p. 33, 1986.
- Heki, K., S. Miyazaki, H. Takahashi, M. Kasahara, F. Kimata, S. Miura, N. F. Vasilenko, A. Ivashchenko, and K. D. An, The Amurian Plate motion and current plate kinematics in Eastern Asia, *Journal of Geophysical Research*, 104(B12), p. 29147, 1999.
- Meade, B. J., and B. H. Hager, Block models of crustal motion in southern California constrained by GPS measurements, *Journal of Geophysical Research*, 110, B03403, doi:10.1029/2004JB003209, 2005.
- Seno, T., T. Sakurai, and S. Stein, Can the Okhotsk plate be discriminated from the North American plate?, *Journal of Geophysical Research*, 101(B5), p. 11305, 1996.
- Steblov, G. M., M. G. Kogan, R. W. King, C. H. Scholz, R. Bürgmann, and D. I. Frolov, Imprint of the North American Plate in Siberia revealed by GPS, *Geophysical Research Letters*, 30(18), 2003.
- Zhang, P. Z., Z. Shen, M. Wang, W. J. Gan, R. Bürgmann, and P. Molnar, Continuous deformation of the Tibetan plateau from global positioning system data, *Geology*, 32(9), p. 809, 2004.

19. Crustal Deformation Along the Northern San Andreas Fault System

Mark H. Murray

19.1 Introduction

The San Andreas fault system in northern California includes three sub-parallel right-lateral faults: the San Andreas, Ma'acama, and Bartlett Springs. This northernmost segment is the youngest portion of the fault system, forming in the wake of the northwestwardly propagating Mendocino triple junction where the Pacific, North America, and Gorda (southern Juan de Fuca) plates meet. The Pacific plate moves about 35-40 mm/yr relative to central California across a broad ~100-km zone in northern California. Additional deformation in eastern California and the Basin and Range province contribute to the total relative Pacific-North America motion of ~50 mm/yr. The San Andreas fault itself has been essentially aseismic and accumulating strain since it last ruptured in the great 1906 San Francisco earthquake, and no major earthquakes have occurred during the historical record on the more seismically active Ma'acama, and Bartlett Springs faults, which are northern extensions of the Hayward-Rodgers Creek and Calaveras-Concord-Green Valley faults in the San Francisco Bay area. Our earlier geodetic studies showed that the inferred slip rate on the Ma'acama fault ($13.9_{-2.8}^{+4.1}$ mm/yr) implied an accumulated slip deficit large enough to generate a magnitude 7 earthquake, posing a significant seismic hazard (Frey Mueller *et al.*, 1999).

Since 2003, we have been resurveying sites measured in our previous studies plus about 40 additional sites, originally surveyed by Caltrans and NGS (Murray, 2004). The additional sites are located along the San Andreas fault system just north the San Francisco Bay and will improve monitoring along the Rodgers Creek and Green Valley faults. Most of the monuments were last observed in 1993–1995, so the new observations significantly improve the velocity estimates and models of average interseismic strain accumulation, including possible spatial variations along the fault system. Additional sites in the region between the southern and northern portions of the network are planned for resurveying in the future. The entire network spans the region from Pt. Reyes to Cape Mendocino. Together with planned PBO stations, it forms a primary monitoring network for future observations to detect temporal variations in deformation.

19.2 Deformation

Figure 13.38 shows site velocities estimated using the GAMIT/GLOBK software package for the 1994-2004 period relative to stable North America, as defined by a set of 20 fiducial stations. We are currently processing the

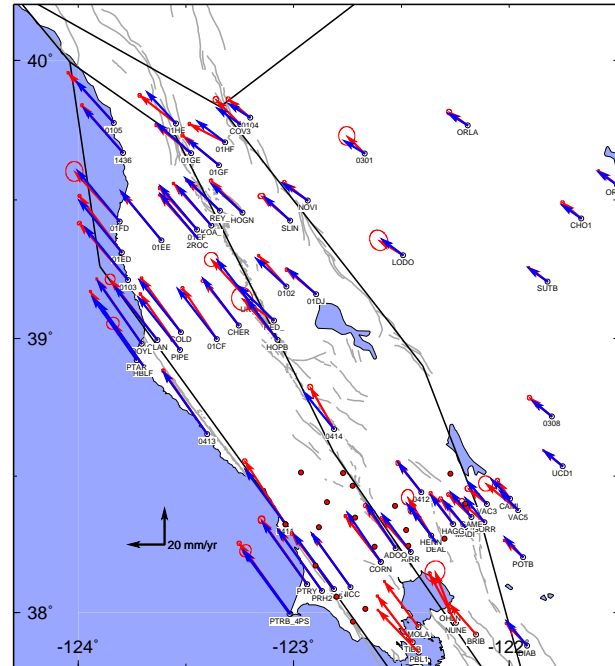


Figure 13.38: Velocities of sites in the Coast Ranges relative to North America, with 95% confidence regions assuming white-noise process only. Included are sites from this study plus sites from the BARD continuous network and the USGS North Bay profile. Arrows with ellipses, observed velocities. Arrows without ellipses, velocities predicted from angular velocity-backslip block model assuming block boundaries (heavy black lines). We assume Pacific, North America, and Sierran-Great Valley blocks, plus 2 small blocks between the San Andreas, Ma'acama, and Bartlett Springs faults. The most significant misfits, such as near Cape Mendocino, can be reduced by refining the fault geometry. Additional sites in the southern portion of the network (circles), have been recently re-measured.

data from the most recent surveys that will provide new estimates of velocities for sites between the southern and northern profiles shown. Most of the velocities are derived from data spanning 8-10 years, whereas those with the largest error ellipses include data from only a 4 year span. The easternmost stations exhibit motions typically associated with Sierran-Great Valley block (ORLA: 12.5 mm/yr NW). The westernmost sites are moving close to the Pacific plate rate (PTAR: 45.9 mm/yr NW). Fault-normal contraction is observed east of the Ma'acama

fault, in the region of the Coast Ranges near the Central Valley where similar contraction has been observed elsewhere (e.g., Murray and Segall, 2001).

Also shown in Figure 13.38 are velocities predicted by angular velocity-fault backslip modeling techniques (e.g., Murray and Segall, 2001) to account for both far-field plate motions and interseismic strain accumulation. We are developing a 3D fault model and applying the same modeling approach that we used in our BAVU study of the San Francisco Bay area (d'Allesio et al., 2005). Preliminary results show that the agreement between observed and predicted velocities is typically less than the 2 mm/yr level. Misfits are larger in a few areas close to faults, such as along the central Ma'acama and near the MTJ, that should be decreased with further refinement of the fault geometry. Total deformation across the San Andreas fault system is 38 mm/yr, in agreement with previous studies, but deep slip is concentrated on the Ma'acama fault (24 mm/yr) and on the Bartlett Springs fault (10 mm/yr), with only 4 mm/yr on the San Andreas. We are currently investigating this result, which is due in part to the high-degree of correlation between the slip rates on the 3 faults, and will test methods for adding geologic and other information using Bayesian techniques, which should reduce the correlations on slip rates and provide better resolution on other parameters such as locking depths.

We are also working with D. Agnew (UCSD), R. King (MIT), and Z-K. Shen (UCLA) to combine these results with the BAVU, SCEC Crustal Motion Model (CMM 3.0), and other studies to provide an integrated California-wide velocity field. The preliminary velocity field is shown in Figure 20. and includes over 2000 stations. Additional stations will be included from the Cape Mendocino triple junction region. Results from this study will be used to develop a state-wide deformation and fault slip model that will be incorporated into a hazard assessment project by the Working Group on California Earthquake Probabilities under the auspices of the USGS. Preliminary results of the WGCEP project are expected in mid-2006.

19.3 Acknowledgements

We appreciate support for this project by the USGS NEHRP through grant numbers 02HQGR0064, 03HQGR0074, and 04HQGR0103. We thank André Basset, Maurizio Battaglia, Dennise Templeton, and especially Todd Williams for assistance conducting the survey.

19.4 References

d'Alessio, M. A., I. A. Johanson, R. Bürgmann, D. A. Schmidt, and M. H. Murray, Slicing up the San Francisco Bay Area: Block kinematics from GPS-derived

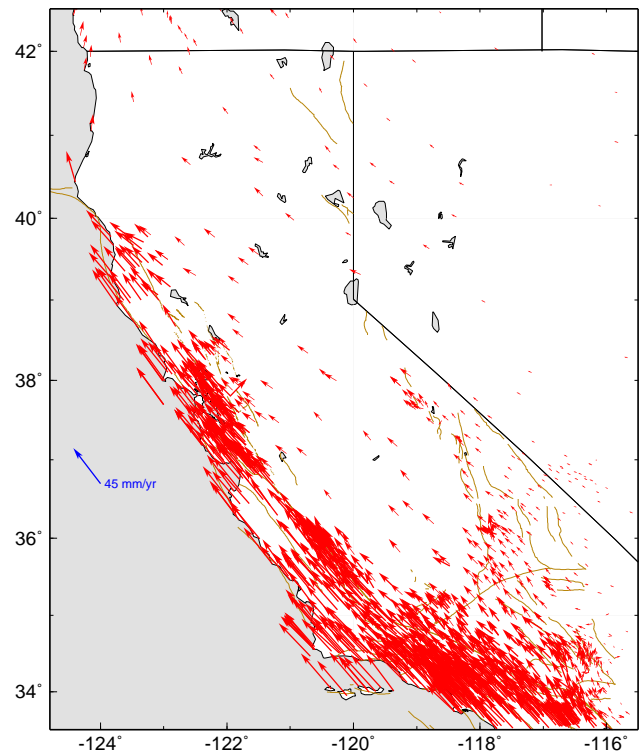


Figure 13.39: Velocities of sites in California relative to stable North America from a combination of velocities from this study, BAVU, the SCEC Crustal Motion Map, and other studies.

surface velocities, *J. Geophys. Res.*, 110, B06403, doi:10.1029/2004JB003496, 2005.

Frey Mueller, J. T., M. H. Murray, P. Segall, and D. Castillo, Kinematics of the Pacific-North America plate boundary zone, northern California, *J. Geophys. Res.*, 104, 7419–7442, 1999.

Murray, M. H., Crustal Deformation Along the Northern San Andreas Fault System From Geodetic and Geologic Data, EOS Trans. AGU, 85(47), Fall Meeting Suppl., Abstract G14A-04, 2004.

Murray, M. H., and P. Segall, Modeling broadscale deformation in northern California and Nevada from plate motions and elastic strain accumulation, *Geophys. Res. Lett.*, 28, 4315–4318, 2001.

20. Strong Ground Motions Derived from Geodetic Slip Models

Junkee Rhie, Douglas S. Dreger, Mark H. Murray

20.1 Introduction

Accurate estimation of near-fault strong ground motion from our basic understanding of faulting mechanisms and seismic wave propagation is an important goal in the field of earthquake engineering. In areas where there are no near-fault recordings of strong ground motions, such estimations can be crucial in producing a strong ground motion ShakeMap for emergency response purposes [e.g., Dreger and Kaverina, 2000; Dreger et al., 2005].

The main goal of this study is to develop a deterministic method to simulate temporal variations of slip from geodetic static displacements, and apply this method to derive reliable near-fault strong ground motion for earthquakes. Geodetic observations offer several advantages. Geodetic inversions can independently determine the orientation and fault finiteness quickly, whereas seismic inversions must first determine a moment tensor, and then test both possible nodal planes. Because geodetic slip-model inversions take less computer time than seismic inversions, this method can more quickly predict strong motion when real-time GPS observations are available. For emergency response, even a small improvement in time can be significant. Geodetic data sets also provide redundancy should seismic data sets be sparse or inaccessible in real-time, or difficulties arise in the multistage processing of the seismic data [e.g., Dreger and Kaverina, 2000].

20.2 Spatio-temporal slip model

Our method is based on the intuitive assumption that larger slip takes longer time to accumulate. This assumption follows from the well-known linear scaling relation between stress drop and slip velocity, which given that stress drop is basically independent of scalar seismic moment, implies that slip velocity is also essentially constant over the range of seismic moment and may be estimated by assuming regionally appropriate values of rigidity and shear wave velocity.

In practice, a spatially variable slip model is defined by a grid of point sources on a fault plane with rupture duration given by multiple time windows. We use empirical relations to define the average and minimum rise time and assume the scalar seismic moment M_0 from seismic or geodetic estimates. The regions with smallest slip take the minimum rise time to finish slipping, while the regions with larger slip require multiple time window based on the ratio of the spatially variable slip to the constant slip velocity. For a given level of slip, a larger assumed stress drop implies that more slip occurs in each

of the time windows resulting in a shorter overall duration (Figure 13.40). A circular rupture front initiates at the hypocenter given by seismic estimates and propagates with constant assumed rupture velocity. Slip is triggered when the rupture front reaches each point source and has a duration determined by the number of time windows appropriate for the level of slip at that point.

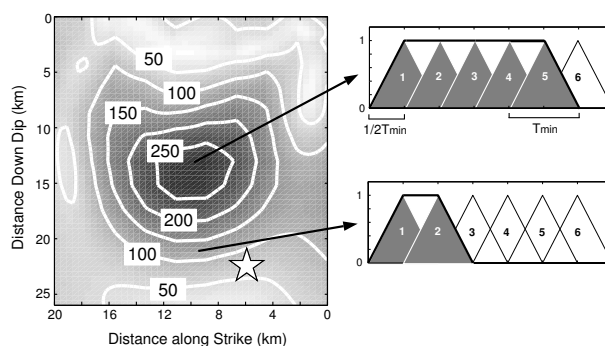


Figure 13.40: A schematic diagram showing how to determine the number of time windows for a variable-slip model. Left column shows the variable slip model on its rupture plane. White star indicates hypocenter of Northridge event. Two small panels on the right indicate necessary time windows (solid gray triangles) and final rise time curve (thick black) associated with slip patches indicated on slip distribution model.

20.3 The Northridge earthquake

We demonstrate the method by simulating strong ground motions from several slip models for the 17 January 1994 Mw 6.7 Northridge earthquake. A model derived from near-source strong ground motions, P and SH teleseismic body waves, and GPS and spirit leveling geodetic data provides reference time histories and peak ground motions for comparison with the motions obtained from the source models inferred from uniform and variable-slip models derived from geodetic data only.

To assess the methodology, we compare the observed and modeled velocity waveforms at near-source stations surrounding the event. To account for site effects, we applied site amplification factors to the waveforms based on the upper 30 m shear wave velocity. Amplification factors are calculated by considering differences in impedances for the rock and soil layers (upper 30 m) for a normal incidence seismic wave.

For most stations and components, predicted strong ground velocities for the reference and variable-slip models are similar to the observed velocities, whereas the uniform-slip model tended to underpredict the velocities. Simulated peak ground velocity (PGV) ShakeMaps for the three models showed similar behavior with the PGV values derived from the uniform-slip model significantly less than the other two models, possibly because the model is too smooth and spread in time. The simulated PGV for reference and variable-slip models showed the roughly the same extent of the 10-20 cm/s contours, the level at which structural damage can occur (Figure 13.41).

Since our objective is to develop a method that is practical in a rapid (on the order of 30 minutes) post-earthquake time frame, we made several simplifying assumptions such as constant slip and rupture velocity. As more information becomes available following an earthquake it may be possible to invert for models to resolve these parameters, but such analysis is not applicable in an automated fashion. Nevertheless, to first order, assuming rupture velocity is constant performs well in describing the overall directivity effect and in simulating peak ground velocity for ShakeMap purposes. Although studies of many events show that the slip velocity is not spatially constant, the assumption is generally applicable given that many spatio-temporal slip models have longer duration for larger slip.

Future work will test this methodology for other large, well-studied events, such as 2003 San Simeon, 1992 Landers, and 2004 Parkfield, to optimize the rules for time variation of slip. Combining the optimized rules and near real-time measurement and inversion of GPS displacement vectors can reduce the estimation time of the extent of near-fault strong ground shaking, and thus could facilitate better emergency response activities.

20.4 Acknowledgements

We appreciate support for this project by the USGS NEHRP through grant numbers 04HQGR0043 and 04HQGR0044.

20.5 References

- Dreger D., and A. Kaverina, Seismic remote sensing for the earthquake source process and near-source strong shaking: A case study of the October 16, 1999 Hector Mine earthquake, *Geophys. Res. Lett.*, 27, 1941-1944, 2000.
- Dreger, D. S., L. Gee, P. Lombard, M. H. Murray, and B. Romanowicz, Rapid finite-source analysis and near-fault strong ground motions - Application to the 2003 Mw 6.5 San Simeon and 2004 Mw 6.0 Parkfield earthquakes, *Seism. Res. Lett.*, 76, 40-48, 2005.

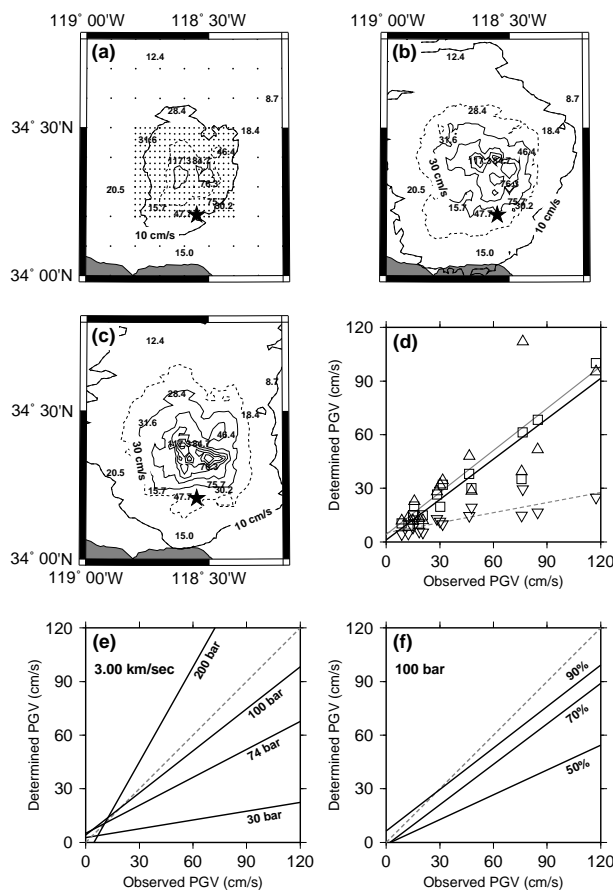


Figure 13.41: (a) PGV ShakeMaps simulated for the Northridge earthquake for model UNI. Black contours of PGV represent the geometric mean of two horizontal PGV components. The minimum level of contour is 10 cm/s and the interval is 20 cm/s. The dotted line is the 20 cm/s contour, indicating the extent of significant structural damage. The black star indicates main-shock epicenter. The black dots are the grid locations where strong motions are derived for ShakeMap. Black bold numbers on the map indicate 15 observed PGV. (b) Same as (a) for model REF. (c) Same as (a) for model VAR. (d) The simulated PGV values at 15 stations as a function of real observations for models VAR (triangles), REF (squares), and UNI (inverted triangles) and the best fitting lines for models VAR (thin grey), REF (thick black), and UNI (dotted grey). (e) The best fitting lines assuming different stress drops for constant rupture velocity of 3.00 km/s. For the reference, the perfect agreement line is indicated with the dotted gray line. (f) The best fitting lines assuming different rupture velocities for constant stress drop of 100 bars.

21. Joint Inversion for 3D Velocity Structure of the Middle East and North Africa to Improve Nuclear Explosion Monitoring

Suzan van der Lee (Northwestern University), Arthur Rodgers (LLNL), Megan Flanagan (LLNL), Michael Pasyanos (LLNL), Federica Marone and Barbara Romanowicz

21.1 Introduction

The need to monitor broader areas and an increasing number of nations with nascent nuclear weapons programs has lead to major challenges to nuclear explosion monitoring research. Agencies must, in fact, be prepared to detect, identify and locate nuclear explosions in wide regions, often aseismic and lacking previous seismic observations from specific test sites. Since the 1980's, the importance of monitoring at regional distances has been well established. However, such monitoring is complicated by the passage of seismic waves through the structurally complex crust and uppermost mantle. As a consequence, traveltimes and amplitudes of regional phases show great variability leading to large uncertainties in event locations and decreased performance of regional discriminants. A major requirement for the accurate modeling of regional seismic data and therefore improved event locations and regional discriminant performance are 3D regional velocity models characterized by high resolution from the crust down to the transition zone.

Our aim is a 3D velocity model of the crust and upper mantle for the geographic region extending from the western Mediterranean to Pakistan, including the aseismic region of North Africa. The joint inversion of different types of seismic data with diverse sensitivity to the crust and mantle is essential to achieve a high resolution image of the structure in this tectonically complex area, where six major tectonic plates and several microplates interact with each other. We expect predictions for seismogram characteristics (phase arrival times, amplitudes, dispersion) based on this new model to match most observations and be useful for event discrimination. Simultaneously, the new model will refine our understanding of the structure and tectonics in the study region.

21.2 Technical approach and dataset

Our 3D S -velocity model will be derived from the joint inversion of regional waveform fits, surface wave group velocity measurements, teleseismic arrival times of S and P waves, receiver functions and published results from active source experiments. The strength of jointly using various datasets lies in their redundancy (increase in the results accuracy) and complementarity (resolving power increase and trade-offs reduction).

The fitting of regional fundamental and higher mode Rayleigh waveforms is being accomplished using the Partitioned Waveform Inversion method (Nolet, 1990). Ex-

amples of recently obtained waveform fits are shown in Figure 13.42. The modeling of both fundamental and higher mode surface waveforms ensures resolution of the entire upper mantle structure down to the transition zone. The inclusion in the inversion of teleseismic arrival times will further boost the resolving power at mid and deep upper mantle levels, while group velocity measurements and constraints on crustal thickness from active-source literature and receiver function analysis will ensure high resolution in the shallow upper mantle.

The seismograms used in this work have been recently recorded by a variety of different stations and networks, both permanent and temporary, operating in the study region: MIDSEA deployment, Kuwait National Seismic Network (KNSN), the United Arab Emirates (UAE) Broadband deployment, the Jordan deployment, the Eastern Turkey Seismic Experiment (ETSE), the Caspian Broadband deployment, the Global Seismic Network (GSN), the International Monitoring System (IMS), MedNet and Geofon. While each of these waveform datasets is valuable on its own, their combination is unique and key to this study.

21.3 Preliminary results

The broad consistency between seismic velocity anomalies inferred from existing and performed measurements of teleseismic arrival times and Rayleigh wave group velocities as well as from regional waveform fits implies that these different types of dataset are at least in part redundant. The consistency further shows that the datasets record the same structural phenomena, despite differences in size and character between typical sensitivity kernels for each dataset.

Preliminary results from data analysis for the Middle East show that the uppermost mantle in this part of the study area is slower on average than typical 1D global velocity models as also previously observed in neighboring regions (e.g. in the Mediterranean (Marone *et al.*, 2004) and beneath the Iranian Plateau (Maggi and Priestley, 2005)).

21.4 Future of the project

The derived 3D S -velocity model will be converted to a 3D P -velocity model, using both published data on elastic properties (and their partial derivatives with temperature and pressure) of mantle rocks and empirical information provided by measured arrival times of teleseismic

P and Pms waves. The corresponding P -wave model will provide an improved ability to locate seismic events.

The prediction and calibration of regional traveltimes and waveforms depend strongly on the methodology used to compute synthetic traveltimes and waveforms from a 3D velocity model. Our goal is to test the obtained S - and P -wave models' ability to predict regional P and S traveltimes, deflect wave paths and deform waveforms using different approximations (e.g. path average vs. exact numerical approaches). We will assess the effects of 3D heterogeneities first on the studied seismograms (traveltimes and waveforms) and subsequently on the 3D models derived from these data.

21.5 Acknowledgements

This work has been financially supported by the National Nuclear Security Administration, Office of Nonproliferation Research and Engineering and Office of Defense Nuclear Nonproliferation (DE-FC52-04NA25542).

21.6 References

Maggi, A. and K. Priestly, Surface waveform tomography of the Turkish-Iranian Plateau, *Geophys. J. Int.*, *160*, 1068-1080, 2005.

Marone, F., S. van der Lee and D. Giardini, 3-D upper mantle S -velocity model for the Eurasia-Africa plate boundary region, *Geophys. J. Int.*, *158*, 109-130, 2004.

Nolet, G., Partitioned waveform inversion and two-dimensional structure under the network of autonomously recording seismographs, *J. Geophys. Res.*, *95*, 8499-8512, 1997.

Pasyanos, M.E., W.R. Walter and S.E. Hazler, A surface wave dispersion study of the Middle East and North Africa for monitoring the Comprehensive Nuclear Test Ban Treaty, *Pure Appl. Geophys.*, *158*, 1445-1474, 2001.

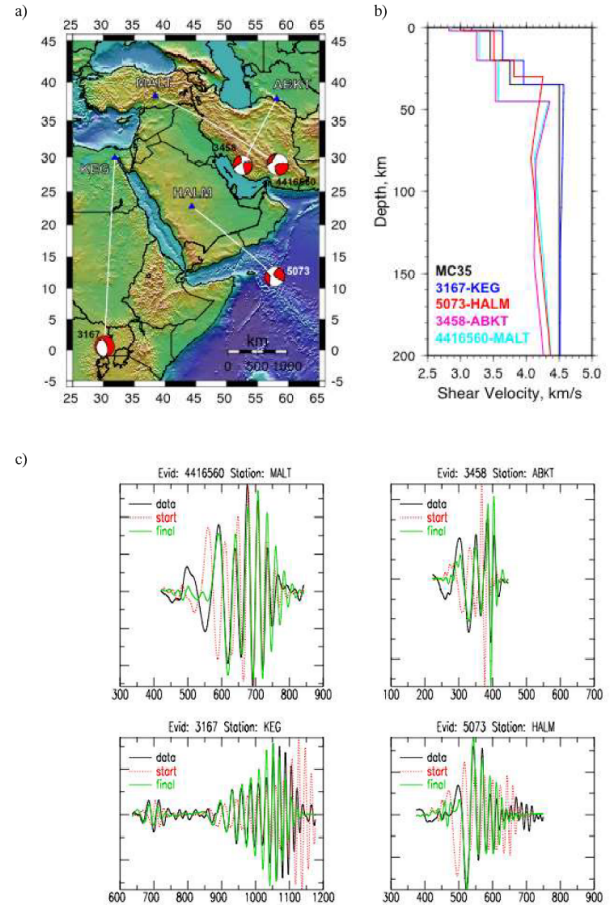


Figure 13.42: a) Map of the Middle East showing four earthquakes and paths for which waveform fits are shown. The events are indicated by their moment tensors. Stations are shown as blue triangles - b) 1D S -velocity models for the four paths shown in a). The used starting model, MC35, is shown in black - c) Fits for vertical component S - and Rayleigh waveforms for the four paths shown in a). In each panel, we show the observed waveform (black), the synthetic waveform computed using the starting (red dashed) and with the final model (green).

22. Constraints on Shear Wave Attenuation in the Earth’s Inner Core from an observation of PKJKP

Aimin Cao and Barbara Romanowicz

22.1 Introduction

Soon after *Lehmann* discovered the earth’s inner core in 1936 through the analysis of travel times of teleseismic body waves, *Birch* (1940) suggested that the inner core should be solid as a result of freezing of liquid iron in the outer core. Thirty years later, the first indirect evidence of the solidity of the inner core was documented by means of seismic normal mode eigenfrequency measurements (*Dziewonski and Gilbert*, 1971). However, the observation of the phase PKJKP, which traverses the inner core as a shear wave, is still a controversial issue, until now attempted by only few investigators. *Julian et al.* (1972) and *Okal and Cansi* (1998) each suggested the detection of PKJKP based on data from short-period seismic arrays in the ~ 1.0 Hz and 0.1-0.5 Hz frequency ranges, respectively. *Deuss et al.* (2000) argued that these two claims were misidentifications, and instead, proposed an observation of pPKJKP+SKJKP, based on stacking data from the global broadband network, in the frequency range 0.01-0.1 Hz. On the other hand, the existing Q_β estimates in the inner core are based solely on normal mode observations (*Dziewonski and Anderson*, 1981; *Widmer et al.*, 1991). There has been no attempt at estimating the shear wave attenuation in the inner core using body wave data.

PKIKP, which traverses the inner core as a compressional wave, is now a routinely observed phase. It should be observed simultaneously with PKJKP in the epicentral distance range 116° to 180° , according to the seismic reference model PREM. The relative amplitude of PKJKP varies strongly with frequency. Although we cannot rule out the possibility of observing PKJKP in the frequency range 0.1 to 0.5 Hz, it is more likely to be found at lower frequencies.

22.2 Data, Method, and Results

We use the high quality data from the broadband Gräfenberg Seismic Array (GRF) in Germany. With an aperture of $\sim 100\text{km} \times 50\text{km}$, GRF provides continuous high quality records at all of its 13 stations since 1980. Its geographical location with respect to frequent large events ($M_w > 7.0$), which occur in the south Pacific Ocean at distances around 140° , make it an ideal broadband seismic array to study PKJKP. We systematically examined large events from 1980 to 1999 and found ~ 20 large events in the vicinity of Tonga and Santa Cruz islands in this time interval. One of them ($M_w=7.3$, depth=76 km, 02/06/1999) is unique for PKJKP obser-

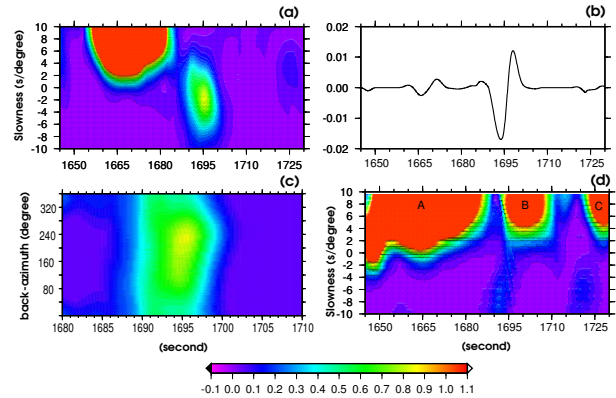


Figure 13.43: Evidence for the observation of PKJKP. (a) Observed vespagram for PKJKP in the slowness and travel time domain. (b) Stacked waveform corresponding to the energy maximum in (a). (c) Observed vespagram in the back-azimuth and travel time domain. The estimated back-azimuth is $\sim 223^\circ$ and the expected back-azimuth of PKJKP is 218° . (d) Synthetic vespagram for the pseudo-liquid inner core model.

vation. We choose the 0.06 to 0.1 Hz band for our analysis.

After aligning the seismograms with respect to the origin time of the event and making an array-sided travel time correction band-pass filtering, normalizing with respect to the first arrival (PKIKP+PKiKP), and stacking using the Phase Weighted Stack (PWS) technique (*Schimmel and Paulssen*, 1997), we computed a vespagram (Figure 13.43a), which corresponds to the predicted window for PKJKP based on the PREM mode. In the negative slowness range, the slowness of the energy maximum is $\sim -1.6\text{s/deg}$, close to the PREM prediction of -1.43s/deg . The arrival time is also compatible with PREM (1695 sec for the maximum energy, compared to a prediction of 1690 sec for the high frequency onset of the pulse). We also observe a clean stacked waveform corresponding to the energy maximum in the PKJKP window (Figure 13.43b). We verified that this phase arrives within 5° of the great circle path from the source, ruling out a scattered near source phase (Figure 13.43c). We further verified that this phase is not a mantle, outer core, or even crust phase (Figure 13.43d). In the negative slowness region there is no energy maximum corresponding to the observation in Figure 13.43a. For this, the in-

roduction of the concept of liquid inner core, as was done by *Duess et al.* (2000), is helpful. If the inner core were liquid, there would not be a PKJKP phase. Therefore, we constructed a synthetic vespagram for an assumed liquid inner core in the relevant time window, using the Direct Solution Method (DSM) to generate complete synthetic seismograms (*Takeuchi et al.* 1996).

The clear PKJKP waveform (Figure 13.43b) allows us to estimate the shear wave attenuation in the inner core. We use the envelope function of PKJKP in the synthetic differential seismogram between the solid inner core and the 'pseudo-liquid' inner core, to constrain the Q_β in the inner core. We process the synthetic differential seismograms in the same way as the observed seismogram and compare the envelope amplitude to the observed one for different values of Q_β in the inner core (Figure 13.44), obtaining a value of $Q_\beta \sim 320$, with an error of ± 150 , accounting for various uncertainties in the measurement. This is significantly higher than obtained from normal mode measurements. Normal modes mainly sample the shallow portion of the inner core, whereas PKJKP samples the central part. Thus, we find that Q_β increases with depth in the inner core, just as Q_α does (*Souriau and Roudil*, 1995). The envelope function modeling also suggests that the observed PKJKP is about 9.0 seconds faster than the synthetic PKJKP. It means that the constrained shear wave velocity in the inner core is $\sim 1.5\%$ faster than that for the PREM model, also in agreement with previous results if one allows for a slight increase in shear velocity with depth in the inner core.

22.3 Acknowledgments

We are grateful to the Gräfenberg Array operators for the long-term high quality maintenance of their array. This work was partially funded by NSF grant EAR-0308750.

22.4 References

Birch, F., The alpha-gamma transformation of iron at high compressions and the problem of the Earth's magnetism, *Am. J. Sci.* 238, 192, 1940.

Deuss, A., Woodhouse, J.H., Paulssen, H., and Trampert, J., The observation of inner core shear waves, *Geophys. J. Int.* 142, 67-73, 2000.

Dziewonski, A.M., and Gilbert, F., Solidity of the inner core of the Earth inferred from normal mode observations, *Nature* 234, 465-466, 1971.

Dziewonski, A.M., and Anderson, D.L., Preliminary reference earth model, *Phys. Earth Planet. Inter.* 25, 297-356, 1981.

Julian, B.R., Davies, D., and Sheppard, R.M., PKJKP, *Nature* 235, 317-318, 1972.

Lehmann, I., *P'*, Bur. Centr. Seismol. Int. A., *Travaux Scientifiques* 14, 87-115, 1936.

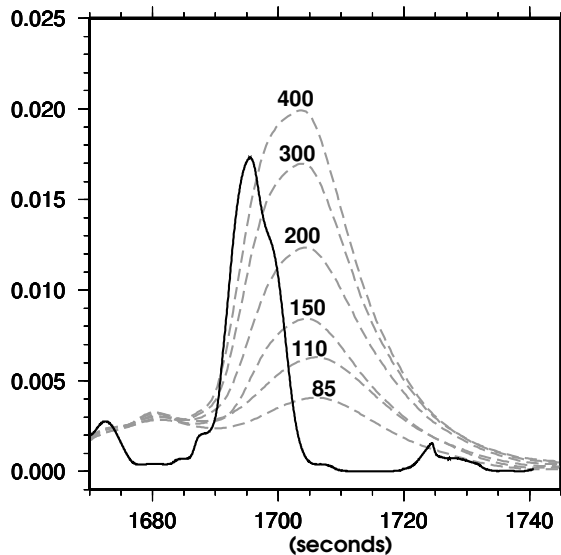


Figure 13.44: Envelope function modeling. The solid black line corresponds to the observed PKJKP, and dashed lines denote synthetic PKJKP with respect to different shear wave quality factors assumed in the inner core.

Okal, E.A., and Cansi, Y., Detection of PKJKP at intermediate periods by progressive multi-channel correlation, *Earth planet. Sci. Lett.* 164, 23-30, 1998.

Schimmel, M., and Paulssen, H., Noise reduction and the detection of weak, coherent signals through phase-weighted stacks, *Geophys. J. Int.* 130, 497-505, 1997.

Souriau, A., Roudil, P., Attenuation in the uppermost inner core from broad-band GEOSCOPE PKP data, *Geophys. J. Int.*, 123, 572-587, 1995.

Takeuchi, N., Geller, R.J., and Cummins, P.R., Highly accurate P-SV complete synthetic seismograms using modified DSM operators, *Geophys. Res. Lett.* 23, 1175-1178, 1996.

Widmer, R., Master, G., and Gilbert, F., Spherically symmetric attenuation within the earth from normal mode data, *Geophys. J. Int.* 104, 541-553, 1991.

23. High Resolution Anisotropic Structure of the North American Upper Mantle from Inversion of Body and Surface Waveform Data

Federica Marone and Barbara Romanowicz

23.1 Introduction

Seismic anisotropy is required for a correct interpretation of the retrieved S -velocity structure in tomographic studies at least in the first 400 km of the upper mantle (Gung *et al.*, 2003). A detailed knowledge of the seismic anisotropic structure of the earth's mantle also provides insight into debated geophysical issues, such as the nature and strength of the lithosphere/asthenosphere coupling, the depth extent of continental sub-regions and the relation of imaged seismic anisotropy to present-day asthenospheric flow and/or past tectonic events recorded in the lithosphere.

To date, our knowledge of the North American anisotropic structure arises mainly from global tomographic models (e.g. Ritsema *et al.*, 1999; Gung *et al.*, 2003) or SKS splitting studies (e.g. Fouch *et al.*, 2000; Savage and Sheehan, 2000), which lack horizontal and vertical resolution respectively, and are limited to either radial or azimuthal anisotropy.

Our goal is a new high resolution model for the North American upper mantle incorporating both radial and azimuthal anisotropy. We aim at unprecedented lateral and depth resolution by improving both data coverage and methodology.

23.2 Dataset

In this study, we consider fundamental and overtone surface waveforms selected from 3 component long period seismograms. Surface wave data for paths relevant to the study region has been extracted from the existing compilation used for global tomography in Panning and Romanowicz (2005). This dataset has been further complemented with waveforms from events at teleseismic and far regional distances ($15^\circ < \Delta < 65^\circ$) recorded at broad band seismic stations in North America. The collected dataset includes data for 540 events from 1993 to 1999, with M_w between 6.0 and 7.0. The main criteria guiding the event selection has been the achievement of the best possible path (Figure 13.45) and azimuthal coverage for the North American continent.

From each deconvolved and filtered seismogram, individual fundamental and higher mode surface wave packets have been extracted using an automated selection algorithm (Panning and Romanowicz, 2005) and subsequently checked by hand, to ensure a high quality dataset.

Our final dataset consists of more than 18,000 fundamental and 20,000 higher mode high quality surface wave



Figure 13.45: Data coverage - Paths of teleseismic events with $M_w \geq 6$ recorded at North American stations (indicated by white triangles), for which high quality fundamental mode Rayleigh wave packets have been selected.

packets. We expect that the achieved fairly homogeneous path and azimuthal coverage for North America will be further improved by taking advantage of the broad band dataset that is being collected under the USArray effort within EarthScope.

23.3 Methodology improvements

We invert seismic long period waveform data simultaneously for perturbations in the isotropic S -velocity structure and anisotropic parameter $\xi = \frac{v_S^2 H}{v_{SV}^2}$, in the framework of normal mode asymptotic coupling theory (NACT - Li and Romanowicz, 1996). The resulting broad band sensitivity kernels allow us to exploit the information contained in long period seismograms for body, fundamental and higher mode surface waves at the same time.

This approach was being applied at the global scale with lateral parametrization in terms of spherical harmonics (e.g. Li and Romanowicz, 1996). Here, we have adapted the procedure to the regional case by implementing a lateral parametrization in terms of spherical splines on an inhomogeneous triangular grid of knots (e.g. Wang and Dahlen, 1995), with the finest mesh for the region of interest, where the data coverage is densest, and a coarser

grid outside the study region. This flexible parametrization approach permits the perturbation of only a subset of the model parameters, for instance the ones falling within the target area, while using the entire set to correct the data for the global 3D heterogeneous structure, in this case using the radial anisotropic global model SAW24AN16 (Panning and Romanowicz, 2005).

Body and surface wave datasets used in mantle seismic tomography are sensitive to crustal structure, but cannot resolve details within the crust. Accurate crustal corrections are therefore essential for the quality of high resolution regional tomographic studies. The effect of shallow-layer features is often removed from the data by assuming an a priori crustal model (e.g. CRUST5.1) and applying linear perturbation corrections. However, lateral variations in Moho depth can be fairly large even over short distances, as for instance at ocean/continent transitions and the adequacy of linear corrections is questionable. In fact, Montagner and Jobert (1988) showed that the non-linearity of shallow-layer corrections is often non negligible even at long periods. In high resolution upper mantle regional tomographic studies, it is therefore important to take the crustal structure into account in a more accurate way. Going beyond the linear perturbation approximation, we follow the approach proposed by Montagner and Jobert (1988) and split the correction into a linear and non-linear part. At each point along a path, we assign a 1D reference model according to the local crustal structure (e.g. extended crust, orogen, ocean, ...). We then correct for the difference between the discontinuities in the chosen a priori crustal model (e.g. CRUST5.1) and the selected 1D local reference model assuming a linear perturbation, and exactly for the difference, if any, between the local reference model and PREM (our global reference model).

23.4 Results

Our 3D radial anisotropic model (Figure 13.46) shares the large scale features of previous regional tomographic studies for North America (e.g. Van der Lee and Nolet, 1997; Grand, 2001). We confirm the pronounced difference in the isotropic velocity structure between the western active tectonic region and the central/eastern stable shield, with the boundary being sharp and almost perfectly coincident with the Rocky Mountain Front. At transition zone depths, we document the presence of subducted material (Juan de Fuca and Farallon plate). Concerning the anisotropic signature, we observe a positive ξ anomaly in correspondence of the cratonic areas between 200 and 300 km depth.

Comparison of models obtained with different crustal correction approaches (linear vs. linear/non-linear perturbation approximation) shows that shallow-layer features can significantly bias the mantle structure down to 400 km depth and therefore confirms that accurate

crustal corrections are an essential step in high resolution regional tomographic studies. Both shape and amplitude of the imaged anomalies can be affected by inaccurate removal of the crustal signature.

23.5 Future of the project

Our final goal is a 3D high resolution tomographic model incorporating both radial and azimuthal anisotropy. Starting from our 3D radial anisotropic structure, we have begun addressing the distribution of azimuthal anisotropy, for which we have extended our NACT formalism. Resolving azimuthal anisotropy's four different components will only be possible with the improved coverage we expect from the USArray data. Meanwhile, using appropriate scaling relationships for the upper mantle, we are developing a preliminary 3D model, which, in addition to the isotropic S -velocity structure and the anisotropic parameter ξ , also incorporates the dominant $2\text{-}\Psi$ variations of anisotropy. Such a model can be interpreted in terms of an orthotropic medium, characterized by radial anisotropy with a symmetry axis of arbitrary orientation and described by the 5 Love parameters plus two angles defining the axis orientation. We hope to obtain constraints on the depth distribution of azimuthal anisotropy and in particular to discriminate between a lithospheric and an asthenospheric origin of the observed SKS splitting.

23.6 Acknowledgements

This work has been financially supported by the National Science Foundation as part of EarthScope (Grant EAR-0345481).

We are grateful to the IRIS Data Management Center (DMC) as well as to the Geological Survey of Canada for providing waveform data used in this study.

23.7 References

- Fouch, M.J., K.M. Fischer, E.M. Parmentier, M.E. Wysession and T.J. Clarke, Shear-wave splitting, continental keels, and patterns of mantle flow, *J. Geophys. Res.*, 105, 6255-6275, 2000.
- Grand, S.P., Mantle shear structure beneath the Americas and surrounding oceans, *J. Geophys. Res.*, 99, 591-621, 1994.
- Gung, Y., M. Panning and B. Romanowicz, Global anisotropy and the thickness of continents, *Nature*, 422, 707-711, 2003.
- Li, X.D. and B. Romanowicz, Global mantle shear-velocity model developed using nonlinear asymptotic coupling theory, *Geophys. J. R. Astr. Soc.*, 101, 22,245-22,272, 1996.
- Montagner, J.-P. and N. Jobert, Vectorial tomography; II. Application to the Indian Ocean, *Geophys. J.*, 94, 309-344, 1988.

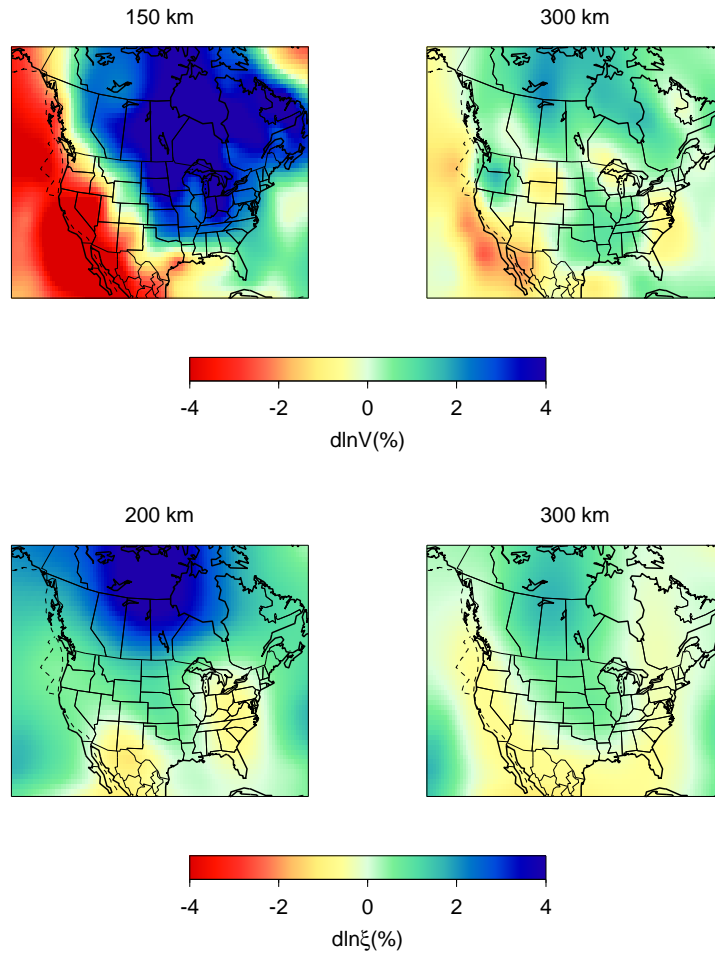


Figure 13.46: Horizontal slices at different depths through our 3D radially anisotropic model - Top: Perturbations in the isotropic S -velocity structure. Anomalies are relative to average - Bottom: Perturbations in the anisotropic parameter ξ . Anomalies are relative to isotropy.

Panning, M. and B. Romanowicz, A three dimensional radially anisotropic model of shear velocity in the whole mantle, *Geophys. J. Int.*, in revision, 2005.

Ritsema, J., H. van Heijst and J. Woodhouse, Complex shear wave velocity structure imaged beneath Africa and Iceland, *Science*, 286, 1925-1928, 1999.

Savage, M.K. and A.F. Sheehan, Seismic anisotropy and mantle flow from the Great Basin to the Great Plains, western United States, *J. Geophys. Res.*, 105, 13715-13734, 2000.

Van der Lee, S. and G. Nolet, Upper mantle S -velocity structure of North America, *J. Geophys. Res.*, 102, 22815-22838, 1997.

Wang, Z. and F. Dahlen, Spherical-spline parametrization of three-dimensional Earth models, *Geophys. Res. Lett.*, 22, 3099-3102, 1995.

24. Development of a Regional Velocity Model Using 3D Broadband Waveform Sensitivity

Mark Panning, Barbara Romanowicz, and Ahyi Kim

24.1 Introduction

We present a new approach to develop and evaluate earth models at the regional scale that utilizes full waveform seismograms. Adequate path calibrations are crucial for improving the accuracy of seismic event location and origin time, size, and mechanism. There is considerable information on structure in broadband seismograms that is currently not utilized. The limitations have been largely theoretical. The development and application to solid earth problems of powerful numerical techniques, such as the Spectral Element Method (SEM), has opened a new era, and it should be possible to compute the complete predicted wavefield accurately without any restrictions on the strength or spatial extent of heterogeneity. This approach requires considerable computational power, which is currently not fully reachable in practice.

We have begun work on an approach which relies on a cascade of increasingly accurate theoretical approximations for the computation of the seismic wavefield to develop a model of structure for the area of Eurasia located between longitudes of 30 and 150 degrees E, and latitudes of -10 to 60 degrees North. The selected area is particularly suitable for the purpose of this experiment, as it is highly heterogeneous, presenting a challenge for modeling, but it is well surrounded by earthquake sources and a significant number of high quality broadband digital stations exist, for which data are readily accessible through IRIS (Incorporated Research Institutions for Seismology) and the FDSN (Federation of Digital Seismic Networks).

24.2 Modeling Approach

The modeling approach utilizes increasingly advanced theoretical frameworks and numerical methods in order to obtain improved models of regional seismic structure. Specifically, a large-scale regional Eurasian model will be developed from a large dataset of seismic waveforms using the path-average approximation (PAVA) and NACT (Non-linear Asymptotic Coupling Theory; *Li and Romanowicz, 1995*), which are well-developed normal-mode based approaches which consider 1D (PAVA) and 2D (NACT) waveform sensitivity in the vertical plane along the great-circle path between source and receiver. This model will then be refined in a smaller region using an implementation of Born single-scattering theory (*Capdeville, 2005*), which more accurately represents the 3D sensitivity of the seismic wavefield. Finally, we will utilize the Spectral Element Method (SEM), a numerical approach that accurately models both 3D and non-linear

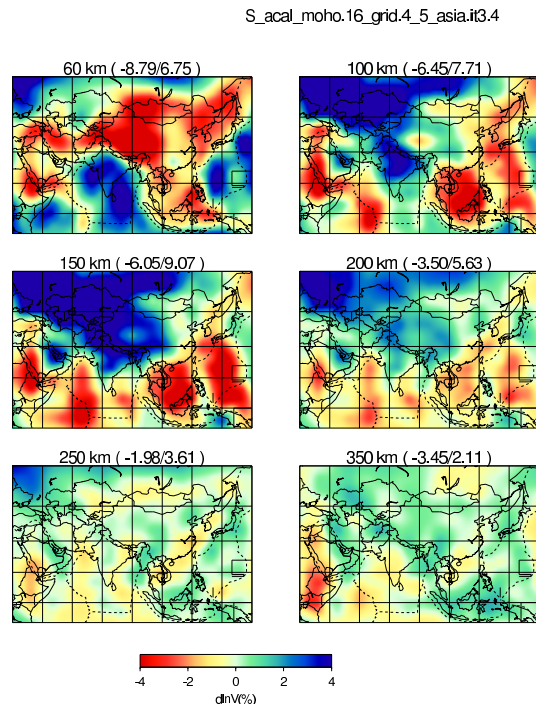


Figure 13.47: Preliminary smooth S velocity model for the upper mantle for the Eurasia developed using PAVA and NACT approaches. Values are the percent perturbations in isotropic velocity from PREM. Model is parameterized in radial splines spaced approximately 100 km, and in level 5 spherical splines (spacing ≈ 400 km).

effects (e.g. *Faccioli et al., 1996; Komatitsch and Vilotte, 1998*). To conserve computational resources we will restrict the use of SEM to the upper mantle by coupling to a normal mode solution (CSEM; *Capdeville et al., 2003*) and applying appropriate boundary conditions.

24.3 Preliminary Results

An initial model for Eurasia has been developed using PAVA and NACT and a global dataset of surface waveforms (Figure 13.47). This dataset includes waveforms both from our existing database (*Li and Romanowicz, 1996; Mégnin and Romanowicz, 2000; Gung et al., 2003; Panning and Romanowicz, 2004*), as well as new data, and includes 38826 3-component waveforms from 476 events recorded at 169 stations. While this model is smooth, it will serve as a starting point for the mod-

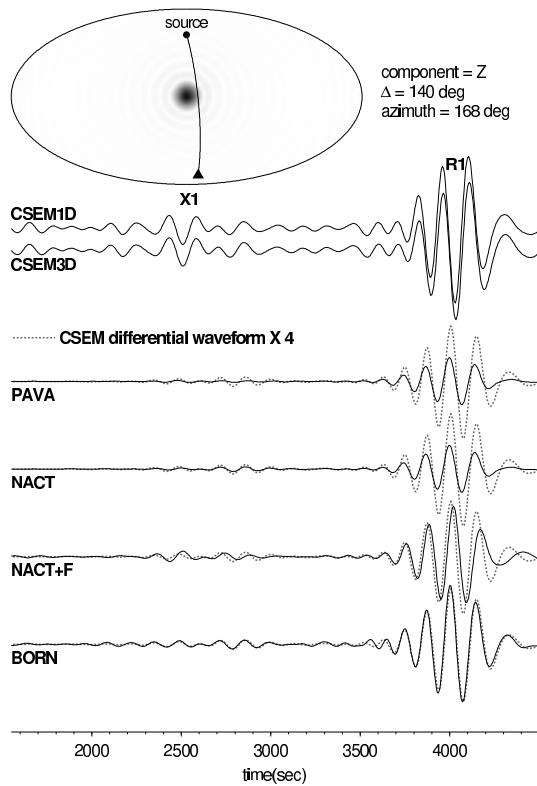


Figure 13.48: Comparison of performance of several mode-based approximations used in tomographic modeling. The map shows the source-receiver geometry and the velocity model, an ellipsoidal anomaly 5% slower than the background centered at 220 km depth. The top two traces are the SEM synthetics calculated from the 1D background model and the 3D model. The remaining traces show the differential waveforms obtained by subtracting the waveform produced by the 1D model. For each approximation, the differential SEM waveform is shown as a dotted line, and the waveform from the approximation is solid. Results are shown for the Path Average approximation (PAVA), Non-linear Asymptotic Coupling Theory (NACT), NACT plus a higher-order focusing approximation (NACT+F), as well as the 3D Born approximation.

els developed using increasingly accurate theoretical approaches.

The next step is to invert the surface wave dataset using the 3D implementation of Born scattering. Using this approach, we can calculate 3D sensitivity kernels with show significant sensitivity to off-path structure. We have performed verification tests that show that this approach can produce much more accurate seismograms for particular source-receiver paths (Figure 13.48).

Future work will include CSEM calculation of synthetics used in the inversion, which will include both 3D ef-

fects as well as the non-linear dependence of the waveforms to velocity structure.

24.4 Acknowledgements

We would like to acknowledge Yann Capdeville for the use of his Born code, and advice in the adaptation of this code to our project. This project has been funded through the Dept. of Energy, National Nuclear Security Administration, contract no. DE-FC52-04NA25543

24.5 References

- Capdeville, Y., E. Chaljub, J.P. Vilotte, and J. P. Montagner, Coupling the spectral element method with a modal solution for elastic wave propagation in global earth models, *Geophys. J. Int.*, 152, 34-66, 2002.
- Capdeville, Y., B. Romanowicz, and Y. Gung, Global seismic waveform tomography based on the spectral element method, abstract, joint AGU/EGS/EUG Meeting, Nice, April 2003.
- Capdeville, Y., An efficient Born normal mode method to compute sensitivity kernels and synthetic seismograms in the Earth, submitted to *Geophys. J. Int.*, 2005.
- Faccioli, E., F. Maggio, A. Quarteroni, and A. Tagliani, Spectral-domain decomposition methods for the solution of acoustic and elastic wave equations, *Geophysics*, 61, 1160-1174, 1996.
- Gung, Y., B. Romanowicz, and M. Panning, Anisotropy and lithospheric thickness, *Nature*, 422, 707-711, 2003.
- Komatitsch, D. and J. P. Vilotte, The spectral element method: an effective tool to simulate the seismic response of 2D and 3D geological structures, *Bull. Seism. Soc. Am.*, 88, 368-392, 1998
- Li, X.D. and B. Romanowicz, Comparison of global waveform inversions with and without considering cross-branch modal coupling, *Geophys. J. Int.*, 121, 695-709, 1995.
- Li, X. D. and B. Romanowicz, Global mantle shear velocity model developed using nonlinear asymptotic coupling theory, *J. Geophys. Res.*, 101, 22,245-22,273, 1996.
- Megnin, C. and B. Romanowicz. The 3D shear velocity structure of the mantle from the inversion of body, surface and higher mode waveforms, *Geophys. J. Int.*, 143, 709-728, 2000.
- Panning, M. and B. Romanowicz, Inferences on flow at the base of Earth's mantle based on seismic anisotropy, *Science*, 303, 351-353, 2004.

25. Toward the Constraints on Lateral S Wave Velocity Gradients and the Shape of the Pacific Superplume

Akiko To, Barbara Romanowicz

25.1 Introduction

We have recently documented that a sharp lateral boundary exists at the southern edge of the Pacific superplume (*To et al.*, 2005). The set of SHdiff wave forms, which graze the South Pacific superplume, have similar features to those observed previously at the southeastern edge of the African superplume. They both show a rapid shift of the arrival time with respect to azimuth and are followed by postcursors. First, we report the postcursors are explained as refractions from the lateral boundary on the D'' region. Second, we report that sharp lateral boundaries also exist not only in the southern edge of the super plume, but also in other regions surrounding the super plume.

25.2 Cause of the secondary arrival in Sdiff waveforms

The Sdiff waveforms which sample South Pacific superplume or the southeastern edge of the African superplume both show a rapid shift of the arrival time with respect to azimuth and they are followed by postcursors. In order to explain these features, we modified a tomographic SH model by increasing the gradient between the fast and slow anomalies, but keeping the shape of the boundary fixed (Figure 13.50 (Right)). We used the coupled mode/spectral element method (CSEM, *Capdeville et al.*, 2003), which can handle strong lateral variations of velocity in the D'', to construct synthetic waveforms. The synthetics from the original tomographic model (Figure 13.49 (Left)) do not generate the secondary arrival or the rapid shift of the first arrival. On the other hand, the synthetics from the modified model with the sharp boundaries (Figure 13.49 (Middle)) capture the features of the observed waveforms. The move out of the secondary arrival, which actually appears in multiple branches, shows a slope which is consistent with observations, although it appears at a slightly different azimuth. Moreover, the jump of the first arrival occurs around the azimuth of 215 degrees, which is also consistent with the observations. Particle motion analysis of observed and synthetic waveforms shows that the first pulse arrives from the southern side and the second pulse arrives from the northern side. Both the first and second arrivals are estimated to be refracted waves and their paths are described schematically in Figure 13.50 by yellow and green lines, respectively. The result suggests that it is important to take into account the heterogeneity outside of the great circle path.

25.3 Sharp lateral boundaries around the Pacific super plume

We have assembled a large dataset of Sdiff waveforms and travel time throughout the Pacific region. Also in other regions bordering the South Pacific superplume, observed Sdiff travel times vary rapidly over small ranges of azimuth and/or distance (Figure 13.51). The observed travel times can be better fit by increasing the amplitude and lateral gradients of the large scale velocity anomalies in a tomographic S velocity model. Modeling the pulses and the travel time jump due to lateral heterogeneity can help constrain the shape and velocity contrast at the superplume boundaries, at the base of the mantle.

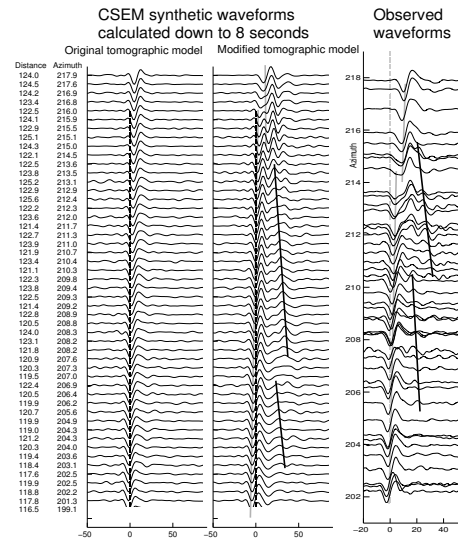


Figure 13.49: Synthetic waveforms calculated by CSEM down to 8 seconds. [Left] The waveforms from the original tomographic model (Figure 13.50 left panel); [Middle] the waveforms from the modified model (Figure 13.50 right panel). Gray lines follow the first trough, black lines follow the secondary arrivals. [Right] Observed velocity waveforms for event 19970904 in Fiji-Tonga (M_w 6.8) recorded in South Africa. Bandpass filtered with corner frequencies at 0.01 and 0.125 Hz. Y-axis shows the back azimuth. The broken line is the expected Sdiff arrival for the PREM model. Gray lines follow the trough of the first pulse. Black solid lines follow the secondary pulse, which is only observed in the vicinity of the structural boundary.

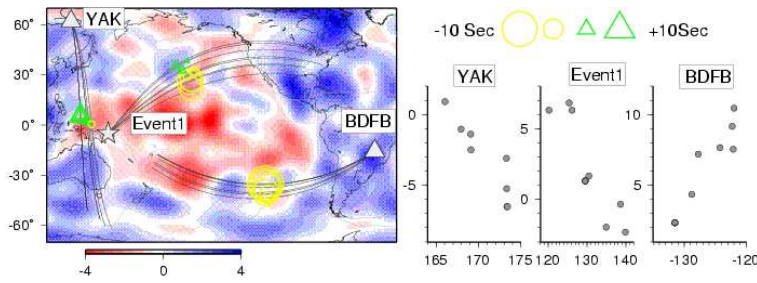


Figure 13.51: [Left] Sdiff ray path distributions where the rapid travel time shifts with respect to azimuth or back azimuth are observed. The background color map shows SAW24B16 model at CMB. Yellow circles and green triangles show the observed Sdiff travel time residuals with respect to PREM. Symbols are plotted at the middle point of the diffracting portion at CMB. White star and white triangles show the epicenter (Event1) and the stations (YAK and BDFB) which are discussed in the right figure. [Right] The Sdiff travel time residuals as a function of azimuth (for Event1) and back azimuth (for YAK and BDFB).

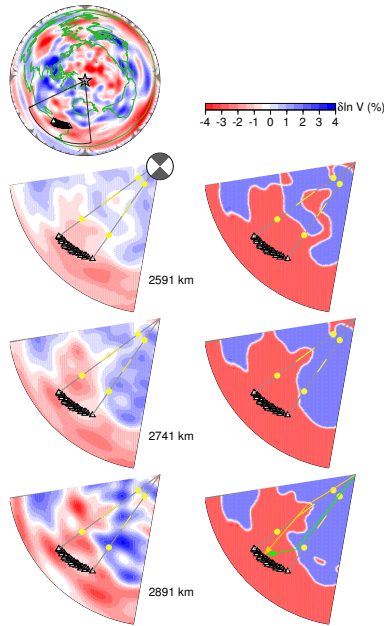


Figure 13.50: Left panel: the original SAW24B16 (Méglin and Romanowicz, 2000) model at three depths in the bottom 300km of the mantle. The source in Fiji Tonga region is located at the apex. The stations in Africa are shown by triangles. Right panel: a model which is modified from SAW24B16. The boundary of the fast and slow anomalies is the contour line of 0% anomaly of SAW24B16. The anomaly jump is from -2.75 to 1.75%. Both models have 1D PREM structure from surface down to 370 km above the CMB. The 3D velocity anomalies linearly increase from 370 to 300 km above the CMB.

25.4 Acknowledgements

The data are downloaded from IRIS DMC and CNSN.

25.5 References

- Capdeville, Y., A. To and B. Romanowicz, Coupling spectral elements and modes in a spherical earth: an extension to the "sandwich" case, *Geophys. J. Int.*, 154, 44-57, 2003
- Méglin C. and B. Romanowicz, The three-dimensional shear velocity structure of the mantle from the inversion of body, surface and higher-mode waveforms. *Geophys. J. Int.*, 143, pp. 709-728, 2000
- To, A., B. Romanowicz, Y. Capdeville and N. Takeuchi, 3D effects of sharp boundaries at the borders of the African and Pacific Superplumes: observation and modeling, *Earth and Planet. Sci. Lett.*, 233, 137-153, 2005

26. Towards Inverting Seismic Waveform Data for Temperature and Composition of the Earth’s Upper Mantle

Fabio Cammarano, Barbara Romanowicz, Lars Stixrude ^(a) and Carolina Lithgow-Bertelloni ^(a)
(a)Department of Geological Sciences, University of Michigan

26.1 Introduction

Unraveling the physical state of the upper mantle, including the transition zone (TZ), is one of the key factors for understanding the Earth’s mantle dynamics. Knowledge of mantle temperature and composition is mainly based on the interpretation of seismological observations based on insights from mineral physics. Despite the progress made to image the 3-D seismic structure of the upper mantle, its interpretation in terms of physical parameters is still challenging and it requires a truly interdisciplinary approach. Due to the better knowledge of the elastic and anelastic properties of mantle minerals at high temperatures and pressures, such an approach is now becoming feasible.

We propose a new waveform inversion procedure, based on a formalism previously developed at Berkeley for global elastic and anelastic tomography, and using our existing collection of long-period fundamental and higher mode surface waveforms. Here, we incorporate mineral physics data at an early stage of the process to directly map lateral variations in temperature and composition, using recent estimates of the temperature and composition derivatives of seismic velocities ($\partial \ln V / \partial \ln T, C$). We show preliminary tests of the inversion. We discuss ways to address the non-linearities, as well as uncertainties in the partial derivatives.

In addition to constraining the lateral variations in temperature or composition, the models can have implications on the average structure of the upper mantle. The most-common accepted physical 1-D structure had problems to satisfactorily fit seismic travel time data, requiring a slower TZ to improve the fit. However, these data do not have sufficient coverage (and resolution) in the TZ. A complementary outcome of our models will be to shed light on whether the seismic data require a modification of the physical structure in the transition zone and if the three-dimensional heterogeneity introduces a significant shift of the average physical structure away from adiabatic pyrolite.

26.2 Mineral physics data

The input parameters from mineral physics are the temperature and compositional partial derivatives of seismic velocities. These values are based on knowledge of elastic and anelastic properties of upper mantle minerals at appropriate pressure and temperature conditions. Compilation of recent data is being used to as-

sess the uncertainties of the temperature partial derivatives throughout the upper mantle (Cammarano *et al.*, 2003). A thermodynamic equation of state that determines jointly the phase equilibria and the elastic properties of the upper mantle has been recently proposed (Stixrude and Lithgow-Bertelloni, 2005). This provides a tool to compute consistently the compositional derivatives.

Anelasticity significantly increase temperature sensitivity in the mantle, but also enlarge notably the uncertainties of the partial derivatives. Moreover, anelasticity introduces a non-linear dependence of the seismic velocities with temperature throughout the upper mantle, and phase-transitions confer a non-linear character to the compositional derivatives as well. However, mineral physics experiments have shown that attenuation is not affected significantly by composition, while it is affected not only by temperature, but also by grain size (e.g. Faul and Jackson, 2005). Uncertainties in composition derivatives are then expected to be smaller, but their assessment will require further work.

26.3 Tests of inversion for temperature

The inversion is based on a normal mode asymptotic coupling mechanism (NACT, Li and Romanowicz, 1996). The seismic data used for the inversion are long period fundamental and overtone spheroidal modes selected on the vertical component of the seismograms included in the existing collection. Including higher modes provide resolution in the transition zone. No crustal correction has been used at this point. The direct inversion of the seismic waveforms for temperature requires $\partial \ln V / \partial \ln T$ (anelastic effects included) as a function of pressure (depth) and temperature and a starting thermal model as well. We choose an adiabat with a potential temperature of 1300° C overlaid by the geotherm for 60 m.y. old oceanic lithosphere.

To test the results of the inversion and assess the best way to address the non-linearities, we test our temperature inversion by performing in parallel an inversion for a physical reference model. The chosen model is one of the best-fit adiabatic pyrolitic models (PREF) for travel-time and fundamental mode data from Cammarano *et al.*, 2005. The models tested span the range of elastic properties for each mineral as inferred from mineral physics and applying different anelasticity models that cover the range of 1-D seismic attenuation models. Note that the thermal structure is exactly the same. An ex-

ample of how a temperature slice may be obtained by inverting with respect to a reference model is given in Figure 13.52

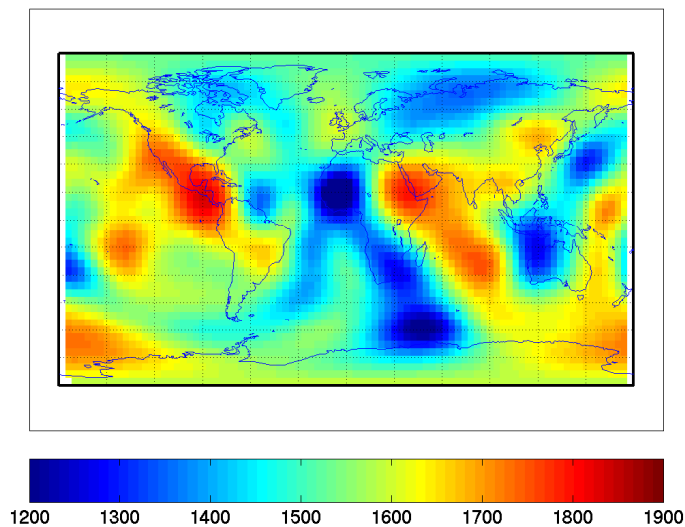


Figure 13.52: Example of horizontal tomographic slice for temperature at 300 km depth. Composition is pyrolitic. Note that the extremely low temperature beneath the African Craton is consistent with a contribution from compositional heterogeneity.

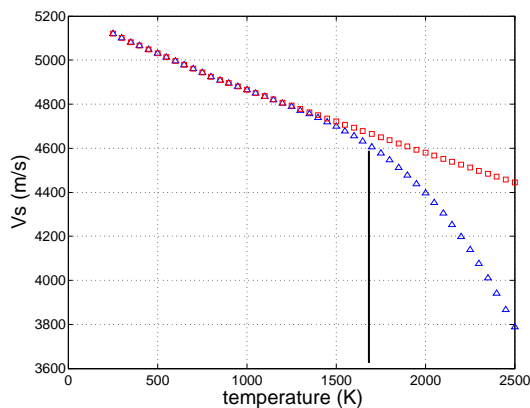


Figure 13.53: Examples of non linearity effects at 300km. Triangles represent variation of V_S with T by including anelasticity effects, squares are without it. Black line indicates the reference T at this depth.

The sensitivity kernels of the seismogram with respect to velocity are translated into temperature by using the partial derivatives. The kernels should be recomputed after each iteration of the inversion because of the non linearity introduced by attenuation. However, knowing how the effect changes as a function of temperature and depth, we will try to correct the model after each iteration. In figure 13.53, we show at a given depth (300

km) how the kernels change around the thermal reference temperature. Note that the kernels (the derivatives of Figure 13.53) change both towards high and low temperature.

26.4 References

Cammarano F., Goes S., Deuss A., Giardini D., Is a pyrolitic adiabatic mantle compatible with seismic data? *Earth and Planetary Science Letters*, 232, 227-243, 2005

Cammarano F., Goes S., Giardini D., Vacher P., Inferring upper mantle temperatures from seismic velocities. *Physics of the Earth and Planetary Interiors*, 138, 197-222, 2003

Li X.D., Romanowicz B., Global mantle shear velocity model developed using nonlinear asymptotic coupling theory. *Journal of Geophysical Res.*, 101, 22245-22272, 1996

Stixrude L., Lithgow-Bertelloni C., Thermodynamics of mantle minerals I, Physical properties. *Geophysical Journal International*, 162, 610-632, 2005

27. Europa Scenarios: Preliminary Physically Consistent Models of Europa

Fabio Cammarano, Vedran Lekic, Mark Panning, Michael Manga, Barbara Romanowicz

27.1 Introduction

Europa, one of the four major moons of Jupiter, presents planetary scientists with a set of fascinating questions, not the least of which concerns the presence of a water ocean beneath its icy surface. Recent magnetometer data acquired by the Galileo flybys seem to have confirmed the presence of Europa's ocean (Kivelson *et al.*, 2000). Additionally, detailed images of the planet allowed the observation of cracks in the ice consistent with flow of warm ice or water below the surface (Greeley *et al.*, 2000) and the near-infrared mapping spectrometer experiment probably detected hydrated salts on the surface (Mc Cord *et al.*, 2001). Nevertheless, any quantitative constraints on the ocean depth and the depth of the ice shell above it require further explorations.

Measurements of the seismic response of Europa remotely from an orbiter or using a lander can greatly expand our knowledge of its internal structure. Despite this potential, the feasibility of a seismic experiment that would exploit natural sound sources (e.g., the opening of the cracks in the ice) to investigate the thickness of the ice shell and the ocean depth, has only recently been considered. In order to determine the potential of seismic signals to discriminate between different possible scenarios for the structure of Europa, it is essential to provide a family of reasonable physical models.

We generate a set of physical models by assuming a three-layer composition: water-ice, silicate mantle (either pyrolytic or chondritic), metallic core (either solid iron or iron+sulfur) and different thermal structures. The thermal structures are based on estimations of the internal heating. Two extreme (cold and hot scenarios) have been considered. Thermodynamic properties as a function of pressure and temperature are computed for each layer by using equation of states based on the most recent mineral physics data (e.g. Wagner and Pruss 2002 for water, Stixrude and Lithgow-Bertelloni 2005 for the silicatic mantle). The depth of the ocean and of the core-mantle boundary are constrained by the mass and moment of inertia for each physical model.

Inversion for ocean depth and core-mantle boundary depth

For any possible combination of thermal structure and composition, we find the depth of the ocean and of the core-mantle boundary which best fits the mass and moment of inertia of Europa. For any physical structure, the uncertainties on those two depths are quite small and are

mainly due to the uncertainty of the gravitational constant (fig. 1).

We choose to not invert for the gravity acceleration (g) profile, which requires tedious iterations because of the feedback with the density profile. Instead, we approximate the gravity profile by pre-computing the values at the core-mantle boundary (assuming an average density of the core, based on the composition used), at the ocean bottom (assuming an average density of the water-ice layer combined with information about Europa's total mass) and by taking the known values at the surface (circa 1.31 m/s^2) and at the center (0) and by interpolating linearly between these points. The resulting gravity profile is sufficiently accurate, and does not noticeably affect our results.

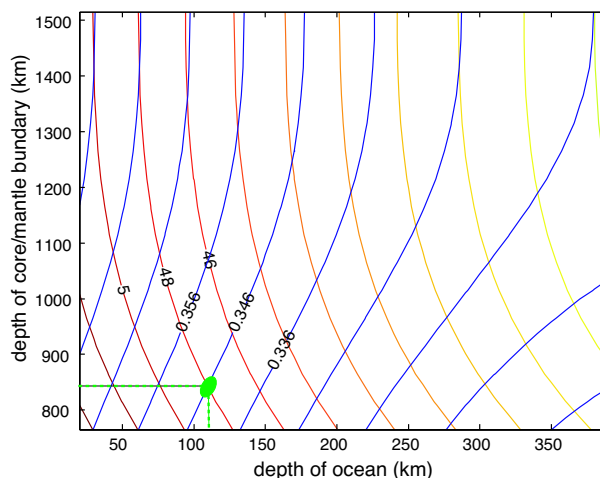


Figure 13.54: Example of determination of the ocean depths and core-mantle boundary for one physical structure. Yello-reddish contours are for mass value, blue for moment on inertia values. The green ellipse is the field of possible combination of the two depths to fit mass and moment of inertia

Anelasticity

Including anelasticity effects is essential to accurately characterize the seismic response of the different physical models. Anelasticity is strongly temperature dependent and it can be used to discriminate between the “cold” and the “hot” scenarios. In fact viscoelastic relaxation at high temperature leads to dispersion (frequency de-

pendence of seismic wave speeds) and dissipation (attenuation). The development of experimental techniques to measure the viscoelastic behavior at high temperature and seismic frequencies is beginning to provide direct constraints on the shear attenuation phenomena (e.g., *Faul and Jackson, 2005*). Extrapolation with pressure, which is still an important issue for the Earth, is less relevant for small planetary bodies where the pressure does not increase dramatically with depth. In this sense, we expect a (strong) constant attenuation throughout the “hot” adiabatic mantle. In the case of a cold mantle, we expect enhanced attenuation at the top of the mantle, and possibly at the core-mantle boundary. For the time being, we test the anelasticity effects using a model derived by *Cammarano et al., 2003*.

Conclusions

We calculate a range of thermodynamically consistent models for the physical structure of Europa, as constrained by the satellite’s mass and moment of inertia. We start with either a pyrolytic or a chondritic mantle composition and with either pure iron or iron plus 20% of sulfur core composition.

Due to the feedback between radiogenic and tidal heating, two extreme thermal profiles are possible in the mantle. Strong dispersion and dissipation is expected in the hot convective mantle, while anelasticity effects will be much weaker in the case of the cold mantle.

There is a strong relationship between different thermal structures and compositions. The “hot” mantle may well keep temperatures high enough to be consistent with a liquid core made of iron plus light elements. In the case of the “cold scenarios”, the possibility of a solid iron core cannot be excluded and it may even be favored.

The depth of the ocean and of the core-mantle boundary are determined with high precision once we assume the composition and thermal structure. In fact, the depth of the ocean is not very sensitive to the core composition used.

27.2 References

- Cammarano F., Goes S., Giardini D., Vacher P., Inferring upper mantle temperatures from seismic velocities. *Physics of the Earth and Planetary Interiors, 138*, 197-222, 2003
- Faul U.H., Jackson I., The seismological signature of temperature and grain size variations in the upper mantle. *Earth and Planetary Science Letters, 234*, 119-134, 2005
- Greeley R., Figueredo P.H., Williams D.A. et al., Geologic mapping of Europa. *J. Geophys. Res.-Planets, 105*, 22559-22578, 2000
- Kivelson MG, Khurana KK, Russell CT, et al., Galileo magnetometer measurements: A stronger case for a subsurface ocean at Europa. *Science, 289*, 1340-1343, 2000

Mc Cord T.B., Orlando T.M., Teeter G., Hansen G.B., Sieger M.T., Petrik N.G., van Keulen L., Thermal and radiation stability of the hydrated salt minerals epsomite, mirabilite, and natron under Europa environmental conditions. *J. Geophys. Res., 106*, 3311-3319, 2001

Stixrude L., Lithgow-Bertelloni C., Mineralogy and elasticity of the oceanic upper mantle: Origin of the low-velocity zone. *J. Geophys. Res., 110*, B03204, doi:10.1029/2004JB002965, 2005

Wagner W., Pruss A., The IAPWS formulation 1995 for the thermodynamic properties of ordinary water substance for general and scientific purpose. *Journal of Physical and Chemical Reference Data, 31*, 387-535, 2002